

STRUCTURAL DYNAMICS OF PHOTOACTIVE YELLOW
PROTEIN

By

SANDIP KALEDHONKAR

Bachelor of Science in Physics
University of Pune
Pune, Maharashtra, India
2002

Master of Science in Physics
University of Pune
Pune, Maharashtra, India
2004

Submitted to the Faculty of the
Graduate College of the
Oklahoma State University
in partial fulfillment of
the requirements for
the Degree of
DOCTOR OF PHILOSOPHY
July, 2013

STRUCTURAL DYNAMICS OF PHOTOACTIVE YELLOW
PROTEIN

Dissertation Approved:

Prof. Aihua Xie

Dissertation Adviser

Dr. Robert J. Hauenstein

Dr. Donghua Zhou

Prof. Wouter D. Hoff

ACKNOWLEDGEMENTS

I am thankful to many persons in my life during my journey towards PhD degree. I take this opportunity to express my gratitude towards them for their kind support.

Firstly, I thank my all family members, specially my father for constant motivation and constant support throughout my life. I thank my beloved wife Sunita for staying by my side and supporting my decisions during this time.

I thank my friends during my Master's degree and members of Sahyadri Explorers Aniket, Bhalchandra, Chaitanya, Dhanajay, Hemant, Manish, and Shailesh with whom I cherish many scientific discussions and Google hangouts on relaxed Sunday mornings. I thank my friends at OSU Srinivasa, Ranjan, Pavan, Vasantha, Shahsidhara, Vijay, Chetan and Phag Phong.

I thank my former colleagues Dr. Beining Nie and Anupama for their help to collect data with time-resolved FTIR experiments. I thank Zhouyang, Shou and Yungxing for their help in numerous activities in Lab and scientific discussions. I especially thank Ningning for providing purified protein samples.

I extend my regards to Susan, Cindy, Tamara, Warren and Melissa for their help in official matters.

I specially thank Dr. Lorand Kelemen and Dr. Johnny Hendriks for their pivotal role in establishing the time-resolved FTIR experimental setup before and during my stay at OSU. I extend my regards to Dr. Lorand Kelemen who initiated the crystallization salt and PYP mutant studies.

Acknowledgements reflect the views of the author and are not endorsed by committee members or Oklahoma State University

I thank all my PhD committee members Prof. Wouter D. Hoff, Dr. Robert J. Hauenstein and Dr. Donghua Zhou. I thank Dr. Yin Guo for serving on my PhD committee during earlier years of my PhD study.

Finally I am grateful to my PhD advisor Prof. Aihua Xie for her motivation and constant support during all these years.

Name: SANDIP KALEDHONKAR

Date of Degree: JULY, 2013

Title of Study: STRUCTURAL DYNAMICS OF PHOTOACTIVE YELLOW PROTEIN

Major Field: PHYSICS

Abstract:

Photoactive yellow protein (PYP) is a blue light photoreceptor protein. PYP is a structural prototype of the PAS domain superfamily of regulating and signaling proteins. Upon absorption of a blue light photon, PYP exhibits a photocycle leading to the signaling state. We study structure-function relation in the PYP family by investigating single point mutants of *Halorhodospira halophila* (Hhal) PYP and homologous PYPs from three different bacteria. We study the role of Asn43 in Hhal PYP, a one of the nine well conserved residues in the PAS domain superfamily. The time-resolved FTIR difference spectroscopy of Asn43Ala PYP shows that this residue plays a key role in regulating kinetics of signaling of PAS domain. The FTIR absorption spectrum of *Idiomarina loihiensis* (Il) and Hhal PYP shows that the secondary structures of the Il PYP are similar to that of Hhal PYP. The decay of long lived putative signaling pB state of Il and Hhal PYP follows similar kinetics, yet these PYP perform different biological functions. We have observed a novel spectral isotopic effect (SIE) in *Salinibacter ruber* (Sr) and Hhal PYP through UV/Vis absorption spectroscopy. SIE offers possibility to examine hydrogen bonding strength in proteins.

Despite extensive studies since 1887 (*Arc. Exp. Pathol. Pharmacol.* 1887, **29**: 1-16), it remains unclear how salt solutions alter stability and solubility of protein. We employ PYP as a model system to study impact of salts on structural dynamics of protein. The time-resolved step-scan Fourier transform infrared spectroscopy (FTIR) with 5 μ s time resolution and time-resolved rapid-scan FTIR with 8 ms time resolution were employed in this study to capture the dynamic structural development of PYP upon light stimulation. We found that salts do not alter photoisomerization of *p*-coumaric acid (*p*CA) and proton transfer pathway from Glu46 to *p*CA upon photoexcitation of PYP. Thus salt do not affect structural changes inside protein. Our study reveals that, salt suppresses conformational changes of PYP strongly, thus formation of signaling state of PYP for bacterial phototaxis is inhibited in high salt solutions. The suppression of conformational changes of PYP signaling state in high salt solution is attributed to effective dehydration of proteins. The knowledge gained may be applied to understand the effect of high salt concentration on stability and solubility of the proteins, which is known as Hofmeister effect.

TABLE OF CONTENTS

Chapter	Page
I. INTRODUCTION	1
1.1 Photoactive Yellow Protein.....	1
1.2 Photocycle of PYP.....	7
1.3 Molecular mechanism of the PYP photoactivation	11
1.4 PAS domain proteins.....	16
1.5 Hofmeister effect and structural changes in protein.....	24
II. METHODS AND MATERIALS	26
2.1 Bacterial growth, PYP over-expression, PYP purification.....	26
2.1.1 Ion Exchange Chromatography.....	29
2.1.2 Size Exclusion Chromatography.....	30
2.2 Buffer and FTIR sample preparation.....	30
2.3 Laser.....	31
2.3.1 Optical Parametric Oscillator	32
2.3.2 Q Switch.....	32
2.4 FTIR system and techniques	33
2.4.1 Principles of Infrared Spectroscopy	33
2.4.2 Vibrational modes and isotopic shift.....	35
2.4.3 Introduction to FTIR instrument.....	36
2.4.4 Michelson Interferometer.....	37
2.5 IR absorption of protein	38
2.6 Time-resolved FTIR spectroscopy	42
2.6.1 Time-resolved rapid-scan FTIR spectroscopy	42
2.6.2 Time-resolved step-scan FTIR spectroscopy	45
2.7 Flash photolysis system	50
III. IMPACT OF CRYSTALLIZATION ON STRUCTURAL DYNAMICS OF PHOTOACTIVE YELLOW PROTEIN	52
Introduction	53
Materials and methods.....	54
Results and discussion.....	57
Conclusions	71

Chapter	Page
IV. STRUCTURE-FUNCTION RELATIONS IN PHOTOACTIVE YELLOW PROTEIN..	73
4.1 Locked chromophore analogs reveal that photoactive yellow protein regulates biofilm formation in deep sea bacterium <i>Idiomarina loihiensis</i>	74
4.2 A conserved Helical capping hydrogen bond in PAS domains controls signaling kinetics in the superfamily prototype photoactive yellow protein.....	100
4.3 Strong ionic hydrogen bonding causes a spectral isotope effect in photoactive yellow protein.....	134
V. CONCLUDING REMARKS	149
5.1 Impact of crystallization salts on structural dynamics of protein	149
5.2 Structure-function relationship in photoactive yellow protein	150
REFERENCES	159
APPENDIX A	176
APPENDIX B	181
APPENDIX C	188
APPENDIX D.....	195
APPENDIX E	203
APPENDIX F	211
APPENDIX G.....	222

LIST OF TABLES

Table	Page
1.1 List of photoreceptor chromophores	3
1.2 List of amino acid and their sequential position in PYP	4
1.3 pKa value of pCA and Glu46 in solution and PYP	5
1.4 Crystallized proteins from the PAS domain superfamily	18
2.1 List of PYPs studied in this dissertation	26
2.2 peak position of Amide bands in mid-IR region	40
3.1 Co-ordination number of ions in first hydration shell	68
3.2 Number of water molecules at various NaCl salt concentration	68
3.3 Distances between charged residues in $\Delta 25$ pG abd pB solution NMR structures for 5 conformations out of 20	69
4.2.1 Effect of the N43S and N43A mutations and deletion of the N-terminal 23 residues on the properties of PYP	112
4.3.1 Experimentally observed shifts in absorbance maxima of Sr PYP and Hh PYP and their E46Q mutants caused by H/D exchange compared to tentative estimates for the strength of the hydrogen bond between the pCA and residue 46	142
5.1 Most conserved residues in PYP family.	155

LIST OF FIGURES

Figure	Page
1.1 The UV/Vis spectra of wtPYP at pH 7.50	5
1.2 Secondary structure of Hhal PYP	6
1.3 The three dimensional structure of PYP	6
1.4 The pCA Photoisomerization.....	9
1.5 Schematics of PYP photocycle	10
1.6 Schematics of molecular mechanism of PYP photoactivation	15
1.7 Crystal structures from PAS domain proteins.....	17
1.8 Sequence comparison of PAS domain proteins	23
2.1 Over-expression of Hhal PYP in E. Coli	27
2.2 The UV/Vis absorption of PYP during purification stages	28
2.3 Layout of experimental setup for time-resolved rapid scan and step-scan FTIR spectroscopy	36
2.4 The second derivative of absorbance of wt-PYP with and without three-sample exchanger	39
2.5 Infrared absorption of Myoglobin from Sperm Whale and wtPYP and Halorhodospira halophila.....	41
2.6 Schematics of quadruple-split rapid-scan time-resolved measurement	44
2.7 The data reproducibility of light induced FTIR difference absorption of PYP	45
2.8 The 3-D representation of an interferogram obtained in time-resolved step-scan FTIR spectroscopy	46
2.9 Infrared interferogram of PYP	47
2.10 The layout for extracting difference absorption from recorded data in step-scan time-resolved FTIR experimental setup	49
2.11 Schematics of flash photolysis system.....	51
3.1 Structural dynamics of PYP in (NH ₄) ₂ SO ₄	59
3.2 Structural dynamics of PYP in NaCl	61
3.3 Light induced pB-pG FTIR difference spectrum of PYP in alkali chloride salts	63
3.4 Protein quake vs electrostatic epicenter of PYP in salt.....	64
3.5 The light induced FTIR difference absorption spectrum of PYP film for hydrated and reduced hydration	64
4.1.1 Regulation of biofilm formation in <i>I. loihiensis</i> by light and <i>p</i> -coumaric acid analogs.....	84
4.1.2 Comparison of the spectroscopic properties of the pG dark state of the PYPs from <i>Idiomarina loihiensis</i> and <i>Halorhodospira halophila</i>	86
4.1.3 Low pH titration of the PYP from <i>I. loihiensis</i>	87
4.1.4 Comparison of the last photocycle step in the PYPs from <i>I. loihiensis</i> and <i>H. halophila</i> at pH 7.5.....	87

Figure	Page
4.1.5 Time-resolved FTIR difference spectroscopy of the PYP from <i>I. loihiensis</i>	90
4.1.6 Model for the regulation of biofilm formation in <i>I. loihiensis</i>	97
4.2.1 Sequence conservation and structural context of Asn43 in PYP.....	103
4.2.2 Side chain hydrogen bonding of Asn43 in PYP.....	107
4.2.3 Effect of the N43A and N43S mutations on the stability of PYP.....	121
4.2.4 Effect of the N43A and N43S mutations on the absorbance maximum and pK _a of the <i>pCA</i> in PYP.....	125
4.2.5 Probing structural deformations of the pG dark state of wtPYP (black) by the N43A (red) and N43S (green) mutations using second derivative FTIR spectroscopy.....	125
4.2.6 Substitutions at Asn43 slow down the kinetics of the last PYP photocycle step.....	127
4.2.7 Structural changes upon pB formation in wtPYP and its N43A and N43S mutants detected by FTIR difference spectroscopy.....	130
4.2.8 Comparison of functional properties of PYP mutants.....	133
4.2.9 Conservation of the side chain hydrogen bonding interactions of residue 43 in the PAS domain superfamily.....	137
4.3.1 Anionic hydrogen bonding of <i>pCA</i> at the active site of PYP.....	133
4.3.2 Spectral isotope effects in PYP.....	133
4.3.3 Effects of H/D exchange on active site hydrogen bonding strength and absorbance maximum in PYP.....	144
4.3.4 Distinction between three types of hydrogen bonds.....	154
5.1 Color coded conserved residues in PYP family.....	155
5.2 Sequence alignment of homologous PYP.....	156

CHAPTER I

INTRODUCTION

1.1 Photoactive Yellow Protein

Discovery of photoactive yellow protein

The first photoactive yellow protein (PYP) was discovered by Terry Meyer (Meyer 1985) while surveying all chromophoric proteins from *Ectothiorhodospira halophila* (*E. Halophila*, strain BN9626), which is renamed to *Halorhodospira halophila* (Hhal) (Imhoff et al. 1996, Meyer et al. 2003). *Halorhodospira halophila* is a purple phototrophic bacterium which lives in extremely halophilic, anoxygenic environment. Meyer found a total of eight chromophoric proteins. One of them is yellow with a peak absorption in the blue at 446 nm (see Fig 1.1) (Meyer 1985). This yellow protein was found to be different from all known chromophoric proteins. The chromophore of this yellow protein was thought to be flavin-like (Meyer 1985) and later as retinal-like (McRee et al. 1986). We will show later in this chapter that this yellow protein contains a new chromophore and form a new family of chromophoric proteins.

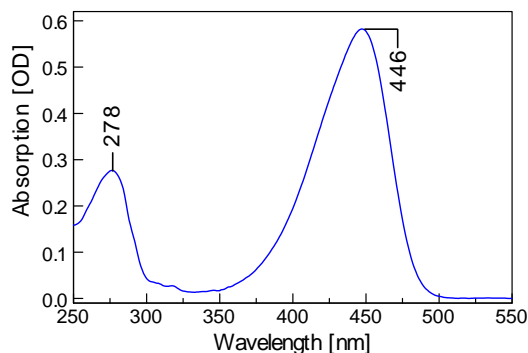


Figure 1.1: The UV/Vis spectra of wt PYP at pH 7.50 and in 50mM phosphate buffer showing a maximum peak at 446 nm from the *pCA* chromophore and another peak at 278 nm from the tyrosine and tryptophan. The purity index (PI) of PYP is defined as the absorption ratio between 278 and 446 nm. The best PI obtained for Hhal PYP is 0.42.

Photo-excitation of this yellow protein at 445 nm leads to cyclic process, with at two intermediate states (Meyer et al. 1987). An early red-shifted intermediate state (λ_{max} : ~460 nm) with a lifetime of approximately 270 microseconds, a blue-shifted intermediate (λ_{max} : ~ 340 nm) with a longer 303 milliseconds before returning to the initial state (Meyer et al. 1987). The light-activated nature of this yellow protein led to a new name, photoactive yellow protein (PYP) (Meyer et al. 1987), which has been used to date.

Hhal PYP is a small water soluble protein with a molecular weight of 14 kilo-daltons (Meyer 1985). The phenylthiohydantoin (PTH) amino acid analysis (Van Beeumen et al. 1993) revealed that Hhal PYP consists of 125 amino acids with the sequence and a chromophore with molecular weight of 147.6 daltons, covalently attached to Cys69. This excludes the possibility of PYP having retinal or flavin as its chromophore. Further structural analysis conclusively determined that the chromophore of PYP is a *p*-coumaric acid (*p*CA) (Fig. 1.2) and is covalently linked to Cys69 via a thioester bond by two research groups in 1994 (Baca et al. 1994, Hoff et al. 1994). Only few chromophores have been reported so far, including retinal, flavin, phytochrome, and tryptophan residues as shown in Table 1.1. This is the first time to find *p*CA as a chromophore in proteins. The *p*CA chromophore represents the latest addition to the small, elite family of biological chromophores. The chromophore family is listed in Table 1.1.

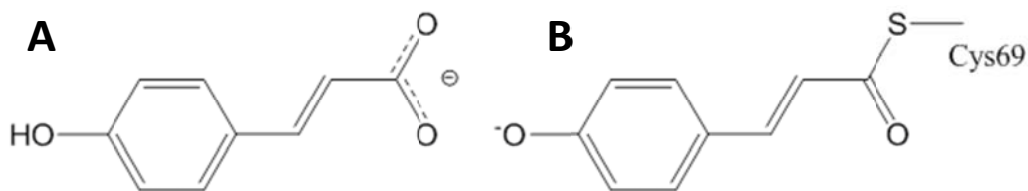
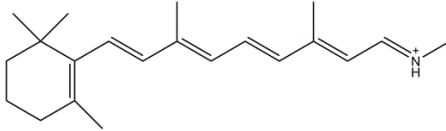
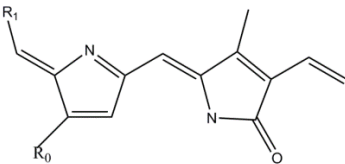
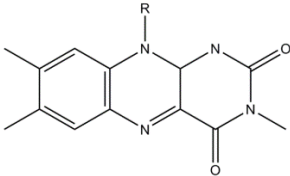
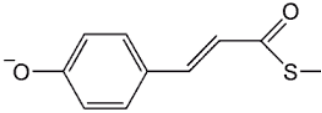
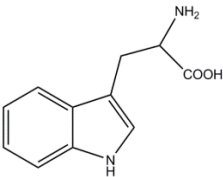


Figure 1.2: Structure of the chromophore (A) the structure of the free *p*CA in solution at neutral pH (B) The *p*CA is attached to PYP through thioester linkage at cys69 residue in PYP. The phenolic group of *p*CA is deprotonated in PYP's dark state.

With *pCA* as its light absorbing chromophore, Hhal is the first member of a new family of colored proteins. The chromophore is the molecule which absorbs the visible light. The chromophore families are listed in Table 1.1. The retinal chromophore is found in rhodopsin family of proteins. The rhodopsin are responsible for black/white vision in animals and color vision in humans (Stryer 1995). After absorbing light, retinal isomerizes to perform the function. The phytochrome chromophore is found in phytochrome receptor family in plants (van der Horst et al. 2004). The proteins from phytochrome family perform various functions as gene-expression governed by light, controlling circadian clock (van der Horst et al. 2004). The flavin derivatives chromophore is observed in light-oxygen-voltage (LOV) and blue light using FAD (BLUF) domains of proteins. In LOV proteins upon absorption of light flavin derivative FMN forms cysteinyl adduct which leads to the signaling state (Kennis et al. 2003). While in BLUF domain protein flavin derivative FAD binds to protein noncovalently (Gomelsky et al. 2002). The BLUF domain protein absorbs the light and initiates photocycle by electron transfer (Masuda et al. 2004, Fukushima et al. 2005). In the recent years tryptophan residues is also categorized as chromophore (Hospes 2012). Upon absorption of light tryptophan residue is activated by disruption of π bond over indole ring (Hospes 2012). The numbers of chromophores in nature are very limited. The *pCA* chromophore was the latest addition to small chromophore family. The *pCA* as a chromophore found from PYP family was the latest addition to the elite family of natural biological chromophores.

Table 1.1 List of chromophores adapted from (van der Horst et al. 2004, van der Horst et al. 2007, Hospes 2012)

Photoreceptor	Structural element of chromophore	Photochemistry
Retinal		Photoisomerization
Phytochrome		Photoisomerization
Flavin		Electron transfer FMN-cysteiny adduct formation
<i>p</i> -Coumaric Acid		Photoisomerization
Tryptophan residues		Disruption of π bond

The Structure of Photoactive Yellow Protein

The PYP from Hhal has 125 amino acids. The composition of amino acids is as following. The PYP has 9 Ala, 9 Val, 7 Leu, 5 Ile, 5 Met, 9 phe, 1 Cys, 1 Trp, 1Arg, 4 Pro, 13 Gly, 5 Ser, 7 Thr, 5 Tyr, 6 Asn, 5 Gln, 12 Asp, 7 Glu, 2 Arg, 2 His, 11 Lys. The PYP has 6 β -strands, 5 α -helices, one 3_{10} helix, and one π -helix which was revealed by x-ray crystallography (Borgstahl et al. 1995). The PYP's amino acid sequence and its secondary structure depicted in Figure 1.3.

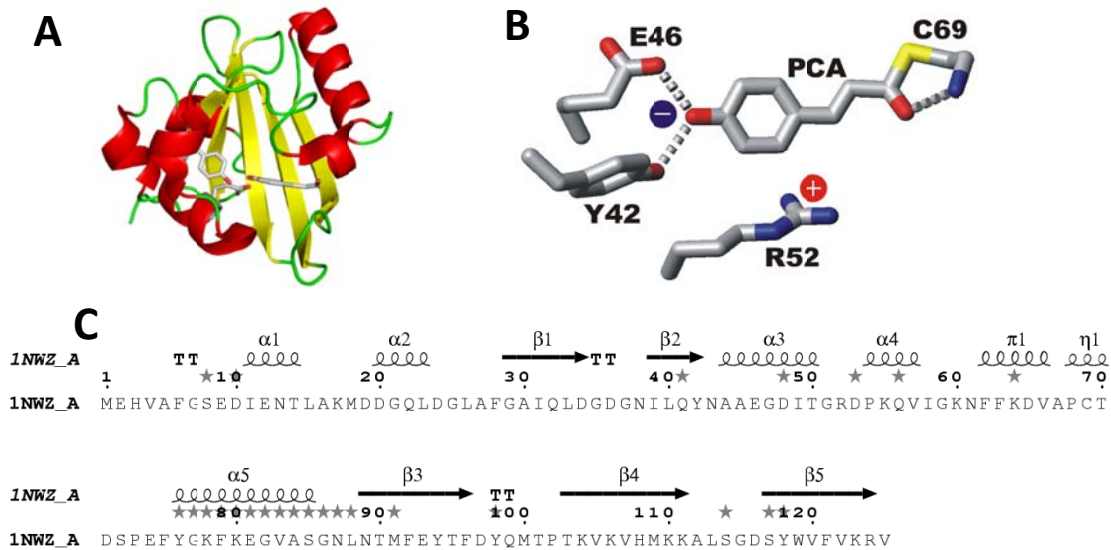


Figure 1.3: Structure of the PYP. (A) The tertiary structure of the PYP PDB ID: 1NWZ) The structures in yellow color represents the β -strands, red color represents α -helix (B) Active site of PYP. At the active site of PYP Glu46 is protonated, *pCA* is negatively charged in pG state, *pCA* makes 2 hydrogen bonds one with Glu46 and other with Tyr42. (C) The secondary structure of Hhal PYP. The coil like structure represents α -helix and arrows represents β -strands.

The active site structure of Photoactive Yellow Protein

The active site structure of PYP consists of negatively charged *pCA* hydrogen bonded with Glu46 and Tyr42 (Hoff et al. 1994, Borgstahl et al. 1995) as shown in Figure 1.2 B. The negative charge on phenolate of *pCA* is delocalized over the ring (Kim et al. 1995). The *pCA* is covalently attached to Cys69 through thioester bond (Hoff et al. 1994, Borgstahl et al. 1995). The *pCA* binding pocket of PYP is highly hydrophobic (Borgstahl et al. 1995, Xie et al. 2001). The binding pocket of *pCA* is consisted of Ile31, Tyr42, Glu46, Thr50, Arg52, Phe62, Val66, Als67, Cys69, Thr70, Phe96, Phe97, Asp97, Tyr98, Met100, V120, and V122 residues.

Table 1.2. List of amino acids and their sequential position in PYP.

Amino Acids	Number of AA	Amino Acid position
Ala (A)	9	A5, A16, A27, A30, A44, A45, A67, A84, A112
Val (V)	9	V4, V57, V66, V83, V105, V107, V120, V122, V125
Leu (L)	7	L15, L23, L26, L33, L40, L88, L113
Ile (I)	5	I11, I31, I39, I49, I58
Met (M)	5	M1, M18, M100, M109
Phe (F)	9	F6, F28, F62, F63, F75, F79, F92, F96, F121
Trp (W)	1	W119
Pro (P)	4	P54, P68, P73, P102
Gly (G)	13	G7, G21, G25, G29, G35, G 37, G47, G51, G59, G77, G82, G86, G115
Ser (S)	5	S8, S72, S85, S114, S117
Thr (T)	7	T14, T50, T70, T90, T95, T101, T103
Cys (C)	1	C69
Tyr (Y)	5	Y42, Y76, Y94, Y98, Y118
Asn (N)	6	N13, N38, N43, N61, N87, N89
Gln (Q)	5	Q22, Q32, Q41, Q56, Q99
Asp (D)	12	D10, D19, D20, D24, D34, D36, D48, D53, D65, D71, D97, D116
Glu (E)	7	E2, E9, E12, E46, E74, E81, E93
Arg (R)	2	R52, R124
His (H)	2	H3, H108
Lys (K)	11	K17, K55, K64, K75, K80, K106, K110, K111, K123

Interestingly the pK_a values of *pCA* and Glu46 are shifted in opposite directions by more than 7 pH units in PYP as compared to solution (Hoff 1995), as shown in Table 1.3. In aqueous solution the phenolic ring of *pCA* is neutral with pK_a of 9.5. The pK_a value of phenolic oxygen of *pCA* is downshifted in PYP to 2 (Hoff 1995). In case of Glu residue the pK_a value in aqueous solution is 4.1. The pK_a of Glu46 residue from solution to the protein is upshifted to 11.7 (Hoff 1995). This unusual shift in pK_a of the *pCA* and Glu46 in PYP aids to photoreception and proton transfer from Glu46 to *pCA* which in turn leads to receptor activation of PYP.

Table 1.3: The pK_a value of *p*CA and Glu46 in solution and PYP

	pK_a in solution	pK_a in PYP pG
<i>p</i> CA	9.5	2.7
Glu46	4.1	11.7

1.2) Photocycle of PYP

The PYP exhibits a photocycle upon absorption of a blue photon by negatively charged *p*CA chromophore (Meyer et al. 1987). The basic photocycle of PYP is consisted of majorly three intermediates states pG, pR, pB' and pB (Xie et al. 1996, Xie et al. 2001, Hellingwerf et al. 2003). The pG state is considered as a ground or dark state, pR state is red shifted intermediate while pB state is blue shifted intermediate from the ground state of PYP (Xie et al. 1996, Xie et al. 2001). The major structural change from pG to pR is photoisomerization, followed by signaling state formation in pB and finally recovery to pG state.

In the literature the nomenclature of PYP photointermediates is different by various research groups. The pR intermediate state of PYP is referred as I_1 or PYP_L, pB state is referred as I_2 or PYP_M. In this dissertation the PYP photointermediates are describes with pG, pR pB' and pB nomenclature and is shown in Figure 1.5.

Upon photoexcitation PYP molecule is excited to pG* intermediate and PYP either enters into the photocycle or returns to its ground state. The pG* is then followed by early short-lived photointermediate I_{510} . The fast intermediate of PYP photocycle during initial stage has been revealed by ultra-fast absorption spectroscopy (Baltuska et al. 1997, Ujj et al. 1998). In those studies red shifted intermediates I_{510} was detected. The I_{510} intermediate is formed ≤ 3 ps, while it decays in ~ 220 ps to form next intermediate I_{510}^\ddagger . The intermediate I_{510}^\ddagger decays into pR₄₆₅ intermediate with time constant of ~ 3 ns. Further pR intermediate leads to pB' followed by pB (Xie et al. 1996, Xie et al.

2001, Hellingwerf et al. 2003). The absorption maximum of pB' and pB intermediate is at 355 nm (Xie et al. 2001). The putative pB intermediate is long lived and believed to be a signaling state of the PYP (Xie et al. 1996, Xie et al. 2001). The long lived pB intermediate recovers to pG state, completing the PYP photocycle.

Photoisomerization of *pCA*

The primary event of the PYP photocycle is photoisomerization of *pCA* involving trans-to cis isomerization (Hoff et al. 1994). The pG structure of the PYP is 7-trans 9-s cis (Baca et al. 1994, Hoff et al. 1994), and after absorption of blue photon the *pCA* changes to its cis configuration (Kort et al. 1996). There are two possibilities how *pCA* can get photoisomerizes. The first possibility is 7-cis 9-s-cis which involves flipping of the *pCA* ring and breaking the Glu46 and *pCA* hydrogen bond while the second possibility is 7-cis 9-s trans isomerization as depicted in Figure 1.4.

The pR-pG FTIR absorbance difference spectroscopy of PYP, reveals that the bond between *pCA* and Glu46 remains intact (Xie et al. 1996) in pR state, thus providing a correct hydrogen bonding structure and orientation of *pCA* in pR intermediate structure of PYP. The experimental evidence obtained in study performed by Xie and coworkers shows that *pCA* isomerizes along C7=C8 and C9-C10 bonds which breaks the hydrogen bond between the *pCA* and Cys69 backbone as shown in Figure 1.4 C.

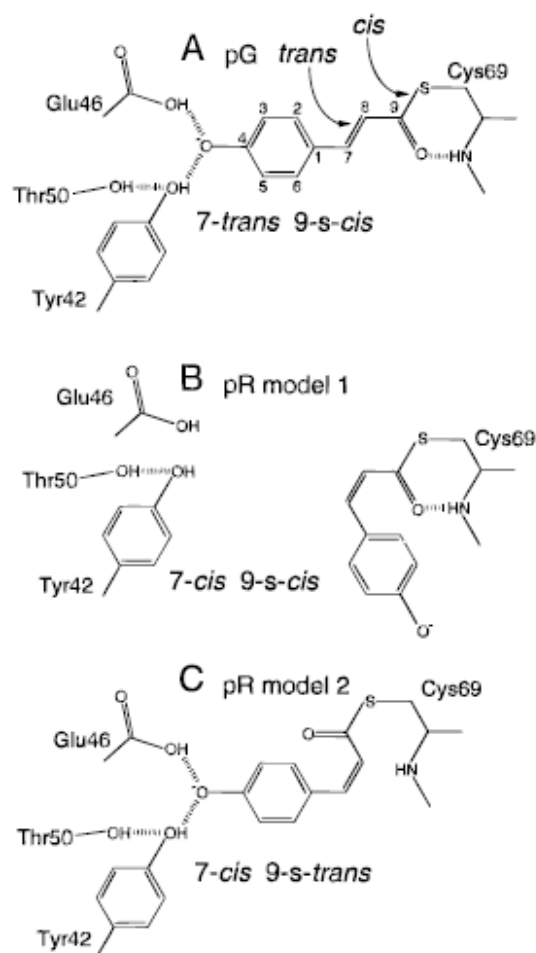


Figure 1.4 The *pCA* photoisomerization. (A) The ground state structure of *pCA* interacting with Glu46 and Tyr42 with 7-*trans* 9-*s-cis* isomer. The two possible *cis* isomers of *pCA* after *trans* to *cis* photoisomerization. (B) 7-*cis* 9-*s-cis* and (C) 7-*cis* 9-*s-trans* isomers of *pCA*. This figure is adapted from (Xie et al. 1996).

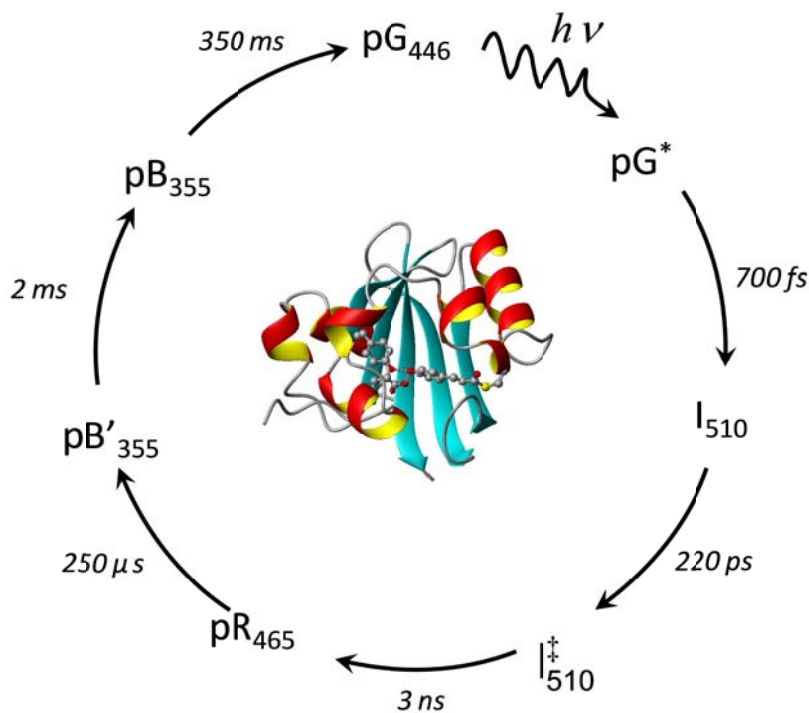


Figure 1.5: Schematics of PYP photocycle. The PYP absorbs a blue photon and the native state (pG) is excited to pG*. This initiates the photocycle of PYP leading to several intermediate states as depicted in the figure.

Structural interpretation of the Photoactive Yellow Protein photocycle

In the pG state, the OH from carboxylic group of Glu46 is hydrogen bonded to the negatively charged phenolic oxygen of pCA (Xie et al. 1996), which is consistent with the X-ray structure of PYP [Figure 1.3A] (Borgstahl et al. 1995). In pG, the pCA is deprotonated and in the 7-trans 9-s-cis conformation [Figure 1.3 B] (Hoff et al. 1994). This buried negative charge on pCA is delocalized over the phenolic oxygen and ring, and is stabilized by specific electrostatic interaction with the positively charged Arg52, as well as by hydrogen bonding interactions with the OH groups of Glu46 and Tyr42 in the pCA binding pocket. Upon absorption of a blue photon, the pCA chromophore is photoisomerized into 7-cis 9-s-trans configuration, leading to the formation of pR (Xie et al. 1996). Glu46 donates a proton to the phenolic oxygen of pCA, forming a putative unstable pB' state (Xie et al. 2001), however the hydrogen bond between pCA and Glu46 is intact in pB'.

This local proton transfer event neutralizes the *pCA*, generates a new buried unstable negative charge of COO⁻ of Glu46, and terminates the *pCA*-/Arg52+ interaction (Xie et al. 2001). This unstable negative charge triggers a large conformational change leading to the formation of a long lived signaling state and hence receptor activation which is repressed by the absence of COO-formation in the E46Q mutant (Xie et al. 2001). The initial dark state of pG is recovered from pB at a longer time scale (250 ms) through a series of steps involving the reisosomerization of *pCA* to 7-trans 9-s-cis conformer, deprotonation of *pCA* and reprotonation of Glu46 (Xie et al. 1996).

1.3) Molecular mechanism of the PYP photoactivation

There have been several models proposed to explain the molecular mechanism behind the photoactivation. The *pCA* of PYP absorbs the blue light and changes the configuration and isomerization which leads to proton transfer from Glu46 to *pCA* and breaking of HB between them. The absorption of blue light by PYP is signal induction process. The proton transfer from Glu46 to *pCA* and breaking of hydrogen bond between *pCA* and Glu46 after blue light absorption of PYP is signal induction process. This signal induction process is followed by intramolecular signal transduction in PYP which leads to signaling state of PYP. The signaling state conformation further transduces signal to other molecules in signal pathways. The process and molecular mechanism of signal induction in PYP is well understood. However the molecular mechanism behind the intramolecular signal transduction in PYP is now well understood.

Hydrophobic collapse Model

The hydrophobic collapse model was proposed by Cusanovich et al. 2003 to explain the signaling mechanism during PYP photoactivation (Cusanovich et al. 2003). According to this hypothesis, the *pCA* exposes to solvent after photoisomerization developing a hydrophobic cavity with F62, F75 and F96. The developed cavity collapses and results in breaking the interaction between N-terminus and central β -sheet as distortion of residuals on *pCA* side I31, V105, V107,

V120, V122. However this hypothesis was developed on the basis of the studies performed by Craven and coworkers (Craven et al. 2000). This hypothesis is put forward on the basis of hydrophobic environment of the pCA chromophore. However this hypothesis lacks the energetic evidence to support the hydrophobic cavity model and thus does not yield a clear molecular mechanism of PYP photoactivation.

Structural change via hydrogen bonding of Asn43 and Glu46

In an another model, proposed by Ihee et al is based on helical capping of N43 (Ihee et al. 2005) in PAS domain (Pellequer et al. 1998). N43 is one of the conserved residues in the PAS domain. This model proposes the interaction hydrogen bond between N43 and backbone of E46 breaks after photoexcitation of the PYP, which leads to the breaking of N-terminus from the central β -sheet. However the study performed by the Masato et al. 2010, clearly shows that N43 plays a crucial role in kinetics of the PYP (Kumauchi et al. 2010). The pB-pG FTIR difference absorption spectrum of N43A PYP presented here (Kumauchi et al. 2010) shows that the PYP photocycle is slower ~ 1000 time after the HB interaction between N43 and E46 is broken, however it retains the larger conformational changes. Thus this model fails to explain the molecular mechanism behind the photoactivation of PYP.

CH/ π Interaction between Phe6 and Lys123

The CH/ π hydrogen bond interaction energy is weak (2-8 kJ/mol) (Nishio 2011). In PYP aromatic ring of Phe6 and side chain of Lys123 forms a weak CH/ π hydrogen bond (Harigai et al. 2006). The pB-pG FTIR difference absorption spectrum of site directed mutants of Phe6 and Lys123 shows that the loss CH/ π interaction reduces the conformational changes in PYP. The energy of the CH/ π hydrogen bond (~ 2 -8 kJ/mol) is much less than typical protein folding energy ~ 40 kJ/mol. The smaller conformational changes in site directed mutants of Phe6 and Lys123 partially supports the

intramolecular signal transduction as PYP is partially unfolded in signaling state which would require energy of $\sim 20\text{-}30$ kJ/mol.

Protein quake due to buried negative charge

The model presented by Xie and coworkers in 2001 proposes that, the Glu46 donates proton to pCA and develops a negative charge inside the protein (Xie et al. 2001). This negative charge inside the protein is energetically unfavorable and the electrostatic energy of this charge is $\sim 28\text{-}30$ kJ/mol. This energy is of the order of the protein folding ~ 40 kJ/mol, which explains partial unfolding of PYP upon photoexcitation. The negative charge developed on Glu46 in pB intermediate state of PYP drives the conformational changes which leads to protein quake (Xie et al. 2001). This protein quake changes the protein conformations leading to signaling state. This model is well supported by structural, kinetic and energetic evidences (Xie et al. 2001).

Still it is elusive that which molecular interaction leads to intramolecular the signal transduction? How the PYP molecule does regain the similar structure of ground state from the signaling state?

The complete photocycle of PYP is accompanied by four major interactions between the anionic chromophore and Glu46 as depicted in Figure 1.3 B. First step is isomerization of the pCA from 7-trans 9-s-cis conformer to 7-cis 9-s-trans conformer (pR state) which takes place on a time scale of ps-ns. At second step intramolecular proton transfers from Glu46 to the anionic pCA chromophore (pB' state) which takes place on a time scale of 250 μs leading to the deprotonation of Glu46. At the next step the negative charge on Glu46 (pB state) triggering a large conformational change resulting in the formation of the long lived signaling state (2 ms). Last step is reisomerization of pCA from 7-cis 9-s-trans to 7-trans 9-s-cis and reprotonation of Glu46 (pG state) on time scale of 350 ms (Xie et al. 2001).

X-ray crystallography has allowed us to determine 3-dimensional structure of proteins in atomic details. Crystalline protein structure helps to understand molecular mechanism of how protein

functions. In 1960's many scientist attempted know how proteins behave in solutions and crystals (Timasheff et al. 1969). It was discovered that enzymatic activity of ribonuclease S (Doscher et al. 1963), carboxypeptidase A(Quiocho et al. 1966) and chymotrypsin (Sigler et al. 1963) was different in solution than crystal. Protein has to change its conformation while activation.

In case of PYP pB intermediate state was determined using P6₃ crystal lattice employing millisecond time resolved X-ray crystallography (Genick et al. 1997). It was claimed that pB state is similar to pG state of PYP. However other observations (Dux et al. 1998, Rubinstenn et al. 1998, Hoff et al. 1999) suggested that pB and pG structure are different from each other. To resolve the dispute Xie and coworkers performed time resolved FTIR spectroscopy on PYP in P6₃ crystals and PYP in solution (Xie et al. 2001).

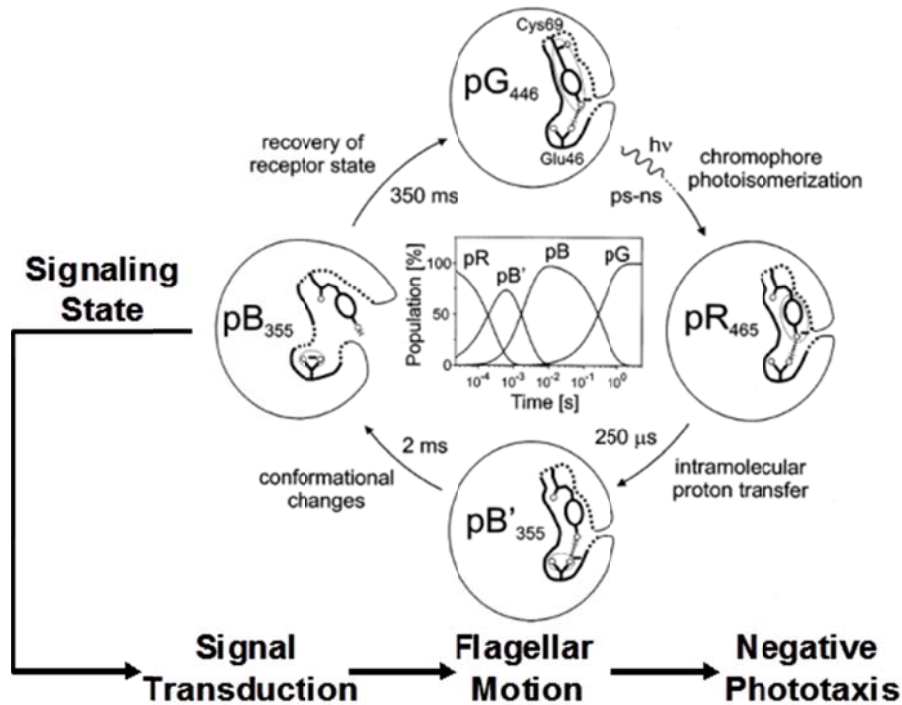


Figure 1.5: Schematics of molecular mechanism of PYP photoactivation. After blue light excitation PYP undergoes into photocycle, the native state (pG) is followed by pR intermediate where chromophore goes under photoisomerization. In next intermediate (pB') intramolecular proton transfer is followed. In succeeding intermediate (pB) PYP undergoes into large conformational changes which is followed by recovery where PYP achieves its native state (pG). The figure is adapted from the ref (Xie et al. 2001)

In this experiment it was clearly observed that pB state did not developed. Further the pB like state in PYP's P6₃ crystal was completely different from that of PYP in solution. Further in order to understand whether this effect is due to lattice or crystallization, time resolved FTIR measurement done on PYP in (NH₄)₂SO₄ concentrations of 0.5 M, 1.0 M, 2.0 M, 2.5 M. Surprisingly it was noted as high salt concentrations increases the putative pB like state is not developed and at 2.5 M (NH₄)₂SO₄ concentration, PYP's pB-pG spectra was similar as pB-pG in P6₃ crystal. The data indicated that Glu46 remains protonated in putative pB state and has smaller conformational changes compared to PYP in solution.

Crystallization suppresses PYP structural dynamics. It was clear that 2.5 M (NH₄)₂SO₄ affected PYP structural dynamics. Next question arises whether salt does changes structural dynamics? Is there different effect due to different salts? This is how we started with exploring protein structural dynamics in high salt concentration solution.

PYP was used as a model system to study the effects on Hofmeister salt on protein as PYP undergoes large structural changes in pB intermediate. We have used time resolved infrared spectroscopy to gain insights of protein's structural dynamics. Infrared spectroscopy is a rich in information and gives information on vibrational modes of molecule. Also, IR spectroscopy can give information about hydrogen bonding.

1.4) PAS domain protein

Lagarias et. al. recognized that PYP is from Pert-Arnt-Sim (PAS) domain superfamily of proteins (Lagarias et al. 1995). PAS domains are involved in signaling proteins and appear in archaea, bacteria and eukaryotes. The structure of the PAS domain is defined by central antiparallel β -sheets flanked by 3 or 4 α -helices (Hefti et al. 2004). PAS domain proteins are mainly signaling and regulating proteins. The PYP was the first crystal structure obtained from the PAS domain and a structural prototype of PAS domain.

The Pfam database version 27.0 has 14831 protein families, and for the PAS fold family has identified 88,093 sequences as PAS domain from 5998 species (Finn et al. 2010). Out of these sequences from PAS domains, only 62 proteins have been crystallized successfully till this date. The list of crystallized protein from the PAS domain is provided in Table 1.4. Other examples of protein from PAS domain are human ERG (HERG) and Light Oxygen Voltage 2 (LOV2) (Byrne et al. 1995, Bernard et al. 2005). The crystal structures of PAS domain proteins are shown in Figure 1.6.

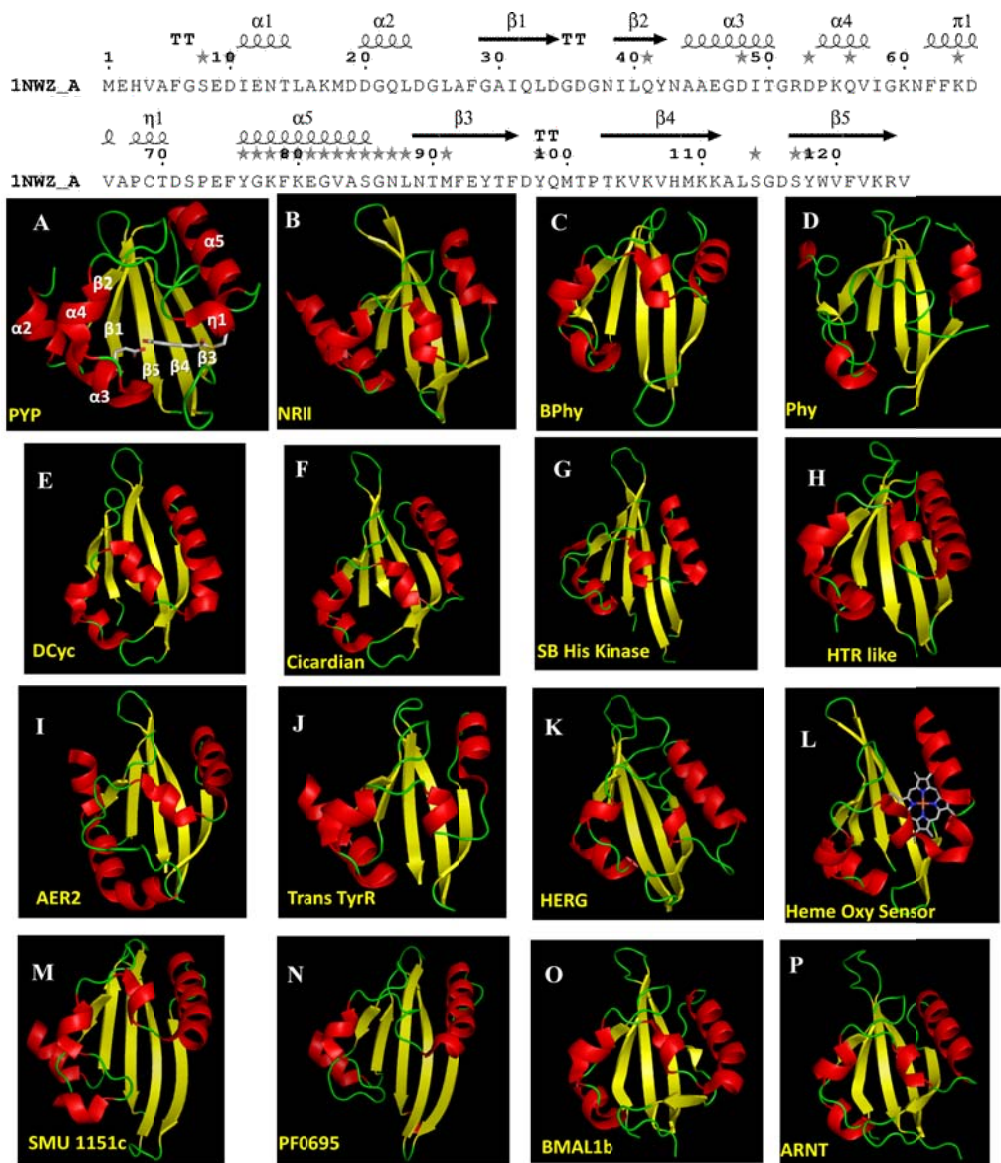


Figure 1.6 Crystal Structures from PAS domain proteins. (A) PYP: photoactive yellow protein, PDB ID: 1NWZ, (B) NRII: nitrogen regulation protein, PDB ID : 3B33, (C) BPhy: Bacterophytochrome PDB ID: 3S7O, (D) Phy: phytochrome CPH1, PDB ID: 2VEA, (E)DCyc: Digunylate Cyclase, PDB ID: 3H9W, (F) Cicardian protein, PDB ID: 3GDI, (G) SB His Kinase: Sensory Box Histidine Kinase, PDB ID: 3LUQ, (H) HTR like protein, PDB ID: 3FC7, (I)AER2: Aerotaxis transducer, PDB ID:3VOL, (J) Trans TyrR: Transcriptional tyrR PDB ID: 2JHE, (K) HERG: Human erg potassium channel PDB ID: 1BYW, (L) Heme oxy sensor DosP PDB ID :1V9Y, (M) Putative uncharacterized protein SMU 1151c, PDB ID:2QKP, (N) uncharacterized protein PF0695, PDB ID: 3CAX. (O) BMAL1b PDB ID: 4F3L, (P) ARNT: Aryl hydrocarbon Receptor Nuclear Translocator PDB ID: 3F1P.

Table 1.4 : Crystallized proteins from the PAS domain superfamily

PAS fold	PAS Domain Protein	Organism	PDB	residues
PAS	Photoactive yellow protein*	<i>Halorhodospira halophila</i>	1NWZ	17-125
PAS	Photoactive yellow protein*	<i>Rhodospirillum centenum</i>	1MZU	16-124
PAS	Circadian locomotor output cycles protein kaput	<i>Mus musculus</i>	4F3L	109 - 188
PAS	Sensor histidine kinase DcuS	<i>Escherichia coli</i>	2W0N	15 - 117
PAS	Sensor protein fixL*	<i>Bradyrhizobium japonicum</i>	2VV6	154 - 256
PAS	Sensor protein fixL*	<i>Sinorhizobium meliloti</i>	1D06	137 - 250
PAS	Nitrogen fixation regulatory protein	<i>Azotobacter vinelandii</i>	2GJ3	25 - 136
PAS	Period circadian protein	<i>Drosophila melanogaster</i>	3RTY	236 - 333
PAS	BMAL1b	<i>Mus musculus</i>	4F3L	146 - 253
PAS	Nitrogen regulation protein	<i>Vibrio parahaemolyticus</i>	3B33	4 - 111
PAS	Sensor histidine kinase	<i>Thermotoga maritima</i>	3A0S	424 - 518
PAS 2	Bacteriophytochrome*	<i>Deinococcus radiodurans</i>	3S7O	24 - 129
PAS 2	Bacteriophytochrome*	<i>Pseudomonas aeruginosa</i>	3NHQ	12 - 113
PAS 2	Phytochrome-like protein cph1*	<i>Synechocystis sp.</i>	2VEA	15 - 125
PAS 2	Bacteriophytochrome (Light-regulated signal transduction histidine kinase) *	<i>Rhodopseudomonas palustris</i>	2OOL	28 - 136
PAS 3	Diguanylate cyclase with PAS/PAC sensor	<i>Marinobacter aquaeolei</i>	3H9W	36 - 123
PAS 3	Period circadian protein homolog 2	<i>Mus musculus</i>	3GDI	342-430
PAS 3	Sensory box histidine kinase/response regulator	<i>Burkholderia thailandensis</i>	3MR0	28-116
PAS 3	Putative light and redox sensing histidine kinase	<i>Haloarcula marismortui</i>	3EEH	34-121
PAS 3	Probable GGDEF family protein	<i>Chromobacterium violaceum</i>	3NJA	26-114
PAS 3	Sensory box histidine kinase/response regulator	<i>Chlorobium tepidum</i>	3ICY	38-111
PAS 4	Putative uncharacterized protein RHA05790	<i>Rhodococcus sp.</i>	3FG8	128-224
PAS 4	HTR-like protein	<i>Haloarcula marismortui</i>	3FC7	144-241
PAS 4	HTR-like protein	<i>Haloarcula marismortui</i>	3BWL	406-508
PAS 4	Sensory box histidine kinase/response regulator	<i>Geobacter sulfurreducens</i>	3LUQ	95-200
PAS 4	Sensory box sensor histidine kinase	<i>Vibrio cholerae serotype O1</i>	3MXQ	12-130
PAS 4	Uncharacterized protein Rv1364c/MT1410	<i>Mycobacterium tuberculosis</i>	3K3C	21-135
PAS 8	Aerotaxis transducer Aer2	<i>Pseudomonas aeruginosa</i>	3VOL	173 - 248
PAS 8	Transcriptional regulatory protein tyrR	<i>Escherichia coli</i>	2JHE	81-148
PAS 9	Aureochrome1	<i>Vaucheria frigida</i>	3UE6	217-322
PAS 9	Oxygen sensor protein DosP	<i>Escherichia coli</i>	1V9Y	30 - 132
PAS 9	Potassium voltage-gated channel subfamily H member 2	<i>Homo sapiens</i>	1BYW	28-134
PAS 9	Blue-light-activated histidine kinase	<i>Brucella melitensis biotype 1</i>	3T50	31 - 137
PAS 9	NPH1-1	<i>Avena sativa</i>	2V0U	413 - 518
PAS 9	PAS domain-containing serine/threonine-protein kinase	<i>Homo sapiens</i>	1LL8	8 - 112
PAS 9	Phototropin-1	<i>Arabidopsis thaliana</i>	2Z6C	199 - 302
PAS 9	Phototropin-2	<i>Arabidopsis thaliana</i>	4EEP	390 - 494
PAS 9	Blue-light photoreceptor	<i>Bacillus subtilis</i>	2PR5	24-128
PAS 9	fungal photoreceptor VVD	<i>Neurospora crassa</i>	3D72	70 - 182
PAS 9	Putative uncharacterized protein	<i>Desulfitobacterium hafniense</i>	3MJQ	9-108
PAS 9	Sensor histidine kinase	<i>Erythrobacter litoralis</i>	3P7N	37-141
PAS 9	Transcriptional regulator, LuxR family	<i>Burkholderia thailandensis</i>	3MQQ	15-116
PAS 9	Sensory box/GGDEF domain protein	<i>Cowellia psychrerythraea</i>	3LYX	17-120
PAS 9	HTR-like protein	<i>Haloarcula marismortui</i>	3BWL	387-490
PAS 9	Sensory box histidine kinase/response	<i>Methylococcus capsulatus</i>	3EWK	219 - 325

	regulator			
PAS 9	Sensory box sensor histidine kinase/response regulator	<i>Geobacter sulfurreducens</i>	2R78	24 - 119
PAS 9	Sensory box protein	<i>Pseudomonas putida</i>	3SW1	15-121
PAS 9	Putative blue light receptor*	<i>Chlamydomonas reinhardtii</i>	1N9N	20-125
PAS 9	Two-component sensor histidine kinase	<i>Nostoc sp.</i>	3OLO	20-113
PAS 9	Vivid PAS protein VVD	<i>Neurospora crassa</i>	2PDT	70-182
PAS 9	PHY3 LOV2*	<i>Adiantum capillus-veneris</i>	1JNU	929-1032
PAS 10	Putative uncharacterized protein SMU_1151c	<i>Streptococcus mutans</i>	2QKP	332 - 442
PAS 10	Putative uncharacterized protein PF0695	<i>Pyrococcus furiosus</i>	3CAX	355 - 459
PAS 11	Aryl hydrocarbon receptor nuclear translocator	<i>Homo sapiens</i>	3F1P	360 - 467
PAS 11	Aryl hydrocarbon receptor nuclear translocator-like protein 2	<i>Homo sapiens</i>	2KDK	317 - 426
PAS 11	Circadian locomotor output cycles protein kaput	<i>Mus musculus</i>	4F3L	273 - 381
PAS 11	Endothelial PAS domain-containing protein 1	<i>Homo sapiens</i>	3F1P	241 - 349
PAS 11	Nuclear receptor coactivator 1	<i>Mus musculus</i>	1OJ5	259 - 367
PAS 11	Period circadian protein homolog 1	<i>Mus musculus</i>	4DJ2	357 - 464
PAS 11	Period circadian protein homolog 3	<i>Mus musculus</i>	4DJ3	267 - 376
PAS 11	Period circadian protein	<i>Drosophila melanogaster</i>	3RTY	388 - 499
PAS 11	BMAL1b	<i>Mus musculus</i>	4F3L	337 - 442

The proteins from PAS 5, PAS 6, and PAS 7 has not been crystallized, hence not listed in this table. The data was obtained from Pfam 27.0 (<http://pfam.sanger.ac.uk/>) and PDB (<http://www.rcsb.org/>) databanks.

* proteins with chromophore

Structure of the PAS Fold

The proteins from PAS domain have unique secondary and tertiary structure as shown in Figure 1.4. The protein folding pattern of PAS domain, known as PAS fold is divided majorly into 3 segments: (i) PAS core consisting 2 β strands with 2-3 α -helices (ii) helical connector which connects two β -strands and (iii) β -scaffold composed of 3 β -strands (Taylor et al. 1999).

The Protein family (Pfam) version 27.0 has divided PAS fold in to 11 sub folds which is listed in Table 1.2. The proteins from PAS 5, PAS 6 and PAS 7 are not been identified but not crystallized yet.

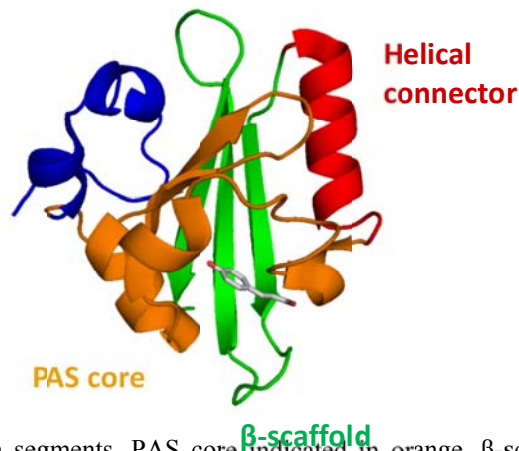


Figure 1.7 The PAS domain segments. PAS core indicated in orange, β -scaffold indicated in green, while helical connector is indicated in red

PAS domain segments

PAS core: The position of the PAS core is towards N-terminus of protein and is 2nd segment of PYP protein fold. PAS sequence is consisted of ~ 50 amino acids (Nambu et al. 1991, Kumauchi et al. 2002, Kurokawa et al. 2004). The PAS core fold is consisted of two antiparallel β strands with 2-3 α -helical structures. The one of the most conserved residues of PAS domain is from PAS core is Asn43 according to PYP sequence from *Hhal* as shown in Figure 1.5 and also discussed in literature (Taylor et al. 1999, Kumauchi et al. 2010). PAS core usually is attached to cofactor of the protein.

Helical Connector: The helical connector connects the central PAS core to the β scaffold region. The length of the helical connector region varies from protein to protein as shown in the Figure 1.4. The length of the helical connector is long in case of Digunylate Cylase, HTR like protein, Heme Oxy Sensor, SMU 1151c and PF0695 proteins as compared to PYP. While the length of helical connector is shorter in case of Nitrogen regulation protein, bacteriophytochrome and Transcriptional TyrR protein compared to PYP.

β -scaffold: The β -scaffold is the last segment in PAS domain protein consisted of three antiparallel β -strand running towards C-terminus. The most conserved residues from β -scaffold region are Asp97,

Val120 and Val125 (See figure 1.7). In PYP it has been proposed that the N-terminus and β -scaffold region interacts with CH/pi hydrogen bond interaction between Phe6 in N-terminus region and Lys123 in β -scaffold region (Harigai et al. 2008). The β -scaffold region dimerizes in Light-oxygen-voltage Histidine –kinase (LOV-HK) (Rinaldi et al. 2012). The dimerization of β -scaffold region LOV proteins transduces signal to effector domain. Thus β -scaffold segment of PAS domain is an important segment to transduce signals towards C-terminal of protein.

Signal transduction in PAS domain

As PAS domain proteins share a common three dimensional fold, an important question evolves whether PAS domain proteins has similar signal transduction mechanism? The cofactors of PAS domain protein are usually linked to PAS core motif. This is a clear indication that PAS core is preliminary component in receiving the signal. The signal is propagated from PAS core to the other domains to conduct the biological function. However, in PAS domain proteins, no common mechanism is found for signal transduction. The answer to this question can be revealed in future by combined approaches of structural biology and bioinformatics.

PYP/1-125

TT αA αB βA → TT βB → LL

1 *10 20 30 40*

PYP/1-125 ..MEHVAFGSEDIENTLAKMDDGQLDGLAFGAIQLDGDGNI..LQYNAA.
 NR11/1-115SNAMDTSLPSAILNNMVTATLILDDGLAI..RYANPA.
 Bphy/1-132SMTGG..QMGGRGMSRDPLPFFPPLYLGGPE
 Phy/1-132 ATTVQLSDQSLRQLETLAIHTAHLIOPHGLVVVLOEPDLTI..SQISAN.
 DCyc/1-115MTKAIPWKINWQTMAF..EYIGPQ.
 Cicardian/311-473YEAPRIPPEKRIFTTTHHTPNCLEF..QAVDER.
 SB_His_Kinase/1-114ERLRLFTEHAPAAALAMFDREMYR..LAVSRR.
 HTR_like/1-125 SNALANRIENVVSQERTRKKFESLVS DSPDGI VHLTTNGTI..LSVNPS.
 AER2/168-289ARIKSALDNVSANVMIA DNDLNI..IYMNRT.
 Trans_TyrR/76-190EREHLALSALLEALPEPVLSVDMKSKV..DMANPA.
 HERG/1-110SRKFIIANARVENCAV..IYCNDG.
 Heme_Oxy_Sensor/20-147GIFFPALQNMMAVLIINENDEV..MFFNPA.
 SMU_1151c/312-450EQANLILNHLPLEITFVNKDDIF..QYVNDSDV
 PF0695/352-473EELKAIFEALPVDVTFIDKDDR..RFFSPG.
 BMAL1c_B/327-447PANGEIRVKSMEYVSRHAIDGKF..VFVDQR.
 ARNT_B/357-467VCQPTRFTISRHNIEGIF..TFVDHR.
 consensus>50e.....v...d.d.i...y.n...

PYP/1-125

αC αD πA ηA αE

..... *50 * * 60 * 70 **** 80****

PYP/1-125 .EGDITGRDPKQVIGKNFFKDVAA...PCTDSPEFYGKFG...KEGVA
 NR11/1-115 .AELIFSQSAKRIVEQS.LSOLII...QHASLDLALITQ.....PLQSG
 Bphy/1-132 ITTENCEREPIHIPGSI.....QPHGALLTADGHSGEVLQMSLNAA
 Phy/1-132 .CTGILGRSPEDLLGRT.LGEVFF...DSFQIDPIQSRLL.....TAGQI
 DCyc/1-115 .IEALLGWPPQGSWKSVEDWATRM...HPEDQEWVNVFCVK....QSECG
 Cicardian/311-473 .AVPILGGLYLPQDLIETP.VLVQL...HPSDRPLMLAIHKKIL...QAGGQ
 SB_His_Kinase/1-114 .WRDYGLGDGDIIGMS.HYDIF...PEIGEWEKSVHRR...GLAGE
 HTR_like/1-125 .MAGRLGADPDTLVGGQ.LSAVM...DSEANQRLKAGKS....AVENG
 AER2/168-289 .VSEMLGRAEADIRKQ..LPNFD...AGRIMGANI DVFHKNPAHQHLLA
 Trans_TyrR/76-190 .SCQLFGQKLDRLRNHT.AAQLI...NGFNFLRWLE.....S
 HERG/1-110 .FCELCGYSRAEVMQRP.CTCDFLHGPTORRAAAQIAQ.....ALLGA
 Heme_Oxy_Sensor/20-147 .AEKLVGKYKREVI GNN.IDMLI...PRDLRPAHPEYIRHNREGGKARV
 SMU_1151c/312-450 PAAEMVFKRTPSQVGRN.VELCH...PKVLDKVKKVF.....ELLRN
 PF0695/352-473 .ERIFTRTPSVLGRP.VQLCH...PKSVYVNNKIL.....KAFKE
 BMAL1c_B/327-447 .ATAILAYLPQELLGTS.CYEYF...HODDIGHLAECHRQV...LQTRE
 ARNT_B/357-467 .CVATVGYQPQELLGKN.IVEFC...HPEDQQLLRDSFQQV...VKLKG
 consensus>50el.g.....dv.g.....e.....p.d.....d.....

PYP/1-125

βC TT βD βE

***90* 100 110 * 120

PYP/1-125 SGNLNTMFEYTFDYQMTPTKVKVHMKKALS...SYWVFKRV...
 NR11/1-115 QSITDSVTVFVV DGRPLMLEVTVSPI..TWQRQL..MLLVEMRKID...
 Bphy/1-132 TFLGQEPTVLRGQTLAALLPEQWPALQAALPPGCP..DALQYRATLDWPA
 Phy/1-132 SSLNPSKLVARVMGDDFVIFDGVFHR.NSDGLLV...CELEPAYTSDNLP
 DCyc/1-115 VDHEADYRALHRDGHYVWIRDVVHVVRDSDGEVE...ALIGFMFDISLEH
 Cicardian/311-473 PFDYSPIRFRTRNGEYITLDTSWSSFINPWSRKI...SFIIGRHKVRVGP
 SB_His_Kinase/1-114 VIRVEEDCFVRA DGRTQVLRWEVRPWEYEGEGRVG...GVVIFTEDIT...
 HTR_like/1-125 TATRSEDVAGGRHYHNQYIPVDSHRKSD.....TFQLVSRDIT...
 AER2/168-289 NLTGVHKAELNLGRRFSLDV.VPVFN DANERLG...SAVQWTDRTTEE...
 Trans_TyrR/76-190 EPQDSHNEHVVI NGQNFLEITPVYLODENDQHVLTVGAVVMLRSTIRMGR
 HERG/1-110 EERKVEIAFYRKDGSCFLCLVDVVPVKNEDGAVI...MFIILNFEVVMMEK
 Heme_Oxy_Sensor/20-147 EGMSRELQLEKKGSKIWTRFALSQVSAEGKVYY...LALVRDASVEMAQ
 SMU_1151c/312-450 GQRDKVNMWFQSERLGKFFVYVTYAAVRDQAGDFQ...GVLEYVQDIKPF
 PF0695/352-473 GRKKEATFWLRLREKYVYIK..YVPLFNEKGEYI...GTLEMTMDIAPYK
 BMAL1c_B/327-447 KITTNCYKFKIKDGSFITLRSRWFSPNPNWTKEV...EYIVSTNTVVLAN
 ARNT_B/357-467 QVLSVMFRFRSKNQEWLWMTSSFTFQNPYSDEI...EYICTNTNV...
 consensus>50dg.....l.....n.....v.....i.....

Figure 1.8: Sequence comparison of PAS domain proteins from subdomains of PAS to compare the secondary structure fold and most conserved residues.

1.5) Hofmeister effect and structural changes in protein

Proteins are biological molecules and plays pivotal role in various cellular functions in organism, such as signaling, catalytic activity and transport of ions. The ability to perform specific function of protein arises due to molecular intra and inter interactions of residues with adjacent molecules and each other, its surface properties, chemical composition. Most of the enzymes are protein which catalyzes chemical reactions. Protein performs its function by changing the conformational changes. Franz Hofmeister a professor of pharmacology from University of Prague published series of seven papers along with his co-workers, titled 'Zur Lehre von der Wirkung der Salze' (About the science of the effect of salts) during late 1880s and 1890s. These papers were written in German and published *Archiv fuer experimentelle Pathologie und Pharmakologie*. The first paper of this series was written by his student S. Lewith in 1887 and Hofmeister was not an author of this paper. Lewith presented the effects of salts on proteins in blood serum. On second paper, Hofmeister was an author and he studied effects of salts on egg white protein. In the third communication Hofmeister withdrew remarkable conclusions on water withdrawing effect of salts.

In 1885, Hofmeister discovered that under high salt concentration albumin proteins got precipitate (Kunz et al. 2004). While the concentration of different salts required precipitating the same protein was found to be varied. Later on salts were categorized to a series based on their precipitation degrees. It was determined that these ions changes the water structure and often ions are classified on water structure maker (more ordered or more hydrogen bonds) or breaker (disordered or less hydrogen bonds) (Cacace et al. 1997).

Hofmeister salts affect many properties of biomolecules. Biomolecules are molecules produced by living organism, e.g. proteins, lipids, nucleic acids. In 1965 Von Hippel and Wong studied the stability of thermal ribonuclease protein under various neutral salt conditions (Vonhippe et

al. 1965). They used optical rotatory spectroscopy to measure the melting temperature of protein, and found that salts highly affect the melting temperature. This concluded that Hofmeister salts greatly affects the stability of biological macromolecules. In later investigations it was reported that Hofmeister salt influence the solubility of biomolecules (Collins et al. 1985). At high salt concentrations protein is either salted in (more soluble) or salted-out (less soluble). Salting out of proteins is often used to get crystalline state of protein. Crystalline state of proteins generates the information of atomic positions of protein from which one can predict proteins secondary and tertiary structure. The information on proteins secondary and tertiary structure helps to understand how protein would be reacting to particular reaction. Recently there have been many attempts done by time resolved X-ray crystallography to understand how protein changes conformation once it is activated. However studying time resolved X-ray crystallography would not yield information on functional details as protein behaves differently in solution than crystal. Our attempt is to understand how proteins structural dynamics changes in high salt concentration.

CHAPTER II

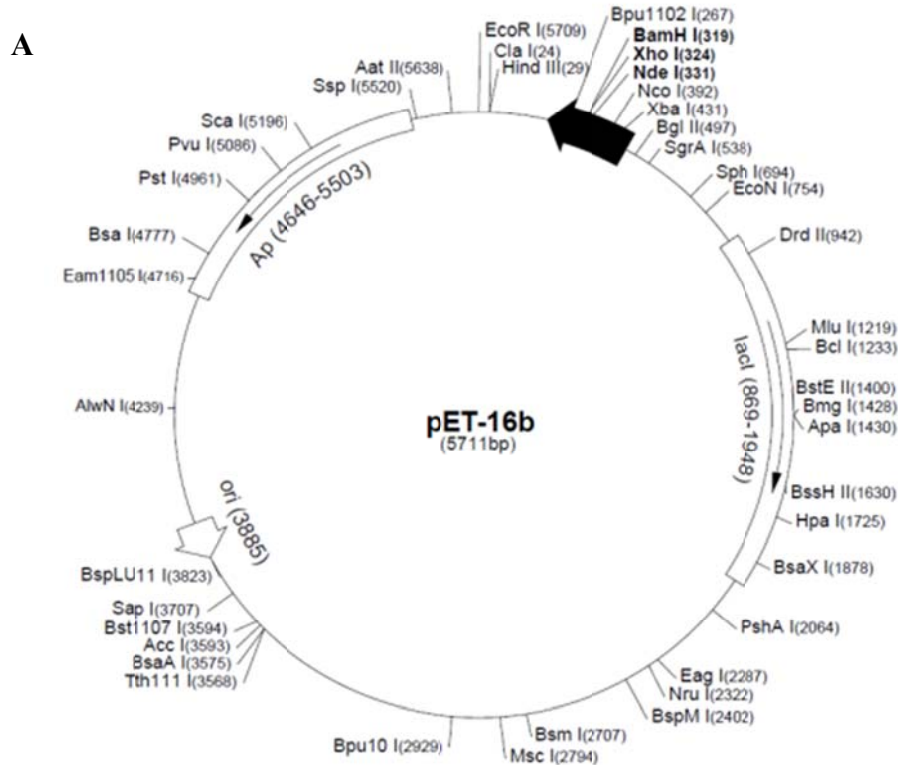
MATERIALS AND METHODS

2.1) Bacterial growth, PYP over-expression, PYP Purification

The yield of PYP from *Hhal* is ~ 1mg/L (Hoff 1995). In order to have better yield, PYP gene was expressed in *Escherichia Coli* (*E.Coli*) by genetic engineering. *E.Coli* is the best studied bacterial system and to obtain better yield, often desired bacterial gene is incorporated into *E.Coli* and protein is over-expressed (Mihara et al. 1997) by inducing factor Isopropyl β -D-1-thiogalactopyranoside (IPTG). Apart from wt PYP from *Hhal*, we have performed experiments with other PYPs which are listed below. The PYPs other than wt-PYP from *Hhal* were obtained from our collaboration with Dr. Hoff's lab.

Table 2.1: List of PYPs used in this dissertation

Protein	Bacteria	amino acid length
wt-PYP	<i>Halorhodospira halophila</i>	125
wt-PYP	<i>Idiomarina lohieinsis</i>	125
wt-PYP	<i>Salinibacter ruber</i>	156
N43A PYP	<i>Halorhodospira halophila</i>	125
N43S PYP	<i>Halorhodospira halophila</i>	125



B

ATGGAA CACGTAGCCTTCGGTAGCGAGGACATCGAGAACCACCCTCGCCAAAG
 ATGGACGACGGCCAGCTCGACGGCCTGGCCTTCGGCGCCATCCAGCTCGAC
 GGCGACGGCAACATCTTCAGTACAACGCCGCGGAGGGCGACATCACCGGC
 CGCGACCCGAAGCAGGTCATCGGCAAGAACTTCTTCAAGGACGTGGCCCG
 TGC ACTGACAGCCCGGAGTTCTACGGCAAGTTCAAGGAAGGGGTGGCCTCG
 GGCAACTGAACACGATGTTTCGAGTACACCTTCGATTACCAAATGACGCC
 ACGAAGGTGAAGGTGCACATGAAGAAGGCCCTCTCCGGCGACAGCTACTGGGTC TTC
 GTC AAGCGGTCTAG

C

MEHVAFGSED IENTLAKMDD GQLDGLAFGA IQLDGDGNIL QYNAAEGDIT
 GRDPKQVIGK NFFKDVAPCT DSPEFYGKFK EGVASGNLNT MFEYTFDYQM
 TPTKVKVHMK KALSGDSYVW FVKRV

Figure 2.1: Overexpression of HhaI PYP in E.coli. Schematic map of pET-16b plasmid which has ampicillin resistance and desired protein is induced by IPTG. The PYP gene is inserted in between BamHI and NdeI sites (A). DNA gene sequence of PYP from HhaI (B) and corresponding amino acids sequence with one letter (C).

PYP was over-expressed in genetically engineered *E.Coli* (BL21DE3) with pET16B plasmid [Figure 2.1]. *E.coli* cells were incubated at 210 rpm, 37°C inside the incubator. *E.Coli* was grown in 50 ml of LB media for 14 hrs. Further these cells were transferred to 1 L LB culture. Apo-PYP was induced by 1 mM IPTG at 0.8 OD of cell culture, after which cells were further incubated for 6 hrs. Cells were harvested at 3900 g for 15 minutes. Cell lysis was carried at 8.0 M urea solution at room temperature for 40 minutes. Cell lysate was precipitated using centrifugal force at 46,000 g for 15 minutes at 10°C. Reconstitution of apo-PYP was carried by adding 2-3 fold of *pCA* anhydride. Further PYP was purified with anion exchange chromatography using DEAE-Sepharose and Q-Sepharose. PYP was purified to highest quality using size exclusion chromatography using Sephadex G-50 superfine media. Purity Index (PI) is calculated as ratio of absorbance at 278 nm to 446 nm. Fractions with 0.43 or better PI were collected. The best purity index obtained with PYP is 0.42. The yield obtained is ~20 mg/l. Purified PYP was concentrated using anion exchange chromatography and eluted at 100 mM NaCl. The improvement in purity index during various stages of purification is shown in Figure 2.2. After purification PYP was stored at -80 °C in deep freezer.

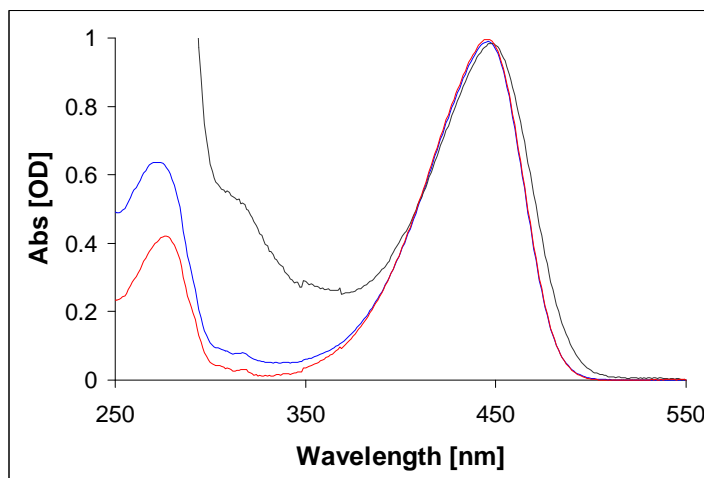


Figure 2.2: The UV-vis absorption of PYP during purification stages. The PI is calculated by taking ratio of Abs_{278 nm}/Abs_{446 nm}. The black spectrum represents PYP solution after dialysis of cell lysate, while blue spectrum is recorded absorption for best fraction obtained after first anion-exchange purification and PI of the sample is 0.65. The red spectrum represents the best fraction obtained 2nd anion-exchange purification and corresponding PI is 0.43.

In UV/visible absorption spectrum of protein, 280 nm band is due to the absorption of UVlight by Tyr, Trp and Cys (disulfide bonds). The extinction coefficient of a protein in water can be found by following formula (Pace et al. 1995).

$$\varepsilon(280)(M^{-1}cm^{-1}) = (\#Trp)(5500) + (\#Tyr)(1490) + (\#Cys)(125) \quad (2.1)$$

2.1.1 Ion Exchange Chromatography (IEX)

Ion-exchange chromatography separates proteins on basis of their net charge. The choice of cation or anion exchanger is decided on the total charge of the protein at particular pH. For example cation exchanger is implemented if protein has net positive charge below its isoelectric point (pI), while anion exchanger is implemented if protein has net negative charge above its isoelectric point. The media used in ion-exchange chromatography is charged beads which interact with protein electrostatically. After applying protein solution to column, protein molecules are adsorbed to ion exchange column. The affinity of protein towards gel media is dependent on the charge of the protein. The separation of the proteins is achieved by washing column with increasing NaCl salt concentration. Proteins with low- affinity towards columns start eluting first while proteins with high affinity elutes at higher concentration of NaCl.

Ion exchange chromatography technique is used during capturing, intermediate purification and polishing stages of protein purification (Protein Purification book (1999)). The capturing of PYP during its purification was performed by the Diethylaminoethyl (DEAE)-Sephacel fast flow, a weak anion-exchanger. The intermediate level PYP purification was performed by Q-sephacel fast flow media a strong anion-exchanger. The particle size of DEAE Sepharose and Q-Sepharose is 45-165 μm , however their binding capacity differs. The capacity of DEAE Sepharose fast flow and Q-Sepharose fast flow media are 0.11-0.16 mmol/ml and 0.18-0.25 mmol/ml. The operating pH range for DEAE Sepharose and Q-Sepharose are 2-9 and 2-12 respectively. The net charge of the protein is dependent on the pH. We exploit this fact to

separate the PYP proteins during the purification stages. The first anion exchange is carried with DEAE Sepharose at pH 8.50, while the second anion exchange is carried with the Q-Sepharose at pH 6.00. The change in pH during successive runs of anion exchange chromatography achieves better separation and yield as the net charge of protein differs at different pH. The experimental pI of PYP is 4.3 (McRee et al. 1986), as a result at pH 6.00 and 8.50 the PYP remains negatively charged while other proteins binding affinity changes resulting the better separation of proteins. The PYP purification procedure is discussed more in protocol E in the appendix of this dissertation.

2.2.2 Size exclusion Chromatography

Size exclusion chromatography method separates molecules on basis of its size. The gel media has small pores which can trap small size particles while particles size more than the pore passes through the gel. This process is based on diffusion. The large size molecules diffuse faster while small size particles diffuse slower, thus the separation is achieved. To achieve better separation sample volume applied to column has to be 0.5-2% of column volume, smaller the better.

The media for size exclusion chromatography was Sephadex G-50 superfine which can be implemented to separate molecules in the range of 1500-30,000 dalton. The molecular weight of PYP is found to be 14021 dalton using mass spectrometry. Apart from purification of proteins this technique can be implements for desalting of proteins.

2.2) Buffer and FTIR sample preparation

Stock buffers of 1.0 M of potassium monobasic phosphate and 1.0 M potassium dibasic phosphate were prepared in D₂O. Further, 50 mM deuterated phosphate buffer was prepared from the stock buffers and pH was adjusted with deuterated hydrochloric acid and deuterated sodium hydroxide to pH 7.50. Based on ionization, pK_a of phosphate buffers are 2.16, 7.21 and 12.32.

The buffers prepared in D₂O pH correction was applied as $pD = \text{actual reading} + 0.4$. Buffers at pH 8.50 and 9.50 were prepared in deuterated borate solution ($pK_a = 9.24$).

All salt solution were prepared at 50 mM deuterated buffer concentration and prepared by volumetric method. For example 1 ml of 4.0 M NaCl was prepared by weighing 58.4 mg of NaCl in final volume of 1 ml. All samples were washed twice using Microcon YM-10 centrifugal devices. First was adjusts pH of sample while 2nd wash reduces H₂O contamination less than 0.1 %.

PYP for FTIR experiments were prepared at protein concentration of ~10 mM in salt solution buffer mentioned above. This was achieved by washing ~10 mM PYP in salt solution buffer twice, through Microcon YM-10 filters at 12,000 rpm. The same procedure was repeated for 0.5 M, 1.0 M, 2.0 M, 2.5 M, 3.0 M, 4.0 M NaCl and also for 2.5 M LiCl, 2.5 M KCl and 2.5 M CsCl. The sample washing time was differed, to obtain ~10 mM PYP concentration.

Each sample solution was made by sandwiching 2.7 μl of PYP between two CaF₂ windows of 15 mm in diameter and 2 mm thick using a 12 μm spacer. For each sample of PYP dark state UV-VIS absorption was measured in the 250-550 nm range.

2.3) Laser

The photocycle of PYP molecule was initiated by the tunable Nd:YAG laser in visible range was implemented to photoexcite PYP molecule from its ground state.

Laser has three basic components

- 1) Active medium to amplify incident Electromagnetic (EM) waves.
- 2) Energy pump which can achieve population inversion of lasing media

3) Optical resonator consisted of two opposite mirrors which stores part of induced emission. It provides selectively feedback of emitted radiation from excited molecules of active medium.

2.3.1 Optical Parametric Oscillator (OPO)

The OPO is based on parametric interaction of strong electromagnetic waves with molecules in crystals. In this interaction pump photon is inelastically scattered by crystal molecule, pump photon is absorbed and generates two new photons. As every photon generates electromagnetic wave, these two photons generate two electromagnetic radiations with different frequencies one of them called as signal wave and other as idler wave. Gain of signal and idler wave depends on intensity of pump and effective nonlinear susceptibility of crystal. Due to high gain of OPO pulsed operation is preferred where Q-switched laser source. OPO tuning can be done by either rotating crystal or controlling temperature.

2.3.2 Q-Switch

Q-Switch technique allows obtaining single and powerful pulse of flashlamp-pumped laser. The cavity losses of laser are kept so high until a selected time t_0 after the start of pump pulse $t=0$, ensuring oscillation threshold has not reached. Optical switch is opened at $t=t_0$ the losses in cavity are lowered so the the Q-value of cavity changes from low to high value. The time profile of the pulse depends on the rise time of Q-switching.

Tunable solid state laser consisted of Neodymium Yttrium Aluminium Garnet (Nd:YAG) crystal was employed to achieve monochromatic light source at 1064 nm. Flashlamp (Quantel, Brilliant) was operated at 1.4 kv at 10 Hz. First harmonics was generated at 1064 nm with 400 mJ. While second and third harmonics generated at 532 nm and 355 nm with 200 mJ and 100 mJ respectively. Optical Parametric Oscillator (OPO) was employed to tune the wavelength from third harmonics to 410-680 nm. The actinic light produced by laser has pulse width of 5 ns.

Flashlamp and Q-switch were triggered using SRS DG-535. PYP photocycle was initiated by actinic light at 475 nm generated by YAG laser. The laser energy obtained after OPO was 22.0 mJ, while at sample position energy was 3.0 mJ over 10 mm diameter area.

2.4) FTIR system and techniques

IR absorption and time-resolved FTIR measurements gives structurally reach information on proteins in actions. IR spectroscopy is sensitive to hydrogen bonding, vibrational modes, and protonation states of amino acids in protein.

A Bruker IFS 66v FTIR spectrometer with a Michelson interferometer was utilized for time-resolved measurements. Global source made of silicon-carbide was used to generate mid infra-red light.

2.4.1. Principles of Infrared spectroscopy

Typically IR absorption is less intense than UV visible as the extinction coefficients of molecules in IR are lower than UV. Thus, IR spectroscopy requires more amount of sample compared to UV. Secondly, water has strong absorption in many regions of infrared where protein and nucleic acids absorbs. This problem can be mitigated by using D₂O solution instead of H₂O solution.

Vibrational modes of a particular molecule are localized and influenced by surrounding environment. Thus, it can probe structural changes which are influenced by changing local environment. e.g. the vibrational mode of hydrogen bonded molecules, or protonated /deprotonated molecule.

The intensity of vibrational band is dependent on the magnitude of light induced dipole. The wavefunction of a molecule Ψ can be separated by electronic and nuclear motion by Born-Oppenheimer principle as shown in equation 2

$$\Psi = \Psi_e(r, R)\Phi_N(R) \quad (2.2)$$

In above equation subscripts e and N represents electronic and nuclear part of wavefunction, respectively. The vibrational transition can be denoted as following

$$\Psi_0(r, R)\Phi_v(R) \rightarrow \Psi_0(r, R)\Phi_{v'}(R) \quad (2.3)$$

Φ_v and $\Phi_{v'}$ represents two different vibrational states; while r and R are the coordinates of electron and nuclei, respectively. Ψ_0 is the ground state of electronic wavefunction. By considering the nuclei stationary, electric dipole operator depends only on electronic coordinates and the transition dipole is given by

$$\langle \Psi_0 \Phi_v | \mu | \Psi_0 \Phi_{v'} \rangle = \langle \Psi_0 | \mu | \Psi_0 \rangle \langle \Phi_v | \Phi_{v'} \rangle = 0 \quad (2.4)$$

As the first integral over r is odd and second integral over R is zero as Φ_v and $\Phi_{v'}$ are orthogonal eigenstates of the Hamiltonian, hence the above equation is zero.

If nuclei are in motion during vibrational mode, then dipole operator is dependent on R as variation in R changes the electron density. The expansion of Taylor series of dipole operator μ is given by following

$$\mu(r, R) = \mu(r, R_0) + \left(\frac{\partial \mu(r)}{\partial R} \right)_{R_0} (R - R_0) + \dots \quad (2.5)$$

The expectation value of first term yield zero as shown in equation 3, however the second term is nonzero and is given as

$$\langle \Psi_0 \Phi_v | \mu | \Psi_0 \Phi_{v'} \rangle = \langle \Psi_0 | \left[\frac{\partial \mu(r)}{\partial R} \right]_{R_0} | \Psi_0 \rangle \langle \Phi_v | R | \Phi_{v'} \rangle \quad (2.6)$$

In above equation first integral is electronic while second integral is vibrational. Electronic integral is change in permanent dipole moment of ground state of molecule.

2.4.2. Vibrations modes and isotopic shift

The vibration of a molecule occurs when the atoms inside molecule moves about its mean position in periodic motion, while molecule has its translational and rotational motion. The polyatomic molecule with N atoms has 3N degrees of freedom. The non-linear molecule has 3 translational and 3 rotational degrees of freedom, while is a linear molecule has 3 translational and 2 rotational degrees of freedom. The total number of vibrational modes for a polyatomic molecule is given by 3N-total number of degrees of freedom. Thus for non-linear polyatomic molecule is vibrational modes are 3N-6 , while for linear polyatomic molecule it is 3N-5. The vibrational frequency of a normal mode can be calculated from following formula.

$$\tilde{\omega}_e = \frac{1}{2\pi c} \sqrt{\frac{f}{\mu}} \quad (2.7)$$

Where f and μ are force constant and reduced mass of molecule, respectively. The force constant and reduced mass can be found as described by following formulae.

$$f = \left(\frac{\partial^2 V(r)}{\partial r^2} \right) \quad (2.8)$$

$$\mu = \frac{m_A m_B}{m_A + m_B}$$

Often the vibrational frequencies are overlapped with different modes of vibration. Sometimes it is difficult to assign a particular vibrational mode to molecule. This issue can be

resolved by using isotopic edited molecule which would downshift the vibrational mode. Using computational and experimental approach the particular vibrational mode can be assigned.

2.4.3 Introduction to FTIR instrument

Before invent of Fourier Transform Infrared Spectrometry (FTIR), infrared instruments were dispersive type. In dispersive IR instruments energy (frequency) was separated by means of grating or dispersion through prism. The modern FTIR systems are built on Michelson interferometer. In our lab all infrared experiments were carried out by IFS 66v FTIR spectrometer (Bruker, Germany). The experimental setup for FTIR absorption and time-resolved FTIR measurement is as shown in Figure 2.3.

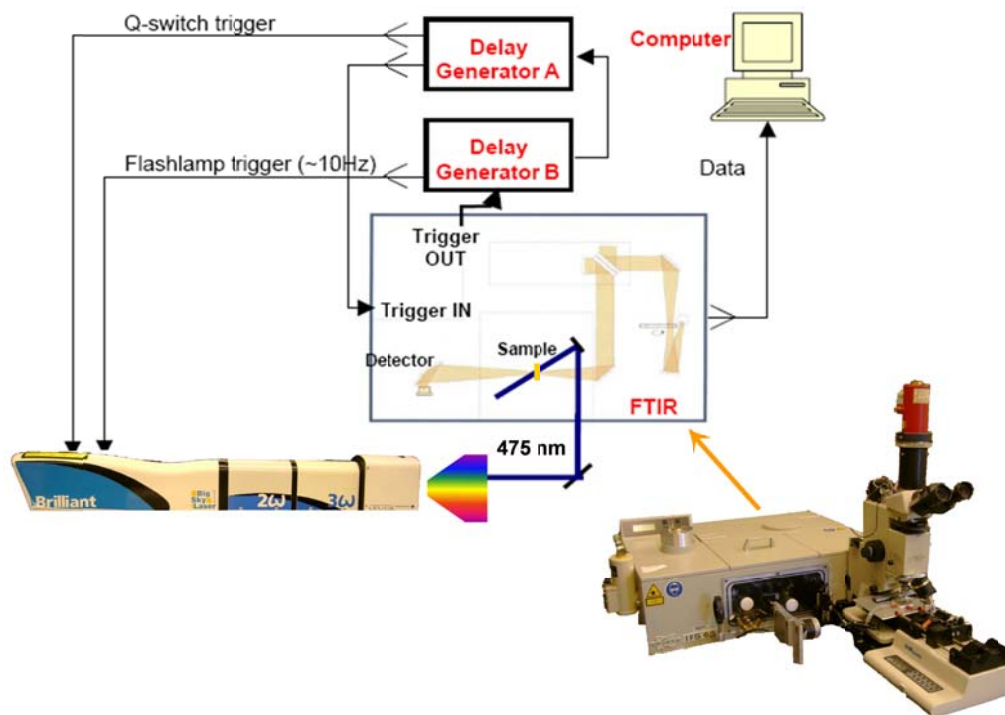


Figure 2.3: Layout of experimental setup for time-resolved rapid-scan and step-scan FTIR spectroscopy.

2.4.4 Michelson Interferometer

Michelson interferometer is consisted of light source, beam splitter and two perpendicular mirrors in which one stationary while other is moving. Light beam from source is ideally divided equally by means of beam splitter resulting 50% reflection and 50% of transmission of beam. Both beams get reflected by mirrors and recombines at the beam splitter. Intensity reached at the detector is addition of the two beams. As moving mirror travels, the optical path difference is created. When the optical path in both arms of interferometer is same the two beams will be in phase ($\delta=0$) and intensity at the detector $I(\delta)$ will be maximum. If the moving mirror travels by distance same as the quarter of the wavelength the optical path difference becomes $\delta=\lambda/2$. In that case the beams are out of phase and results in destructive interference. As mirror moves further by quarter of wavelength or total of $\lambda/2$, the path difference becomes $\delta=\lambda$ and produces constructive interference. The maxima is created if the path difference is multiple wavelengths, while minima is created if path difference is half multiple of half wavelengths. Thus interferogram with intensity $I(\delta)$ is produced as a function of the mirror position. The interferogram can be explained by infinitely long cosine of wave and written as

$$I(\delta) = 4A^2 \cos^2(\pi\lambda\delta) \quad (2.9)$$

$$I(\delta) = 2A^2 (1 + \cos(2\pi\lambda\delta)) \quad (2.10)$$

Intensity measured by detector for light of spectral intensity $B(\lambda)$ is given by

$$I(\delta) = \int_0^{\infty} B(\lambda)(1 + \cos(2\pi\lambda\delta))d\lambda \quad (2.11)$$
$$I(\delta) = \int_0^{\infty} B(\lambda)d\lambda + \int_0^{\infty} B(\lambda)\cos(2\pi\lambda\delta)d\lambda$$

$$\text{When } \delta=0, I(\delta) = I(0) = 2\int B(\lambda)d\lambda \quad (2.12)$$

$$I(\delta) - \frac{1}{2}I(0) = \int_0^{\infty} B(\lambda) \cos 2(2\pi\lambda\delta) d\lambda \quad (2.13)$$

Above equation represents the interferogram and Fourier-transform of above equation gives intensity at wavelength.

$$B(\lambda) = \int_0^{+\infty} [I(\delta) - \frac{1}{2}I(0)] \cos(2\pi\lambda\delta) d\delta \quad (2.14)$$

. Spectral resolution and Apodization

Resolution of FTIR spectrometer is inversely proportional to total displacement of the mirror in one direction. In practice, moving mirror cannot move $-\infty$ to $+\infty$, and has finite movement resulting truncating interferogram. However to extract best information out of interferogram, it has to be treated with special mathematical treatment called as apodization.

2.5) IR absorption of Protein

Protein sample with 2.7-3.0 μ l were sandwiched in between two CaF_2 (15 mm X 2 mm) separated by 12 μ m spacer. IR absorption was collected by 3-sample exchanger driven by stepper motor (Si3540, Applied Motion products, USA) and movement of 3-sample exchanger was controlled translational direction. The 3-sample exchanger was maintained at a constant temperature of 300K using water circulating temperature controller (RTE 111 D3, NESLAB Instruments, Inc., USA). The step motor driver of 3-sample exchanger is externally triggered by the spectrometer in rapid-scan mode to synchronize the data collection and changing sample position. Sample position was stabilized before collecting the interferogram. IR absorption

collected by 3 sample exchanger was better than normal IR absorption as it reduces signal from water vapor (see Figure 2.4). Sample chamber was purged with nitrogen gas to reduce water vapors. The scanning rate and spectral resolution were 40 kHz and 2.0 cm^{-1} , respectively in IR absorption measurement.

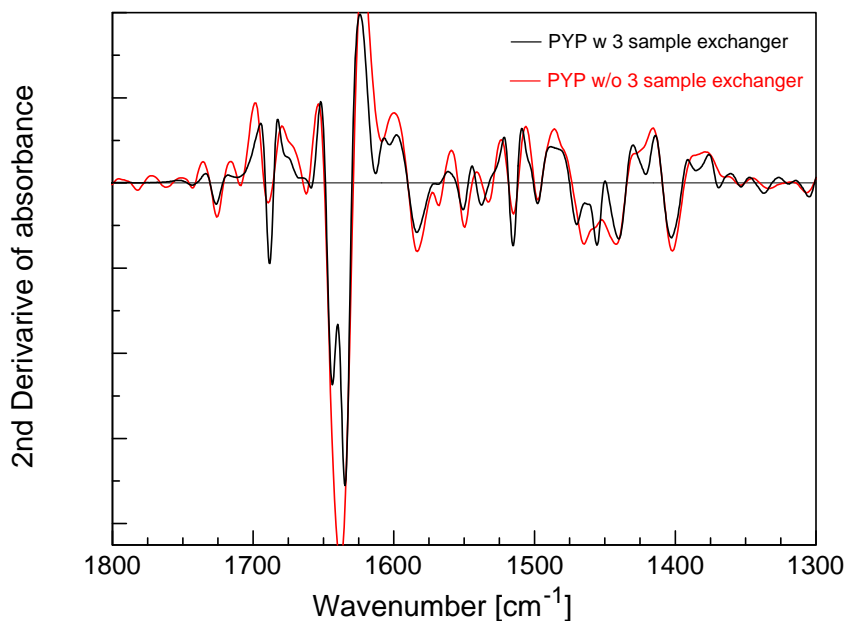


Figure 2.4. The second derivative of absorbance of wt-PYP with (black) and without three-sample exchanger (red). The 2nd derivative of absorption without 3-sample exchanger shows the strong absorption bands of water in region of 1800-1400 cm^{-1} .

Proteins has five major bands due to amide vibrations in mid-IR region, as described in

Table 2.2

Table 2.2. Peak position of Amide bands in mid-IR region. Adapted from (Tamm et al. 1997)

Designation	Wavenumber (cm^{-1})	Assignment
Amide-A	~3300	N-H stretching in resonance with overtone (2 X amide II)
Amide-B	~3110	
Amide-I	1600-1700	80% C=O stretching; 10% C-N stretching; 10% N-H bending
Amide-II	1510-1580	60% N-H bending; 40% C-N stretching
Amide-III	1200-1400	30% C-N stretching; 30% N-H bending; 10% C=O stretching; 10% O=C-N bending; 20% other

The amount of secondary structure in the protein can be estimated by infrared absorption spectroscopy (Tamm et al. 1997). In this case usually Amide-I band is used to fit with number of peaks to estimate amount of secondary structure. The protein absorption of two different proteins in Amide-I region is different with same concentration. For example we have compared absorption of PYP with myoglobin at ~ 10 mM concentration as depicted in the Figure 2.5. The myoglobin has predominately α -helices, while PYP is consisted of β -sheet flanked α -helices. The peak of Amide-I band in case of myoglobin is at 1650 cm^{-1} , while in case of PYP 1642 cm^{-1} . The structural details of each protein can be revealed by obtaining the second derivative of absorption.

The mid infrared spectrum is greatly affected by water vapor spectrum. The implementation of three sample exchanger cancels out water vapor absorption from reference and sample spectrum as they are measured at same time. The absorption of sample is calculated by $Abs = -\log \frac{Sample}{Reference}$. The water vapor spectrum is observed in $2000\text{-}1400\text{ cm}^{-1}$ region which is overlapping region for Amide-I , Amide-II absorption of protein. In Figure 2.4 the second derivative of absorption of PYP is compared with and without 3 sample exchanger. The PYP absorption without 3 sample exchanger is greatly affected in region of $1800\text{-}1400\text{ cm}^{-1}$ region. The Amide-I band at $\sim 1640\text{ cm}^{-1}$ of PYP without 3 sample exchanger is resolved into two bands with 3 sample exchanger.

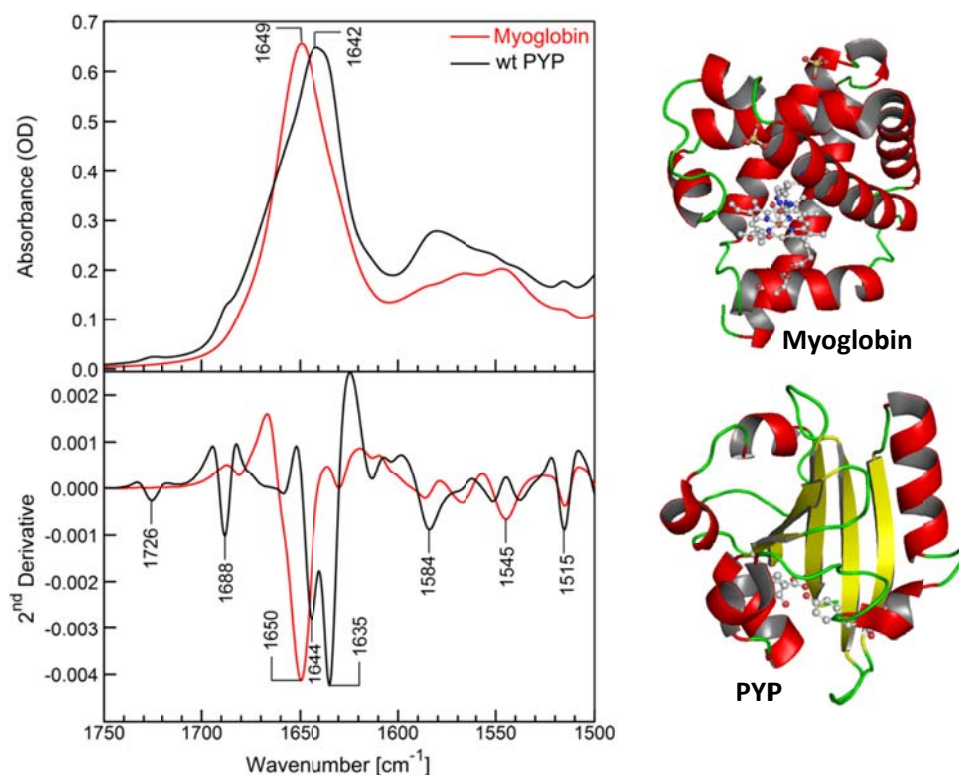


Figure 2.5: Infrared absorption of Myoglobin from Sperm Whale (*Physeter catodon*) and wtPYP from *Halorhodospira halophila*. The top panel shows infrared absorption for Myoglobin (red) and PYP (black), the corresponding 2nd derivative of absorption is plotted in bottom panel. The Amide-I absorption peak of both proteins are different. Myoglobin has α -helical structure while PYP has both α -helices and β -strands. (PDB IDs: Myoglobin :1A6M, PYP:1NWZ)

2.6 Time-resolved FTIR spectroscopy

The time-resolved FTIR spectroscopy technique provides information of relaxation dynamics of molecules vibrational and rotational states. To understand the reaction dynamics of the biomolecule, structural information of intermediate state has to be gained. The time-resolved FTIR spectroscopy can provide structural details of intermediate states of a reaction. Specially, time-resolved FTIR spectroscopy is advantageous over other techniques. Firstly, the probe IR beam is nondestructive to sample. Secondly IR beam it can monitor nonchromophoric systems, and finally measurements can be performed in physiological conditions without changing energy landscape of the molecule. Currently, time-resolved FTIR spectroscopy can monitor dynamics of

reaction from ns to seconds time scale with utilization of different data collection processes. This time scale covers dynamics of all collective motions inside a biomolecule, thus allowing to probe events like proton transfer, conformational changes, protonation and deprotonation of side chain of amino acids. The time-resolved FTIR spectroscopy is further divided into mainly two areas. Time-resolved step-scan FTIR spectroscopy can probe molecular events from ns- μ s and μ s-ms time range. While time-resolved rapid scan FTIR spectroscopy probes molecular events from ms to second time scale.

2.6.1) Time-resolved rapid-scan FTIR spectroscopy

Time resolved rapid-scan measurements were performed in spectral range of 4000-900 cm^{-1} , at spectral resolution of 4.5 cm^{-1} with 200 kHz mirror speed. The PYP photocycle was triggered using laser pulses with pulse duration of 4 ns and energy of 3 mJ at 475 nm. Measuring IR beam was 5 mm in diameter, while laser beam diameter 10 mm. The light induced FTIR absorption changes were measured with 8 ms time resolution using the rapid scan method. The 4 ns long actinic light flash for the time-resolved FTIR measurements was provided by a YAG laser (Quantel, Brilliant laser) pumped OPO (Opotek) tuned to 475 nm.

The normal rapid scan FTIR measurement can yield time resolution of 25 ms at 4.5 cm^{-1} spectral resolution and 200 kHz scanning rate of moving mirror. To achieve improvement in time resolution of rapid-scan FTIR, one full scan was divided into 4 equal paths (Q1 to Q4), that each yields in principle identical information. However, the data obtained, in reality, shows some noticeable differences. These differences arise from the slight variation in the zero path difference of the interferogram. To overcome this technical difficulty, experiment was repeated four times, such that the laser flash excites the sample at the start of each of the 4 quarters. The delay generators (DG 535, Stanford Research System) were synchronized with FTIR master clock.

The schematics of data collection for quadruple-split rapid-scan FTIR measurement is shown in figure 2.6. Combining these four quarters right after laser excitation from four experiments to generate the first full scan interferogram which is then Fourier transformed to an infrared difference spectrum. This method is known as quadruple-split rapid scan FTIR measurement and yields 8 ms time resolution at 4.5 cm^{-1} spectral resolution and 200 kHz scanning rate of moving mirror.

The scan 'A' recorded before laser flash is treated as the reference spectrum (Figure 2.6). The single beam spectrum is generated by Fourier transform of the interferogram resulting four single beams spectra per scan. The FTIR instrument and laser are synchronized by delay generators. The actinic laser flash comes before every quarter of the scan. The laser flash photoactivates PYP starting of the four interferograms in four measurements. This results in four different measurements of rapid-scan FTIR, each with different delay time of laser flash. In our experiment for 4.5 cm^{-1} spectral resolution with 200 kHz scanner velocity the delay time for lasers were adjusted to 10 ms, 23 ms, 59 ms and 72 ms.. Finally the difference absorption spectrum is obtained by taking logarithmic difference between single beam spectrum of each quarter of scan. The mathematical formula for same is below.

$$\Delta Abs(\nu)_i = -\log \left(\frac{\text{Single Beam}_{Bi}}{\text{Single Beam}_{Ai}} \right) \quad (2.15)$$

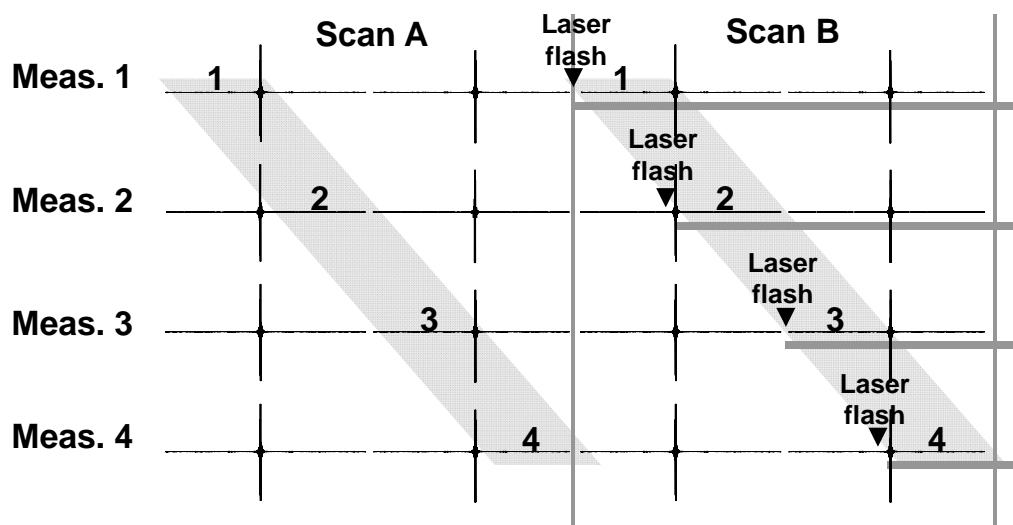


Figure 2.6. Schematics of quadruple-split rapid scan time resolved measurement. Each forward and backward scan is divided into two equal interferograms resulting total of four interferograms per scan. The scan ‘A’ recorded before laser flash is treated as the reference spectrum. The single beam spectrum is generated by Fourier transform of the interferogram resulting four single beams spectra per scan.

Data analysis

Data was analyzed using OPUS software provided by manufacturer. The FTIR difference absorbance obtained is highly reproducible as shown in Figure 2.7. Each FTIR difference absorption spectra was accumulated with 256 flashes and average with total of 768 accumulations. Data from OPUS was extracted in ASCII format and plotted using Matlab. Time - resolved FTIR difference spectra were calculated using the preflash data (pG_{446}) as a reference and averaged over repetitive measurements.

The difference spectra are measured using the Rapid Scan method and show a strong variation with salt concentration. The spectra are normalized to the 1497 cm^{-1} (deprotonation of *pCA*) and 1515 cm^{-1} (protonation of *pCA*) band which has effectively the same difference amplitude throughout pG and pB.

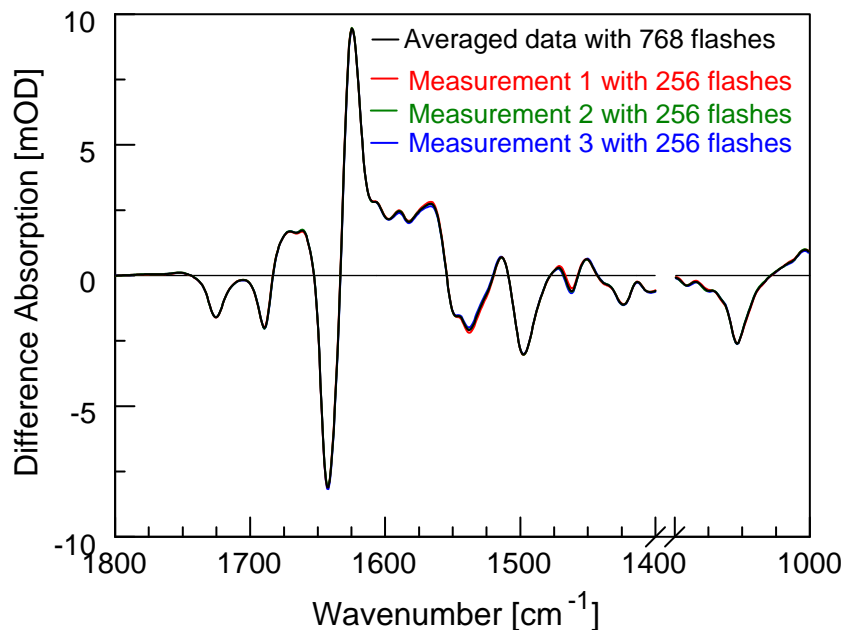


Figure 2.7: The data reproducibility of light induced FTIR difference absorption of PYP. Three different measurements were averaged; each measurement was averaged with 256 accumulations of PYP photocycle.

2.6.2) Time-resolved step-scan FTIR spectroscopy

The time-resolved step-scan spectroscopy technique provides time resolution of ns and μ s. In time-resolved step-scan FTIR spectroscopy interferometer is held at each fixed position and time course signal is recorded using digitizer. Thus by moving mirror stepwise interferogram is recorded with transient signal at each sampling point (Figure 2.8). Further the data is Fourier transformed to obtain the data set containing spectral changes. In this method the time resolution is regulated by 1) detector rise-time, 2) Analogue to Digital (AD) converter and 3) strength of the signal.

The Bruker IFS 66v FTIR spectrometer was employed to implement time-resolved step-scan FTIR spectroscopy. The photovoltaic MCT detector from Kolmar Technologies (KMPV50-0.5-J2) with build-in preamplifier was used for microsecond time resolution step-scan

experiment. The build-in preamplifier of MCT detector has AC and DC outputs. The signals from DC output was digitized by 8 bit, 200 MHz digitizer (PAS82) provided by Bruker Optics.

In time-resolved step-scan FTIR measurement, mirror position of moving mirror is increased in step-wise at each step position transient signal is collected. Then mirror is moved and fixed to adjacent position. Then the signal at each mirror position is processed to obtain a 3-D interferogram as shown in Figure 2.8. The typical interferogram during time-resolved step-scan FTIR experiment is shown in Figure 2.9. The number of mirror positions is dependent on the spectral resolution. For example 6 cm^{-1} spectral resolution takes only 382 mirror positions while 4 cm^{-1} spectral resolution takes 522 mirror positions to obtain spectrum in $1858\text{-}929\text{ cm}^{-1}$ region.

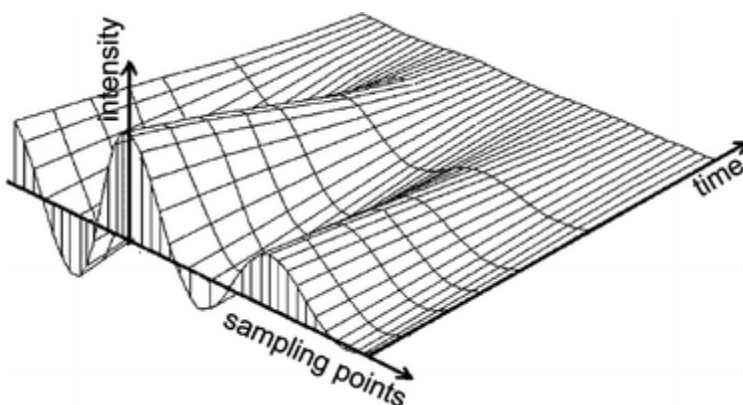


Figure 2.8. The 3-D representation of interferogram obtained in time-resolved step-scan FTIR spectroscopy. The sampling point axis represents the change in mirror position; intensity axis represents intensity of interferogram. At each mirror position the reaction is evoked by laser flash and transient intensity is recorded. Adapted from (Radu et al. 2009)

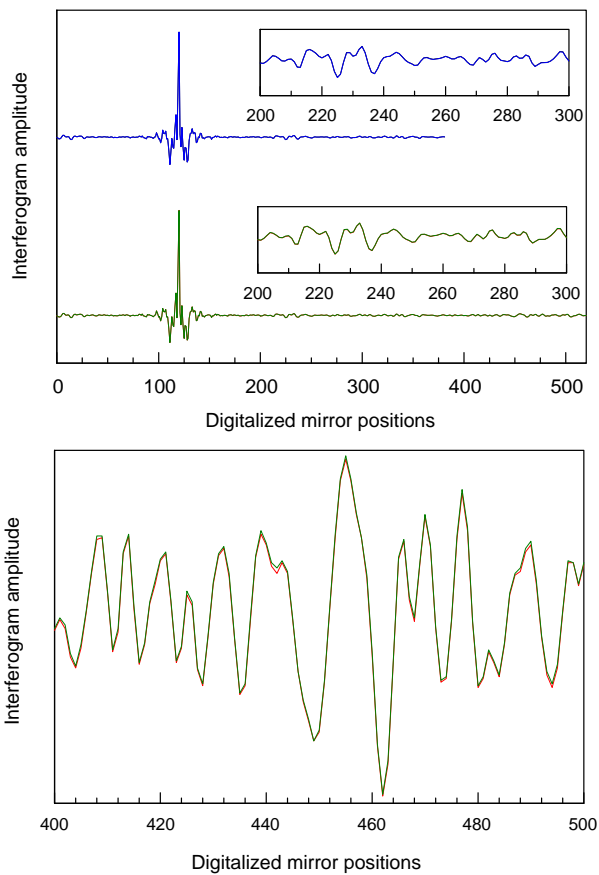


Figure 2.9. Infrared interferogram of photoactive yellow protein (PYP) (A), with 6.0 cm^{-1} spectral resolution generating 382 mirror positions and (B) with 4.0 cm^{-1} spectral resolution generating 522 mirror positions. Each interferogram was averaged over 32 scans with 16 cm^{-1} phase resolution. Insets are magnified by factor of 20. Inset B, two repeated measurements red & green interferogram are nearly identical, show high reproducibility. A cutoff filter with 10% transmission at 1856 cm^{-1} was used and according to folding limit is adjusted to 1858 cm^{-1} - 929 cm^{-1} . Magnified infrared interferogram of PYP with 4.0 cm^{-1} spectral resolution, in region of 400-500 mirror positions (C).

To obtain the FTIR difference spectrum from the collected data following procedure is applied. The single beam spectrum $S(\nu)$ is obtained from static interferogram $I(x)$ and corresponding phase spectrum $\Phi(\nu)$ is stored. The Mertz algorithm was implemented to correct the phase. Further the change in interferogram intensity with time at fixed mirror position $\Delta I_x(t)$ is rearranged to interferogram at fixed time $\Delta I_t(X)$. The intensity difference spectrum $\Delta S_t(\nu) = S_t(\nu) - S_0(\nu)$ is calculated. Finally the absorption difference spectrum is obtained by following formula

$$\Delta A_t(\nu) = -\log\left(\frac{S(\nu) + \Delta S_t(\nu)}{S(\nu)}\right) \quad (2.16)$$

The procedure to extract the FTIR difference absorption in step-scan mode is depicted in Figure 2.10.

In our time-resolved step-scan FTIR experiment, moving mirror, homemade 3-sample exchanger, laser trigger and electronic shutter were synchronized with delay generators (DG 535,

Standford Research System). The Analogue to digital converter with 8 bit digitizer was implemented to record the intensity of signal. The homemade 3-sample exchanger reduces the time for data collection as during recovery of the protein sample position is switched to adjacent sample position.

The time-resolved step-scan measurement was performed from 5 μs to 7 ms time scale at 4.5 cm^{-1} spectral resolution. The scanning mirror velocity was set to 100 kHz. The FTIR setup was positioned on vibrational isolated optical table. The 3-sample exchanger was used to change the sample position. On each sample position 6 coaddition were done (2 for each sample), total coadditions on one sample were 180. IR cutoff filter was used to eliminate signals greater than 1850 cm^{-1} and spectra was collected in range of 1850-990 cm^{-1} . Data was collected on quasi-logarithmic time scale with 5 μs time resolution with 504 mirror points. Laser flash, 3-sample exchanger and actual measurement time were synchronized with help of the delay generator (DG). The details of time-resolved step-scan FTIR measurement is provided in appendix D.

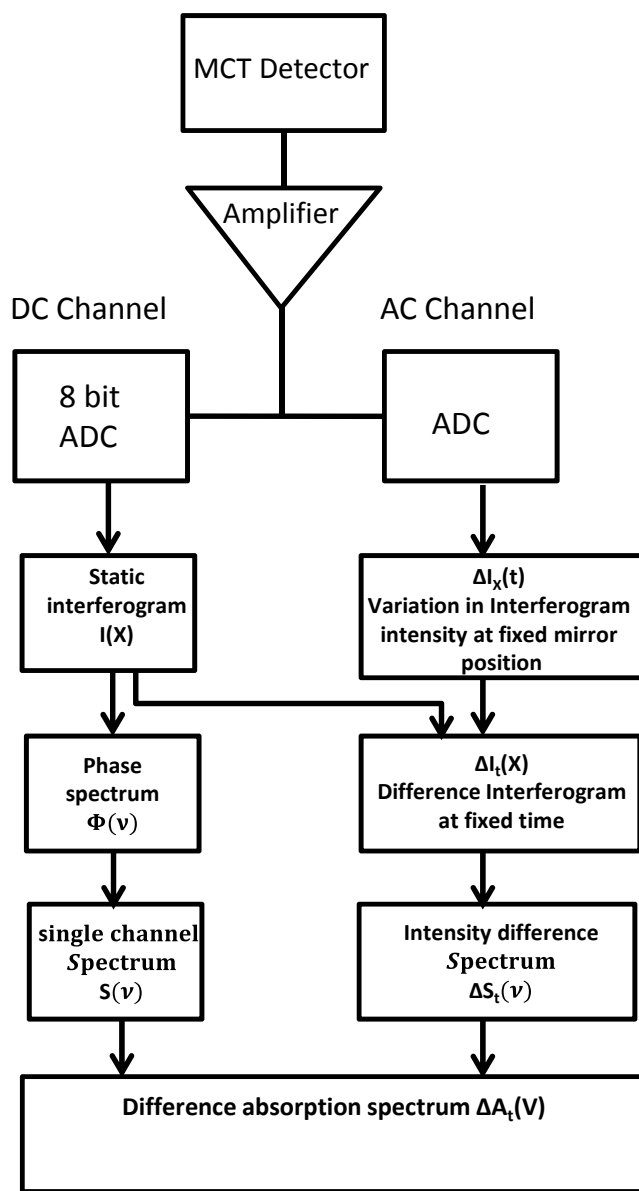


Figure 2.10. The layout for extracting difference absorption from recorded data in step-scan time-resolved FTIR experimental setup.

2.7) Flash photolysis system

Homemade flash photolysis system was used to find out recovery time of PYP photocycle in different salt conditions. White light source was generated by flashlamp (ORIEL, 66001). A water bath was placed in front of the flashlamp to absorb excess heat. Monochromator (CM110, 1/8 monochromator) was used to obtain probe light from flashlamp. A second monochromator placed in front of photomultiplier (Hamamatsu, R928). The probe light was set to 430 nm by setting both monochromators at 430 nm. The amplifier (FEMTO) was employed to amplify the signal at PMT. The pump beam was aligned with an angle with the probe beam to avoid pump beam photons reaching at the PMT. The flash photolysis measurements were carried out at room temperature. The schematic of flash photolysis system is shown in Figure 2.11.

Photocycle was initiated by actinic flash of laser pulse at 475 nm, while probe beam was at 430 nm. The laser beam spot at the sample was ~ 6.0 mm in diameter while laser energy at the sample was ~ 3.0 mJ/pulse. Data was collected on quasi-logarithmic time scale, 200 ns being the smallest time resolution.

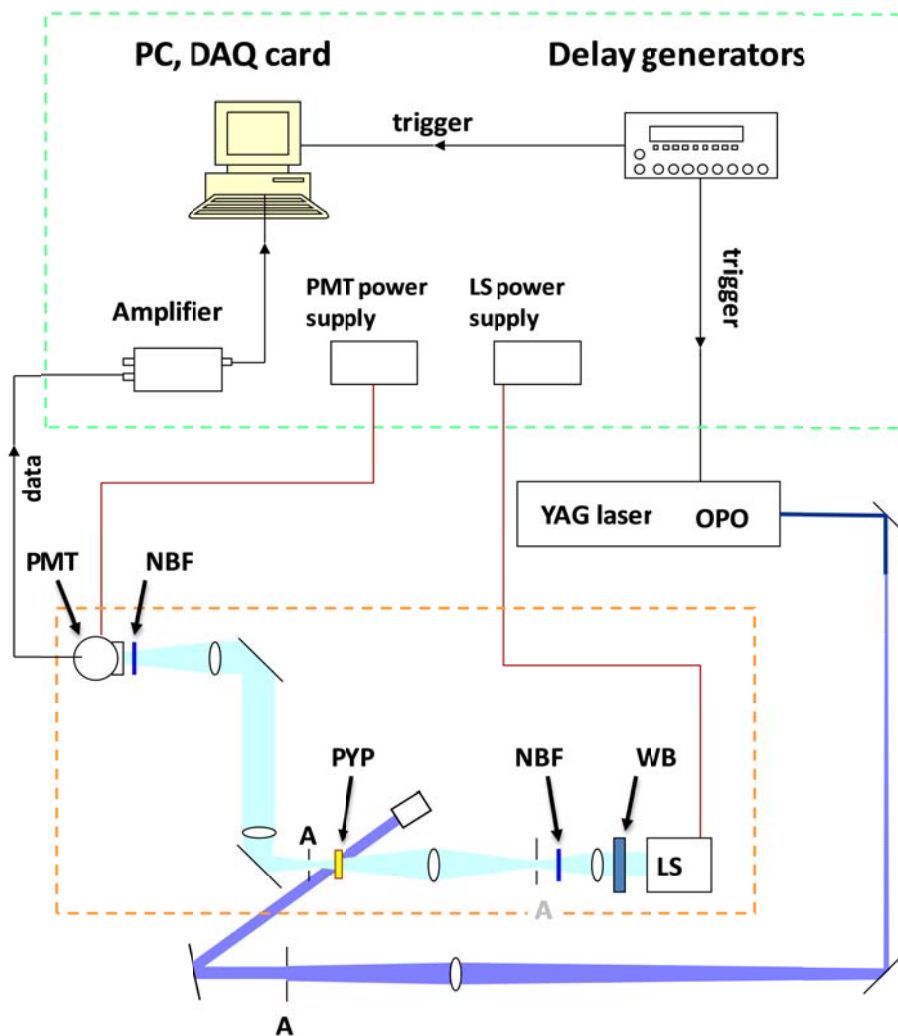


Figure 2.11. Schematics of flash photolysis system. The laser flash time was synchronized by delay generator. The abbreviations are as follows. LS: Light Source, WB: water bath, NBF: monochromator

CHAPTER III

IMPACT OF CRYSTALLIZATION SALT ON STRUCTURAL DYNAMICS OF PHOTOACTIVE YELLOW PROTEIN

Abstract

Water is essential for protein functions. Without water, most proteins would lose their biological activities. Solutions with high salt concentration change the stability and solubility of proteins. Despite extensive studies, it remains unclear how salts alter the properties of proteins. We report the effects of crystallization salts on the structural dynamics of photoactive yellow protein (PYP) which is an excellent model system. PYP is a structural prototype of PAS domain superfamily, a blue light photoreceptor protein for bacterial negative phototaxis. Time-resolved infrared difference spectroscopic technique is employed to capture the dynamic structural development of this protein upon light stimulation. Our data show that high salt concentration strongly suppresses protein conformational changes. The knowledge gained may be applicable to understand the other effects of salts on proteins, which is known as Hofmeister series.

Introduction

The proteins are dynamic in nature and its dynamics is regulated by the energy landscape of protein (Austin et al. 1975, Ansari et al. 1985). Proteins are complex molecules with different motions on the time scale from femto-seconds to few seconds (McCammon 1984, Henzler-Wildman et al. 2007). These motions in protein are broadly categorized into localized motions and collective motions

Photoactive yellow protein and its structural dynamics

Photoactive yellow protein (PYP) is a structural prototype of PAS domain proteins which are mainly regulating and signaling proteins. PYP is a blue light photoreceptor protein from *Halorhodospira halophila* (Hhal), discovered by T.E. Meyer in 1985 (Meyer 1985). In the receptor state of PYP (pG), negatively charged chromophore *p*-Coumaric acid (*p*CA) absorbs a blue light and drives PYP into photocycle. The PYP has a central β -sheet flanked by α -helices (Borgstahl et al. 1995). The *p*CA is attached to Cys69 through thioester linkage (Hoff et al. 1994). In the dark state (pG) of PYP *p*CA forms hydrogen bonds with Glu46 and Tyr42 (Borgstahl et al. 1995).

Upon absorption of blue light *p*CA photoisomerizes from 7-trans 9-s-cis conformation to 7-cis 9-s-trans configuration (Xie et al. 2001). The PYP signaling state is formed through large amplitude structural transformation. The photocycle of PYP is accompanied by four major steps and initiated by absorbing blue photon by anionic *p*CA. First step is isomerization of the *p*CA from 7-trans 9-s-cis conformer to 7-cis 9-s-trans conformer (pR state) which takes place on a time scale of ps-ns. At second step intramolecular proton transfers from Glu46 to the anionic *p*CA chromophore (pB' state) which takes place on a time scale of 250 μ s leading to the deprotonation of Glu46. At the next step the negative charge of COO⁻ of Glu46 (pB state) triggers a large conformational change resulting in the formation of the long lived signaling state. Last step is reisomerization of *p*CA from 7-cis 9-s-trans to 7-trans 9-s-cis and reprotonation of Glu46 (pG state) on time scale of 350 ms.

PYP undergoes large conformational changes in the signaling state (pB), however there was contradiction with different experimental techniques. The time-resolved X-ray study on protein suggested that the receptor state (pG) and signaling state (pB) are similar (Genick et al. 1997), however other studies contradict this experiment (van Brederode et al., 1996; Rubinstenn et al., 1998; Hoff et al., 1999). The issue was resolved by performing time-resolved FTIR spectroscopy on PYP crystal and PYP in solution (Xie et al. 2001). The experiment reveals that structural changes in solution during signaling state are suppressed in case of crystal. Further we conducted experiment on PYP in crystalline solutions (unpublished), which reveals that PYP structural changes in signaling state are reduced and interestingly the kinetics of PYP in crystalline solution 2.5 M $(\text{NH}_4)_2\text{SO}_4$ remains same as PYP solution. In PYP crystal photocycle kinetics is accelerated by ~ 10 times (manuscript in preparation). These results provide us motivation to study structural dynamics of PYP in high salt concentration.

The stability of biomolecules at high salt concentration has been studied for many years (Collins 2004), however the structural dynamics of proteins at high salt concentration has not been studied to our knowledge. Here we study structural dynamics of PYP at high salt concentration. To our knowledge this is the first study reporting on protein structural dynamics in crystalline salt solution. We employ time-resolved FTIR spectroscopy to study structural dynamics of photoactive yellow protein in high salt concentration solution.

Materials and methods

Protein purification. PYP gene was overexpressed in *E. Coli* BL21(DE3) as described in ref (Kumauchi et al. 2010). *E. Coli* Cells were grown in LB media with ampicillin 1000mg/L. Apo-PYP was induced by 1 mM IPTG, followed by cell lysis in 8 M urea. Apo-PYP was reconstituted with *p*-hydroxycinnamic anhydride as described in ref (Mihara et al. 1997). Purity index (PI) of PYP is defined by the ratio of $\text{Abs}_{278}/\text{Abs}_{446}$. The PYP was purified with successive anion exchange chromatography. The first anion exchange chromatography was performed with DEAE

Speharose at pH 8.5, followed by second anion exchange chromatography with Q-sepharose at pH 6.0. The 0-100 mM NaCl was used for gradient elution of protein. Purified PYP fractions with PI 0.43 or better were collected to perform the experiments.

Sample preparation: For FTIR absorption and time-resolved FTIR experiments, PYP samples were prepared in high salt concentration of $(\text{NH}_4)_2\text{SO}_4$ (CAS 7783-20-2, Sigma-Aldrich) and NaCl (CAS 7647-14-5, Sigma-Aldrich) as described below. The solution of 0.5 M $(\text{NH}_4)_2\text{SO}_4$ in D_2O was prepared and evaporated under dry N_2 flow until saturation to get 4.1 M $(\text{ND}_4)_2\text{SO}_4$. PYP samples with ~10 mM in deuterated 50 mM NaHPO_4 at pH * 6.90 were prepared in 0 to 2.5 M $(\text{ND}_4)_2\text{SO}_4$ by mixing various amount of buffered PYP in saturated $(\text{ND}_4)_2\text{SO}_4$ solution and centrifuged twice with microcon YM-10 filter at 14000 g. The solutions of 50 mM deuterated potassium phosphate buffer with 0.5 M, 1.0 M, 1.5 M, 2.0 M, 2.5 M, 3.0 M, and 4.0 M NaCl at pH* 7.50 were prepared. PYP sample were washed twice by adding 400 μl of NaCl buffer and centrifuged with microcon YM-10 at 14000 g to achieve ~ 10 mM PYP concentration.

The IFS 66v FTIR spectrophotometer (Bruker, Germany) was employed for FTIR absorption and time-resolved rapid-scan FTIR measurements.

FTIR absorption. The 2.7 μl of PYP samples were sandwiched in between two CaF_2 windows of 15 mm in diameter and 2 mm thick separated by 12 μm spacer. The Spectral resolution for FTIR absorption was 2 cm^{-1} with scanning mirror velocity of 40 kHz and 16 phase resolution. Water vapors were removed from optical path by vacuum. Sample chamber was purged with dry N_2 constantly at 4.47 liters per minute to reduce water vapors.

Further, home-made 3-sample exchanger driven by stepper motor (SI3540, Applied motion products) synchronized with FTIR spectrophotometer was implemented to record the IR absorbance spectra, which cancels water vapor absorbance significantly. This home-made 3-sample exchanger changes position of sample in translational direction upon receiving trigger from the FTIR instrument. Once sample position is changed, scan was recorded after 200 ms wait

time so that sample is stabilized at the position. The temperature of 3-sample exchanger was maintained to 300 K using water circulation system (Neslab, RTE-111).

Time-resolved FTIR difference spectroscopy: Time resolved measurements were performed in spectral range of 4000-900 cm^{-1} , at spectral resolution of 4.5 cm^{-1} with 200 kHz speed of scanning mirror and 16 phase resolution. The time-resolved FTIR difference spectroscopy for PYP samples in NaCl salt solutions were measured with 40 ms time resolution. Each of the spectra is the average of accumulations of 256 flashes. In case of PYP samples in $(\text{NH}_4)_2\text{SO}_4$ salt solutions, quadruple-split rapid-scan FTIR technique was employed to achieve better time resolution. In this technique one scan is divided into four equal parts by splitting the forward and backward scan into two, the resulting time-resolution obtained is 8 ms. The spectral resolution was 4.5 cm^{-1} with 200 kHz scanning velocity and 16 phase resolution. The laser flash was synchronized such that it arrives before starting of each quarter scan resulting the time resolution of 8 ms. The PYP photocycle was triggered by actinic laser pulses generated by a YAG laser (Quantel, Brilliant laser) pumped OPO (Opotek) tuned to 475 nm with pulse duration of 4 ns and energy of 3.0 mJ. The laser was synchronized with the FTIR spectrophotometer by delay generators (DG 535, Stanford Research System). The laser beam size at the sample was 6 mm in diameter. Time-resolved FTIR difference spectrums were computed by macro programming developed in OPUS software. The difference absorption spectrum was as the difference between the pB and pG states of PYP as

$$\Delta A(t, \nu) = d \cdot C_{\text{pB}}(t) \cdot [\epsilon_{\text{pB}}(\nu) - \epsilon_{\text{pG}}(\nu)].$$

The FTIR difference spectrum of PYP in various salt concentration solution was normalized with peak to peak amplitudes of 1497 and 1515 cm^{-1} signal. This normalization normalizes other chromophore bands i.e. 1162 cm^{-1} , 1054 and 1002 cm^{-1} as shown in supplementary figure 2.

Water molecules per ion in NaCl salt solutions: NaCl salt solutions were prepared at 27 °C in 10 ml water solution to calculate number of water molecules available per ion. NaCl was purchased

from sigma Aldrich (CAS no. 7647-14-5). To prepare 0.5 M, 1.0 M, 2.0 M and 4.0 M amount of NaCl was weighed as shown in table 2. The weighed amount of NaCl was transferred to 10 ml graduated cylinder. Then 7 ml of water was added to dissolve NaCl completely. Then water was added to make 10 ml of the solution. Water concentration of NaCl solution was estimated on the basis of added water to NaCl.

Results and discussion:

Crystallization salt suppresses PYP structural dynamics

We have studied effect of crystallization salt solution on structural dynamics of PYP with $(\text{NH}_4)_2\text{SO}_4$ and NaCl. These two inorganic salts are most frequently used as crystallization reagents to obtain protein crystals (Lu et al. 2012). The first PYP crystal structure with $P6_3$ symmetry was obtained at 2.5 M $(\text{NH}_4)_2\text{SO}_4$ (Borgstahl et al. 1995). The three dimensional plots from time-resolved FTIR difference absorption signals of PYP photocycle in $(\text{NH}_4)_2\text{SO}_4$ salt solutions is plotted in Figure 1A. The positive and negative amplitudes in difference absorption spectra correspond for photointermediate state and dark state of PYP during its photocycle respectively. The three dimensional plot shows a 2D plot on bottom which reflects the amplitude change on the three dimensional difference absorption plots.

Effect of ammonium sulfate on PYP structural dynamics

The series of three dimensional FTIR difference absorption plots shows that the concentration of $(\text{NH}_4)_2\text{SO}_4$ is increased, the amplitudes for bands 1642 and 1624 cm^{-1} decreases. The positive signal at 1624 cm^{-1} decays in case of PYP in no salt solution. However in case of PYP in $(\text{NH}_4)_2\text{SO}_4$ salt solutions with concentration from 0.5 M to 2.5 M $(\text{NH}_4)_2\text{SO}_4$ the signal at 1624 cm^{-1} rises initially and decays later for as shown in Figure 3.1A.

Structural markers of PYP in FTIR difference absorbance: The light induced time-resolved FTIR difference spectrum of PYP yields changes in molecular structure. The following

are important structural markers of PYP in FTIR pB-pG difference spectrum during PYP photocycle which has been discussed previously (Xie et al. 1996, Hoff et al. 1999, Xie et al. 2001). (i) 1726 cm^{-1} : The negative signal at 1726 cm^{-1} arises due to νCO of protonated carboxylic group of Glu46 in pG. (ii) 1689 cm^{-1} : This signal is related to structural transition during protein quake of PYP after photoexcitation. (iii) $1642/1624\text{ cm}^{-1}$: these signals arise due to C=O stretching of protein backbone (Amide I), (iv) $1497/1515\text{ cm}^{-1}$: these signals arise due to pCA deprotonation (1497 cm^{-1}) in pG and pCA protonation (1515 cm^{-1}) in pB.

The light induced pB-pG FTIR difference absorption spectrum of PYP in $(\text{NH}_4)_2\text{SO}_4$ salt solutions with concentration from 0.5 M to 2.5 M $(\text{NH}_4)_2\text{SO}_4$ at 17 ms reveal the structural changes after the photoexcitation. Increase in the concentration of $(\text{NH}_4)_2\text{SO}_4$ salt reduces amplitudes at 1624 cm^{-1} , 1642 cm^{-1} and 1689 cm^{-1} . The reduction in amplitudes at 1624 cm^{-1} and 1642 cm^{-1} shows that protein conformational changes are smaller in presence of $(\text{NH}_4)_2\text{SO}_4$ salt solutions. The new positive peak arises in FTIR difference absorption spectrum of PYP in $(\text{NH}_4)_2\text{SO}_4$ salt solutions at 1751 cm^{-1} . The peak in the region of $1700\text{-}1780\text{ cm}^{-1}$ corresponds for C=O stretching of protonated carboxylic group (Xie et al. 1996, Xie et al. 2001, Nie et al. 2005). The 1751 cm^{-1} signal shows that Glu46 is remaining protonated in pB intermediate state of PYP. Also as the C=O stretching frequency of Glu46 is upshifted shows that Glu46 has lower hydrogen bond partners and has more hydrophobic environment in pB intermediate than pG (Nie et al. 2005).

Apart from these signals, the positive peaks at 1605 , 1591 , 1561 cm^{-1} in pB intermediate of PYP in 0 M $(\text{NH}_4)_2\text{SO}_4$ are diminished in case of high salt concentration of $(\text{NH}_4)_2\text{SO}_4$ (Figure 1B). The $1610\text{-}1560\text{ cm}^{-1}$ region corresponds for different polar side chain groups with double bonds (Venyaninov et al. 1990). The change in structural transition of PYP in $(\text{NH}_4)_2\text{SO}_4$ salt solutions after photoactivation is plotted in Figure 3.1C. The structural transition is directly corresponds to amount of change in the conformation of PYP after photoactivation. At 1.5 M in $(\text{NH}_4)_2\text{SO}_4$ salt solution PYP's structural transitions are suppressed significantly.

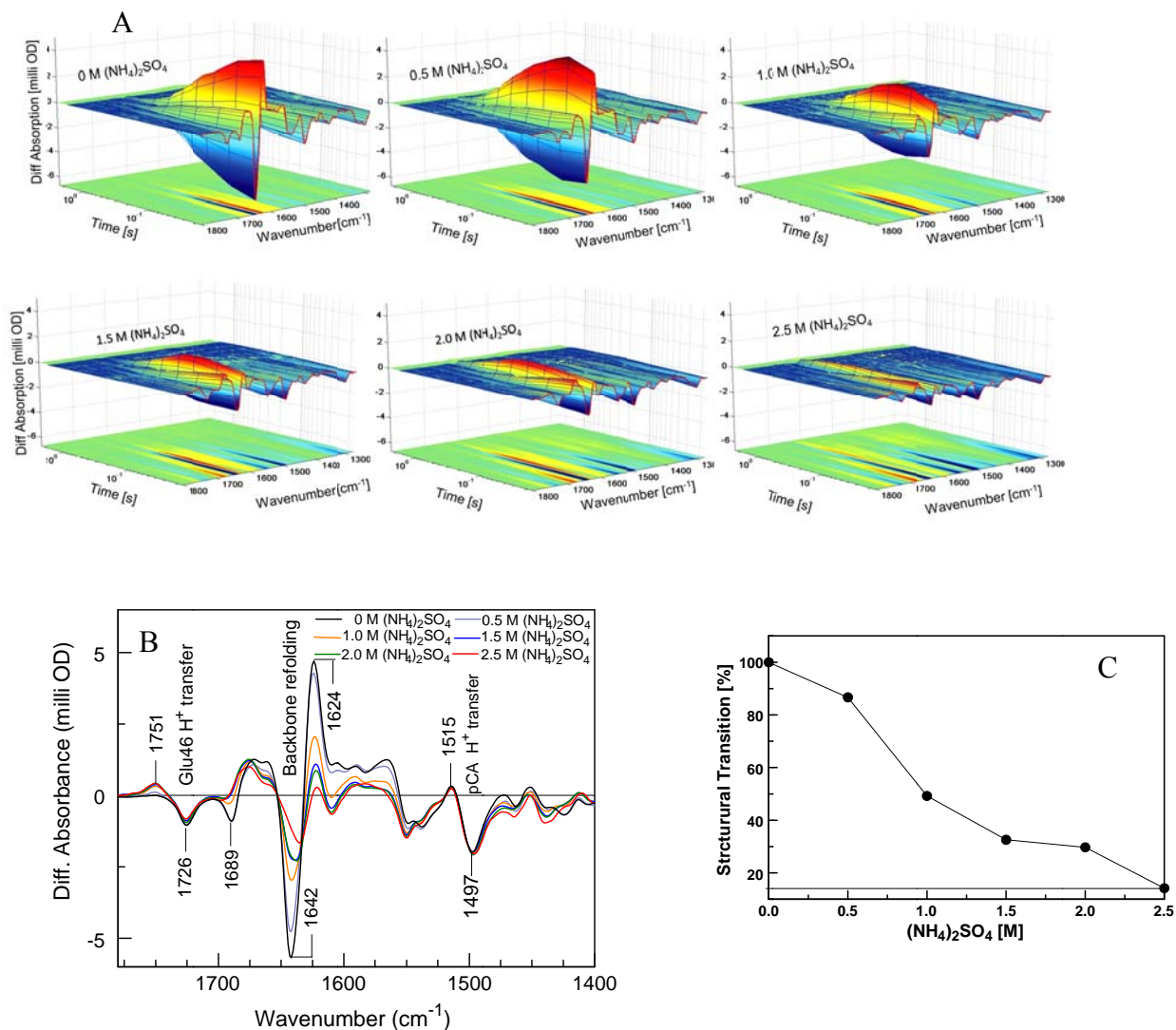


Figure 3.1: 3-D time-resolved FTIR difference absorption spectroscopy of PYP in series of $(\text{NH}_4)_2\text{SO}_4$ salt concentrations recorded from 17 ms to 2 s at pH* 7.00 and 300 K. The large amplitude in 3D plot corresponds to amide-I (backbone structure) of PYP, at 0M salt concentration these amplitudes are larger, as salt concentration increases the amplitude of amide-I reduces (A). The amplitude of amide-I (1642 and 1624 cm^{-1}) in pB-pG difference spectra reduce as salt concentration is increased (B). The structural transition of PYP (peak to peak amplitude of amide-I in pB-pG difference absorption) versus $(\text{NH}_4)_2\text{SO}_4$ salt concentration (C).

In case of NaCl salt series, PYP solution was prepared at pH* 7.50 as, below pH* 7.50 the PYP's light induced difference absorption shows a small positive peak at 1750 cm^{-1} which shows that Glu46 is protonated in pB state (unpublished). This signal is a structural feature of pB-pG light induced FTIR difference spectrum. If Glu46 is fully deprotonated in pB it yields largest amide-I amplitude, otherwise amide-I amplitude is smaller. So we performed experiments for PYP in NaCl salt solution series at pH* 7.50.

Effect of NaCl on PYP structural dynamics: We examine effect of NaCl on structural dynamics of PYP during photocycle by performed time-resolved rapid-scan FTIR difference absorption spectroscopy (Figure 3.2). The secondary structure of PYP remains same even at 4.0 M NaCl concentration (See supplement Figure 1), indicating pG or dark state of PYP remains same and overall protein folding is retained same as in native state. The 3-dimensional plot of time-resolved provides information of structural changes as well as kinetics during photocycle of PYP.

In presence of NaCl high salt concentration ($> 1.0\text{M}$), the amide-I peak to peak difference absorption of PYP light induced IR infrared spectrum reduces this clearly shows that at high salt concentration PYP conformations are suppressed during signaling state. The amplitude of the 1624 cm^{-1} positive and the 1641 cm^{-1} negative bands become smaller at high salt concentration. At 3.0 M NaCl concentration PYP conformational changes in pB state are completely suppressed at 3.0 M NaCl salt concentration. The structural changes of pB state in NaCl salt concentration. For the lowest 0.5 M concentration the difference amplitude between 1624 cm^{-1} and 1641 cm^{-1} band is 12.6 mOD, while for 4.0 M one it is only 2.7 mOD. This suggests that the signaling state of high salt containing PYP sample has different conformation than that of 0 M salt (Figure 3.2B).

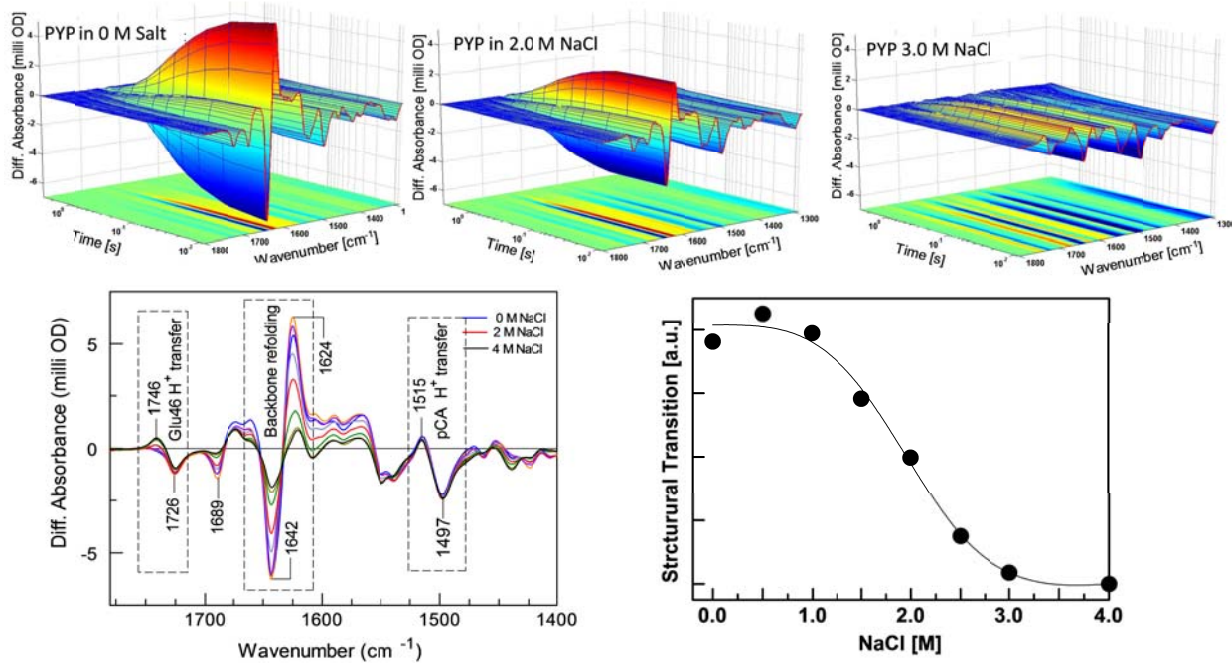


Figure 3.2: 3-D time-resolved FTIR difference absorption spectroscopy of PYP in series of NaCl salt concentrations recorded from 40 ms to 8 s at pH* 7.50 and 300 K. (A). The normalized (see methods) light induced FTIR difference absorbance spectra of PYP at 40 ms after photoexcitation in series of NaCl salt concentrations (B). The structural transition of PYP (peak to peak amplitude of amide-I in pB-pG difference absorption) versus NaCl salt concentration (C).

The pB state of PYP in high salt concentration, the positive peak at 1746 cm^{-1} is due to C=O stretching of protonated Glu46. The upshift in C=O stretching of Glu46 show that in pB state of PYP has lower hydrogen bonds (Nie et al. 2005) than in pG state and Glu46 in pB is in more hydrophobic environment than that of pG state. The band negative band at 1689 cm^{-1} and positive peaks in the region of $1620\text{-}1550\text{ cm}^{-1}$ are reduced in amplitude.

The structural features at high salt concentrations are altered and similar as $(\text{NH}_4)_2\text{SO}_4$. Only major difference in case of NaCl is, in pB state the C=O stretching frequency of Glu46 is at 1742 cm^{-1} compared that to 1751 cm^{-1} in case of $(\text{NH}_4)_2\text{SO}_4$. The peak at 1751 cm^{-1} due to C=O stretching is also observed in case of PYP at low pH. The change in C=O stretching in pB like state of PYP in presence $(\text{NH}_4)_2\text{SO}_4$ and NaCl can be attributed to two things. Firstly, in presence of $(\text{NH}_4)_2\text{SO}_4$ the E46 is experiencing more hydrophobic environment compared to NaCl since the ν_{CO} is higher in case of $(\text{NH}_4)_2\text{SO}_4$ (Nie et al. 2005). Secondly it could happen that the E46 in different salt condition has different configurations specially the hydroxyl group of carboxylic side.

Structural transition

Comparative structural suppression of PYP in high salt concentration can be studied by finding difference amplitude of amide-I in pB and pG state. We have plotted structural transition of amide-I band at different salt concentration (Figure 3.2C). At 2.0 M NaCl, the amplitude of amide-I suppressed by ~50% compared to 0 M salt concentration (Figure 3.2C). At 3.0 M and 4.0 M NaCl, the conformational changes of PYP in pB state are reduced to such extent that structural transitions are saturated (Figure 3.2C). Structural transitions are most sensitive at 2.5 M NaCl, because transitions are suppressed to more than half compared to 0 M salt concentration. Based on this fact, we choose 2.5 M salt concentration to study effect of cations on the structural dynamics of PYP.

Effect of cations on PYP structural dynamics

The effect of cations on structural dynamics of PYP was studied at 2.5 M alkali chloride concentration. The alkali ions were Li^+ , Na^+ , K^+ and Cs^+ . The difference absorption of PYP in alkali chloride has similar features to NaCl series. However the suppression of structural dynamics at same concentration of alkali chloride differs. We found that Na^+ is most suppressive, while Cs^+ is least suppressive in terms of change in conformations of PYP after photoexcitation (Figure 3.3), by comparing peak to peak amide-I signal. These ions have same charge but their ionic radius and co-ordination number in first hydration shell are different (see Table 3.1). The ionic radius for Li^+ , Na^+ , K^+ , Cs^+ is 0.59, 1.02, 1.37, 1.67 Å, respectively (Lide et al. 1997-1998). The order of the suppression of structural dynamics does not follow the Hofmeister series. The suppression of structural dynamics is due to two elements ionic radius and coordination number of ion. Both of these factors influence the hydration of protein and results in different structural suppression.

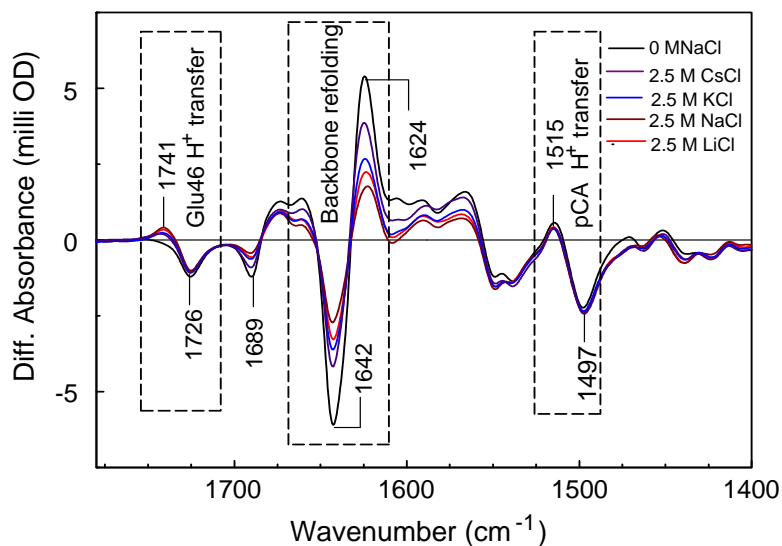


Figure 3.3. Light induced pB-pG FTIR difference absorption spectrum of PYP in alkali chloride salts at 40 ms after photoexcitation at pH* 7.50 and 300 K. The difference absorption spectrum shows that NaCl suppresses conformational dynamics most comparative to other alkali chloride salts.

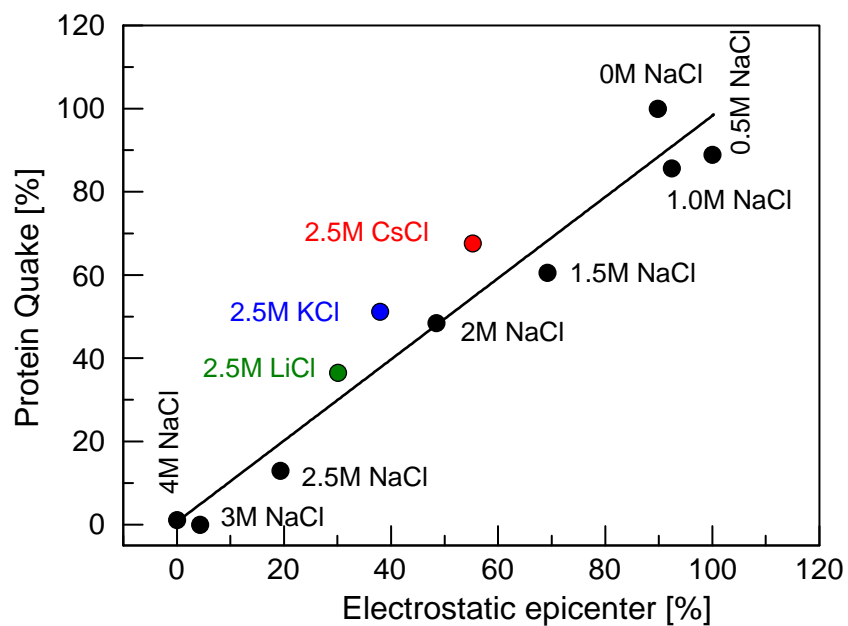


Figure 3.4: Change in the Amide-I amplitude while pG to pB transition represents protein quake, while amount of Glu46 deprotonation in pB represents electrostatic epicenter.

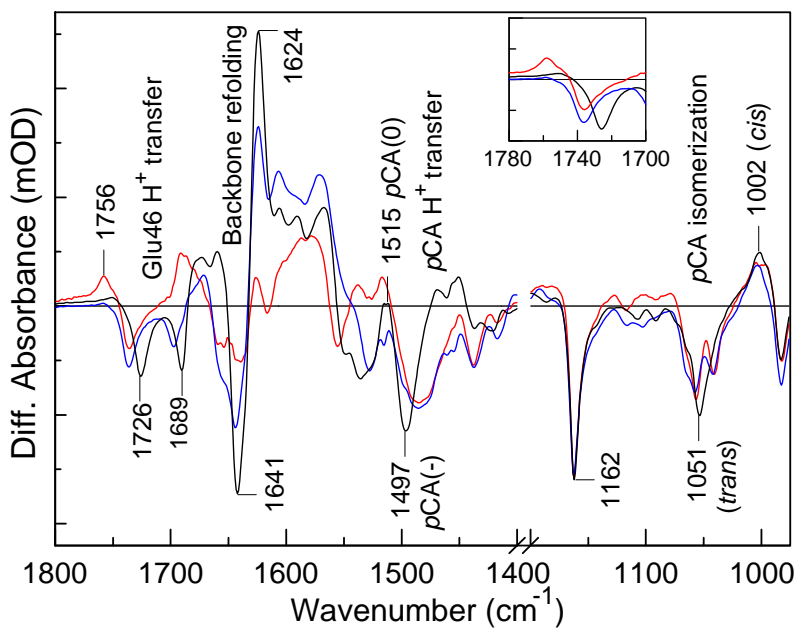


Figure 3.5. The light induced FTIR difference absorption spectrum of PYP film for hydrated in H₂O(blue) hydrated in D₂O (black) and reduced hydration (red).

Effective dehydration of PYP at high salt concentration

The conformational changes are smaller for the putative signaling pB intermediate state of PYP at high salt concentration (Figure 3.1 & 3.2). The protein conformation changes are assisted by its environmental conditions. To perform the biological function protein undergoes a structural change. The transition from a one structure to other structure of protein is energy driven as protein molecule finds a local minimum on energy landscape (Frauenfelder et al. 1991). The equilibrium can be shifted by changing reaction coordinate, for instance, pH, temperature or pressure (Frauenfelder et al. 2009).

Proteins are dynamic in nature and it needs water molecules to guide the conformational changes. At room temperature hydration of protein is divided into three layers. The first hydration layer of water is closest to protein surface and this layer is strongly in interaction with protein through hydrogen bonding. The water in second hydration layer interacts with water in first hydration layer and third hydration layer is the surrounding bulk water (Fenimore et al. 2004). The molecular dynamics simulations indicate the hydration layer of a biomolecule is ~ 10 Å (Ebbinghaus et al. 2007) which is more than 3 times of diameter of water molecule. However experimental result with terahertz absorption spectroscopy reveals that dynamic hydration layer of a biomolecules is larger than 10 Å and is up to 18 Å from molecule surface (Born et al. 2009). This concludes that a biomolecule has at least two layers of water molecules for its hydration.

The PYP film with low hydration level and high hydration level has ~ 350 and ~ 1000 water molecules respectively (Hoff, 1999). The light induced FTIR difference spectrum of PYP film with low and high hydration is shown in figure 5. The high hydration film shows a large change in the conformation after photoactivation while film with low hydration of shows smaller conformational change (Figure 5). The low hydration level suggests that PYP is hydrated to its first hydration shell while in 2nd hydration shell is weakly hydrated. As PYP molecule is highly

hydrated the 2nd and 3rd hydration shells of PYP are complete and protein is able to retain its conformational changes

The diameter of PYP molecules is $\sim 30 \text{ \AA}$ (Getzoff et. al 2003). Here we approximate first hydration layer around PYP molecule is 3 \AA away from surface of PYP. To estimate water molecules in first hydration shell of PYP. The volume between first hydration layer and protein surface is $\sim 10300 \text{ \AA}^3$. The density of liquid water is 1 g/cm^3 at room temperature, which yields volume of 1 water molecule to be $\sim 30 \text{ \AA}^3$. This suggests that the PYP will have ~ 350 water molecules for its first hydration shell. Again we approximate the second hydration layer of PYP molecules is 3 \AA distance from the first hydration layer. The volume between first and second hydration layer yields $\sim 14360 \text{ \AA}^3$, thus there will be ~ 470 water molecules. Thus combining first two hydration shells yields ~ 830 water molecules per PYP molecule.

Crystalline PYP in space group $P6_5$ and $P6_3$ contains ~ 390 and ~ 325 water molecules per PYP molecule respectively (Yeremenko et al. 2006), which is of the order of low hydration level as explained by Hoff et al. 1999 (Hoff et al. 1999).

The dehydration effects of protein on conformational changes have been noticed in bacteriorhodopsin (bR) (Varo et al. 1987), lysozyme (Careri 1979) by employing IR spectroscopy. In case of bacteriorhodopsin, conformational change is significant when hydration level is $0.05\text{-}0.06 \text{ g H}_2\text{O/ g bacteriorhodopsin}$ (Varo et al. 1987), however the saturation of conformational changes occurs when hydration level is $\sim 0.1 \text{ g H}_2\text{O/g bacteriorhodopsin}$. This ratio suggests that $\sim 150\text{-}200$ water molecules are required per bR protein molecule to retain its full functional form. The bR is a trimer protein molecule, and the exposed surface area of bR on intracellular and extracellular is $\sim 780 \text{ \AA}^2$. (PDB ID : 1M0L) (Schobert et al. 2002). The water molecules available for 780 \AA^2 will be ~ 75 . So when bR is hydrated with $h=0.05$ hydration ratio, the exposed solvent area has minimum of 1 layer of water molecules. This was confirmed by

monitoring absorption of amide-I and amide-II bands using infrared spectroscopy. Thus dehydration of protein leads to smaller conformational changes during its activation.

The qualitative reasoning for dehydration of PYP in high salt concentration is provided below. The hydration shells of ions and proteins in high salt solutions are affected. The ion hydration has three shells of water molecules surrounding it. The first shell of ion hydration has strongly ordered water molecules, second hydration shell has semi ordered water molecules. The water molecules beyond first and second hydration shells of ion are treated as a bulk water molecule. The first hydration shell is strongly organized and has a definite number of water molecules. In case of Na^+ and Cl^- ions the first hydration shell has 5 and 7 water molecules respectively in equilibrium (Mason et al. 2006). The water concentration is 55.5 M at 27°C. As salt concentration is increased the water concentration is reduced. We estimated water concentration at various NaCl salt concentrations. At 4.0 M NaCl concentration, the water concentration in solution reduces to 50 M (See Table 3.3). As one molecule of NaCl dissociate after dissolving into water, it would require 12 water molecules to complete the first hydration shell. Thus at 4.0 M NaCl salt concentration at least 48 M of water molecules are engaged in first hydration shell leaving only 2.0 M water molecules for second hydration shell and bulk water.

The interaction between protein, water and ions is dynamic process. The water molecule in the hydration shell of ion can be exchanged and also reoriented. This result shows that ionic solutions influences water structure beyond first hydration shell. Overall ions disorder the water structure and orients water molecule away from tetrahedral structure.

When protein is dissolved in water containing high salt concentration, both protein and ions will be competing for water molecules. Our estimation of water concentration at high salt solution suggests both protein and ions will be deprived of second shell and bulk water molecules of hydration. Thus proteins are effectively dehydrated at high salt concentration.

Table 3.1: Co-ordination number of cations in first hydration shell

Solute	Concentration	Co-ordination number	Ion-Oxygen Distance (Å)	Method	Reference
Li⁺					
LiCl	18.5 m	4 (±1)	2.25	X-ray Diffraction	(Narten et al. 1973)
LiCl	3.6 m	6.0 (±0.30)	1.95 (±0.04)	NDIS	(Howell et al. 1996)
LiCl	1 m	6.5 (±0.65)	1.96 (±0.04)	NDIS	(Howell et al. 1996)
Na⁺					
NaCl	4 m	5.0 (±0.25)	2.3	ND Null Water	(Mason et al. 2006)
NaCl	1 M	8	2.50 ±0.10	ND	(Ohtomo et al. 1980)
K⁺					
KCl	4 m	5.3 (±0.32)	2.6	ND	(Neilson et al. 1985)
KCl	1 M	8	3.10±0.05	ND	(Ohtomo et al. 1980)
Cs⁺					
CsCl	10 m, 5m	2-3	3.15	X-ray Diffraction	(Lawrence et al. 1967)
CsCl	2.5 m	3-4	3.15	X-ray Diffraction	(Lawrence et al. 1967)
Cl⁻					
LiCl	10 m	6-7	3.20	X-ray Diffraction	(Lawrence et al. 1967)
LiCl	5 m	5-9	3.20	X-ray Diffraction	(Lawrence et al. 1967)
NaCl	4 m	7.4 (0.59)	-	ND Null Water	(Mason et al. 2006)
KCl	2.75 m	6	-	X-ray Diffraction	(Terekhova et al. 1969)

m: molality, M: Molarity NDIS: Neutron diffraction and isotopic substitution, ND: Neutron Diffraction

Table 3.2. Number of water molecules at various NaCl salt concentrations.

NaCl (M)	NaCl (mg)	water (ml)	H ₂ O Concentration (M)	Number of H ₂ O molecules per ion
0	0	10	55.5	0
0.5	292.2	9.84	54.4	54.4
1.0	584.4	9.74	54.4	26.95
2.0	1168.8	9.58	53.0	13.25
4.0	2337.6	9.03	50.0	6.25

Table 3.3. Distances between charged residues in $\Delta 25$ pG and pB solution NMR structures for 5 conformations out of 20

Residue pair	$\Delta 25$ pG structure (PDB ID:1XFN)					$\Delta 25$ pB structure (PDB ID:1XFQ)				
	Å					Å				
D53-K55	10.0	12.5	11.5	7.4	7.1	5.4	3.4	11.1	11.3	3.7
D65-K60	3.6	3.7	7.1	6.2	3.3	9.9	12.3	3.5	4.4	10.5

The protein surface develops charges as charged amino acids are exposed to the environment. In PYP, there are 17 negative and 6 positive charged amino acids exposed to surface, while 1 negative and 8 positive charges are partially exposed on the protein surface at neutral pH (Getzoff et al. 2003). The charged side chain on protein surface can interact with each other through electrostatic interaction. The change in electrostatic interaction energy between two charges is calculated by $\Delta u = \frac{q_1 q_2}{4\pi\epsilon_0\epsilon_r} \left(\frac{1}{r_2} - \frac{1}{r_1} \right)$, where q_1 and q_2 are charges, r is the distance between two charges, and

In PYP there are mainly 3 regions which undergoes into large structural changes in pG to pB transition. These regions are residue 1 to 25, 44 to 77 and 94 to 103 (Bernard et al. 2005). So ~50% of PYP residues undergoes structural transition from pG to pB state. We predict that such transition can be inhibited in presence of high salt concentration as protein becomes effectively dehydrated. We have identified residues which can interact through electrostatic interaction on protein surface in the regions mentioned above by studying high resolution crystal structure.

Electrostatic interactions of residue Lys110 with residues Glu9, Asp10, and Glu12 are shown in Figure 3.6 A. The separation distance between ionic atoms of Glu12 and Lys110 is 2.69 Å and 3.49 Å. Similarly the separation distance between ionic atoms of Asp48 and Arg124 is 2.91 Å and 3.92 Å (Figure 6B). Also the separation distance between Lys60 and Asp65 is 5.13 and 5.57 Å (Figure 3.6C).

The native environment of protein is water. As PYP changes its conformation from pG to pB transition these charged residues are separates further. Approximating the closest distance

between charged residue pair to $\sim 5.0 \text{ \AA}$ in the pG state of PYP, yields the magnitude of electrostatic energy between these charge pair on surface $\sim 275 \text{ kJ/mol}$ in the vacuum or dry, while the same charged residues yields $\sim 3 \text{ kJ/mol}$ interaction energy when PYP is fully hydrated. One conformation among 20 of $\Delta 25 \text{ pG}$ and $\Delta 25 \text{ pB}$ structure of solution NMR shows that in pG state the distance between charged residues Asp65 and Lys60 could be as close as 3.3 \AA while in pB state these residues are separated by 12.3 \AA apart (see Figure 3.7 and Table 3.4) (Bernard et al. 2005). The electrostatic interaction energy between these residues will be $\sim 187 \text{ kJ/mol}$ in vacuum (dry) and $\sim 1.5 \text{ kJ/mol}$ in water. The electrostatic energy difference between these two residues in pB and pG state in will be $\sim 187 \text{ kJ/mol}$ and 1.5 kJ/mol in vacuum and water respectively. In case of water the energy difference is of the order of thermal energy, while in vacuum or dry environment the energy difference is so high that protein may not be able to change the conformation as it is energetically unfavorable. This gives a relative idea that protein in water has energetically favorable conditions than the vacuum (dry) and protein conformational changes are energetically favorable in water than in its dry form.

The conformation change of protein requires the water molecules. In high salt concentration, data presented here suggest that protein is able to change the conformation, however they are smaller. At high salt concentration, the hydration shell of protein and salt has water molecules available for first hydration shell. The exchange of water molecules from the hydration shell of protein and salt seems to be slower in case of high salt concentration salt. Thus at high salt concentration it appears that the conformational dynamics is slowed due to the exchange between the hydration shells. This hypothesis should be confirmed by designing the mutants with slower photocycle of PYP N43 or M100 which has longer lifetime for pB intermediate (Kumauchi et al. 2010, Philip et al. 2010).

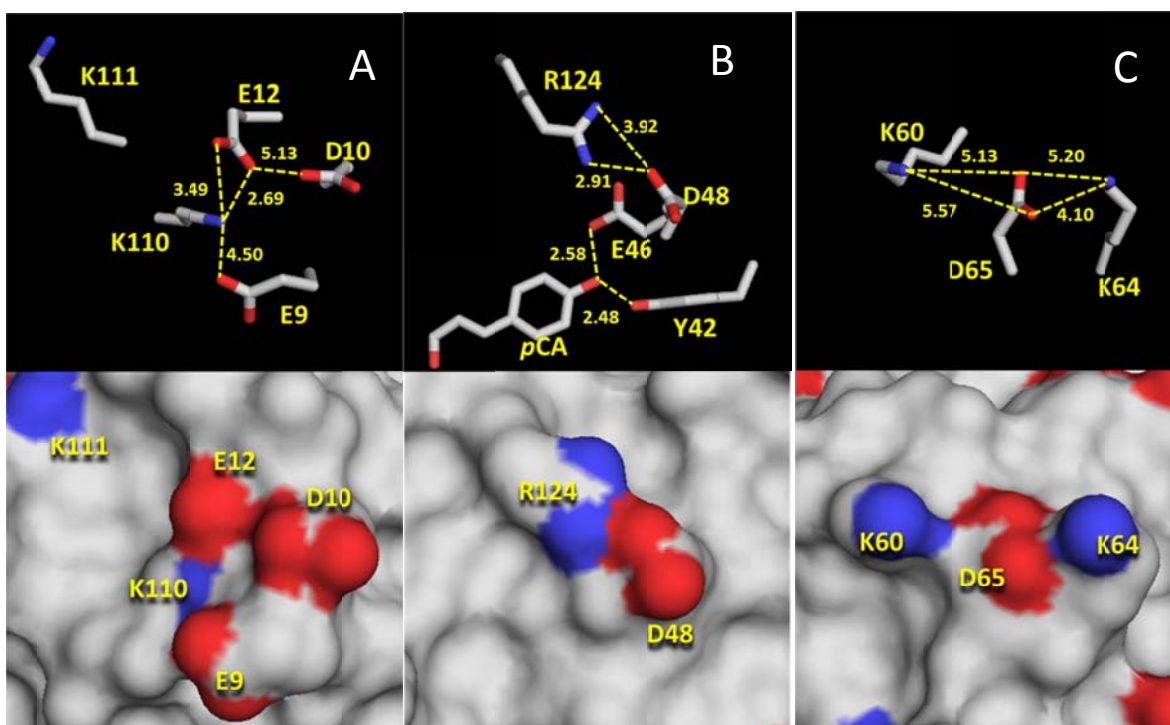


Figure 3.6: Electrostatic interaction of residues on PYP surface: Electrostatic interaction between Glu9-Lys110, Asp10-Lys110, Glu12-Lys110 (A), Asp48-Arg124 (B) and Lys60-Asp65 (C). The top panel shows side chain residues and their separation between ionic atoms in Å, while lower panel shows same view of residues with solvent exposed surface (calculated with 1.4 Å probe by pymol, PDB ID: 1NWZ)

Conclusions

We study structural dynamics of PYP at high salt concentration. High salt solutions suppress structural transition and structural dynamics of PYP.

Proteins structural dynamics is influenced by its microenvironment, altering the microenvironment changes energy landscape of protein. In case of PYP, high salt concentration reduced structural motions in signaling state. In physiological conditions PYP undergoes large structural changes during its signaling state. The large structural change is mainly due to motion of N-terminus region and flexible regions from residue 44-78 (Bernard et al. 2005) . These

collective motions appear to reduce in presence of high salt concentration. Data presented here suggests that protein at high salt concentration protein dynamics can affect processes like protein-protein interaction, protein-ligand binding.

The stability of protein in high salt concentration has been addressed in many research articles. The data presented here provides insight to understand the structural dynamics events of protein in functional state and it can be applied to understand Hofmeister effect?

Acknowledgements: AX acknowledges support from OCAST grants HR02-137R and HR10-078.

Supporting information Available: The structural stability of PYP at high salt concentration by FTIR absorbance; Normalization of light induced FTIR difference absorption spectrum of PYP in salt concentration w.r.t. peak to peak difference of 1515 cm^{-1} and 1497 cm^{-1} signal.

CHAPTER IV

STRUCTURE-FUNCTION RELATIONS IN PHOTOACTIVE YELLOW PROTEIN

Protein functions are highly dependent on its native state structure. If proteins are not folded properly, it cannot perform its usual function.

So far in PYP family 14 PYP has been found from different bacteria (Kumauchi et al. 2008). These PYP varies in their structural similarity. The most studied PYP is from Hhal. Here we report two different approaches to unravel structure function relation in PYP. The native structure similarity was deciphered by IR absorbance, while structure after activation of PYP was deciphered by time-resolved FTIR difference spectroscopy.

CHAPTER 4.1

Locked chromophore analogs reveal that photoactive yellow protein regulates biofilm formation in the deep sea bacterium *Idiomarina loihiensis*

Michael A. van der Horst¹, T. Page Stalcup², **Sandip Kaledhondar**³, Masato Kumauchi²,

Miwa Hara², Aihua Xie³, Klaas J. Hellingwerf¹, and Wouter D. Hoff^{2#}

¹Department of Molecular Microbial Physiology, Swammerdam Institute for Life Sciences, University of Amsterdam, the Netherlands; ²Department of Microbiology and Molecular Genetics and ³ Department of Physics, Oklahoma State University, Stillwater, OK 74078, USA.

[#]To whom correspondence should be sent: Department of Microbiology and Molecular Genetics, Oklahoma State University, 307 Life Sciences East, Stillwater OK 74078. E-mail: wouter.hoff@okstate.edu

Reprinted with permission from (J. Am. Chem. Soc. 2009, 131: 17443-17451) Copyright (2009) American Chemical Society

Abstract: *Idiomarina loihiensis* is a heterotrophic deep sea bacterium with no known photobiology. We show that light suppresses biofilm formation in this organism. The genome of *I. loihiensis* encodes a single photoreceptor protein: a homolog of photoactive yellow protein (PYP), a blue light receptor with photochemistry based on *trans* to *cis* isomerization of its *p*-coumaric acid (*pCA*) chromophore. The addition of *trans*-locked *pCA* to *I. loihiensis* decreases biofilm formation, while *cis*-locked *pCA* increases it. This demonstrates that the PYP homolog regulates biofilm formation in *I. loihiensis*, revealing an unexpected functional versatility in the PYP family of photoreceptors. These results imply that *I. loihiensis* thrives not only in the deep sea but also near the water surface, and provide an example of genome-based discovery of photo-physiological responses. The use of locked *pCA* analogs is a novel and generally applicable pharmacological tool to study the *in vivo* role of PYPs irrespective of genetic accessibility. Heterologously produced PYP from *I. loihiensis* (II PYP) absorbs maximally at 446 nm, and has a

*p*CA pK_a of 3.4. Photoexcitation triggers the formation of a pB signaling state that decays with a time constant of 0.3 seconds. FTIR difference signals at 1726 cm⁻¹ and 1497 cm⁻¹ reveal that active site proton transfer during the photocycle is conserved in Il PYP. It has been proposed that a correlation exists between the lifetime of a photoreceptor signaling state and the timescale of the biological response that it regulates. The data presented here provide an example of a protein with a rapid photocycle that regulates a slow biological response.

4.1.1 Introduction

Living organisms use a limited number of types of photoreceptor proteins to obtain information about their ambient light climate. These photoreceptor proteins can be grouped into different families, based on their structure and light-absorbing co-factor (Van der Horst et al. 2004). Until very recently, such photoreceptor proteins had been found exclusively in phototrophic microorganisms. However, genome sequencing projects have uncovered many examples of photoreceptor proteins in chemotrophic microorganisms (van der Horst et al. 2007, Purcell et al. 2008). Bioinformatics analyses showed that members from most known photoreceptor protein families are present in chemotrophic Bacteria. Most of these have not been characterized regarding their *in vivo* function or *in vitro* biochemical and photophysical characteristics. The wide-spread occurrence of as yet unstudied photosensory proteins revealed by genome projects indicates that many additional unanticipated photobiological responses in chemotrophic bacteria remain to be discovered.

One example of a chemotrophic bacterium with a photoreceptor encoded in its genome is the deep-sea bacterium *Idiomarina loihiensis*. This organism belongs to the group of γ -proteobacteria, and was isolated at 1 km depth in the Hawaiian ocean (Donachie et al. 2003). The genome of *I. loihiensis* contains a cluster of 32 genes that encode proteins involved in the production and secretion of polysaccharides (Hou et al. 2004). This prompted us to study biofilm

formation in *I. loihiensis*. In parallel, we examined the genome of *I. loihiensis* for the presence of photoreceptor proteins from all five established photoreceptor families that can be unambiguously recognized based on their sequence (Van der Horst et al. 2004), and a single photoreceptor gene was identified (van der Horst et al. 2007). This gene encodes a protein that shows clear homology to photoactive yellow protein (PYP) (van der Horst et al. 2007, Kumauchi et al. 2008). This blue-light photoreceptor protein was first found in *Halorhodospira halophila* (Meyer 1985, Meyer et al. 1987), and its physico-chemical properties have been well characterized (Cusanovich et al. 2003, Hellingwerf et al. 2003, Imamoto et al. 2007). Studies on the properties of 9 additional PYPs have been initiated (see (Kumauchi et al. 2008) for a review). This work has led to a detailed understanding of PYP photochemistry. Light activation of the initial pG state of PYP (λ_{\max} 446 nm) involves the photo-isomerization of the vinyl bond of its *p*-coumaric acid (*pCA*) chromophore from *trans* to *cis*, resulting in the short-lived, red-shifted pR state. Subsequent protonation of the *pCA* by Glu46 (Xie et al. 1996, Xie et al. 2001) causes formation of the pB' state, and subsequently leads to structural changes in the protein that result in the formation of the blue-shifted pB state (λ_{\max} 355 nm). The pB state is the presumed signaling state of PYP. The protein then thermally recovers to its pG groundstate on a time scale that ranges from 1 millisecond for the PYP from *Rhodobacter sphaeroides* (Haker et al. 2000), to ~0.5 seconds for the PYP from *H. halophila* (Hh PYP) (Meyer et al. 1987, Hoff et al. 1994), to ~1 hour for the PYP from *Salinibacter ruber* (Kumauchi et al. 2008, Memmi et al. 2008).

Examination of the *I. loihiensis* genome (Hou et al. 2004) indicates that its *pyp* gene is located in the immediate vicinity of a gene encoding a diguanylate cyclase. Since c-di-GMP, a recently discovered bacterial signaling molecule, is a central regulator for the synthesis of the exopolysaccharides that are involved in biofilm formation (Paul et al. 2004, Hickman et al. 2005, Ryjenkov et al. 2005, Cotter et al. 2007), we examined the role of light in regulating biofilm

formation in *I. loihiensis*. This revealed that photoactivation of PYP suppresses biofilm formation in this organism.

4.1.2. Experimental Section

Culturing and attachment of *I. loihiensis*. *I. loihiensis* strain L2-TR(T) was cultured in Marine Broth (Difco) at 30°C with gentle shaking. Biofilm assays were performed at 20°C, in a well-thermostated room, using a method adapted from (O'Toole et al. 1998). An overnight culture of *I. loihiensis* was diluted ten times and incubated in 96-well flat-bottom PVC microtiter plates (Costar 3595). One plate was covered with black cloth, another with transparent plastic foil. Plates were illuminated with a white light bulb (50 W, Philips) at ~ 80 cm distance, resulting in a light intensity of ~ 80 microeinsteins m⁻² s⁻¹. Care was taken to minimize effects of illumination on other physical parameters in the experimental setup, such as temperature and humidity. To this end, the experiment was also carried out in an incubator/shaker, thermostated at 20°C. The incubator was not rotating and illumination was carried out from the outside, through the glass shield in the lid of the incubator. To ensure that the position in the 96-wells plate did not alter the behavior of the cells, the addition of *pCA* and its analogs was randomized over the plate, and plates were incubated as described above. After 24 hours, non-attached cells were removed by washing the plates three times with demi water.

Attached cells were stained for 60 minutes with 1% crystal violet. Non-bound crystal violet was removed by washing three times with demi water. Crystal violet was resolublized in 80% ethanol / 20% acetone, and cell attachment was quantified by measuring the absorbance at 595 nm in a plate reader (Spectramax plus, Molecular devices). To test the effect of *pCA* and its analogs on cell attachment, concentrated solutions of the chromophores (*pCA*, *trans*-locked, and *cis*-locked) in DMF were added to the cultures in the wells to a final concentration of 1 mM. The final concentration and solvent used for adding these three chromophores to *I. loihiensis* cell

cultures were identical. The values for of biofilm formation in the dark and light, and in the dark in the presence of *pCA* and the two *pCA* analogs as determined by crystal violet binding were averaged over 6 wells in a 96 wells microtiter plate, and the reproducibility of the resulting values was confirmed in two independent experiments. Attachment of the cells to the wall of the wells prevented exact quantitation of growth by OD600 measurements. Visual inspection of the 96 well plates indicated that there is only limited growth during overnight incubation in the wells. Addition of chromophores did not noticeably affect cell growth.

Synthesis of *pCA* analogs. The *cis*-locked chromophore analog 2-(4-Hydroxy-phenyl)-cyclopent-1-enecarboxylic acid was synthesized from ethyl-2-oxocyclopentane carboxylate as described in the supplemental information. The identity and purity of the intermediate and final products was determined using FTIR and NMR spectroscopy and mass spectrometry.

Cloning of the II *pyp* gene. Based on the genome sequence of *I. loihiensis*, the oligonucleotides 5'-AGGTAACACCATGGAGATTGTTCAATT-3' and 5'-TGAGTCTGGATCCTTATAGTCGCTTAACGAATA-3' were used as the sense primer and anti-sense primer, respectively, for PCR amplification of the *pyp* gene from this organism, thereby introducing *NcoI* and *BamHI* restriction sites. Purified *I. loihiensis* genomic DNA was used as the template in the PCR reaction. The amplified gene was cloned into the pET-16b vector (Novagen) using the *NcoI* and *BamHI* restriction sites. The nucleotide sequence of the cloned II PYP was confirmed by DNA sequence analysis (BigDye™-terminated reaction analyzed on ABI Model 3730 DNA Analyzer, Recombinant DNA and Protein Core Facility at Oklahoma State University). Plasmid DNA was transformed into *E. coli* BL21 (DE3) for apoPYP overproduction.

Overproduction and purification of Hh PYP and II PYP. PYP from *H. halophila* was produced and isolated as described in (Kort et al. 1996) as hexa-histidine tagged apo-protein in *Escherichia coli*. The apoprotein was reconstituted with the 1,1-carbonyldiimidazole derivative of

the respective chromophore (*i.e.* 4-hydroxy-cinnamic acid (*p*CA), 7-hydroxy-coumarin-3-carboxylic acid (*trans*-locked; Molecular Probes, Invitrogen), 2-(4-Hydroxy-phenyl)-cyclopent-1-enecarboxylic acid (*cis*-locked), see Figure 4.1.1C) as described in (Hendriks et al. 2002). Hh PYP was used in 10 mM Tris-HCl, pH 8.0 without removal of the N-terminal hexahistidine tag.

Overproduction of II apoPYP was induced by the addition of 1 mM IPTG, extracted from *E. coli* BL21 (DE3) using 8 M urea and reconstituted with *p*-hydroxycinnamic anhydride (Sigma-Aldrich) (Imamoto et al. 1995) following the procedure described for the PYP from *H. halophila* (Mihara et al. 1997). The apoPYP from *I. loihiensis* readily reconstituted upon the addition of the *p*CA anhydride, yielding a bright yellow protein with an absorbance maximum at 446 nm. The reconstituted holo-II PYP was purified by anion-exchange chromatography using DEAE-sepharose CL-6B (Pharmacia) and sodium chloride as the eluent. The purified protein had a purity index (ratio of absorbance at 280 nm and 446 nm) of 0.48. Possible proteolytic damage of the purified protein was examined by mass spectrometry (Applied Biosystems Voyager-DE Pro MALDI-TOF MS, Recombinant DNA and Protein Core Facility at Oklahoma State University). This yielded a mass of 14,121 Da, indistinguishable within the error of the instrument from the theoretical mass of 14,131 Da.

UV/vis absorbance spectroscopy. UV-visible absorption spectra were measured at room temperature using an HP-8453 (Hewlett-Packard) diode array spectrophotometer and a monochromator-based Cary300Bio (Varian) spectrophotometer. The relative value of the molar extinction coefficient of the II PYP was determined based on the effect of denaturing the protein in 10 mM Tris-HCl pH 7.5 by the addition of 2% SDS on its absorbance spectrum (Imamoto et al. 2001). The extinction coefficient of II PYP was derived by comparing the amplitude of the absorbance band at 345 nm of the denatured II PYP to that of native and SDS-denatured wild type *H. halophila* PYP, which has a known extinction coefficient at 446 nm ($45,500 \text{ M}^{-1} \text{ cm}^{-1}$) (Meyer et al. 1989). A 150 W halogen quartz light source (Cuda) with a broadband blue filter (band pass

filter 59855 Oriel, CT) was used to initiate the photocycle of Il PYP in 10 mM Tris-HCl pH 7.5. After approximately 15 seconds of illumination the actinic light was shuttered, and the thermal recovery of the dark state was measured with a time resolution of 100 milliseconds. The photocycle recovery kinetics at 446 nm and 355 nm was biexponential. A mixed buffer (Glycine, Succinate, MES and MOPS, 100 mM each) was used for pH titration measurement in the pH range from 2.0 to 12.0. The pH was adjusted using 1N NaOH or HCl. The acid titration was carried out in a darkened room using the minimal intensity of red light needed for handling of the samples and reading of the pH values. The pH dependence of the sample absorbance at its absorption maximum (446 nm) was described using the Henderson-Hasselbalch equation.

FTIR spectroscopy. Il PYP and Hh PYP samples for FTIR spectroscopy were prepared at 8 mM in 50 mM phosphate buffer in D₂O at pH* 6.6 as described (Xie et al. 1996). For each sample, 2.7 μ l PYP was sandwiched between two CaF₂ windows (15 mm diameter and 2 mm thickness) with a 12 μ m spacer. Steady state and time-resolved infrared measurements were measured using a Bruker IFS 66v FTIR spectrometer (Billerica, Massachusetts) with a liquid nitrogen-cooled Mercury Cadmium Telluride (MCT) detector. Water vapor in the optical path was removed by vacuum, except for the sample compartment, which was purging with dry nitrogen gas (2.2 L/min). Sample temperature was controlled at 300 K using a water circulator (Neslab, RTE- 111) in all the FTIR measurements. FTIR absorption spectra of steady state PYP samples were measured in the spectral range of 4000 – 850 cm⁻¹ at 2 cm⁻¹ spectral resolution and 40 kHz scanning velocity, and averaged over 175 scans, using CaF₂ windows as a reference. The 2nd derivative of the absorbance was calculated using the Bruker OPUS software based on Savitzky-Golay algorithm with 13 smoothing points.

For time-resolved FTIR spectroscopy, the photocycle of PYP was triggered with blue laser pulses (475 nm, 4 ns pulse duration, and ~3 mJ per pulse) from a Quantel, Brilliant laser with an Oportek OPO. The repetition rate of the pump laser was set at 0.25 and 0.125 Hz,

respectively, for Hh PYP and Il PYP. Light-induced infrared absorption changes of PYP were measured in rapid-scan FTIR mode at 4.5 cm^{-1} spectral resolution with 200 kHz scanning velocity, and averaged over 256 repetitions. A quadruple splitting technique was employed so that the time resolution for the first spectrum was improved from 46 ms (without splitting) to 8 ms. For proper synchronization between the scanning mirror of the Bruker FTIR system and the laser flashes, a triggering system was designed and utilized where the FTIR system served as the master clock, and two delay generators (SRS, DG535) that were externally triggered by the FTIR system (coupled to the scanning mirror), were used to trigger the laser flash lamps ($\sim 10 \text{ Hz}$), the laser Q-switch, and rapid-scan FTIR data acquisition.

A macro program was designed and employed to compute the time resolved infrared difference spectra, $\Delta A(t, \nu) = C_{pB}(t) \cdot d \cdot [\epsilon_{pB}(\nu) - \epsilon_{pG}(\nu)]$, using the infrared absorption of the pG state (preflash spectrum) as the baseline. The peak-to-peak signal of the first infrared difference spectrum of Il PYP was 10 mOD in the Amide I region, with a noise level of 0.03 mOD (3×10^{-5} OD).

Bioinformatics analysis. The genome of *I. loihiensis* was examined for the presence of *pcl* and *tal*, and for genes encoding photoreceptor proteins using NCBI genomic BLAST tools at: http://www.ncbi.nlm.nih.gov/sutils/genom_table.cgi. Domain architecture was examined using SMART (<http://smart.embl-heidelberg.de/>) and Pfam (<http://pfam.sanger.ac.uk/>) databases.

4.1.3 Results

Light-regulated cell attachment. During the culturing *I. loihiensis* in glass flasks or tubes, cells were observed by eye to stick together in aggregates or attach to the glass culturing tube in a ring at the air-liquid interface. These aggregates were several millimeters in size and appeared after overnight culturing. In PVC 96-well microtiter plates, cells tended to stick more to the wall of the well, instead of to each other. To examine if light regulates this biofilm formation

process, we determined the effects of white light on the attachment of *I. loihiensis* to 96-well microtiter plates. Bacterial cell attachment to the PVC was quantified using a crystal violet staining method (O'Toole et al. 1998). This revealed that the presence of light reproducibly suppresses attachment of *I. loihiensis* cells to the PVC surface by ~35% (Fig. 4.1.1A).

Since the only photoreceptor protein identified in the genome of *I. loihiensis* is a PYP homolog (van der Horst et al. 2007), we designed an approach to study the role of this photoreceptor in the light regulation of biofilm formation. Because no genetic system is available for *I. loihiensis*, we utilized available knowledge on the effects of locked *pCA* analogues on PYP photochemistry (Fig. 4.1.1C) (Cordfunke et al. 1998, van der Horst et al. 2007). To block PYP photoexcitation we used 7-hydroxy-coumarin-3-carboxylic acid as a *trans*-locked *pCA* to essentially lock the protein in its pG dark state. The remaining photochemistry of PYP reconstituted with this *pCA* analog (Cordfunke et al. 1998) occurs with very low quantum efficiency. The *cis*-locked *pCA* analog 2-(4-hydroxy-phenyl)-cyclopent-1-enecarboxylic acid would be expected to permanently activate PYP by locking it in its pB state (Van der Horst 2004). Both chromophores readily attach to Hh PYP. As expected, *trans*-locked *pCA* results in an absorbance spectrum resembling the pG state (λ_{\max} 443 nm), while *cis*-locked *pCA* resembles the absorbance spectrum of the pB state (Fig. 4.1.1D). PYP reconstituted with *cis*-locked *pCA* exhibits a characteristic peak at ~350 nm, but in addition displays a peak at 310 nm. The free form of this chromophore has absorption maxima at 267, 283 and 340 nm at pH 3, 7 and 10, respectively (data not shown). The 310 nm peak may arise from a combination of increased scattering and the n-to- π transition of the carbonyl group of the chromophore. The increased scattering of the solution suggests partial aggregation of PYP reconstituted with *cis*-locked *pCA*.

Incubation of *I. loihiensis* with these two *pCA* analogs significantly affected biofilm formation in the dark. The addition of *trans*-locked *pCA* resulted in a 45% increase in cell attachment, whereas *cis*-locked *pCA* resulted in a 75% reduction of attachment, when compared

to the addition of *pCA* or no chromophore addition (Fig. 1B). In the presence of both chromophore derivatives the cells no longer exhibited the light-induced suppression of biofilm formation. The addition of exogenous *pCA* to the cells did not alter the photoresponse (compare Fig. 1A in the dark and 1B in the presence of *pCA*). This result shows that *I. loihiensis* cells synthesize *pCA*, and that the addition of the small amount of DMF used as solvent for the chromophores to the cell culture does not affect biofilm formation. These data provide strong evidence that PYP is the photoreceptor for the light regulation of biofilm formation in *I. loihiensis*. We therefore decided to examine the spectroscopic properties of Il PYP.

Spectroscopy of Il PYP. The UV/vis absorbance spectrum of Il PYP is essentially identical to that of Hh PYP (Fig. 4.1.2A). The extinction coefficient of the characteristic 446 nm absorbance band was determined to be $43,350 \text{ M}^{-1}\text{cm}^{-1}$, very similar to the value of 45,500 for *H. halophila* PYP (Meyer et al. 1989).

The structure of the pG state of Il PYP was compared to that of the PYP from *H. halophila* using FTIR absorption and second derivative spectroscopy (Fig. 4.1.2B, C). The FTIR absorbance spectrum of a protein in the $1800\text{-}1350 \text{ cm}^{-1}$ region contains contributions from the protein backbone and from all polar and charged side chains. The peak positions of these overlapping bands are better resolved in the second derivative of the FTIR spectrum (Dong et al. 1992). Thus, the second derivative of the FTIR absorbance of a protein provides a sensitive “fingerprint” for the structure of a protein (He et al. 1991, Dong et al. 1992). The second derivative FTIR spectra of the pG states of the PYPs from *I. loihiensis* and *H. halophila* are highly similar, demonstrating that they share a very similar three-dimensional structure. This is in line with the 75% sequence identity shared by these two PYPs.

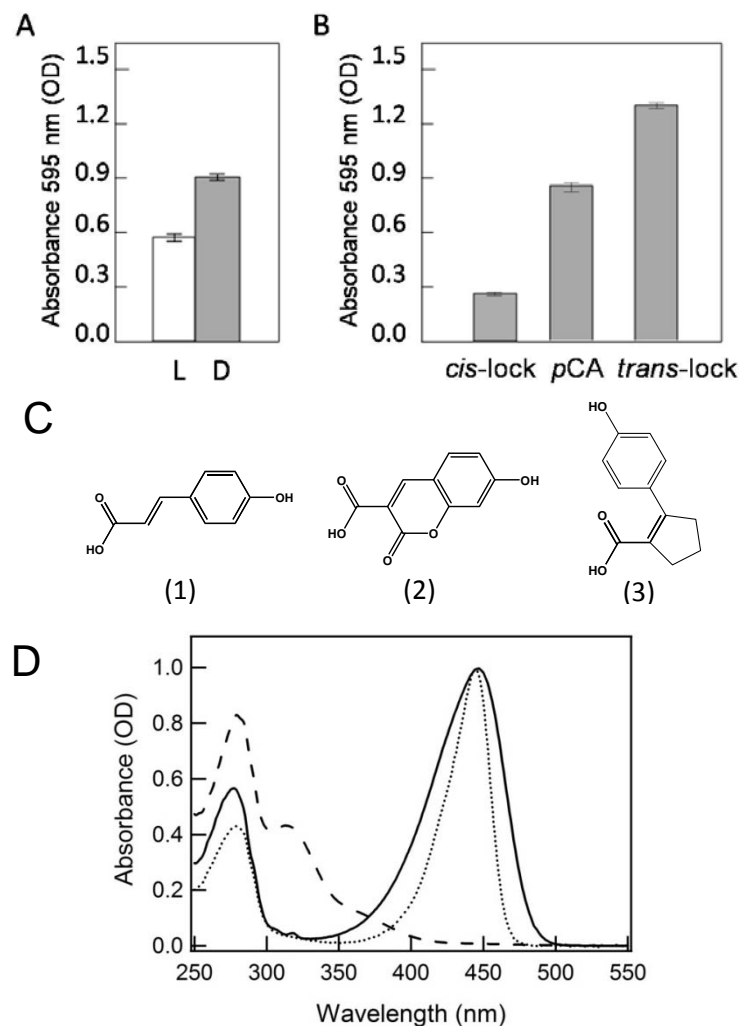


Figure 4.1.1. Regulation of biofilm formation in *I. loihensis* by light and *p*-coumaric acid analogs. Error bars indicate standard deviations. (A) Biofilm formation in growing *I. loihensis* cultures was measured in the light (open bars) and in the dark (gray bars), revealing that light suppresses biofilm formation. The absorbance of crystal violet at 595 nm is shown, providing a measure for the amount of cells attached to the PVC microtiter plate well. (B) The effect of the addition of *p*CA, *cis*-locked *p*CA, and *trans*-locked *p*CA on biofilm formation in *I. loihensis* cultures grown in the dark. The error in panel (A) and (B) were calculated for values of 6 wells in a 96 well microtiter plate. (C) The *p*CA chromophore analogs used to lock PYP into its pG and pB states. The structures of the chromophore used in this study are shown: 4-hydroxy-cinnamic acid (*p*CA, 1), (2) 7-hydroxy-coumarin-3-carboxylic acid (*trans*-locked, 2), and 2-(4-hydroxy-phenyl)-cyclopent-1-enecarboxylic acid (*cis*-locked, 3). (D) UV/Vis absorbance spectra of Hh PYP containing *p*CA (solid), *trans*-locked *p*CA (dotted), and *cis*-locked *p*CA (dashed).

The pK_a of the *pCA* chromophore in Il PYP was determined by acid titration using UV/vis absorbance spectroscopy. At pH values below 4 the native pG state was converted to a pB_{dark} species (Meyer 1985, Hoff et al. 1997) with a protonated *pCA* chromophore and an absorbance maximum at 352 nm (Fig. 4.1.3A). The transition was described by a single pK_a value of 3.4, with an n value of 1.3 (Fig. 4.1.3B). In Hh PYP this transition occurs with a pK_a of 2.8 (Meyer 1985, Hoff et al. 1997).

The photochemical activity of the protein was examined by exposing it to blue light at pH 7.5. This revealed the formation of a pB photocycle intermediate with an absorbance maximum at 350 nm (Fig. 4.1.4). The pB state decayed to the initial pG state in a biphasic process with time constants of 0.3 s (79%) and 5 seconds (21%) (Fig. 4). Thus, the *yyp* gene in the *I. loihiensis* genome encodes a genuine, photochemically active PYP. The kinetics of pB decay in the PYP from *I. loihiensis* is very similar to that of the PYP from *H. halophila* (Meyer et al. 1987, Hoff et al. 1994).

The molecular events that occur upon pB formation in Il PYP were examined using rapid-scan FTIR difference spectroscopy in D_2O (Fig. 4.1.5A). The pB – pG FTIR difference spectrum for Il PYP is quite similar to that of Hh PYP (Fig. 4.1.5B). Thus, the published assignments of FTIR signals in Hh PYP (Xie et al. 1996, Xie et al. 2001) can be applied to Il PYP. The negative signal at 1726 cm^{-1} is caused by the deprotonation of Glu46, and matches the signals at 1497 and 1515 cm^{-1} caused by *pCA* protonation. The signal at 1726 cm^{-1} also shows that hydrogen bonding between the side chain of Glu46 and the phenolic oxygen of the *pCA* in the pG state is essentially identical in the two PYPs. The main differences in the pB – pG difference spectrum for Il PYP are a ~20% reduction in the amide I difference signals at 1624 cm^{-1} , and a reduction in the unassigned side chain signal at 1590 cm^{-1} . This indicates that the light-induced conformational changes in Il PYP are similar but somewhat smaller compared to those in Hh PYP.

To complement the detection of the kinetics of pB decay in Il PYP by visible absorbance spectroscopy (Fig. 4.1.4), we extracted the time dependence of the amplitude between the negative amide I difference signal at 1642 cm^{-1} and the positive amide I peak at 1624 cm^{-1} (Fig. 4.1.5C). This revealed a biphasic decay with a major fast phase of 0.30 s and a minor slow phase of 3.6 seconds, very similar to the values obtained by visible absorbance spectroscopy. The kinetics of the amide I signals of Il PYP during pB decay were compared to those obtained for Hh PYP, confirming that the kinetics of the last photocycle step in these two proteins is very similar (Fig. 4.1.5C).

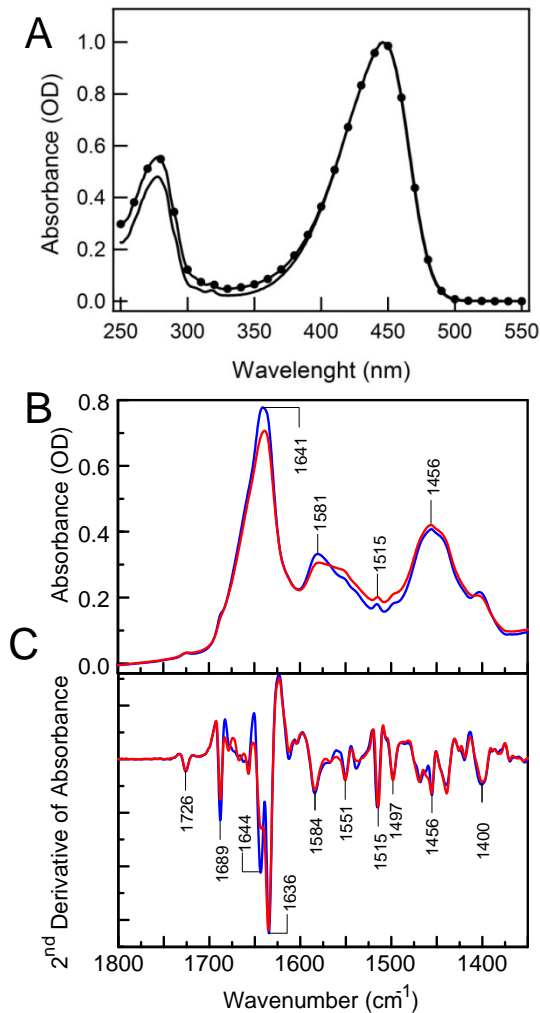


Figure 4.1.2. Comparison of the spectroscopic properties of the pG dark state of the PYPs from *Idiomarina loihiensis* and *Halorhodospira halophila*. (A) UV/vis absorbance spectra of Il PYP (dotted line) and Hh PYP (solid line). FTIR spectroscopic comparison of the structure of the pG dark state of Il PYP (red) and Hh PYP (blue) based on infrared absorbance spectra (B) and second derivative spectra (C) in D_2O at pH* 6.6.

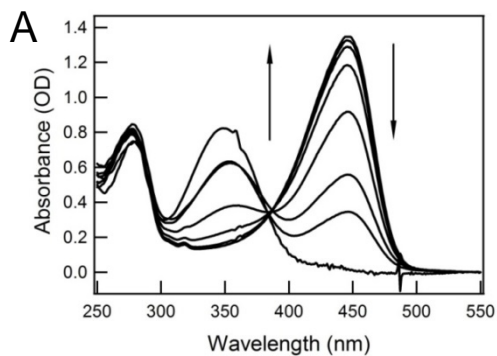


Figure 4.1.3. Low pH titration of the PYP from *I. loihiensis*. (A) UV/vis absorbance spectra of Il PYP as a function of pH. Arrows indicate the direction of the change in the amplitudes of the bands at 446 and 350 nm at increasingly lower pH values. (B) The pH dependence of the absorbance at 446 nm as a function pH, fit to the Henderson-Hasselbalch equation.

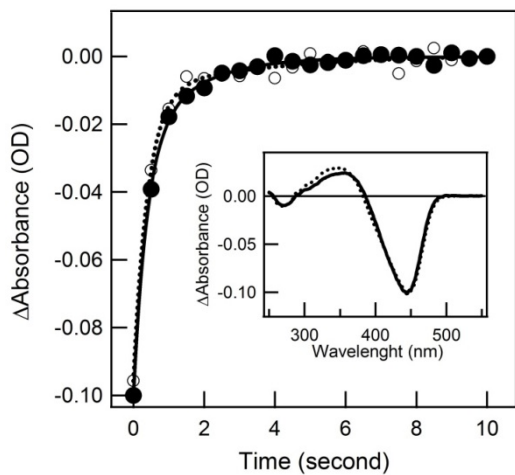
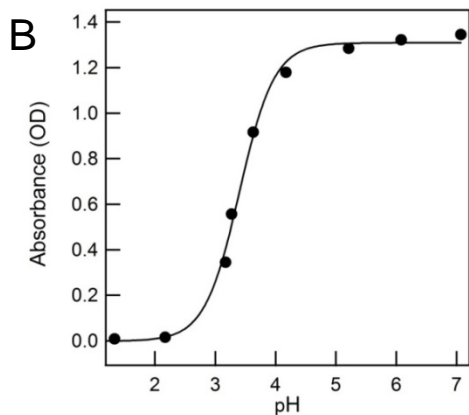


Figure 4.1.4. Comparison of the last photocycle step in the PYPs from *I. loihiensis* and *H. halophila* at pH 7.5. Kinetics of pB decay in Il PYP (solid line and closed circles) and Hh PYP (dotted line and open circles) detected at 446 nm. In both PYPs the decay is biexponential. The time constants for Il PYP were 230 milliseconds (80%) and 5.7 seconds (20%), and for Hh PYP 380 milliseconds (75%) and 1.6 seconds (25%). The inset depicts the light-dark UV/vis difference spectra of Il PYP (solid) and Hh PYP (dotted) calculated using the absorbance spectra at $t=0$ and $t=10$ seconds.

Identification of TAL and pCL in *I. loihiensis*. The *in vivo* functioning of PYP requires the biosynthesis of its *pCA* chromophore and covalent attachment to apoPYP. In *Rhodobacter capsulatus* this is achieved by the activity of two proteins: tyrosine ammonia lyase (TAL) and *p*-coumaryl:CoA ligase (*pCL*) (Kyndt et al. 2003). TAL converts tyrosine into *pCA* and *pCL* activates the *pCA* by attachment to coenzyme A. The coumaryl CoA then reacts with apoPYP, resulting in the formation of a thioester bond between *pCA* and the conserved Cys side chain at the active site of PYP. Since the *I. loihiensis* genome encodes a functional *pyp* gene, we examined the presence of possible *tal* and *pcl* genes in its genome.

The *I. loihiensis* genome encodes two proteins with significant sequence similarity to the known TAL from *Rb. capsulatus* (Supplemental Fig. 1). The product of gene IL135 shares 31% sequence identity and 46% sequence identity with the TAL from *Rb. capsulatus*; for gene IL2450 these numbers are 28 and 43%. The two TAL candidates in *I. loihiensis* are fairly divergent: they share 28% sequence identity and 49% similarity. In *H. halophila* the *pyp* gene is present in an apparent three-gene operon, together with a *tal* and a *pcl* gene (Kort et al. 1996). The TAL from *H. halophila* is 32% identical to product of gene IL2450 and 26% identical to product of gene IL135. These four proteins all are approximately 500 amino acids in length.

A highly conserved Ala-Ser-Gly fragment of ammonia lyases undergoes spontaneous cyclization to form the 4-methylene-imidazole-5-one cofactor of the enzyme (Baedeker et al. 2002). This ASG sequence is conserved in the two TAL candidates in *I. loihiensis*. The crystal structure of the TAL from *Rb. Sphaeroides* (Louie et al. 2006) has revealed 9 residues that form the substrate binding pocket. Of these 9 residues 8 are conserved (Tyr60, Phe66, His89, Leu153, Tyr300, Arg303, Asn435, and Gln436) in the two *I. loihiensis* proteins. His89 is of particular importance, because hydrogen bonds with the phenolic oxygen of the Tyr substrate, and mutagenesis has shown that this residue is critical for its substrate specificity (Louie et al. 2006). In view of this high level of conservation of functionally critical residues, the products of *I.*

loihiensis genes IL135 and IL2450 are very likely to encode functional TALs. Both of these genes are not in the immediate vicinity of the *pyp* gene (*I. loihiensis* gene IL2385). This is in contrast to the situation in *H. halophila* (Kort et al. 1996), and in *Rb. Capsulatus* (Kyndt et al. 2004) where *tal* is located very close to the *pyp* gene.

A single gene with high sequence similarity to the *pcl* genes from *Rb. capsulatus* and *H. halophila* is present in the *I. loihiensis* genome (Supplemental Fig. 2). This gene (IL2385) encodes a protein with ~28% sequence identity and ~43% sequence similarity to the known *pCL*s from *Rb. sphaeroides* and *H. halophila*; (Kort et al. 1996, Kyndt et al. 2003) all three proteins are ~400 residues in length. The crystal structure of the 4-chlorobenzoate:CoA ligase from *Alcaligenes sp. AL2007* has been reported (Gulick et al. 2004). This structure revealed functionally important residues in the substrate binding pocket. Comparison with the protein encoded by gene IL2385 reveals that key residues in the substrate binding pocket are conserved: His204, Ile303, and Gly305 (numbering for 4-chlorobenzoate:CoA ligase). In CoA ligases for small acyl substrates Gly305 is substituted with Trp, supporting the conclusion that the *I. loihiensis* enzyme binds the larger *p*-coumaryl substrate. Finally, Val205 in the 4-chlorobenzoate:CoA ligase is substituted with Ile in the CoA ligase in *I. loihiensis*. In plant *p*-coumaryl:CoA ligases this position is important for substrate specificity, and contains Ile (Schneider et al. 2003), as does the *I. loihiensis* enzyme. Interestingly, gene IL2385 in *I. loihiensis* is located immediately downstream of the *pyp* gene in an apparent operon (Fig. 4.1.6A). This is strong independent support for its functional assignment as a *pCL*.

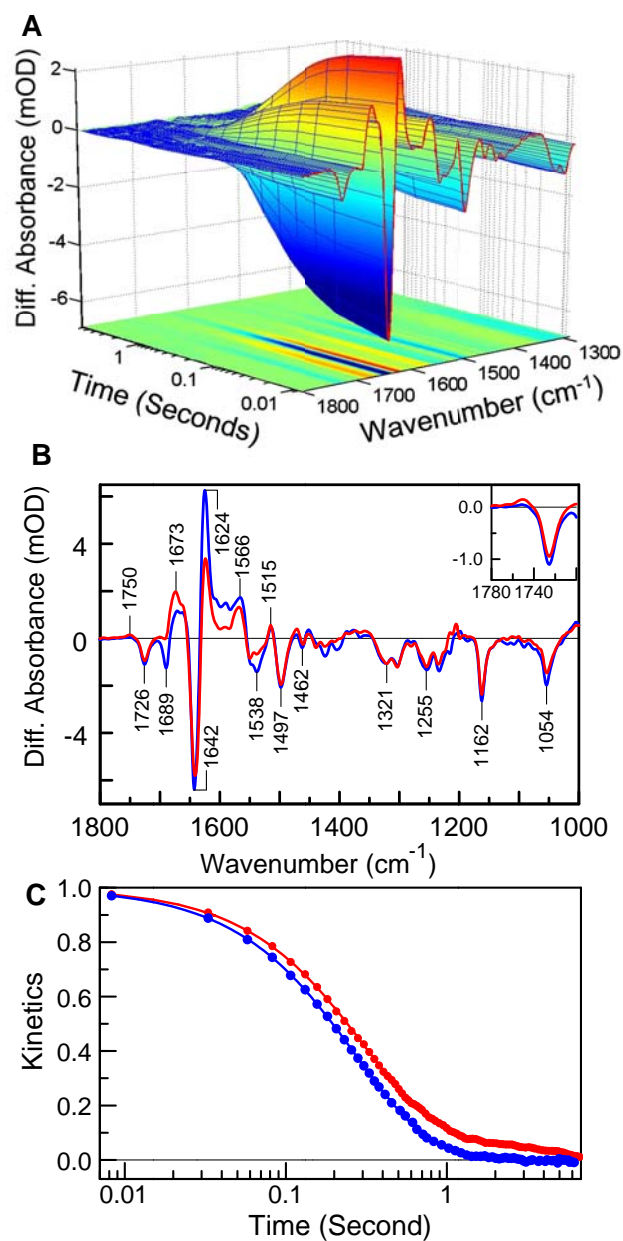


Figure 4.1.5. Time-resolved FTIR difference spectroscopy of the PYP from *I. loihiensis*. (A) Three-dimensional plot of the time resolved rapid-scan FTIR difference absorbance signals during the photocycle of II PYP in D₂O at pH* 6.6. (B) Light-induced FTIR difference spectra between the long-lived pB intermediate and the initial pG state for the PYPs from *I. loihiensis* (red) and *H. halophila* (blue). In the inset the difference spectra in the spectral region 1780-1760 cm⁻¹ are enlarged. (C) Kinetics of the last step in the PYP photocycle of II PYP (red) and Hh PYP (blue) monitored by the peak difference between the amide I signals at 1642 and 1624 cm⁻¹. The solid lines are a bi-exponential fits of the data, with time constants of 0.30 seconds (89%) and 4 seconds (11%) for II PYP, and 0.26 seconds (92%) and 0.8 seconds (8%) for Hh PYP.

4.1.4 Discussion

Functional diversity in the PYP family. Hh PYP and II PYP share 75% sequence identity. This level of sequence similarity ensures that the two proteins have very similar three-dimensional structures. However, this sequence-based conclusion does not transfer to their functional properties. For example, the absorbance spectra of the red and green pigments in human color vision differ by 30 nm, while these proteins share 96% sequence identity (Nathans et

al. 1986). Similarly, the absorbance peaks of the green and blue variants of proteorhodopsin differ by 35 nm, but their amino acid sequences are >78% identical (Man et al. 2003). The lifetime of the pB state in the PYP family varies from milliseconds to hours, and single point mutations can greatly alter pB decay kinetics in Hh PYP (Kumauchi et al. 2008). The results reported here demonstrate that the properties of Hh PYP and Il PYP are highly similar despite their very different biological functions.

In *Rhodocista centenaria*, a PYP-phytochrome hybrid containing a histidine kinase domain regulates the activity of chalcone synthase, which is involved in the biosynthesis of photoprotective pigments (Jiang et al. 1999). The PYP from *H. halophila* functions as the photoreceptor for negative phototaxis (Sprenger et al. 1993). The biological function of the PYP from *Thermochromatium tepidum* is not known, but it is part of a larger protein that also contains a diguanylate cyclase domain (Kyndt et al. 2004). The data reported here reveal that the biological function of the PYP from *I. loihiensis* is to photo-regulate biofilm formation. This indicates a high level of functional versatility in the PYP family. The difference in function between Il PYP and Hh PYP is in striking contrast with the high level of conservation in both amino acid sequence and a range of functional properties: the pCA absorbance maximum and pK_a, pB lifetime, and photocycle-associated active site proton transfer and conformational changes. These data suggest a recent divergence in the biological function of these two PYPs.

The diversity of output signals generated by PYP photoexcitation (phototaxis, pigment synthesis, and biofilm formation) appears to be a general theme in photobiology. Also in the case of LOV (Crosson et al. 2003), BLUF (Gomelsky et al. 2002), and phytochromes (Sharrock 2008) great diversity is seen for the output domains connected to the photosensors and in the biological responses that they trigger.

An approach to study *in vivo* PYP function. For 9 of the 12 bacteria known to contain PYP⁶ no genetic tools are available. This presents an important barrier to studies on the *in vivo* function of PYP, and has precluded genetic confirmation of the function of Hh PYP in negative phototaxis. Here we develop and apply the use of locked *pCA* analogs to examine the involvement of PYP in light-regulated biofilm formation in *I. loihiensis*. This provides a generally applicable tool for studies on the *in vivo* role of PYP, even in organisms that are not genetically accessible. Thus, while the biological function of the highly studied PYP from *H. halophila* as the photoreceptor for negative phototaxis still has not been conclusively determined, the results reported here provide compelling biochemical evidence for the biological function of the PYP in *I. loihiensis*.

Since PYP is the only photoreceptor known to contain *pCA* as a cofactor, the detection of opposing biological effects upon the addition of *trans*-locked and *cis*-locked *pCA* provides strong evidence for a role of this photoreceptor in the photoresponse studied. Coumaric acids are known to pass the microbial cell envelope relatively easily (Baranowski et al. 1983). Presumably, after passing the cell membrane, the *pCA* analog will be incorporated into PYP by *p*-coumaryl:CoA ligase (*pCL*) (Kyndt et al. 2003), depending on the substrate specificity of the *pCL*. *De novo* biosynthesis of PYP and PYP turnover will thus result in the incorporation of *pCA* analogs into PYP. The difference between cells exposed to *trans*-locked and *cis*-locked *pCA* would be expected to reveal the maximal physiological response triggered by PYP. This presents a generally applicable chemical approach to examine the involvement of PYP in a photoresponse.

The degree of biofilm formation by *I. loihiensis* in the presence of *trans*-locked *pCA* would be expected to be identical to that for cultures grown in absolute darkness. However, the experiments (Fig. 4.1.1) showed a somewhat lower degree of biofilm formation for cultures grown in darkness. Two possible explanations for this observation are (i) that small amounts of light reached the cultures during the course of the experiments, or (ii) that a small amount of dark

noise occurs in PYP reconstituted with native *pCA* so that even in the absence of light a basal level of signal is generated. The current data do not allow these two effects to be distinguished.

Correlating the time scales of receptor activation and biological response. The photocycling rates of photosensory proteins cover a wide range of time scales, from milliseconds to hours. In the PYP family the lifetime of the pB state varies from minutes and hours for the PYPs from *Rhodocista centenaria* (Jiang et al. 1999) and *Salinibacter ruber* (Kumauchi et al. 2008, Memmi et al. 2008) to hundreds of milliseconds for the PYP from *H. halophila*. (Meyer et al. 1987, Hoff et al. 1994) The photocycles for the PYPs from *Rb. sphaeroides* and *Rb. capsulatus* are even faster (Haker et al. 2000, Haker et al. 2003, Kyndt et al. 2004).

Interestingly, the lifetime of the signaling states (Yan et al. 1991) in a photocycle appears to match the typical time scale of the biological response that they trigger (Jung et al. 2003, van der Horst et al. 2005). A correspondence between the lifetime of an activated signaling component and the time scale of the biological response that it triggers has also been reported for two-component regulatory systems. In this case the lifetime of phosphorylated response regulators varies according to the duration of the response (Janiak-Spens et al. 1999, Thomas et al. 2008). Hh PYP and the archaeal sensory rhodopsins both exhibit a photocycling time of ~0.5 seconds and both trigger phototaxis responses, which occur on a sub-second to second time scale (Sundberg et al. 1986, Sprenger et al. 1993). The slower photocycling time of the PYP from *R. centenaria* (~50 seconds) corresponds to its function in the regulation of gene expression (Jiang et al. 1999). A similar correspondence is seen in BLUF domain proteins (Gomelsky et al. 2002). The BLUF domain protein AppA functions as an antirepressor, and exhibits a photocycle of 15 minutes (Masuda et al. 2002). In contrast, the BLUF protein PixD is a photoreceptor for phototaxis in *Synechocystis*, with a photocycle time of ~10 seconds (Masuda et al. 2004, Okajima et al. 2005). The LOV-based phototropins in plants (Swartz et al. 2001), which trigger

phototropism, chloroplast movement, and stomatal opening, also exhibit slow photocycling times (from minutes to hours).

Here, we present an example of a photosensory protein that does not follow this trend. Il PYP exhibits a fast photocycling time but triggers a slow biological response: biofilm formation. Strikingly, despite the highly distinct biological functions of the PYPs from *I. loihiensis* and *H. halophila*, their photocycling times are essentially identical. Thus, the overall kinetics of a photocycle cannot be directly used to infer information regarding the time scale of the biological response that it triggers. This result also has implications for modeling of signaling pathways in the living cell based on kinetic information for the individual signal transduction components.

Biofilm formation in *I. loihiensis* exposed to *trans*-locked versus *cis*-locked *pCA* differs by a factor ~ 5 , while incubation in the dark versus light results in a difference by a factor ~ 1.6 . The smaller effect of light exposure is in line with the fairly short lifetime of the pB state of Il PYP. The difference between the two locked *pCA* analogs provides an estimate of the maximal amplitude of this physiological response. Apparently, the light intensities used in the experiments reported here do not trigger this maximal response. In view of the pB lifetime of Il PYP, this light intensity would be expected to yield a photostationary state in which 5 to 10% of the PYP molecules in the cell are in the pB state, which may yield a sub-maximal response. This analysis suggests that Il PYP functions as a photoreceptor for relatively high light intensities, providing an explanation for the apparent mismatch between the photocycling time of Il PYP and the time scale of the biological response that it triggers.

Light regulation of biofilm formation. Biofilm formation is a complex process. Two key external stimuli known to regulate biofilm formation are nutrient availability and quorum sensing (Stanley et al. 2004, Boehm et al. 2009). Here we report a novel external stimulus that affects biofilm formation: light.

Recently it was reported that cell attachment in *Caulobacter crescentus* is regulated by blue light via the LOV-histidine kinase photoreceptor protein LovK (Purcell et al. 2007). Key differences with the results reported here are that (i) attachment of *C. crescentus* occurs not via exopolysaccharides but through a specialized stalk, (ii) in *I. loihiensis* a *pCA*-based PYP and not a flavin-based LOV photoreceptor regulates cell attachment, (iii) blue light inhibits biofilm formation in *I. loihiensis* but promotes cell attachment in *C. crescentus*, and (iv) the photocycling time of the LovK is on the hours time scale, while that of Il PYP occurs on the sub-second time scale. For LovK it has been proposed that light provides information on the position of the organism in the water column (Purcell et al. 2007). A similar biological role is plausible for light-regulated biofilm formation by PYP in *I. loihiensis*.

A number of features in the *I. loihiensis* genome suggest a model for the signal transduction chain in PYP-directed light regulation of biofilm formation. The Il *pyp* gene is present in an apparent operon with a downstream gene encoding a *pCL* (Fig. 4.1.6A). The two-gene *pyp-pcl* operon is immediately adjacent to a gene encoding a multi-domain signaling protein that is transcribed convergently with the *pcl* gene and overlaps with it by three base pairs. This signaling protein consists of two N-terminal PAS domains and a C-terminal GGDEF domain (Fig. 4.1.6B). The latter domain presumably exhibits diguanylate cyclase activity, which catalyzes the conversion of GTP into c-di-GMP (Paul et al. 2004, Hickman et al. 2005, Ryjenkov et al. 2005). Recently c-di-GMP has emerged as a central regulator for biofilm formation (Cotter et al. 2007). The *I. loihiensis* genome encodes 32 genes encoding enzymes involved in exopolysaccharide synthesis and transport, 34 proteins containing an GGDEF domain, and 22 proteins containing an EAL domain (Hou et al. 2004). The EAL domain is involved in the breakdown of c-di-GMP through its phosphodiesterase activity (Schmidt et al. 2005). In addition, the *I. loihiensis* genome contains 3 proteins that have been annotated to contain a PilZ domain, which function as a receptor for c-di-GMP (Cotter et al. 2007). These observations suggest the

possibility that Il PYP regulates the diguanylate cyclase activity of the downstream GGDEF protein (Fig. 6C). A functional link between PYP and c-di-GMP is confirmed by the PYP from *Thermochromatium tepidum*, which contains a diguanylate cyclase domain (Kyndt et al. 2004).

Genome-based identification of photobiology in chemotrophs. *I. loihiensis* was identified in samples taken 35 km off the coast of Hawai'i at 1,300 meters below the water surface near a hydrothermal vent, and is closely related to an uncultivated organism found at 11,000 m depth in the Mariana Trench (Donachie et al. 2003). Thus, *I. loihiensis* is regarded as a deep sea bacterium. At such depths no sun light penetrates, and organisms in this environment live in complete darkness. *I. loihiensis* is an aerobic heterotroph capable of amino acid catabolism (Donachie et al. 2003) and has not been reported to exhibit photobiological responses.

The results reported here that *I. loihiensis* contains a functional PYP and exhibits light-induced suppression of biofilm formation are strong evidence that this organism also lives in a part of the ocean's water column where its biology is influenced by light. The inhibition of biofilm formation by light suggests that planktonic *I. loihiensis* cells are favored in the light, while biofilms form at greater depths. The metabolism of *I. loihiensis* is centered around amino acid catabolism, and it has been proposed that the organism grows on the proteinaceous particles that are present near deep sea hydrothermal vents. *I. loihiensis* is likely to form biofilms on such particles and may be dispersed when such particles flow to the ocean's surface.

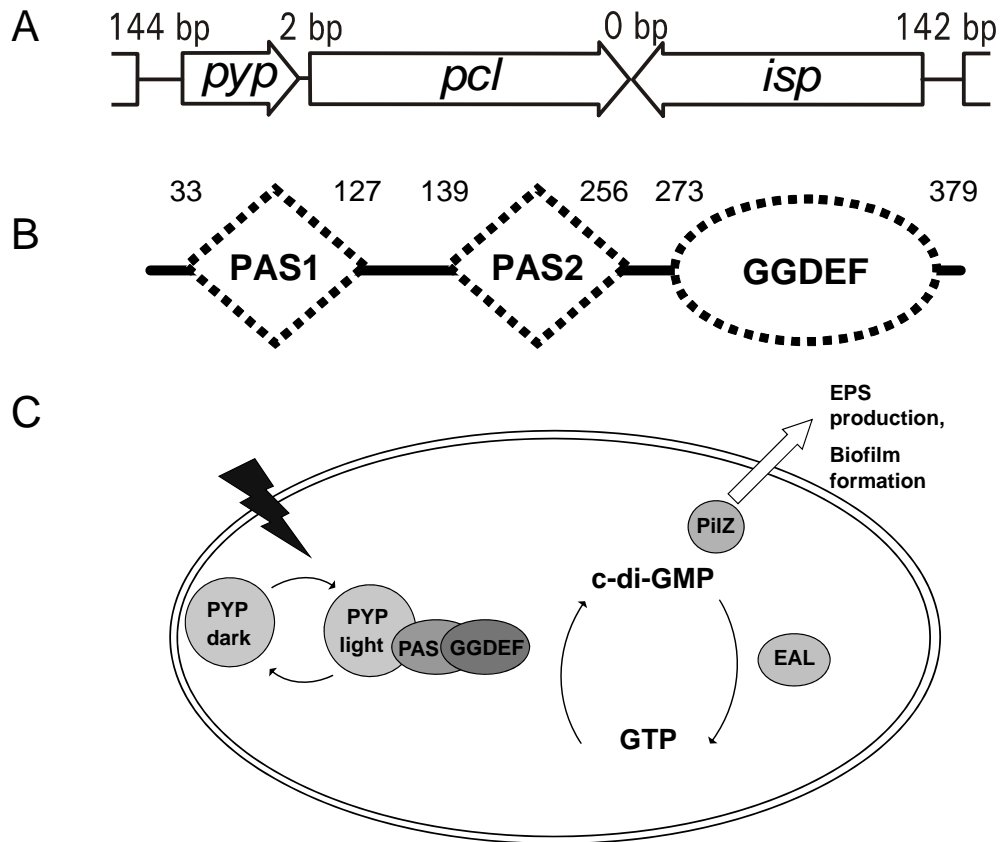


Figure 4.1.6. Model for the regulation of biofilm formation in *I. loihensis*. (A) Genetic context of the *Il pyp* gene. Genes are represented to scale as arrows: *pyp* is photoactive yellow protein (125 residues, IL2385), *pcl* is *p*-coumaryl:CoA ligase (422 residues, IL2386), *isp* is intracellular signaling protein, see panel B (392 residues, IL2387). The length (number of basepairs) of the intergenic regions is also indicated. (B) Domain architecture of the intracellular signaling protein (IL2387) immediately downstream of the *pcl* gene. The numbers of the residues at the start and end of each domain are indicated. (C) Model for light-regulated biofilm formation in *I. loihensis*. The proposed effect of PYP photoexcitation on the synthesis of c-di-GMP is indicated, together with the resulting physiological changes that result in biofilm formation.

4.1.5. Conclusions

I. loihiensis can form biofilms, and this process is inhibited by light. This light regulation of cell physiology is unexpected for a chemotrophic deep sea bacterium, and indicates that the organism also occurs in illuminated areas of the water column, close to the ocean surface. Genome sequencing projects have revealed photoreceptors in many chemotrophic bacteria. Thus it is likely that many novel light responses remain to be discovered in these organisms.

A novel approach to study *the in vivo* function of PYP was developed based on the use of *trans*-locked and *cis*-locked derivatives of the *pCA* chromophore in PYP, which results in constitutively inactive and constitutively active PYP derivatives, respectively. This approach was used to demonstrate that PYP is the photoreceptor for light-induced suppression of biofilm formation in *I. loihiensis*. This approach is generally applicable, and is particularly valuable for studies on organisms for which no genetic tools are available.

The genome of *I. loihiensis* encodes two enzymes that are likely to have TAL activity, and in addition it contains a *pcl* gene that forms an apparent operon with the *pyp* gene. This indicates that *I. loihiensis* contains the two enzymes for *pCA* synthesis and activation that allow holoPYP production.

The identification of II PYP as the photoreceptor for biofilm regulation in *I. loihiensis* broadens the range of biological processes regulated by PYP. Such diversity in output signals is an emerging theme from studies on different types of photoreceptors.

Heterologously overproduced II PYP is a yellow and photoactive protein. Its visible absorbance maximum, *pCA* pK_a , active site proton transfer, and pB lifetime are very similar to the well-studied PYP from *H. halophila*, despite the very different biological function of Hh PYP. The genome of *I. loihiensis* encodes proteins with clear homology to *pCL* (immediately

downstream of the *pyp* gene) and TAL for the synthesis and activation of the *pCA* chromophore of PYP.

The fast kinetics of pB decay in Il PYP do not match the slow biological that it triggers, providing a counterexample for a proposed correlation between the time scales for the photocycle of a photoreceptor and the biological response that it triggers.

Acknowledgements. WDH gratefully acknowledges support from NIH grant GM063805 and OCAST grant HR07-135S, and from startup funds provided by Oklahoma State University. KJH was supported by the “Molecules to cells” program from NWO.

The authors thank Dr. Shaobin Hou and Dr. Maqsdul Alam (University of Hawaii) for providing genomic DNA of *I. loihiensis* and Hans Bieräugel and Dr. Jan van Maarseveen for synthesis of chromophore analogs.

Supporting Information Available. Synthesis method for locked chromophores; TAL multiple sequence alignment; *pCL* multiple sequence alignment. This information is available free of charge via the Internet at <http://pubs.acs.org/>.

CHAPTER 4.2

A Conserved Helical Capping Hydrogen Bond in PAS Domains Controls Signaling Kinetics in the Superfamily Prototype Photoactive Yellow Protein

Masato Kumauchi¹, **Sandip Kaledhonkar**², Andrew F. Philip³, James Wycoff¹, Miwa Hara¹,
Yunxing Li², Aihua Xie,^{*2} and Wouter D. Hoff^{1*}

Department of Microbiology and Molecular Genetics¹ and Department of Physics², Oklahoma State University, Stillwater, Oklahoma, 74078, USA, and Department of Biochemistry and Molecular Biology³, The University of Chicago, Chicago, Illinois, 60637, USA.

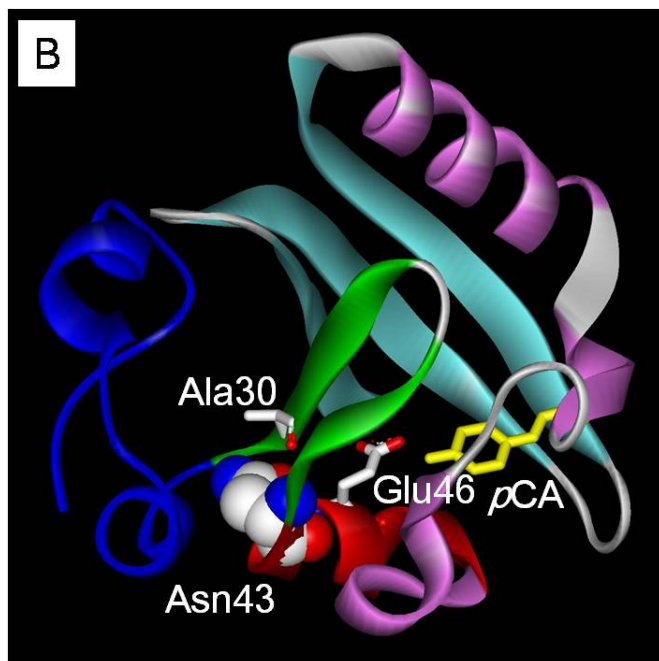
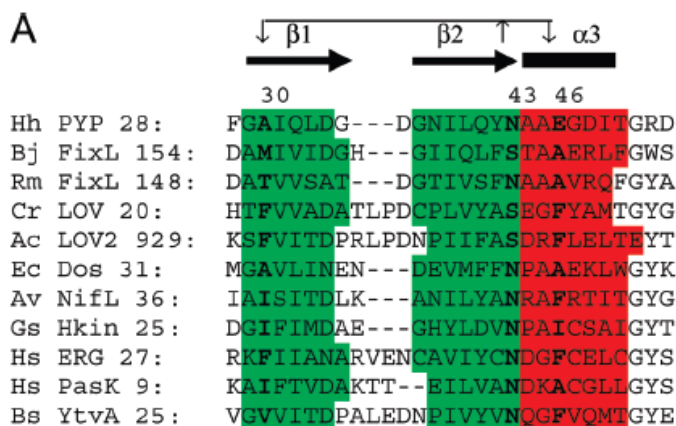
*To whom correspondence should be addressed: Wouter D. Hoff, 307 Life Sciences East, Stillwater, OK 74078. Tel: 405-744-4449; Fax: 405-744-6790; E-mail: wouter.hoff@okstate.edu or Aihua Xie, 145 Physical Sciences II, Stillwater, OK 74078. Tel: 405-744-6589; Fax: 405-744-6811; E-mail: xaihua@okstate.edu.

Reprinted with permission from (J. Am. Chem. Soc. 2010, 132:15820-15830) Copyright (2010) American Chemical Society

Abstract: PAS domains form a divergent protein superfamily with more than 20,000 members that perform a wide array of sensing and regulatory functions in all three domains of life. Only 9 residues are well-conserved in PAS domains, with an Asn residue at the start of α -helix 3 showing the strongest conservation. The molecular functions of these 9 conserved residues are unknown. We use static and time-resolved visible and FTIR spectroscopy to investigate receptor activation in the photosensor photoactive yellow protein (PYP), a PAS domain prototype. The N43A and N43S mutants allow an investigation of the role of side chain hydrogen bonding at this conserved position. The mutants exhibit a blue-shifted visible absorbance maximum and up-shifted chromophore pK_a . Disruption of the hydrogen bonds in N43A PYP causes both a reduction in protein stability and a 3,400-fold increase in the lifetime of the signaling state of this photoreceptor. A significant part of this increase in lifetime can be attributed to the helical capping interaction of Asn43. This extends the known importance of helical capping for protein structure to regulating functional protein kinetics. A model for PYP activation has been proposed in which side chain hydrogen bonding of Asn43 is critical for relaying light-induced conformational changes. However, FTIR spectroscopy shows that both Asn43 mutants retain full allosteric transmission of structural changes. Analysis of 30 available high resolution structures of PAS domains reveals that the side chain hydrogen bonding of residue 43 but not residue identity is highly conserved, and suggests that its helical cap affects signaling kinetics in other PAS domains.

4.2.1. Introduction

Photoactive yellow protein (PYP) is a blue light receptor from the halophilic photosynthetic proteobacterium *Halorhodospira halophila* (Meyer 1985, Meyer et al. 1987) and is a prototype PAS domain (Pellequer et al. 1998, Cusanovich et al. 2003). PYP was the first PAS domain for which the three-dimensional structure was reported (Borgstahl et al. 1995, Getzoff et al. 2003), and remains the PAS domain that is best understood in terms of biochemistry and biophysics at the protein level (Hellingwerf et al. 2003). The PAS domain is a ubiquitous protein module with a common three-dimensional fold involved in a wide range of regulatory and sensory functions in all domains of life (Taylor et al. 1999). Amino acid sequence analysis indicates that over 20,000 proteins in the protein sequence database contain a PAS domain, with 43 PAS domains present in the human genome as listed in the SMART database (Schultz et al. 1998). The term PAS is derived from the first letter of the name of the three founding members of the superfamily: the *Drosophila* period protein (Per), the aryl hydrocarbon receptor nuclear translocator protein (Arnt) and the *Drosophila* single-minded protein (Sim). PAS domains have been identified in a wide range of signaling proteins (Ponting et al. 1997, Taylor et al. 1999), including transcription factors, circadian clock proteins, phytochrome, and other proteins involved in regulation, photosensing, and oxygen/redox sensing. Interestingly, all members of this diverse set of proteins appear to be involved in sensing or regulation. Medically important PAS domains include the human ERG potassium channel. Mutations in various domains of this protein, including its PAS domain, cause cardiac arrhythmias (long QT syndrome) (Chen et al. 1999). The PAS domain protein hypoxia-inducible factor is involved in myocardial and cerebral ischemia (Semenza 2000) and in tumor hypoxia (Maxwell et al. 1997).



shown in red, while β -strand 1 and 2 are indicated in green. The *pCA* chromophore is depicted in yellow, and the N-terminal region of PYP in dark blue.

Figure 4.2.1. Sequence conservation and structural context of Asn43 in PYP. (A) Multiple sequence alignment of the N-terminal region of PAS domains with conserved side chain hydrogen bonding at residue 43. The PAS domain residue numbering used here is based on the PYP from *Halorhodospira halophila*. The number of the first depicted residue of each PAS domain is shown. The sequence alignment was adjusted based on the known three-dimensional structure of these PAS domains. Secondary structure is indicated: α -helices are shown in red and by the thick black bars; β -strands are indicated in green and by the black arrows. Residue 43 and its two key hydrogen bonding partners in β -strand 1 and α -helix 3 are highlighted in bold. The conserved side chain hydrogen bonds of residue 43 with the backbone amide groups of these two residues are indicated by arrows. Hh = *Halorhodospira halophila*; Bj = *Bradyrhizobium japonicum*; Rm = *Rhizobium meliloti*; Cr = *Chlamydomonas reinhardtii*; Ac = *Adiantum capillus-veneris*; Ec = *Escherichia coli*; Av = *Azotobacter vinelandii*; Gs = *Geobacter sulfurreducens*; Hs = *Homo sapiens*; Bs = *Bacillus subtilis*. (B) Schematic representation of the crystal structure of PYP highlighting Asn43. The side chain of Asn43 is shown in CPK coloring. As in panel (A), α -helix 3 is

PYP consists of 125 residues divided into two regions (Fig. 1b): (i) a typical PAS domain fold (Hefti et al. 2004) with a central antiparallel 6-stranded β -sheet flanked by three α -helices (residue 28 – 125; referred to below as the PAS domain core of PYP); and (ii) two N-terminal α -helices (residues 1 – 27) not present in most other PAS domains (referred to below as the N-terminal region). The two N-terminal helices pack against the central β -sheet, forming a second, small hydrophobic core in PYP (Borgstahl et al. 1995). Six of the nine residues that are fairly highly conserved in PAS domains are present in PYP. PYP has been studied extensively by site-directed mutagenesis (summarized in (Kumauchi et al. 2008)). A systematic study examining the effects of mutating each of the 13 Gly residues in PYP to Ala revealed that substitution of the three Gly residues in PYP that are conserved in the PAS domain superfamily (Gly31, Gly51, and Gly59) result in fairly small changes in its biochemical properties (van Aalten et al. 2002, Imamoto et al. 2008).

PYP functions as the photoreceptor for negative phototaxis in *H. halophila* (Sprenger et al. 1993). It exhibits a light-triggered photocycle (Meyer et al. 1987) based on its *p*-coumaric acid (*p*CA) chromophore (Baca et al. 1994, Hoff et al. 1994). In the initial pG dark state of PYP the *p*CA is in the *trans* conformation and its phenolic oxygen is deprotonated due to its pK_a of 2.8 (Meyer 1985, Hoff et al. 1997), which is strongly down-shifted from the pK_a of 8.8 for *p*CA in solution (Kroon et al. 1996). The *p*CA forms functionally critical hydrogen bonds with active site residues Tyr42 and Glu46 (Genick et al. 1997, Imamoto et al. 1997). Light initiates the PYP photocycle through the photoisomerization of the *p*CA (Kort et al. 1996), followed by *p*CA protonation from Glu46 (Xie et al. 2001) and subsequent large protein conformational changes (Hoff et al. 1999, Xie et al. 2001, Imamoto et al. 2002) that result in the formation of the pB intermediate. This pB state is believed to be the signaling state of PYP, and spontaneously decays to the initial pG dark state of PYP in a few hundred milliseconds. Spectroscopic evidence indicates that upon pB formation the N-terminal region of PYP dissociates from its PAS domain

core, and becomes largely unfolded (van der Horst et al. 2001, Imamoto et al. 2002, Harigai et al. 2003). This is a striking example of allosteric transmission of a structural change across a protein, since the photoactive site of PYP and the N-terminal region are separated by the rigid central β -sheet in PYP. The changes in electrostatic interactions caused by proton transfer from Glu46 to the *p*CA have been identified as a key mechanism in triggering large conformational changes during the “protein quake” that results in pB formation (Xie et al. 2001, Derix et al. 2003). However, the mechanism for the allosteric transmission of conformational changes in PYP from the chromophore binding pocket to the N-terminal region has not yet been identified. Here we examine the role of Asn43 in this mechanism. The role of Asn43 in receptor activation in PYP is of interest for the more general question of allosteric signal transmission (Goodey et al. 2008, Tsai et al. 2009).

The side chain of Asn43 in PYP forms four hydrogen bonds, all of which are buried: with the backbones of Leu23 in α -helix 2, Phe28 and Ala30 in β -strand 1, and Glu46 in α -helix 3. These side chain hydrogen bonds of Asn43 thus hold three secondary structure elements together. The side chain hydrogen bond between Asn43 and the backbone of Glu46 forms an α -helical cap (Aurora et al. 1998) (Fig. 1 and 2), which likely stabilizes α -helix 3. The term “helical cap” is occasionally used to describe a terminal helical domain in a protein. Here we use it to designate the specific hydrogen bonding pattern of a side chain at the end of an α -helix with a backbone amide in this helix. The side chain hydrogen bonds to Phe28 and Ala30 anchor β -strand 1 at the start of the PAS domain fold to the rest of PYP. Finally, the hydrogen bond to Leu23 contributes to the docking of the N-terminal region of PYP to the central β -sheet. Below we refer to the hydrogen bond between Asn43 and Ala30 as the structural bridging hydrogen bond and that between Asn43 and Glu46 as the helical capping hydrogen bond. Since the side chain hydrogen bonds of Asn43 are structurally implicated in linking the N-terminal region to the central β -sheet of PYP, light-induced changes in hydrogen bonding of this residue are a clear candidate for the

mechanism of allosteric transmission of conformational changes at the photoactive site of PYP to its N-terminal region during pB formation. Evidence for such a model has been reported based on time-resolved X-ray crystallographic studies of PYP (Rajagopal et al. 2005). Here we report experiments that provide an experimental test of this proposal.

A major recent development in the molecular life sciences is the determination of the amino acid sequences of large numbers of proteins due to improvements in DNA sequencing technology. Sensitive methods to identify weak amino acid sequence similarities in databases have revealed that many proteins contain short (~100 residues) conserved domains (Schultz et al. 1998, Bateman et al. 2004), and that shuffling of such domains is an important process in protein evolution (Orengo et al. 2005). These conserved domains typically form large protein superfamilies that share a common three-dimensional fold, but are highly diverse with respect to both amino acid sequence and functional properties. Classical protein families have a common active site and therefore contain conserved active site residues. However, protein superfamilies often exhibit a high degree of variation in their active sites. This raises a novel question: what is the molecular role of the conserved amino acids in protein superfamilies? Are these residues required for stability and folding or are they functionally critical? It has been proposed that highly conserved residues form a folding nucleus, but this proposal is debated (Mirny et al. 2001, Larson et al. 2002). We explore these issues for the most conserved residue in the PAS domain superfamily.

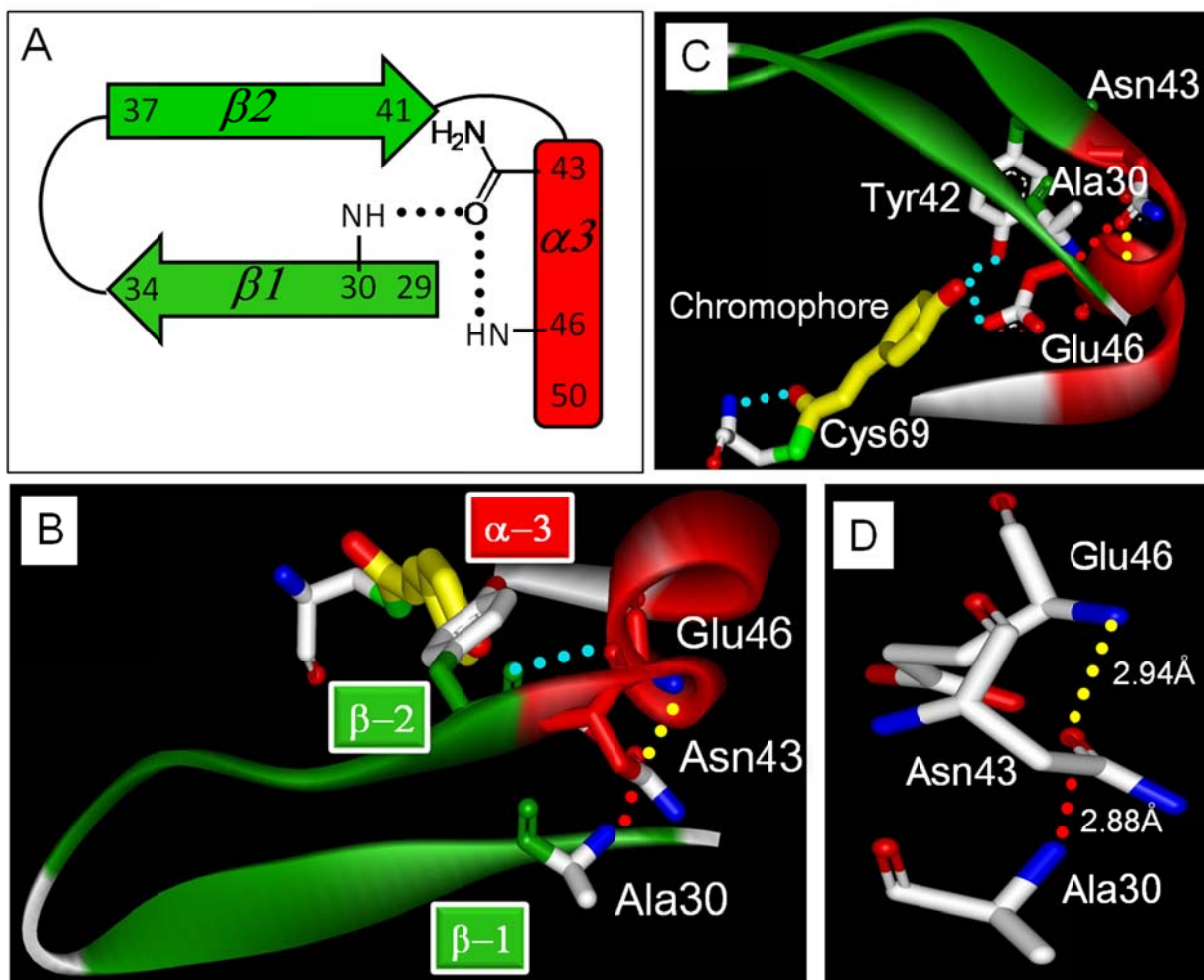


Figure 4.2.2. Side chain hydrogen bonding of Asn43 in PYP. (A) Cartoon of the conserved hydrogen bonding pattern (residue numbering for PYP). (B and C) Residue 28 to 50 of PYP (1NWZ) shown in two orientations, together with the *pCA*. Selected hydrogen bonds are shown as dotted lines, α -helices are shown in red, and β -strands in green. The helical capping hydrogen bond is shown in yellow, the structural bridging hydrogen bond in red. (D) Zoom in to highlight the hydrogen binding interactions of Asn43.

The PAS domain was initially identified through its weak sequence conservation (Ponting et al. 1997, Taylor et al. 1999). The subsequent determination of the three-dimensional structure of a number of proteins from this superfamily revealed that they share a common protein fold (Pellequer et al. 1998, Hefti et al. 2004). While PAS domains are ~100 residues in length, only nine residues show fairly strong conservation. Three-quarters of PAS domains contain 4 to 7 of the 9 conserved residues, with Asn43 (residue numbering based on the PYP from *Halorhodospira halophila*) as the most conserved residue (Taylor et al. 1999). PAS domains can bind a variety of cofactors, including heme and flavin, but some function in the absence of cofactors. Thus a conserved active site is not expected. The residues conserved in PAS domains could be required for the folding or stability of the PAS domain fold or be part of a conserved signaling mechanism. If these residues are functionally important, they may be involved in some aspect of a conserved allosteric switch for PAS domain signaling.

Since the residues conserved in PAS domains are not part of the active site, they have not been selected in structure-based site-directed mutagenesis studies. Therefore, the functional role that these 9 moderately conserved residues play in PAS domains is not known. This indicates that important gaps in understanding remain in current approaches to evaluating three-dimensional structures of proteins to identify residues that are critical for function. Here we report that Asn43, the most highly conserved residue in PAS domains (Fig. 1a), affects signaling kinetics in PYP.

The role of helical capping interactions, such as the side chain of Asn43, in determining protein stability had been extensively studied (Serrano et al. 1992, Doig et al. 1995). The propensity for helical capping varies strongly for different side chains (Doig et al. 1997, Aurora et al. 1998). Whereas Asn and Ser are often observed to form N-terminal α -helical capping interactions, this capacity is fully lacking in Ala. We therefore probe the role of side chain hydrogen bonding by residue 43 in PYP using the N43S and N43A mutants. The results show that the helical capping hydrogen bond strongly affects both the stability and signaling kinetics of

PYP. This extends the importance of helical capping from protein structure and stability (Serrano et al. 1992, Doig et al. 1995, Doig et al. 1997, Aurora et al. 1998) to regulating the kinetics of functional transitions, and provides a specific functional molecular role for the most highly conserved residue in PAS domains.

4.2.2. Experimental Section

Mutagenesis and protein purification. Mutagenesis was performed using Stratagene's QuikChange site-directed mutagenesis kit with primers designed to introduce the N43A and N43S substitutions. A pQE-80A plasmid (QIAGEN) containing the *pyp* gene inserted between *Bam*HI and *Hind*III sites was used as template. The PCR products were digested with *Dpn*I and transformed into *E. coli* DH5 α . DNA was purified using a QIAprep Spin Miniprep kit (QIAGEN), used for DNA sequencing to confirm the mutation in the intact *pyp* gene, and transformed into *E. coli* BL21 (DE3) cells grown on LB agar with ampicillin (200 μ g/mL). Overproduction of apoPYP was induced by the addition of 1 mM IPTG, and the protein was extracted from *E. coli* BL21 (DE3) using 8 M urea, and reconstituted with *p*-hydroxycinnamic anhydride (Sigma-Aldrich) following the procedure described in (Mihara et al. 1997).

UV/vis absorbance and fluorescence spectroscopy. UV/vis absorption spectra were measured at room temperature using an HP-8453 (Hewlett-Packard) diode array spectrophotometer and a monochromator-based Cary300Bio (Varian) spectrophotometer. A 150 W halogen quartz light source (Cuda) with a broadband blue filter (band pass filter 59855, Oriel) was used to initiate the photocycle of PYP in 10 mM Tris-HCl pH 7.5. After 15 seconds of illumination the actinic light was shuttered, and the thermal recovery of the dark state was measured with a time resolution of up to 100 milliseconds. Photocycle kinetics at 445 nm were described as a monoexponential or biexponential decay as needed. A mixed buffer (glycine, succinate, MES and MOPS, 100 mM each) was used for pH titrations from pH 1.5 to 10.0. The

acid titration was carried out in a darkened dark room using the minimal intensity of red light needed for handling of the samples. The pH dependence of the sample absorbance at its visible absorption maximum was described using the Henderson-Hasselbalch equation. Thermal unfolding curves were measured at pH 7.5 using an HP-8453 spectrophotometer equipped with a Peltier element. Denaturant titrations with guanidinium hydrochloride (Gdn-HCl) were performed at pH 7.5 in 10 mM Tris buffer at 25 °C in the same spectrophotometer and analyzed as described in (Lee et al. 2001).

Aromatic fluorescence emission measurements were performed at room temperature in a FluoroMax3 (Yobin Yvon) fluorimeter. Excitation was at 280 nm using a 3 nm slit width and PYP in 10 mM TrisHCl pH 7.5 with an OD of 0.2 at 441 nm. Titrations were performed using a buffered 6 M Gdn-HCl stock solution. For every measurement a fresh protein sample at a specific denaturant concentration was prepared.

FTIR spectroscopy. For FTIR spectroscopy PYP and its N43A and N43S mutants were used at 8 mM protein concentration in 50 mM phosphate buffer in D₂O at pH* 6.6, obtained by washing and concentration with a Microcon (YM-10, 10,000 MWCO, Millipore) centrifuge filter. An FTIR sample consisted of 2.7 µl of PYP sandwiched between two CaF₂ windows (15 mm diameter), separated by a 12 µm spacer. Sample temperature was controlled at 300 K. A Bruker IFS 66v spectrometer was utilized for static and time-resolved infrared measurements in the spectral range 4000-850 cm⁻¹ using a liquid nitrogen-cooled Mercury Cadmium Telluride (MCT) detector. The spectrometer sample chamber was purged with dried nitrogen gas. Light-induced infrared absorption changes in PYP were measured using rapid-scan FTIR spectroscopy at 4.5 cm⁻¹ spectral resolution with 200 kHz scanner velocity. The photocycle was triggered by 6 mJ laser pulses of 4 ns duration at 462 nm (Continuum Surelite-II pumped OPO laser). Laser repetition rate was set to 0.0033 Hz and 0.0166 Hz for N43A and N43S respectively, while the laser spot size on the FTIR sample was ~6 mm in diameter. Time resolved FTIR measurements

on N43A PYP were performed at room temperature and 4 cm^{-1} spectral resolution using a Nicolet 740 FTIR instrument with DTGS detector with dry air purging. A Cuda I-150 light source with a water filter and 420 nm cutoff filter was used to initiate the photocycle. Time resolved spectra were recorded on quasi-logarithmic time scale. Difference absorption spectra were calculated using single beam spectra of the sample immediately before illumination and single beam spectra at specific time points after shuttering the visible excitation. The resulting FTIR difference spectra were corrected for reproducible systematic baseline drift.

Analysis of three-dimensional structures. Swiss pdb viewer 3.7, WebLabViewerPro, and Pymol were used to examine three-dimensional structures of PAS domains, and for the automatic placement of hydrogen atoms in the structures. For four PAS domains (2O9C, 2OOL; 2VLG; 2Z6C) visual inspection of the automatic placement of the hydrogen atoms revealed an unfavorable hydrogen bonding geometry for the side chains of the residue corresponding to Asn43 in PYP. In these four cases, Swiss pdb viewer 3.7 was used for energy minimization, which converged to an alternative placement of the hydrogen atoms involved that resulted in a favorable hydrogen bonding geometry. Only hydrogen atoms moved in this optimization.

Table 4.2.1. Effect of the N43S and N43A mutations and deletion of the N-terminal 23 residues on the properties of PYP.

Property	wt	N43S	N43A	$\Delta 23$ PYP ^a
T_m (°C)	80.5 ± 0.4	76.3 ± 0.2	57.4 ± 0.3	nd
ΔG_U (kJ/mol)	44.9 ± 0.2	41.0 ± 1.8	(11.2 ± 1.1) ^d	nd
$[Gdm]_{1/2}$	2.8 ± 0.05	2.4 ± 0.05	(2.2 ± 0.05) ^d	nd
m (M ⁻¹)	6.6 ± 0.5	7.1 ± 0.3	(4.5 ± 0.9) ^d	nd
λ_{max} of pG (nm)	446	441	442	442
pK _a of pCA in pG	3.0	3.4	4.6	2.7
pB – pG amide I	100%	133%	138%	60%
pG Glu46 C=O (cm ⁻¹)	1737 ^b /1726 ^c	1725 ^c	1725 ^c	1736 ^c
pB lifetime (s)	0.5	17	1640	590

^a References (Imamoto et al. 2002, van der Horst et al. 2001, Harigai et al. 2003); ^b Measured in H₂O; ^c Measured in D₂O; ^d Derived assuming single transition (see main text); nd indicates not determined.

4.2.3. Results and Discussion

Differential effects of the N43A and N43S mutations on the stability of PYP. The effects of the N43A and N43S mutations on various functional properties of the initial pG state of PYP were determined, as summarized in Table 1. We first studied the effect of the N43A and N43S mutations on the stability of PYP (Table 1; Fig. 3; supplemental Fig. 1 and 2). In these experiments UV/vis absorbance spectroscopy was used to monitor thermal melting and equilibrium denaturant titrations. All three samples exhibited a thermally induced transition with an isosbestic point near 385 nm in which the native absorbance band near 445 nm is converted into an unfolded species with an absorbance maximum near 335 nm (supplemental Fig. 1). For wtPYP and the N43S mutant the entire thermal unfolding transition could be monitored. Thermal unfolding of the N43A mutant caused aggregation at temperatures above 80 °C. The midpoint temperature for thermal melting T_m of wtPYP (80.5°C) was only slightly reduced in the N43S mutant (76.3°C), but significantly decreased by the N43A mutation (57.4°C).

In the denaturant titrations wtPYP and the N43S mutant exhibited apparent two-state behavior with an isosbestic point near 380 nm (supplemental Fig. 2). The free energy for unfolding ΔG_U of wt PYP (44.9 ± 0.2 kJ/mol) derived from Gdn-HCl titrations with UV/vis absorbance detection (Fig. 3b) was decreased only slightly in N43S PYP (41.0 ± 1.8 kJ/mol). The ~ 4 kJ/mol reduction in ΔG_U caused by the N43S mutation is smaller than the destabilization of ~ 8 kJ/mol that is typically observed for mutants that disrupt a buried hydrogen bond (Fersht et al. 1985, Shirley et al. 1992, Byrne et al. 1995, Aurora et al. 1998, Takano et al. 1999, Pace et al. 2001, Deechongkit et al. 2004). This indicates that hydrogen bonding remains largely intact in N43S PYP.

In the case of the N43A mutant two distinct isosbestic points were observed: at 385 nm up to 0.8 M Gdn-HCl and at 375 nm at higher denaturant concentrations (supplemental Fig. 3). The spectral changes during the first part and last part of the denaturant titration were distinctly

different (Supplemental Fig. 3B). As for wtPYP and the N43S mutant, the denaturant dependence of the absorbance at 445 nm could be fitted as a single transition. However, this yielded a significantly reduced denaturant m value (Table 1). Based on this observation and on the non-isosbestic nature of the transition, we conclude that unfolding of N43A PYP by Gdn-HCl involves one or more partially unfolded intermediates. To test this proposal, we used fluorescence emission from aromatic amino acids to probe the unfolding of N43A PYP. These data reveal a transition that deviates from the one observed using 441 nm absorbance as a probe (Fig. 3C). This confirms that the denaturant-induced unfolding of N43A PYP deviates from two-state folding. While these data do not allow a complete description of the denaturant-induced unfolding of N43A PYP, they reveal that the N43A mutation strongly impairs the stability of PYP and disrupts the cooperativity of the folding process in PYP.

These results indicate that the side chain hydrogen bonds at position 43 contribute significantly to the stability of PYP, and that the stabilizing side chain hydrogen bonding interactions of Asn43 can also be performed by a serine at this position. This is in line with the shared propensity of Asn and Ser to form a helical capping hydrogen bond to residue $i + 3$ (Doig et al. 1995, Aurora et al. 1998). In addition, in various PAS domains containing a Ser at this position the helical capping hydrogen bond is maintained (see below). Part of the reduction in stability of N43A PYP can be attributed to the loss of the helical capping hydrogen bond of Asn43 (Serrano et al. 1992, Doig et al. 1995).

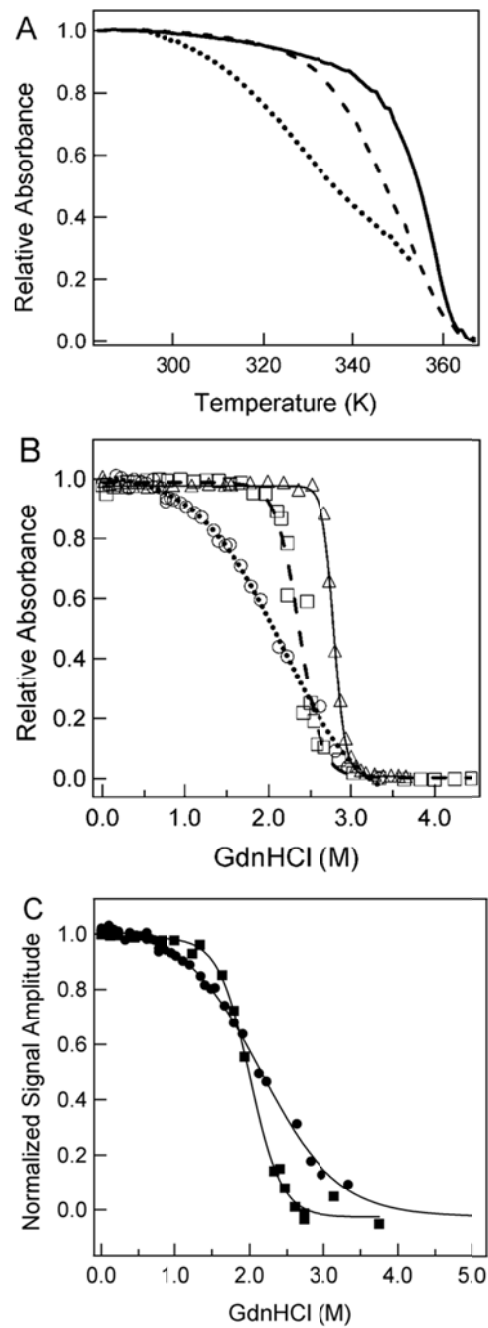


Figure 4.2.3. Effect of the N43A and N43S mutations on the stability of PYP. Thermal unfolding (A) and denaturant titration (B) of wtPYP (solid line), N43S PYP (dashed line), and N43A PYP (dotted line) probed using visible absorbance at 446 nm for wtPYP and 441 nm for the mutants. The data for the thermal unfolding of N43A PYP are truncated at the point where aggregation started to occur. The lines in (B) are fits of the denaturant titration data as single transitions. (C) Comparison of the denaturant titration of N43A PYP as detected by absorbance at 441 nm (circles) and aromatic fluorescence emission at 350 nm (squares).

Tuning of the properties of the pG dark state of PYP by Asn43. The absorbance spectrum (λ_{max}) of N43S and N43A PYP is blue-shifted by 5 nm, from 446 nm in wtPYP to 441 nm in the mutants (Fig. 4a). The overall shape of the absorbance spectra is essentially unchanged in the mutants. This shows that the side chain of Asn43 is involved in tuning the λ_{max} of PYP. Since the same blue-shift in the λ_{max} of the pG state is observed in N43A and N43S PYP, this spectral tuning is caused by an effect for which the hydrogen bonding interactions offered by the Ser side chain are not sufficient.

The protonation of the *pCA* chromophore at low pH in the mutants was monitored by UV/vis absorbance spectroscopy as the loss of the native absorbance band near 445 nm and the concomitant population of a new species with a λ_{max} near 345 nm (supplemental Fig. 4). This transition is described by the Henderson-Hasselbalch equation, revealing that the N43A mutation causes an up-shift in the pK_a of the *pCA* by 1.6 units, from 3.0 in wtPYP to 4.6 in the mutant (Fig. 4b). In contrast, the pK_a of the N43S mutant is up-shifted by only 0.4 pH units to 3.4. Thus, the removal of side chain hydrogen bonding at position 43 in the N43A mutant significantly increases the pK_a of the *pCA* in the pG state of PYP.

The effect of the N43S and N43A mutations on the structure of the pG state was studied by second derivative FTIR absorbance spectroscopy. The FTIR spectrum of a protein in the 1800-950 cm^{-1} region contains contributions from the protein backbone and from all polar and charged side chains. The peak positions of these overlapping bands are better resolved in the second derivative of the FTIR spectrum (Dong et al. 1992). Thus, the second derivative of the FTIR absorbance of a protein provides a sensitive “fingerprint” for the structure of a protein (He et al. 1991, Dong et al. 1992). This approach has been extensively applied to the amide I region, revealing that it provides a sensitive probe for changes in secondary structure (Dong et al. 1990, Zhang et al. 2005). The N43A mutation could result in a release and partial unfolding of the two

N-terminal helices of PYP. This would be sensitively detected in the amide I region of the second derivative FTIR spectrum.

The second derivative of the infrared absorbance spectrum of the pG dark state of wtPYP is very similar to that for the N43S and N43A mutants of PYP (Fig. 5). Specifically, the strong amide I signals at 1644 and 1635 cm^{-1} are essentially unchanged. This is strong evidence that the N43A mutation does not significantly perturb the secondary structure of PYP, indicating that the two N-terminal helices are still packed against PYP in the pG state of these two mutants. Most signals from side chains, for example at 1726 and 1689 cm^{-1} , are also largely unaltered. These results indicate that the side chain hydrogen bonds provided by Asn43 are not required for the docking of the N-terminal region of PYP in the pG dark state. Apparently, the N43A mutant reduces the stability of the pG state (see Fig. 3) while not significantly altering the structural properties of the folded state.

Careful inspection of the second derivative spectra indicates that the amplitude of the peak at 1726 cm^{-1} , which originates from the C=O stretching mode of the side chain of Glu46 (Xie et al. 2001), is reduced in the N43A mutant. Since the amplitude of signals in the second derivative spectrum is highly sensitive to the width of the peak in the infrared absorbance spectrum, this observation indicates a slight increase in the width of the Glu46 C=O stretching mode. This suggests a slight increase in the structural heterogeneity of the Glu46 side chain, without a change in its average properties.

Mechanism of active site tuning in the pG state of PYP by Asn43. Free *pCA* thioester compounds in water exhibit a pK_a near 8.8, and a λ_{max} near 400 nm in the ionized state (Kroon et al. 1996). These values are significantly shifted compared to the pK_a of 2.8 (Meyer 1985, Hoff et al. 1997) and λ_{max} of 446 nm (Maxwell et al. 1997) in native PYP. The mechanisms involved in tuning the pK (Yoda et al. 2001, Philip et al. 2008) and λ_{max} (Kroon et al. 1996, Yoda et al. 2001,

Yamato et al. 2007, Philip et al. 2008, Philip et al. 2010) in PYP have attracted significant attention, and are of more general relevance (Kochendoerfer et al. 1999, Harris et al. 2002). Both of these properties are affected by the N43A and N43S substitutions. The X-ray structure of the pG state PYP (Borgstahl et al. 1995, Getzoff et al. 2003) provides a framework to evaluate the structural basis for these effects. The side chain of Asn43 is 7.5 Å removed from the *pCA*, indicating that the effects of the N43A and N43S mutations on the properties of the *pCA* in the pG state are caused by an indirect mechanism.

Since Asn43 forms hydrogen bonds with the backbones of Leu23 in α -helix 2, Phe28 and Ala30 in β -strand 1, and Glu46 in α -helix 3, the observed effects caused by the N43A and N43S substitutions may be caused by three possible effects: (i) deformation of α -helix 3 due to a change in helical capping, (ii) a change in the docking of the N-terminal region, or (iii) a structural change in the PAS domain core of PYP by the disruption of the structural bridge between α -helix 3 and β -strand 1. We consider these three possibilities for altering the λ_{\max} and pK_a of the *pCA* in the pG dark state of the mutants. In the first option the loss of the helical capping interaction of α -helix 3 would result in an altered structure/position of this helix and thus of the critical active site residues Glu46 and Tyr42 that it contains. This would likely alter the λ_{\max} and pK_a of the *pCA*, since substitutions at these two residues significantly alter these properties (Genick et al. 1997, Mihara et al. 1997, Imamoto et al. 2001, Meyer et al. 2003). A reduction in the hydrogen bonding strength between the *pCA* and residue 46 in the E46Q mutant causes a red-shift in the λ_{\max} of PYP (Genick et al. 1997, Mihara et al. 1997). The absorbance spectra of the N43A and N43S mutants are essentially identical, and both are blue-shifted by 5 nm compared to wtPYP. This implies that it is not a change in the side chain hydrogen bonding interactions of residue 43 that blue-shifts the absorbance spectra in the mutants. In addition, FTIR spectroscopic results presented below show that the position of the negative signal at 1726 cm^{-1} in

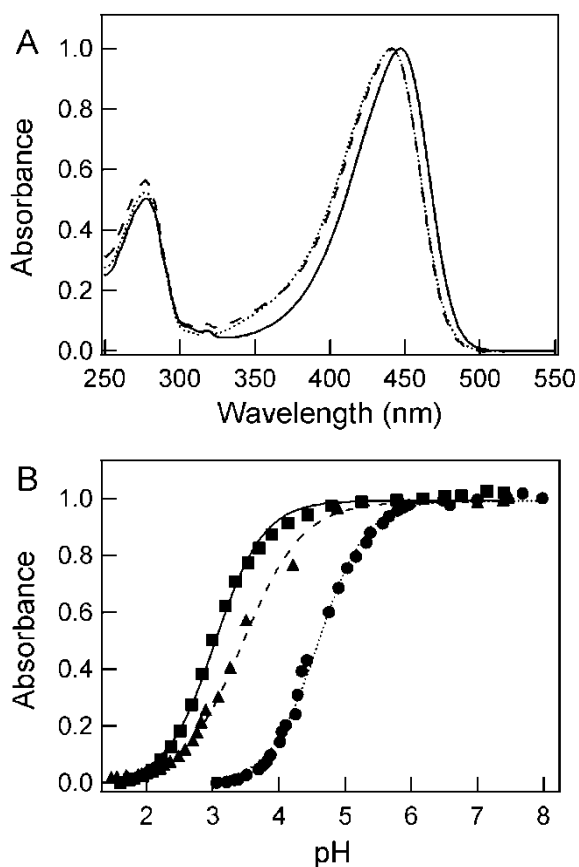


Figure 4.2.4. Effect of the N43A and N43S mutations on the absorbance maximum and pK_a of the *pCA* in PYP. Absorbance spectra at pH 7.1 (A) and pH titrations fit with the Henderson-Hasselbalch equation (B) are depicted, with data for wtPYP (solid lines and squares), N43S PYP (dashed lines and triangles), and N43A PYP (dotted lines and circles). The titration curves were obtained at 446 nm for wtPYP and 441 nm for the mutants. The pK_a and n values for these three proteins are 3.0/1.2, 3.4/1.0, and 4.6/1.2, respectively. The amplitudes of the data were normalized at their visible absorbance maximum.

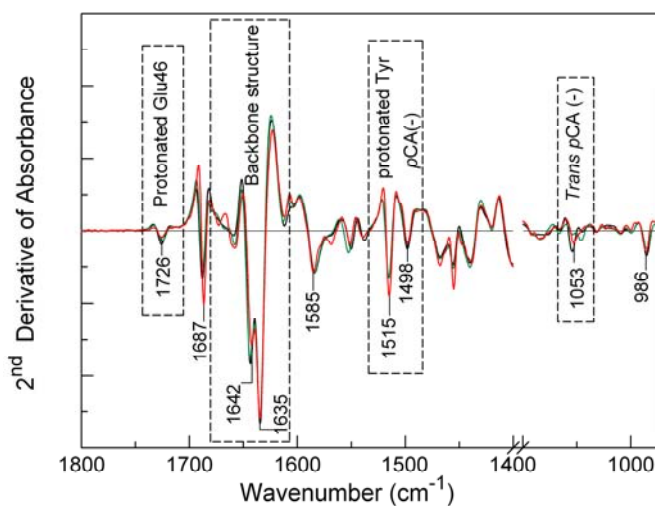


Figure 4.2.5. Probing structural deformations of the pG dark state of wtPYP (black) by the N43A (red) and N43S (green) mutations using second derivative FTIR spectroscopy. The FTIR absorbance spectrum of the three protein samples was measured at 2 cm^{-1} resolution, and was used to calculate the second derivative to facilitate comparison of spectral features in the three spectra. Selected peak positions are indicated.

the pB – pG difference spectrum caused by Glu46 deprotonation (Xie et al. 2001) is unaltered in both mutants (see Fig. 7), demonstrating that the hydrogen bond between Glu46 and the *pCA* is

not changed in the pG state of the two mutants. This argues against a change in the location of α -helix 3 or a structural disruption of the PAS domain core of PYP in the N43A and N43S mutants.

We also considered the possibility that mutations at position 43 cause a change in the strength of the hydrogen bond between the *pCA* and Tyr42. Spectroscopic analysis of active site mutants of PYP has indicated that mutations that weaken the *pCA*-Tyr42 hydrogen bond also affect the *pCA*-Glu46 hydrogen bond (Joshi et al. 2009, Sigala et al. 2009). Thus, the observation that the position of the C=O stretching mode of Glu46 at 1726 cm^{-1} is unaltered in the Asn43 mutants makes it unlikely that the Tyr42-*pCA* H-bond is significantly changed in these mutants.

Mutants lacking the N-terminal 23-27 residues of PYP exhibit a blue-shifted λ_{max} (442 nm) (van der Horst et al. 2001, Imamoto et al. 2002, Bernard et al. 2005), similar to that of the N43A and N43S mutants. This suggests that the blue-shift in the two mutants reported here is caused by an altered interaction between the PAS domain core of PYP and its N-terminal region. The second derivative FTIR spectra indicate that the N-terminal helices of PYP remain docked on the rest of PYP in the N43A and N43S mutants. This implies that an altered docking of the N-terminal region of PYP is involved in the blue-shifted λ_{max} of N43A and N43S PYP.

While the absorbance spectra of the N43A and N43S mutants are essentially identical, their *pCA* pK_a is significantly different: 3.4 for the N43S mutant and 4.6 for the N43A mutant. This result indicates that the side chain hydrogen bonds of residue 43 reduce the pK_a of the *pCA* by up to ~ 1.6 pH units. This could be due either to the capping function of residue 43 or to its role in holding the N-terminal region of PYP in place by its hydrogen bonds to Leu23, Phe28, and Ala30. Since the pK_a of the *pCA* in mutants lacking the N-terminal region is essentially unperturbed (below 3.0) (van der Horst et al. 2001), we propose that a change in the helical capping interaction is a key factor in the altered pK_a of the N43A mutant. Protonation of the *pCA* at low pH causes significant structural changes that have been described as acid denaturation.²¹

The capping interaction likely stabilizes α -helix 3, and the reduced stability of this helix in the N43A mutant can explain the reduced acid stability of the protein (Fig. 4.2.4b).

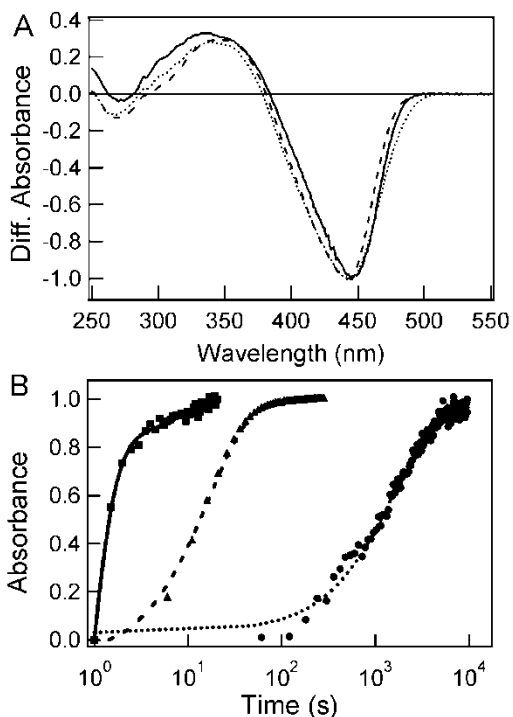


Figure 4.2.6. Substitutions at Asn43 slow down the kinetics of the last PYP photocycle step. The pB-pG UV/vis absorbance difference spectra (A) and kinetics of the pB to pG transition (B) for wtPYP (solid lines and squares), N43S PYP (dashed lines and triangles), and N43A PYP (dotted lines and circles) at pH 7.1 are shown. The difference spectra were normalized for the extent of bleaching of the pG state. The kinetics of the wtPYP photocycle were fitted as a biexponential decay, those of N43A and N43S PYP as a monoexponential decay. The amplitudes of the kinetic traces were normalized; the optical densities of the samples at their visible absorbance maxima near 445 nm were in the 0.35 – 0.45 range

The side-chain hydrogen bonds of residue 43 strongly affect the lifetime of the pB state.

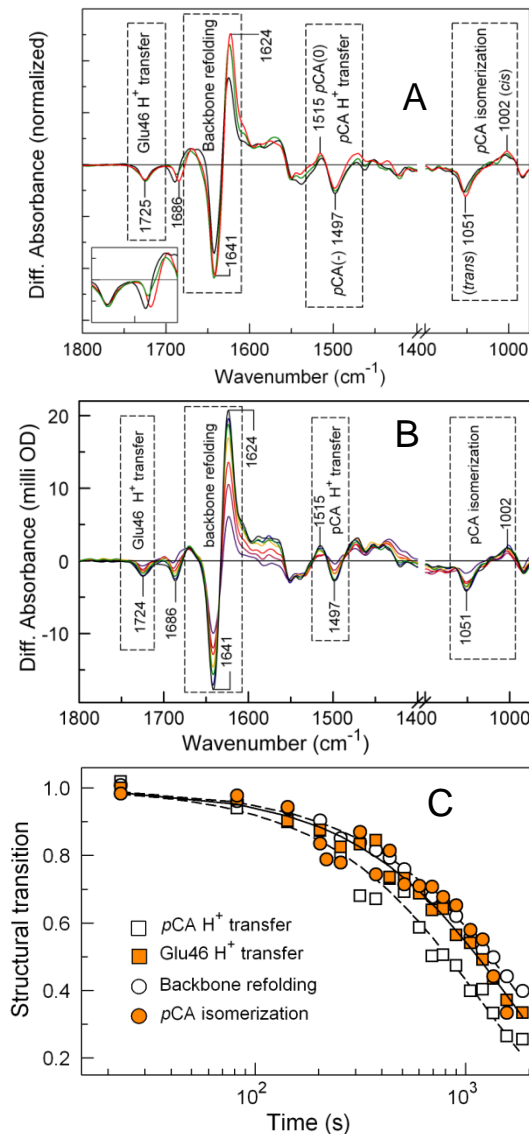
The kinetics of the last photocycle step in the N43A and N43S mutants was determined. The light – dark UV/Vis absorbance difference spectra of the two mutants show the formation of a pB state with a characteristic λ_{max} near 350 nm, very similar to that in wtPYP (Fig. 6a). For both mutants the decay of the pB state is significantly slowed down (Fig. 6b). However, the degree of deceleration greatly depends on the substitution at position 43. In wtPYP the decay of the pB state is biphasic, with the major fast component (90%) decaying with a time constant of 0.48 ± 0.04 seconds. In the N43S mutant the lifetime of the pB state is extended to 17 ± 0.2 seconds, while in N43A PYP it is $1,640 \pm 19$ seconds. These results reveal that the side chain hydrogen bonds of residue 43 have a strong effect on the lifetime of the pB state.

Substitutions at four positions have been reported to greatly slow down the kinetics of pB decay: Met100 (Devanathan et al. 1998, Kumauchi et al. 2002), Glu46 (Devanathan et al. 1999), Phe96 (Morishita et al. 2007), and Gly29 (Imamoto et al. 2008). For the G29A, E46D, M100K, and F96A mutants the lifetime of pB is 210, 385, 600, and 1,075 seconds, respectively. Thus, the N43A mutant of PYP exhibits the most dramatic increase in pB lifetime reported to date.

Structural changes during pB formation in the N43A and N43S mutants. To examine proton transfer events and structural changes during the formation of the pB intermediate in the N43A and N43S mutants, we performed time-resolved rapid-scan FTIR difference spectroscopy (Fig. 7). The negative signal at 1726 cm^{-1} caused by the deprotonation of Glu46 and the signals at 1497 and 1515 cm^{-1} caused by the protonation of the chromophore (Xie et al. 2001) are unchanged in the two mutants (Fig. 4.2.7), indicating that the proton transfer process from Glu46 to the *p*CA proceeds in the mutants as in wtPYP. The pB – pG FTIR difference spectra of wtPYP and the two Asn43 mutants can be convincingly scaled using these signals. This comparison reveals that the amplitude of the amide I difference signals at 1643 and 1623 cm^{-1} are increased by ~35% in the two mutants. This result shows that photoexcitation still triggers a large protein quake in the two Asn43 mutants, and that the amplitude of the protein quake is somewhat larger than in wtPYP. The increase in the amplitude of the amide I signals indicates that the Asn43 side chain somewhat constrains the structural changes that occur upon pB formation in a manner that cannot be achieved by Ala or Ser.

Close inspection of the pB – pG FTIR difference spectra indicates that the negative feature at 1689 cm^{-1} and the positive band at 1669 cm^{-1} are somewhat altered by the N43S and N43A mutations. Since these vibrational modes are still present in the mutants, they do not originate from the C=O stretching mode of the side chain of Asn43. These signals have not yet been assigned, precluding a further structural interpretation at this point.

Since the side chain of Asn43 forms multiple hydrogen bonds that bring together multiple regions of PYP, it is possible that pB decay in the N43A mutant is greatly slowed down because of a lack of cooperativity for the multiple structural changes that occur during the last part of the PYP photocycle. This possibility is supported by the loss of cooperativity in the unfolding of N43A PYP (Fig. 4.2.3C). To test this possibility we performed time-resolved FTIR measurements during the decay of the pB state in N43A PYP (Fig. 4.2.7B). In these measurements PYP in D₂O buffer was used to allow accurate measurements in the amide I region. We probed pB decay using infrared signals for four key events in the PYP photocycle:



reprotonation of Glu46 using the signal at 1725 cm⁻¹; protein conformational changes at 1641 and 1624 cm⁻¹, pCA protonation at 1515 and 1497 cm⁻¹, and pCA re-isomerization at 1051 cm⁻¹ (Fig. 4.2.7C). Each of these processes followed monoexponential decay, with an average time constant of 1,590 s. This is essentially identical to the rate observed using changes in visible absorbance at 441 nm. The rates for the four processes varied within a factor 1.25 (Fig. 4.2.7C). Since the very slow photocycle of N43A PYP reduces the quality of the FTIR spectra due to contamination of the sample with H₂O and water vapor signals, we conclude that the N43A mutations leaves the cooperativity of the pB decay process essentially intact.

Figure 4.2.7. Structural changes upon pB formation in wtPYP and its N43A and N43S mutants detected by FTIR difference spectroscopy. (A) The pB – pG infrared difference spectra at 4 cm⁻¹ resolution for wt (blue), N43A (red), and N43S (green) PYP (pH* = 6.6) were derived from flash-induced time-resolved rapid scan FTIR spectra. The inset shows a magnification of the peaks near 1726 and 1689 cm⁻¹. (B) Time-resolved FTIR difference spectroscopy during pB decay in N43A PYP. The plotted spectra range from 8 to 1,862 seconds. The region 1100-1140 cm⁻¹ is not shown because it does not contain relevant vibrational marker signals. (C) Amplitude-normalized kinetics of structural events during pB decay in N43A PYP. The data from (B) were used to extract the kinetics of Glu46 protonation (1724 cm⁻¹), pCA deprotonation (1515 and 1497 cm⁻¹), pCA reisomerization (1051 cm⁻¹), and backbone conformational changes (1641 and 1624 cm⁻¹). The transitions were fitted as monoexponential decays (lines), yielding lifetimes of 1,640, 1,190, 1,630, and 1,880 s (see main text).

Role of Asn43 in PYP receptor activation and deactivation. We examined the role of Asn43 in determining two aspects of the pB signaling state: its lifetime and its structural properties. Elimination of side chain hydrogen bonding in the N43A mutant results in a dramatic increase in the lifetime of the pB intermediate. We first consider altered docking of the N-terminal region as a factor in the affecting the lifetime of the pB state in N43A PYP. Two lines of evidence indicate that docking of the N-terminal region accelerates pB decay. First, substitutions at Phe6 in the minor hydrophobic core of PYP that weaken docking of the N-terminal region prolong the lifetime of the pB state by ~25-fold (Harigai et al. 2006) Second, mutants lacking 6, 15, 23, 25, or 27 N-terminal residues exhibit a reduced rate for pB decay ranging from 18 to 590 seconds (Harigai et al. 2001, van der Horst et al. 2001, Imamoto et al. 2002). These results show that the N-terminal region is not required for pB decay but does accelerate it. Above we concluded that the blue-shift in λ_{\max} in the Asn43 mutants is caused by an altered docking of the N-terminal region of PYP, which could affect pB lifetime However, the effect of the N43A mutation on the

lifetime of the pB state is at least a factor ~ 3 stronger than that of mutants lacking the entire N-terminal region. This indicates that factors other than docking of the N-terminal region are involved in causing the prolonged pB lifetime in N43A PYP.

Both the structural bridging hydrogen bond of Asn43 to Ala30 and its helical capping hydrogen bond to Glu46 may contribute to the increased pB lifetime in N43A PYP. The large conformational changes that occur upon pB formation (VanBrederode et al. 1996, Hoff et al. 1999, Imamoto et al. 2001, Lee et al. 2001) have been studied in detailed by NMR spectroscopy (Bernard et al. 2005). This revealed that formation of the pB state involves unfolding of α -helix 3 and disruption of the helical capping hydrogen bond of Asn43, while the hydrogen bond from Asn43 to Ala 30 remains intact. We therefore propose that refolding of α -helix 3, which contains key active site residue Glu46, is facilitated by the capping interaction of Asn43 during the re-formation of this helix upon pB decay. Thus, the formation of the helical capping hydrogen bond of Asn43 during pG recovery is a key interaction regulating the lifetime of the pB state. In this analysis both the refolding/re-docking of the N-terminal region and the re-establishment of the helical cap in α -helix 3 are key events in determining the lifetime of the pB signaling state. This provides a specific molecular functional role for a PAS-conserved residue.

The N43A mutation strongly affects both ΔG_U and pB lifetime. While no general trend has been reported that destabilizing mutations slow down functional turnover, the possibility exists that pB lifetime is directly related to the ΔG_U of PYP. Published data on the M100A and R52A mutant argue against this proposal. The ΔG_U of M100A PYP is reduced by 3.8 kJ/mol, while its pB lifetime is ~ 550 seconds (Devanathan et al. 1998). The R52A mutant exhibits a very similar reduction in ΔG_U , but its pB lifetime is 0.8 seconds (Genick et al. 1997). We conclude that the N43A mutation has a specific effect on the kinetics of the PYP photocycle.

Receptor deactivation kinetics are of direct importance for *in vivo* signal transduction. The lifetime of signaling states in microbial sensory rhodopsins has been shown to alter the sensitivity of the *in vivo* response (Yan et al. 1991), and appears to match the typical time scale of the biological response triggered by the receptor (Jung et al. 2003). Two-component regulatory systems also show a correspondence between the lifetime of an activated signaling component and the time scale of the biological response involved (Janiak-Spens et al. 1999, Thomas et al. 2008). Thus, the effects of the N43A and N43S mutations on pB lifetime would be expected to be biologically relevant.

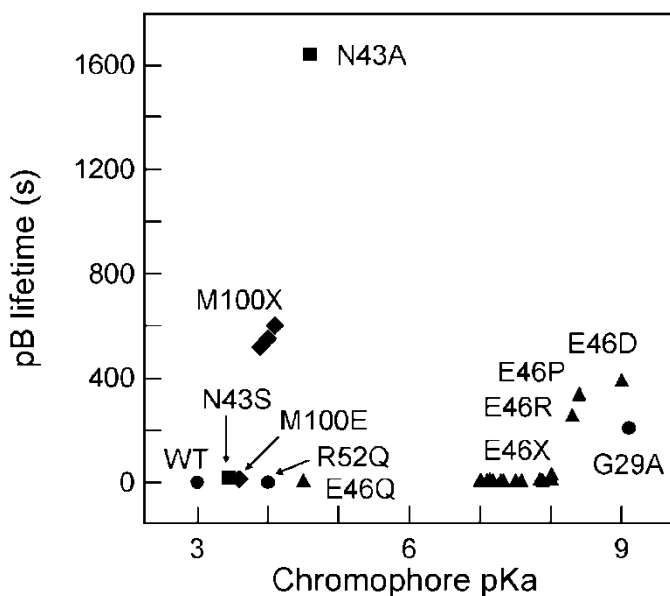


Figure 4.2.8. Comparison of functional properties of PYP mutants. The pK_a of the pCA in the pG state and the lifetime of the pB state for all mutants for which both of these properties have been reported is depicted. Substitution mutants at position Asn43 are indicated as squares, those at Glu46 as triangles, and at Met100 as diamonds; the remaining proteins are depicted by circles. The cluster of mutants indicated as M100X consists of the A, L and K substitution mutants of Met100; cluster E46X contains the A, C, G, H, I, K, L, N, S, T, V, W and Y substitutions of Glu46.

Regarding the role of Asn43 in determining the structure of the pB state, the finding that the N43A mutant exhibits light-induced structural changes that are somewhat larger than in wtPYP (Fig. 7) has important implications for the mechanism of receptor activation in PYP. X-ray crystallographic studies of PYP have suggested a role for the side chain hydrogen bonds of Asn43 in the allosteric transmission of conformational changes at the photoactive site of PYP to its N-terminal region during pB formation (Rajagopal et al. 2005). However, large light-induced conformational changes are observed in the N43A mutant. If the N43A mutation would cause the

release of the N-terminal region in the pG state, the amplitude of the light-induced amide I signals would be expected to be smaller, contrary to the rapid-scan FTIR results. In addition, the negative signals in the pB – pG FTIR difference spectrum, which originate from the pG state and thus provide a probe for the structure of the pG state, are largely unaffected by the two substitutions. This confirms the conclusion from the analysis of the second derivative FTIR absorbance spectrum of the pG state of the N43A mutant that the N-terminal region remains bound to the rest of PYP before photoexcitation. The data reported here show that even in the absence of side chain hydrogen bonding at residue 43 (the N43A mutant), large light-induced structural changes occur upon pB formation. This argues against a major role for photocycle-associated changes in side chain hydrogen bonds of residue 43 in triggering the release of the N-terminal region of PYP during pB formation.

The FTIR difference spectra of the N43A and N43S mutants of PYP are highly similar, while their pB lifetime is very different. This indicates that the structure of the pB intermediate in these two mutants is very similar, and that it is the transition state for pB decay that is differentially affected by the two mutations. Apparently it is not the altered pB structure of the two mutants detected in the FTIR difference spectrum but the lack of side chain hydrogen bonds to promote recovery of the pG state that greatly reduces the rate of pB decay in N43A PYP. In summary, the data reported here indicate that side chain hydrogen bonding at position 43 is a key factor in regulating the lifetime of the pB state, but not in triggering allosteric conformational changes upon pB formation.

A functionally important helical capping hydrogen bond. The data reported here allow a structural dissection of the role of Asn43 in determining key functional properties of PYP. The results indicate that the blue-shift in the λ_{\max} of PYP in the N43A and N43S mutations is not caused by the loss of the helical capping hydrogen bond of Asn43, and that allosteric transmission of structural changes upon pB formation can proceed in the absence of this helical capping

hydrogen bond. Our results provide evidence for the importance of the helical capping hydrogen bond of Asn43 in determining two functional properties of PYP. The analysis presented above indicates that the upshift in the pK_a of the *pCA* in the pG state of N43A PYP is caused by the disruption of the helical capping hydrogen bond of Asn43. In addition, a significant fraction of the dramatic increase in the lifetime of the pB state caused by the N43A mutation can be attributed to the removal of this helical capping hydrogen bond. This interpretation is strongly supported by the observation that the *pCA* pK_a and pB lifetime are largely unchanged in the N43S mutant but greatly altered in the N43A mutant (Fig. 8).

A number of studies have shown the importance of N-terminal α -helical capping interactions on protein stability (Serrano et al. 1992, Doig et al. 1995). Asn43 in PYP provides an example of an N-terminal helical capping hydrogen bond with functional importance. Since helical capping interactions are common in proteins, the importance of this interaction in regulating functional properties as reported here for PYP is likely to also be applicable to other proteins.

PYP has been studied extensively by site-directed mutagenesis, resulting in the identification of a number of mutations that alter its functional properties (Imamoto et al. 2008, Kumauchi et al. 2008). A summary of the effects of these mutations on the pK_a of the *pCA* in the pG state of PYP and on the lifetime of the pB state is provided in Figure 8. This analysis reveals that the N43A mutation causes a unique combination of strong changes in these two properties of PYP.

Table 4.2.2. Conservation of Hydrogen bonding interactions of Asn43 in PYP and other PAS domain

protein (PBD)	conserved residue	helical cap helix 3		link to β -strand 1	
			Length (Å)		Length (Å)
Hh PYP (1NWZ)	Asn43	Glu46	2.9	Ala30	2.9
Rm FixL (1D06)	Asn163	Ala166	2.8	Thr150	2.8
Av NifL (2GJ3)	Asn51	Phe54	2.9	Ile38	3.0
Ec DOS - O2 (1VB6)	Asn46	Ala49	2.9	Ala33	2.8
Ec DOS + O2 (1S67)	Asn46	H ₂ O	2.6		
Hs ERG (1BYW)	Asn45	Phe48	2.9	Phe29	3.2
Hs PasK (ILL8)	Asn25	Ala28	3.2	Ile11	3.4
Bs YtvA (2PR5)	Asn43	Phe46	2.9	Val27	2.9
Bj FixL (1DP6)	Ser169	Ala172	3.4	Met156	3.2
Ac LOV2 (1G28)	Ser947	Phe950	3.3	Phe931	3.0
Cr LOV1 (1N9L)	Ser38	Phe41	3.2	Phe22	3.1

^a Hh = *Halorhodospira halophila*; Rm = *Rhizobium meliloti*; Av = *Azotobacter vinelandii*; Ec = *Escherichia coli*; Hs = *Homo sapiens*; Bs = *Bacillus subtilis*; Bj = *Bradyrhizobium japonicum*; Ac = *Adiantum capillus-veneris*; Cr = *Chlamydomonas reinhardtii*. ^b Hydrogen bond from the side chain of Asn43 and corresponding residues to the backbone NH group of the indicated residue. ^c Hydrogen bonding length is indicated in Å.

Side chain hydrogen bonding of residue 43 is highly conserved in PAS domains. To examine a possible general role of side chain hydrogen bonding of residue 43 in the PAS domain superfamily, we used the DALI server (Holm et al. 2008) to identify proteins that are structurally related to PYP. We examined the three-dimensional structure of each of the 28 different PAS domains identified in this search. Six of these structures were determined by the Protein Structure Initiative (Grabowski et al. 2007). This analysis revealed that in 66% of the PAS domain structures the hydrogen bonding pattern of residue 43 (and the equivalent position in other PAS domains) is identical to that observed in PYP (Table 2 and supplemental Table 1). In an

additional 28% of the structures both hydrogen bonds were observed, but in an $n+1$, $n+2$, or $n+4$ capping configuration. The average dihedral angle Θ at the hydrogen atom for the structural bridging hydrogen bonds in this set of PAS domain structures is at an energetically favorable value of 156 ± 14 . In the case of the $n+3$ helical capping hydrogen bond the values of Θ are 146 ± 16 , slightly lower than ideal but still clearly in the allowed region (Kortemme et al. 2003). The three-dimensional structures of the region involved in the interactions of residue 43 with α -helix 3 and β -strand 3 are highly similar in most PAS domain structures (Fig. 9). Thus, the pattern of side chain hydrogen bonding interactions of residue 43, forming a helical cap for α -helix 3 and a structural bridge to β -strand 1, is highly conserved in the PAS domain superfamily. These conserved helical capping and structural bridging hydrogen bonds are indicated in Figs. 1, 2, and 9.

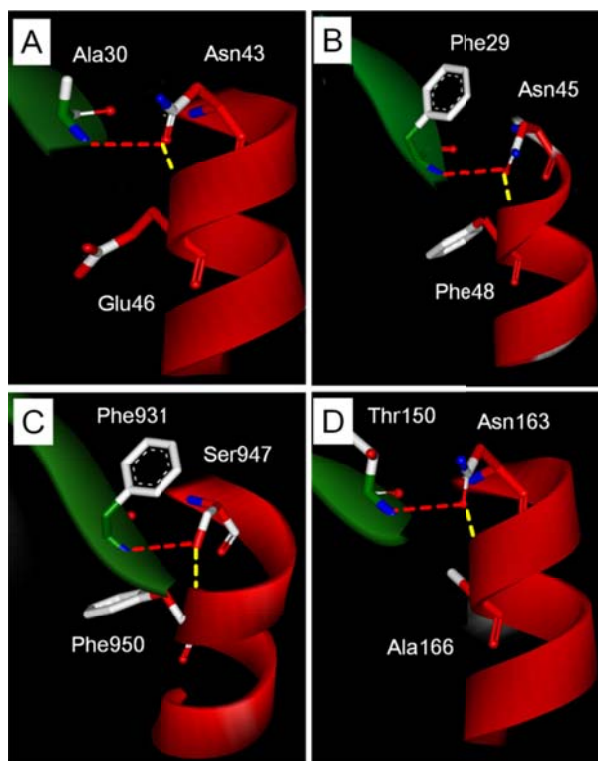


Figure 4.2.9. Conservation of the side chain hydrogen bonding interactions of residue 43 in the PAS domain superfamily. Depicted are the relevant regions of the PYP from *H. halophila* (A), human ERG (B), LOV2 from *Adiantum capillus-veneris* (C), and FixL from *B. japonicum* (D). α -Helix 3 is shown in red and β -strand 1 in green. The residues in the PAS domains corresponding to Asn43 in PYP are indicated with their side chain hydrogen bonds (dashed lines). The helical capping hydrogen bond is shown in yellow, the structural bridging hydrogen bond in red.

The 28 PAS domains with conserved side chain hydrogen bonding for residue 43 (PYP numbering) have very little sequence similarity. The residue corresponding to Asn43 in PYP is

conserved as Asn in 13 of these proteins, and is substituted by Ser, Asp, and Thr in 11, 2, and 1 PAS domain, respectively (Table 2 and supplemental Table 1). These substitutions retain side chain hydrogen bonding capability at position 43. Within the PYP family, Asn43 is fully conserved (Kumauchi et al. 2008), except for the PYP from *Thermochromatium tepidum* (Kyndt et al. 2004), where it is substituted with Ser. Multiple sequence alignments (Getzoff et al. 2003) of the PAS domain superfamily show that Ser is the most common substitution for Asp at position 43, providing support for an important role of side chain hydrogen bonding by residue 43 in the PAS domain superfamily. This analysis indicates that the side chain hydrogen bonding interactions of residue 43 are strongly conserved in PAS domains despite significant variation in the side chain found at this position. Thus, not residue identity at position 43 but the pattern of side chain hydrogen bonding interactions is conserved in this protein superfamily.

The high level of evolutionary conservation of the side chain hydrogen bonds of residue 43 in PAS domains suggests the possibility that it plays a conserved role in the function of this diverse protein superfamily as a whole. This is confirmed by analysis of hydrogen bonding in the heme-containing PAS domain from the oxygen sensor DOS from *E. coli*. (Kurokawa et al. 2004). The side chain hydrogen bonds of Asn46 that form the helical cap and the structural bridge to β -strand 1 in this PAS domain (Table 2) are intact in the absence of oxygen. However, O₂ binding causes conformational changes that disrupt both of these hydrogen bonds. This supports the notion that the functional importance of the side chain hydrogen bonds of Asn43 in PYP is conserved in other members of the PAS domain superfamily. This analysis indicates the possibility that the side chain hydrogen bonds of residue 43 modulate the kinetics of signaling in many members of the PAS domain superfamily.

4.2.4. Conclusions

Disruption of the side chain hydrogen bonds of Asn43 in N43A PYP significantly reduces the stability of PYP and causes an up-shift in the pK_a of the pCA (from 3.0 to 4.6), likely because of the removal of the helical capping hydrogen bond to the backbone of Glu46. In both the N43A and N43S mutants the λ_{max} is blue-shifted to 441 nm, which is attributed to a slightly altered docking of the N-terminal region.

The N43A mutation causes a dramatic increase in the lifetime of the pB state, largely attributed to the loss of side chain hydrogen bonding at this position. Analysis of the available data indicates that the helical capping hydrogen bond of residue 43 plays an important role in regulating the kinetics of receptor resetting in PYP. Thus, α -helical capping is not only important for protein structure and stability, but can also be a key factor for regulating functional kinetics. These results provide a clear molecular role for the most conserved residue in the PAS domain superfamily.

It has been proposed that the side chain hydrogen bonds of Asn43 are a key part of the mechanism of allosteric transmission of structural changes from the active site of PYP to its N-terminal region. However, time-resolved FTIR difference spectroscopy shows that the N43A mutant still exhibits large light-induced conformational change. Thus, side chain hydrogen bonding at this position is not an essential part of the allosteric trigger but affect the lifetime of the pB state.

Analysis of the structure of PYP together with a set of 28 PAS additional domains shows that the two side chain hydrogen bonds of the residue corresponding to Asn43 in PYP are highly conserved despite significant variation in the residue at this position: the structural bridging hydrogen bond to the start of β -strand 1 and the helical capping hydrogen bond. Analysis of published crystal structures of the oxygen sensor DOS from *E. coli* shows that O₂ binding

disrupts these side chain hydrogen bonds, suggesting that they play a functional role in a number of different PAS domains.

Acknowledgements. WDH gratefully acknowledges support from NIH grant GM063805 and OCAST grant HR07-135S, and from startup funds provided by Oklahoma State University. AX was supported by OCAST grant HR02-137R and the Oklahoma State Regents for Higher Education. We acknowledge help of Zhouyang Kang in data collection for the N43A time-resolved FTIR measurements. WDH acknowledges helpful discussions with Peter T. S. van der Gulik.

Supporting Information Available. UV/vis absorbance spectra during pH titrations, Gdn-HCl titrations, and thermal melts of the N43A and N43S mutants; table with hydrogen bonding interactions of Asn43 (and corresponding residues) in 29 PAS domains with known structure.

CHAPTER 4.3

Strong ionic hydrogen bonding causes a spectral isotope effect in photoactive yellow protein

Sandip Kaledhonkar^{1‡}, Miwa Hara^{2‡}, T. Page Stalcup², Aihua Xie¹, Wouter D. Hoff^{2,3*}

¹Department of Physics, Oklahoma State University, Stillwater OK 74078, USA; ²Department of Microbiology and Molecular Genetics, and ³Department of Chemistry, Oklahoma State University, Stillwater OK 74078, USA

Key words: Deuterium bond; H/D exchange; ionic hydrogen bond; isotope effects; spectral tuning.

Background: The role of ionic hydrogen bonds in protein active sites is not well understood.

Results: The absorbance spectrum of photoactive yellow protein is shifted in D₂O.

Conclusion: An active site ionic hydrogen bond explains this spectral isotope effect.

Significance: The spectral isotope effect can reveal and probe the unique properties of ionic hydrogen bonds in proteins.

Abstract: Standard hydrogen bonds are of great importance for protein structure and function. Ionic hydrogen bonds often are significantly stronger than standard hydrogen bonds and exhibit unique properties, but their role in proteins is not well understood. We report that hydrogen/deuterium exchange causes a redshift in the visible absorbance spectrum of photoactive yellow protein (PYP). We expand the range of interpretable isotope effects by assigning this spectral isotope effect (SIE) to a functionally important hydrogen bond at the active site of PYP. The inverted sign and extent of this SIE is explained by the ionic nature and strength of this hydrogen bond. These results show the relevance of ionic hydrogen bonding for protein active sites, and reveal that the inverted SIE is a novel tool to probe ionic hydrogen bonds. We propose a

classification of hydrogen bonds that distinguishes ionic hydrogen bonds from both standard and low barrier hydrogen bonds.

Since the classic work by Pauling, Corey and Branson in 1951 (Pauling et al. 1951), the central importance of hydrogen bonding for protein structure and function has been widely recognized (Kabsch et al. 1983). Backbone hydrogen bonding results in the formation of α -helices and β -sheets, while side chain hydrogen bonds provide specific interactions in the native state of proteins. Functionally important hydrogen bonds are ubiquitous at protein active sites (Gutteridge et al. 2005), and are key elements for enzymatic function (Shan et al. 1996). Biochemically relevant variations on the hydrogen bonding theme, such as low-barrier hydrogen bonds (LBHB) (Cleland et al. 1994), and C-H \cdots O hydrogen bonds (Manikandan et al. 2004), have attracted intense attention. However, many key questions remain unresolved, as was summarized by Perrin and Nielson in their influential review: “For all the importance of hydrogen bonding in chemistry and biology, it is remarkable that we understand it so poorly” (Perrin et al. 1997). Here we study how the unique properties of ionic hydrogen bonds, in which the hydrogen bond donor-acceptor pair carries a formal charge, affect the properties of proteins. We propose a hydrogen bonding classification that distinguishes between ionic hydrogen bonds in LBHBs.

We examine ionic hydrogen bonding in photoactive yellow protein (PYP), a small protein that serves as a model system for protein-ligand interactions at active sites (Cusanovich et al. 2003, Hellingwerf et al. 2003). PYP (Meyer 1985) exhibits a light-triggered photocycle based on its *p*CA chromophore (Hoff et al. 1994). The PYP from the photosynthetic bacterium *Halorhodospira halophila* (Hh PYP) is a highly studied (Cusanovich et al. 2003, Hellingwerf et al. 2003) member of a growing family of bacterial blue-light receptors (Kumauchi et al. 2008). The crystal structure of Hh PYP consists of a central antiparallel 6-stranded β -sheet flanked by five α -helices (Getzoff et al. 2003). The structure of the *p*CA binding pocket indicates Tyr42 and

Glu46 as key residues interacting with the phenolic oxygen of the *p*CA chromophore (Fig. 4.3.1a,b).

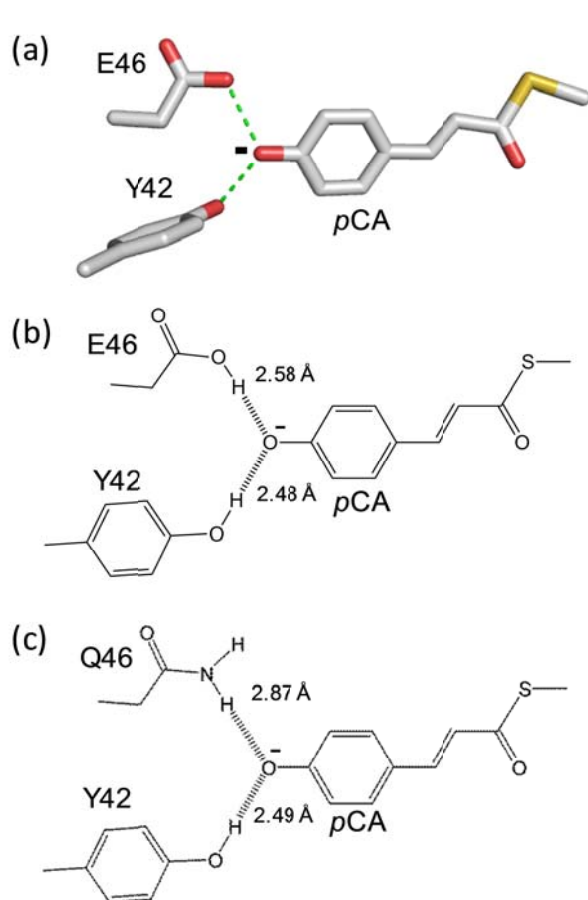


Figure 4.3.1. Anionic hydrogen bonding of *p*CA at the active site of PYP. A 3-dimensional depiction of hydrogen bonding of the anionic *p*CA at the active site of wtPYP based on its crystal structure (PDB ID 1NWZ) (A). A 2-dimensional depiction of hydrogen bonding of the *p*CA with residues 42 and 46, including hydrogen bonding lengths based on the crystal structures of wtPYP (B) and E46Q PYP (C) (PDB IDs: 1NWZ and 1OTA).

The active site of PYP exhibits a number of unusual properties. The protonation states of the *p*CA chromophore and Glu46 in PYP are opposite compared to the situation in solution. This causes the *p*CA to be present in its deprotonated form (Xie et al. 1996, Xie et al. 2001) and allows for biologically important proton transfer events during the PYP photocycle (Xie et al. 1996, Xie et al. 2001). In addition, the absorbance maximum (λ_{max}) of the *p*CA in PYP is strongly shifted from its value in solution, providing an example of the phenomenon of biological spectral tuning that is also at the basis of human color vision. Three major factors contribute to spectral tuning

effect PYP (Kroon et al. 1996). First, the formation of the thioester bond between the *pCA* and Cys69 results in a red-shift from 284 to 335 nm. Secondly, the deprotonation of the phenolic oxygen of the *pCA* causes a further shift to 400 nm. Finally, specific protein-chromophore interactions cause the final red-shift to 446 nm in the case of Hh PYP (Meyer 1985) and 432 nm for Sr PYP (Memmi et al. 2008).

The hydrogen bond between Glu46 and the *pCA* has been shown to be important in determining the λ_{\max} of Hh PYP. Weakening of this hydrogen bond in the E46Q mutant (Fig. 4.3.1c) (Anderson et al. 2004, Sugishima et al. 2004, Sigala et al. 2009) results in a red-shifted of the λ_{\max} to 460 nm, (Genick et al. 1997, Mihara et al. 1997) and its deletion in the E46I, V, and L mutants causes a further red-shift to 478 nm (Philip et al. 2008). High-resolution crystal structures (Getzoff et al. 2003, Anderson et al. 2004) and NMR spectroscopy (Sigala et al. 2009) have revealed a length of 2.6 Å for the Glu46-*pCA* hydrogen bond. In the E46Q this hydrogen bond is lengthened by 0.3 Å (Anderson et al. 2004, Sugishima et al. 2004). Previously, we have demonstrated that hydrogen bonding between residue 46 and the *pCA* changes the λ_{\max} of PYP by affecting not the energy gap between the ground and electronically excited state, but by specifically changing the width of the excited state energy potential (Philip et al. 2010). Thus, a precise description of the relation between hydrogen bond strength and λ_{\max} is complex, because it involves the identification of vibrational modes coupled to the optical transition, the determination of how these vibrational modes are affected by changes in electron delocalization caused by hydrogen bonding, and an evaluation of the Franck-Condon factors associated with these vibrational modes. Here we utilize the known empirical dependence of the λ_{\max} of PYP on the strength of the hydrogen bond between residues 46 and the *pCA*).

EXPERIMENTAL PROCEDURES

Mutagenesis and protein purification – The *pyp* gene from *S. ruber* was obtained by direct PCR amplification using lyophilized cell material and primers that introduced *NcoI* and *BamHI* restriction sites. The resulting PCR product was cloned into the pET-16b vector (Novagen), transformed to *Escherichia coli* XL1, and confirmed by DNA sequence analysis. The recombinant plasmid DNA was transformed into *E. coli* BL21 (DE3). The E46Q mutant of Sr PYP E46Q mutation was obtained by PCR using the corresponding mutagenic primers.

Hh PYP was obtained as described in (Imamoto et al. 1995). Sr PYP *apoprotein* was overexpressed in *E. coli* BL21 (DE3) following a similar procedure. Cells were harvested by centrifugation (2,700×g, 20min) and lysed in 8M urea. Cell debris was removed by centrifugation (17,200×g, 20min). The supernatant was diluted two-fold in Tris-HCl buffer (pH7.5), and the anhydride of *p*-coumaric acid was added. The resulting reconstituted protein was dialyzed against 10mM Tris buffer overnight at 4°C and applied to a DEAE Sepharose fast flow (GE Healthcare) chromatography column. Elution was performed using an NaCl gradient in Tris buffer; Sr PYP eluted at 300mM NaCl-Tris buffer (pH7.5). DNase I was added to the pooled yellow Sr PYP fractions. After overnight dialyzed at 4°C the chromatography was repeated until an optical purity index (Abs_{276}/Abs_{432}) of 1.0 was achieved. Hh PYP and Sr PYP were then exchanged to 50 mM potassium phosphate buffer (pH 7.0) and concentrated using Centricon and Microcon (Millipore) membrane filters (Amicon; YM-10, 10,000 MWCO). Protein samples in D₂O were obtained using the same procedure by washing the protein sample in a potassium phosphate buffer in D₂O (pH* 7.0) and concentration with a Microcon centrifuge filter.

Absorbance spectroscopy – UV/vis absorbance spectra were measured using a Cary 300 UV-Visible spectrophotometer (Varian) in double beam mode using a spectral bandwidth of 2.0

nm, a data interval 1.0 nm, and a scanning rate of 150 nm per minute. The wavelength accuracy of this spectrophotometer is ± 0.04 nm near the visible absorbance peak of PYP.

RESULTS AND DISCUSSION

Prediction and experimental detection of a spectral isotope effect in PYP – The exchange of the hydrogen atom in a hydrogen bond to deuterium modestly alters the strength of the hydrogen bonding interaction. In water hydrogen bonds are weaker than deuterium bonds by ~ 0.6 kJ/mol, which corresponds to a 5% weakening (Benjamin et al. 1963, Scheiner et al. 1996). In contrast, both experimental gas phase studies on small molecules and computational studies have revealed that ionic hydrogen bonds are characterized by the opposite effect, with a deuterium bond that is $\sim 5\%$ weaker (Scheiner et al. 1996, Scheiner 2000). The effect of H/D exchange on hydrogen bonding strength is based on subtle changes in intramolecular donor-acceptor vibrational modes across the hydrogen bond, which results in opposite effects upon H/D exchange for neutral versus ionic hydrogen bonds (Scheiner et al. 1996, Scheiner 2000). Based on the empirical dependence of the λ_{\max} of PYP on the strength of the hydrogen bond between residue 46 and the *p*CA, and reported effects of H/D exchange on hydrogen bonding strength, the effect of H/D exchange of the side chain of Glu46 on the λ_{\max} of PYP can be predicted. Since the Glu46–*p*CA hydrogen bond is ionic and therefore expected to be weakened upon H/D exchange, and because a weakened Glu46–*p*CA hydrogen bond results in a red-shift, we expect that the λ_{\max} of PYP in D₂O is slightly red-shifted. We refer to changes in position of the peak of an electronic transition λ_{\max} upon H/D exchange as a spectral isotope effect (SIE).

An estimate of the size of this SIE *p*CA can be obtained if both the change in hydrogen bonding strength upon H/D exchange ($\Delta\text{HBS}_{\text{H/D}}$) and the shift in λ_{\max} caused by a change in hydrogen bonding strength ($\Delta\lambda_{\max,\text{HBS}}$) are known:

$$\text{SIE} = \Delta\text{HBS}_{\text{H/D}} * \Delta\lambda_{\text{max,HBS}}$$

We estimate the dependence of the λ_{max} of Hh PYP on the hydrogen bonding strength between residue 46 and the *p*CA based on the spectral shifts caused by the E46Q and E46V mutations (Genick et al. 1997, Mihara et al. 1997, Philip et al. 2008). The E46Q mutation causes a 14 nm redshift (from 446 to 460 nm). We use the approximation that the E46Q mutation reduces the hydrogen bonding strength between the *p*CA and residue 46 by half (estimated at ~25 kJ/mol, i.e., half of a “typical” ionic hydrogen bond, see below), corresponding to a 721 cm^{-1} redshift in λ_{max} for a ~2,000 cm^{-1} reduction in hydrogen bond strength (see Table 4.3.1). These data yield a value for $\Delta\lambda_{\text{max,HBS}}$ of ~0.6 nm red-shift per 1 kJ/mol loss in hydrogen bond strength. A similar estimate is obtained when the 32 nm shift in λ_{max} upon the complete deletion of this hydrogen bond (estimated at ~50 kJ/mol) in E46V PYP is considered. Based on published results (Scheiner et al. 1996), we use a value of a 5% reduction in the strength of the ionic hydrogen bond between residue 46 and the *p*CA upon H/D exchange. Therefore, a 5% reduction (2.5 kJ/mol) in the strength of the Glu46–*p*CA hydrogen bond caused by H/D exchange would be expected to result in a ~1.5 nm red-shift in the λ_{max} of PYP. We experimentally tested this prediction for both the highly studied PYP from *H. halophila* (Hh PYP) and the recently identified PYP from the extremely halophilic bacterium *Salinibacter ruber* (Sr PYP), which was found to exhibit significantly different spectral and kinetic properties (Kumauchi et al. 2008, Memmi et al. 2008).

We determined the effect of H/D exchange of the side chain of Glu46 by measuring the UV/vis absorbance spectra of Hh PYP and Sr PYP in buffered H_2O and D_2O solutions (pH 7.0). This measurement revealed small but measurable shifts in the absorbance spectra of both Hh PYP and Sr PYP (Fig. 2, Table 1). The first derivatives of the absorbance spectra were used to extract the exact peak positions of the chromophore absorbance bands. This quantification of the SIE in

Hh PYP and Sr PYP yielded two key observations. First, the λ_{\max} of Hh PYP at 445.7 nm exhibits a 1.8 nm red-shift in D₂O (Fig. 2), consistent with previous results (Hendriks et al. 2003). Upon incubation in D₂O, the λ_{\max} of Sr PYP at 431.8 nm is red-shifted by 5.3 nm (Fig. 4.3.2). Thus, for both PYPs a SIE is observed. The direction of this SIE is consistent with the shift expected for an ionic hydrogen bond. We refer to this effect as an inverted SIE, because it is opposite of what would be expected for a standard hydrogen bond. Secondly, the inverted SIE for Sr PYP is larger by a factor three compared to that for Hh PYP.

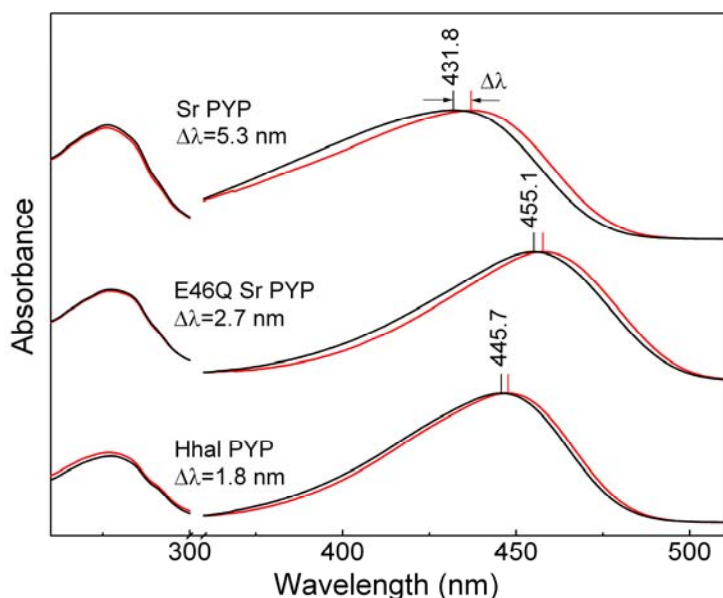


Figure 4.3.2. Spectral isotope effects in PYP. The UV/vis absorbance spectra of the PYPs from *S. ruber* (top two curves) and *H. halophila* (bottom two curves) and the E46Q mutant of Sr PYP (middle two curves) in H₂O (black) and D₂O (red). The shifts in the chromophore absorbance bands upon dissolving the proteins in D₂O are indicated.

Assignment and analysis of the SIE to the Glu46-*p*CA hydrogen bond – As a first step towards a solid assignment of the H/D exchanging group responsible for the observed inverted SIE in PYP, we note that the ionized *p*CA molecule in PYP does not contain any exchangeable protons (see Fig. 1). Therefore, any shifts in λ_{\max} upon H/D exchange are caused by interactions between the *p*CA and exchangeable groups in its protein binding pocket; particularly the phenolic OH group of Tyr42 and the COOH group of Glu46 stand out as likely candidates.

Table 4.3.1. Experimentally observed shifts in absorbance maxima of Sr PYP and Hh PYP and their E46Q mutants caused by H/D exchange compared to tentative estimates for the strength of the hydrogen bond between the *pCA* and residue 46.

Protein	Absorbance maximum		Tentative estimate of <i>pCA</i> –residue 46 HB strength ^a	
	nm	cm ⁻¹	kJ/mol	cm ⁻¹
Sr PYP				
H ₂ O	431.8	23,158	50.2	4,179
D ₂ O	437.1	22,878	47.7	3,970
Δ by H/D	5.3	280	2.5	209
Sr E46Q PYP				
H ₂ O	455.1	21,973	25	2,089
D ₂ O	457.8	21,843	23.8	1,989
Δ by H/D	2.7	130	1.3	100
Δ by mutation	23.3	1185	25	2,090
Hh PYP				
H ₂ O	445.7	22,436	45	3,761
D ₂ O	447.5	22,346	43	3,594
Δ by H/D	1.8	90	2	167
Hh E46Q PYP				
H ₂ O	460.5	21,715	23	1,922
D ₂ O	461.5	21,668	22	1,839
Δ by H/D	1.0	47	1	83
Δ by mutation	14.8	721	22	1880

^aThe depicted values are estimates based on the following assumptions: (i) *pCA*–Glu46 hydrogen bond in Sr PYP is 50 kJ/mol, a typical value for ionic hydrogen bonds. (ii) This hydrogen bond is 10% weaker in Hh PYP. (iii) The E46Q mutation weakens this hydrogen bond by 50% in both Sr PYP and Hh PYP. (iv) H/D exchange reduces the strength of this hydrogen bond by 5% in both Sr PYP and Hh PYP.

To experimentally test the possibility that the significant SIE in Sr PYP is due to the hydrogen bonds of the *pCA* with Tyr42 or Glu46, and to dissect the contributions of these two interactions to the SIE, we prepared the Y42F and E46Q mutants of Sr PYP. These mutants strongly diminish their hydrogen bonding to the *pCA* and therefore also any SIE associated with these hydrogen bonds. Y42F Sr PYP exhibited a very low expression yield and significant instability, precluding its purification for spectroscopic studies. For the E46Q mutant of Sr PYP we detected a 2.7 nm

red-shift in its λ_{\max} at 455 nm upon incubation in D₂O (Fig. 2). The ~2-fold reduction in SIE of E46Q Sr PYP compared to wt Sr PYP establishes that the strong hydrogen bonding interaction between Glu46 and the *pCA* is directly involved in this effect.

Structural and spectroscopic studies provide a framework for the interpretation of these spectroscopic data, and indicate two factors that are important for understanding the inverted SIE of PYP. The first factor is that the hydrogen bonds of Tyr42 and Glu46 with the *pCA* are short. X-ray crystallographic studies at 0.82 and 1.00 Å resolution have revealed that the hydrogen bonds of side chains of Glu46 and Tyr42 to the *pCA* chromophore are 2.6 and 2.5 Å, respectively (Getzoff et al. 2003, Anderson et al. 2004) (Fig. 1b), and thus are significantly shorter than standard hydrogen bonds. Neutron diffraction studies confirmed the presence of these short hydrogen bonds (Fisher et al. 2007, Yamaguchi et al. 2009). Independent information on the presence of these strong short hydrogen bonds with the *pCA* was obtained by both Fourier transform infrared (FTIR) spectroscopy of the C=O stretching mode of the side chain of Glu46 in Hh PYP (Xie et al. 1996, Xie et al. 2001) and by NMR spectroscopy of the far-downfield proton NMR signals of Tyr42 and Glu46 (Sigala et al. 2009). The second consideration is that the side chains of Tyr42 and Glu46 are neutral, while the *pCA* in PYP is ionized. Thus, the negatively charged phenolic oxygen of the *pCA* interacts with the neutral side chains of Tyr42 and Glu46 via a forked ionic hydrogen bond (Getzoff et al. 2003, Anderson et al. 2004, Yamaguchi et al. 2009). The short length and ionic nature of the Glu46–*pCA* hydrogen bond are in excellent agreement with the assignment of a SIE to this interaction.

The observation that the inverted SIE for Sr PYP is significantly larger than that for Hh PYP leads to the proposal that the Glu46–*pCA* hydrogen bond in Sr PYP is stronger than that in Hh PYP. This would be unexpected, since in Hh PYP this hydrogen bond already is quite strong and short (Getzoff et al. 2003, Anderson et al. 2004, Sigala et al. 2009, Yamaguchi et al. 2009). Two considerations provide direct support for this interpretation. First, the λ_{\max} of Sr PYP is

significantly blue-shifted compared to that of Hh PYP. An increase in the strength of the Glu46–*p*CA hydrogen bond would be expected to cause such a blue-shift. Secondly, the E46Q mutation causes a strong 1185 cm⁻¹ red-shift in the λ_{max} of Sr PYP at 457.8 nm (Fig. 4.3.2) compared to the smaller 721 cm⁻¹ red-shift caused by the same mutation in Hh PYP (Genick et al. 1997, Mihara et al. 1997). These results support the notion that the extent of the SIE in PYP reflects the strength of the ionic hydrogen bond between Glu46 and the *p*CA. In Fig. 4.3.3 we summarize the spectroscopic readout of the strength of the ionic hydrogen bond between residue 46 and the *p*CA at the PYP active site through an inverted SIE.

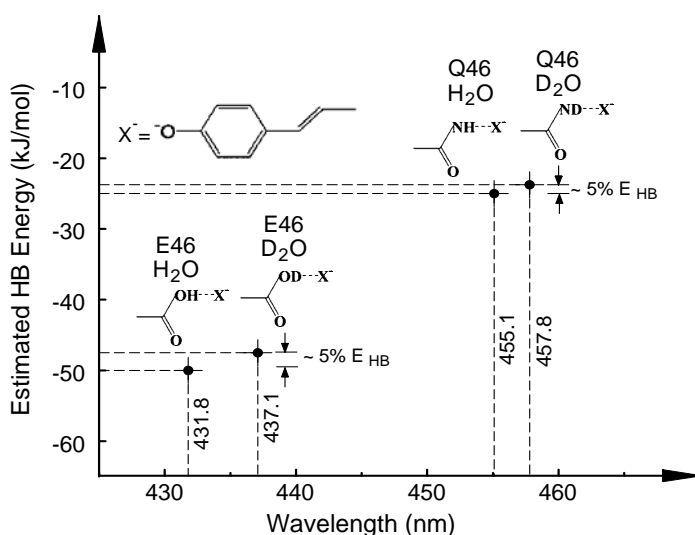


Figure 4.3.3. Effects of H/D exchange on active site hydrogen bonding strength and absorbance maximum in PYP. The estimated weakening of the hydrogen bond between residue 46 and the chromophore upon H/D exchange, and the resulting experimentally detected red-shift in absorbance maximum are depicted for the PYP from *Salinibacter ruber* and its E46Q mutant

Proposed classification of hydrogen bonds – Currently the most useful classification of hydrogen bonding interactions in proteins is debated. Some authors have proposed a classification based on hydrogen bonding strength, with strong (60-170 kJ/mol), moderate (15-60 kJ/mol), and weak (<15 kJ/mol) hydrogen bonds (Steiner 2002). Others have emphasized the shape of the hydrogen bonding potential as double-well, single-well, and LBHB (Guthrie 1996). Yet another classification, introduced in studies on the role of C-H...O hydrogen bonds, focusses on the atom type to which the hydrogen atom forming the hydrogen bond is connected (Manikandan et al. 2004). Particularly the role that ionic hydrogen bonds (Perrin et al. 1997, Meot-Ner 2005), in

which a net charge is present on the hydrogen bond donor-acceptor pair, play in proteins remains unclear.

Based on the results reported here in combination with analysis of the wealth of biophysical data available on PYP (see(Cusanovich et al. 2003, Hellingwerf et al. 2003)) and drawing on the large body of information available on hydrogen bonding (Perrin et al. 1997, Steiner 2002, Meot-Ner 2005), we propose that it is helpful to distinguish three types of hydrogen bonds involving N and O atoms (Fig. 4.3.4). We characterize these hydrogen bonds based on their behavior along two key reaction coordinates. First, the distance between the heteroatoms in the hydrogen bond donor-acceptor pair defines the length and strength of the hydrogen bond (Fig. 4a). Second, the position of the proton between these two heteroatoms describes proton transfer along the hydrogen bond (Fig. 4b). This approach leads us to propose the following three types of hydrogen bonds: (i) standard hydrogen bonds, such as those that hold together α -helices, with a length close to 2.8 Å and a typical strength of approximately 15 kJ/mol,(Steiner 2002) ionic hydrogen bonds, with a length close to 2.6 Å and a typical strength near 50 kJ/mol (Perrin et al. 1997, Meot-Ner 2005), and LBHBs with a length close to 2.4 Å and a typical strength of ~100 kJ/mol (Cleland et al. 1994, Perrin et al. 1997). While the lengths of these three types of hydrogen bonds are quite well defined, their energies are likely to vary substantially depending on the chemical details and molecular environment of the hydrogen bond. Of these three types of hydrogen bonds only the LBHB acts as a single well system for proton transfer. This analysis implies that the presence of a short, ionic hydrogen bond is distinct from a LBHB. Thus the “strong short” hydrogen bonds often referred to in various protein systems (e.g.,(Mildvan et al. 2002)) can in fact involve two distinct types of hydrogen bonding.

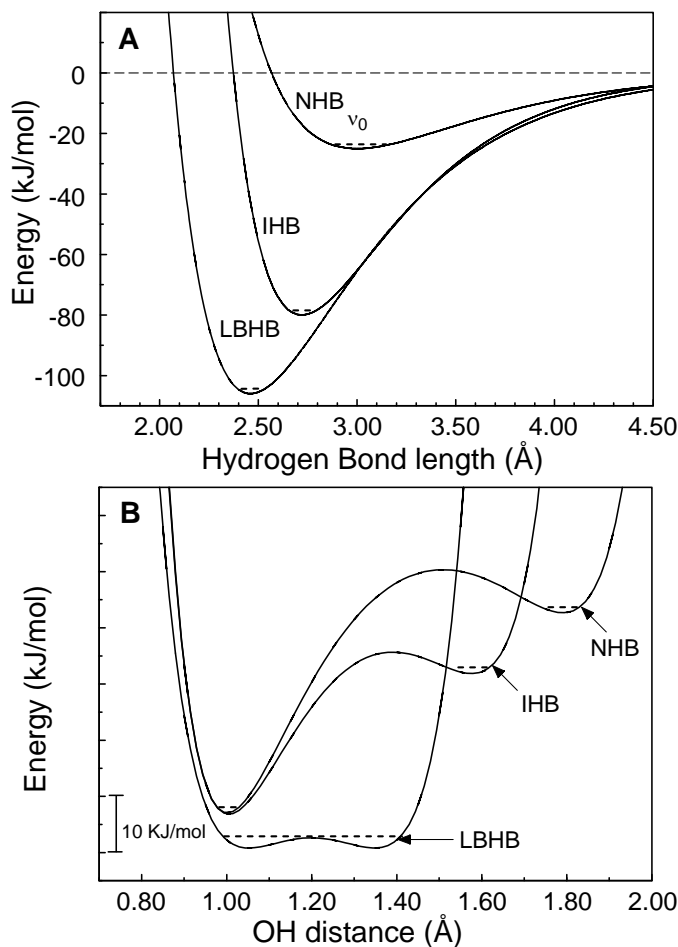


Figure 4.3.4. **Distinction between three types of hydrogen bonds.** The distance between heteroatoms in the hydrogen bond donor-acceptor pair (A) define the equilibrium length and strength of hydrogen bonds, while the position of the proton along this hydrogen bond (B) determines the potential energy for proton transfer between the hydrogen bond donor and acceptor. These two reaction coordinates lead to a distinction between normal hydrogen bonds (NHB) with a length of 3.00 (± 0.20) Å, ionic hydrogen bonds (IHB) with a length of 2.72 (± 0.10) Å, and low barrier hydrogen bonds (LBHB) with a length of 2.46 (± 0.03) Å. The depicted potential energy curves are intended to reflect the qualitative differences between the three types of hydrogen bonds, while depicting physically reasonable values. Quantitative information on the shapes of these energy landscapes were obtained from (Sadhukhan et al. 1999, Herzog et al. 2006, Freindorf et al. 2012). While ionic hydrogen bonds and LBHBs are both considerably stronger than standard hydrogen bonds, the values for their strength are less well defined and

likely to vary considerably depending on the details of the chemical nature of the donor-acceptor pair and their physical environment. Likewise, the exact values for the barriers and energy differences for proton transfer in panel B are intended to illustrate the differences between the three types of hydrogen bonds; the absolute energies of the left well are for illustrative purposes only. The depicted values were chosen to reflect hydrogen bonds involving O (and N) heteroatoms. Normal hydrogen bonds occur abundantly in proteins; ionic hydrogen bonds are found at some active sites and occur often on the surface of protein. LBHBs are rare and often are present at the active site of the protein

Relevance of ionic hydrogen bonding for proteins – The value of the above classification of hydrogen bonds is illustrated by the recent debate about a functionally important and short hydrogen bond at the active site of PYP: different research groups have reported that this hydrogen bond is (Yamaguchi et al. 2009) or is not (Fisher et al. 2007, Saito et al. 2012) a LBHB. We propose that the truth is likely to be in between, namely that this active site hydrogen bond is a strong, ionic hydrogen bond without being a LBHB, i.e., the second class of hydrogen bonds

depicted in Fig. 4. This proposal reconciles the short length of the hydrogen bond with vibrational spectroscopy showing that in the dark state of PYP the side chain of Glu46 is protonated (Xie et al. 1996, Xie et al. 2001) while the *pCA* is ionized, and is in line with recent computational results (Saito et al. 2012).

Ionic hydrogen bonds in proteins are of considerable biological interest. They are substantially shorter and often much stronger than standard hydrogen bonds (Perrin et al. 1997, Meot-Ner 2005), and have been implicated to be important features at the active sites of a range of proteins, including green fluorescent protein (Brejc et al. 1997), serine protease (Fuhrmann et al. 2006), HIV protease (Das et al. 2010), acetylcholinesterase, ketosteroid isomerase (Mildvan et al. 2002) and PYP (Yamaguchi et al. 2009, Saito et al. 2012). However, until recently these structural and spectroscopic results have often been interpreted without taking into account the unusual properties of the ionic hydrogen bond. A relevant example is that the hydrogen bonds between the *pCA* and the side chains of Tyr42 and Glu46 have been described as “unusually short” (Anderson et al. 2004, Fisher et al. 2007). However, the length of these hydrogen bonds is what would be expected for an ionic hydrogen bond, and therefore is unusual only if the properties of these hydrogen bonds are considered within the framework of standard hydrogen bonds. The unique properties of ionic hydrogen bonds are also responsible for the inverted nature of the SIE reported here.

Isotope effects in proteins are widely used in both infrared spectroscopy to assign vibrational modes and via kinetic isotope effects (KIE) in studies of enzyme reaction mechanisms. Here we report and assign a SIE in the electronic absorbance spectrum of the bacterial blue light receptor PYP. Previously, small shifts in the absorbance peaks of both PYP (Hendriks et al. 2003) and GFP (Shi et al. 2007) were reported as un-interpreted observations. We provide a conceptual framework for understanding such spectral isotope effects, report the experimental assignment of the inverted SIE to the ionic Glu46-*pCA* hydrogen bond, and demonstrate how SIE effects can be

used as a spectroscopic readout of the presence and strength of such ionic hydrogen bonds. Determining hydrogen bonding strength in proteins remains an important challenge in protein biophysics, and the values reported in Table 1 are tentative estimates. However, the results and analysis presented here allow a firm assignment and analysis of the SIE in PYP, and lead us to point out the importance of distinguishing between ionic and LBHB interactions. These results are likely to be widely applicable to systems that exhibit predictable spectral shifts in an electronic transition upon changes in hydrogen bonding and indicate that the inverted SIE provides a novel tool to probe ionic hydrogen bonds.

FOOTNOTES

* This work was funded by NSF grant MCB-1051590 to W.D.H. and OCAST grant HR10-078 to A.X.

Author Contributions: ‡These authors contributed equally.

The abbreviations used are: FTIR; Fourier transform infrared; GFP: green fluorescent protein; KIE: kinetic isotope effect; λ_{\max} ; absorbance maximum; *pCA*; *p*-coumaric acid; PYP, photoactive yellow protein; SIE, spectral isotope effect

CHAPTER V

CONCLUDING REMARKS

5.1 Impact of crystallization salts on structural dynamics of protein

Protein molecules in living organism are nano-machines which regulate many processes, supports structural elements like membrane, communicate between various cell elements. The structure of a protein molecule is related to its functional properties. The structural dynamics of protein plays an important role to perform its function (Austin et al. 1975, McCammon 1984). Also, the structural dynamics of protein is dependent on microenvironment surrounding it (Fenimore et al. 2004).

In chapter 3, we have studied impact of crystallization salt on structural dynamics of protein. In high salt concentration solution, the conformational change in PYP in pB state are suppressed. We find that the suppression of conformational changes in pB state is partially due to dehydration of PYP in high salt concentration. Also the electrostatic interaction energy between two charge residues becomes higher in high salt concentration as protein is partially dehydrated. The increase in electrostatic energy confines the change in conformations. Thus interaction of salt with protein alters the energy landscape of protein.

The mechanism understood here can be applied to understand effects of Hofmeister series on protein. The salts from Hofmeister series are often used to prepare crystalline protein. The functional properties of protein in crystalline state can be different than its native state (Doscher et al. 1963, Sigler et al. 1963, Quioco et al. 1966, Xie et al. 2001). We predict that crystallization salt solutions alter the energy landscape of protein. The energy landscape of protein in crystallization salt solution can be

explored by changing temperature and pressure. However there are other ways to explore energy landscape of protein by mutating residue resulting in increased lifetime of pB state of PYP.

5.2 Structure-function relationship in photoactive yellow protein

Protein functions are dependent on its structure; an alteration in structure may lead to severe diseases like cancer. In this dissertation I have studied homologous PYP and mutants of Hhal PYP to find out their functional properties by employing FTIR absorption and time-resolved difference absorption spectroscopy.

Mutation of Asn43 in Hhal PYP

The PAS domain proteins are found in archaea, bacteria, fungi, plants, insects and vertebrates indicating its presence in all of kingdoms of life (Lagarias et al. 1995, Taylor et al. 1999). The PAS domain proteins has a characteristic folding, the core protein fold is an anti-parallel β -sheets flanked by 4-5 α -helices (Taylor et al. 1999). The proteins from PAS domain mainly perform signal transductions and regulatory functions in organism. PAS domain proteins have length of \sim 100 residues, among which nine residues are well conserved (Taylor et al. 1999). The Asn43 residue of PYP is one of the most conserved residues in PAS domain. Asn43 side chain interacts with backbone of Glu46 resulting helical capping for α -helix 3. The PAS domain fold in PYP starts from β -strand 1, or residue Gly29. The hydrogen bond between side chain of Asn43 and backbone of Glu46 is referred as helical capping hydrogen bond. The hydrogen bond between Leu23 and Asn43 docks N-terminal region (residue 1-27) to central β -sheet as shown in figure 5.1.

The mutation of Asn43 in Hhal PYP causes dramatic increase in the lifetime of long lived pB intermediate state (Kumauchi et al. 2010). We attribute this increase in lifetime of pB state of Ans43 mutation to loss of hydrogen bonding of Asn43 to other structural elements as explained above paragraph. Thus side chain hydrogen bonding interaction of Asn43 in PYP is a key factor in controlling the lifetime of pB signaling state.

Previously it has been reported that Asn43 may play a key role in allosteric transmission of PYP from its active site to the N-terminus region (Ihee et al. 2005, Philip et al. 2010). The FTIR difference spectroscopy of N43A mutant shows large conformational changes after photoactivation (Kumauchi et al. 2010). It shows that Asn43 is not an essential part of allosteric transition. The analysis provided here suggests the possibility of regulation of kinetics signaling of PAS domain superfamily by side-chain hydrogen bonds at residue 43.

***Idiomarina loihiensis* PYP**

The PYP from *Idiomarina loihiensis* (Il) has 83% of sequence similarity to Hhal PYP (refer Chapter 4 for more details). The Il PYP has very similar properties to well-studied PYP from Hhal. Its pK_a of *pCA*, visible absorption and pB lifetime are similar to that of Hhal PYP (van der Horst et al. 2009). The FTIR absorption spectrum of Il shows that the secondary structure of Il is very similar to that of Hhal PYP. Interestingly both PYP follow similar kinetics for long lived pB decay, however the functional properties are different (van der Horst et al. 2009). The Il PYP controls biofilm formation while Hhal PYP has negative phototaxis (van der Horst et al. 2009). Despite the high sequence similarity between Hhal and Il PYP, the functional properties are different.

Spectral Isotopic Effect (SIE)

The SIE value is larger in *Salinibacter ruber* (Sr) PYP than Hhal PYP indicates that hydrogen bond between Glu46 and *pCA* is stronger in Sr PYP than Hhal PYP (refer Chapter 4 for more details). However it is unusual as hydrogen bond between Glu46 and *pCA* is already short and strong in Hhal PYP. However there are two considerations to support this evidence. The first consideration is that λ_{max} of Sr PYP is already blue shifted compared to Hhal PYP. The blue shift in Sr PYP indicates that increase in strength of hydrogen bond between Glu46 and *pCA*. The second consideration is red shift of λ_{max} in E46Q Sr PYP at 457 nm. This suggests that E46Q weakens the hydrogen bond between Glu46 and *pCA*.

Isotopes effects in proteins are widely applied in vibrational spectroscopy to assign vibrational frequencies and kinetic isotope effects in studies of enzyme reaction mechanism. We report novel spectral isotopic effect observed through absorption spectroscopy of bacterial blue light photoreceptor PYP.

Time-resolved FTIR difference spectroscopy

Our main tool to explore structure-function relation in protein is infrared spectroscopy and time-resolved FTIR difference spectroscopy. Information provided by FTIR spectrum of a protein is rich in signals. It is challenging to assign each peak position for particular vibrational mode from residues. The vibrational modes are sensitive to hydrogen bonding and protonation state and environment. Sometimes the signals from different vibrational modes are overlapped and it makes difficult to assign vibrational mode associated to particular signal. As time-resolved FTIR difference spectroscopy allows to see PYP molecule in action, it is important to know each mode of vibration contributing to structural change during photoactivation and recovery of PYP. Assignment of vibrational modes can be assisted by combination of site directed mutagenesis of protein, isotopic edited proteins samples and computational calculations for determining vibrational mode. Many of PYP vibrational modes are not assigned and these bands can reveal more about structural changes during PYP photocycle. Below, I discuss one example to assign the vibrational mode and its strategy.

The 1689 cm^{-1} signal in pB-pG FTIR difference spectroscopy is assigned for structural transition during PYP photocycle (Xie et al. 2001). Our preliminary analysis shows that this signal is sensitive to H/D exchange (unpublished) and most probably this signal arises due to vibrational mode of $-\text{CONH}_2$ groups. Further we have predicted most probable candidates to assign this vibrational mode and according to our prediction it should be Gln41 which forms a hydrogen bond network and stabilizes central β -sheet with N-terminus.

Prediction of hypothetical PYPs from conserved residues

The number of PYPs is increasing in PYP family over fast few years through genomic analysis. In 2008 only 14 PYP from different bacteria were reported (Kumauchi et al. 2008). However recently there has been surge in PYP proteins through genomic analysis (Meyer et al. 2012) and they have reported total of 63 PYPs. However in their analysis, Cys69 is not considered as 100% conserved residue. The PYP chromophore *p*CA binds at the Cys69 via thioester bond. Hence it is very critical when determining hypothetical PYP from sequence alignment.

As most important phenomenon in photoactivation of PYP from Hhal are known, it can be applied to understand photoactivation of other PYP's. The functional properties of PYP are very diverse and it would be interesting to explore PYP's function *in-vivo*.

The hypothetical PYPs were identified through genomic analysis by using Basic Local Alignment Search Tool (BLAST) algorithm (Altschul et al. 1990). The protein sequences obtained from BLAST search carefully analyzed to propose hypothetical PYPs. Our main criteria to propose the hypothetical PYPs are finding conserved residues. The protein sequences thus obtained were further aligned with Constraint-based Multiple Protein Alignment Tool (COBALT) to obtained conserved domains (Papadopoulos et al. 2007). Further the multiple sequence alignment obtained through COBALT was feed to ConSurf to estimate conservation in sequence (Ashkenazy et al. 2010). The 3-D structure of PYP with color coded conserved residue was obtained by online ConSurf server and corresponding 3-D structure is shown in Figure 5.3. The obtained multiple sequence alignment through COBALT with organism name and protein sequence is shown in Figure 5.2.

Here we identify total of 52 PYPs from different organisms. Out of these 52 PYPs 14 PYPs has been already known (Kumauchi et al. 2008). Sequence comparison of protein may show a possible candidate for new PYP, however it is not necessary that possible candidate has to be PYP. For the hypothetical PYPs, it might not express itself in bacterial cells. So until and unless the PYP expression is

not found in the original cell it cannot be assigned as protein from PYP family. The list of hypothetical PYP along with existing PYP is provided in appendix G of this dissertation.

According to our analysis residues Gly29, Phe63 and Cys69 are 100% conserved in the PYP family. The sequence comparison shows that the most conserved residue in PYP family are Gly29, Asn43, Glu46, Phe63, Ala67, Pro68, Cys69, Phe75, Val105. These residues have range of normalized conservation score from 1.30 to 1.52.

The next most conserved residues are Asp24, Ile31, Asp34, Gly37, Ile39, Tyr42, Thr50, Gly51, Val57, Gly59, Phe62, Val66, Thr70, Gly77, Phe79, Gly82, Leu88, Tyr94, Phe96, Asp97, Met100, Val107, Met109 with normalized conservation score from 0.85 to 1.12. All conserved residues are listed in Table 5.1.

In the PAS domain superfamily 9 amino acids are very well conserved (Taylor et al. 1999). Our analysis shows that out of these 9 amino acids, 6 amino acids are very well conserved in PYP which are Asp34, Gly37, Ile39, Asn43, Gly51 and Gly59 according to amino acid sequence number in *Hhal* PYP. The other three conserved residue position in PAS domain is highly variable in PYP sequences. The alanine scan of wtPYP from *Hhal* shows that the Ile39 and Asn43 functional properties have been significantly altered. Thus one can predict that these two residues may play a crucial role in signal transduction in PAS domain superfamily. Among these two residues we have studied structural and functional properties of Asn43 with time-resolved FTIR difference spectra (Kumauchi et al. 2010). By understanding the role of conserved amino acids in PAS domain a common signaling mechanism can be predicted which can be applied to all PAS domain proteins.

The PYP's conserved active site residues are Ile31, Tyr42, Glu46, Phe62, Val66, Ala67, Pro68, Cys69 and Phe96 (Kumauchi et al. 2008). Our analysis shows that these amino acids are very well conserved in hypothetical PYPs. The signaling mechanism understood from well- studied PYP from *Hhal* can be employed to new PYPs to understand their structure-function relation.



Figure 5.1: Color coded conserved residues of PYP. The inset at the bottom left corner depicts the color grade of conservation of amino acids. The color coded 3D structure of PYP was generated by ConSurf Server (<http://consurf.tau.ac.il/>). The color grades 1 is least conserved while color grade 9 is most conserved amino acids. (PDB ID: 1NWZ)

Table 5.1. Most conserved residues in PYP family. The range of magnitude of normalized conservation scores are provided in the bracket.

Color code	Conserved residue position in Hhal PYP
Code 9 (1.30 to 1.52)	Gly29, Asn43, Glu46, Phe63, Ala67, Pro68, Cys69, Phe75, Val105
Code 8 (0.85 to 1.12)	Asp24, Ile31, Asp34, Gly37, Ile39, Tyr42, Thr50, Gly51, Val57, Gly59, Phe62, Val66, Thr70, Gly77, Phe79, Gly82, Lue88, Tyr94, Phe96, Asp97, Met100, Val107, Met109
Code 7 (0.54 to 0.81)	Phe7, Ala30, Leu33, Gly47, Arg52, Asn61, Ser72, Lys78, Asn89, Phe92, Tyr98, Pro102, Thr103, His108, Ala112, Val122

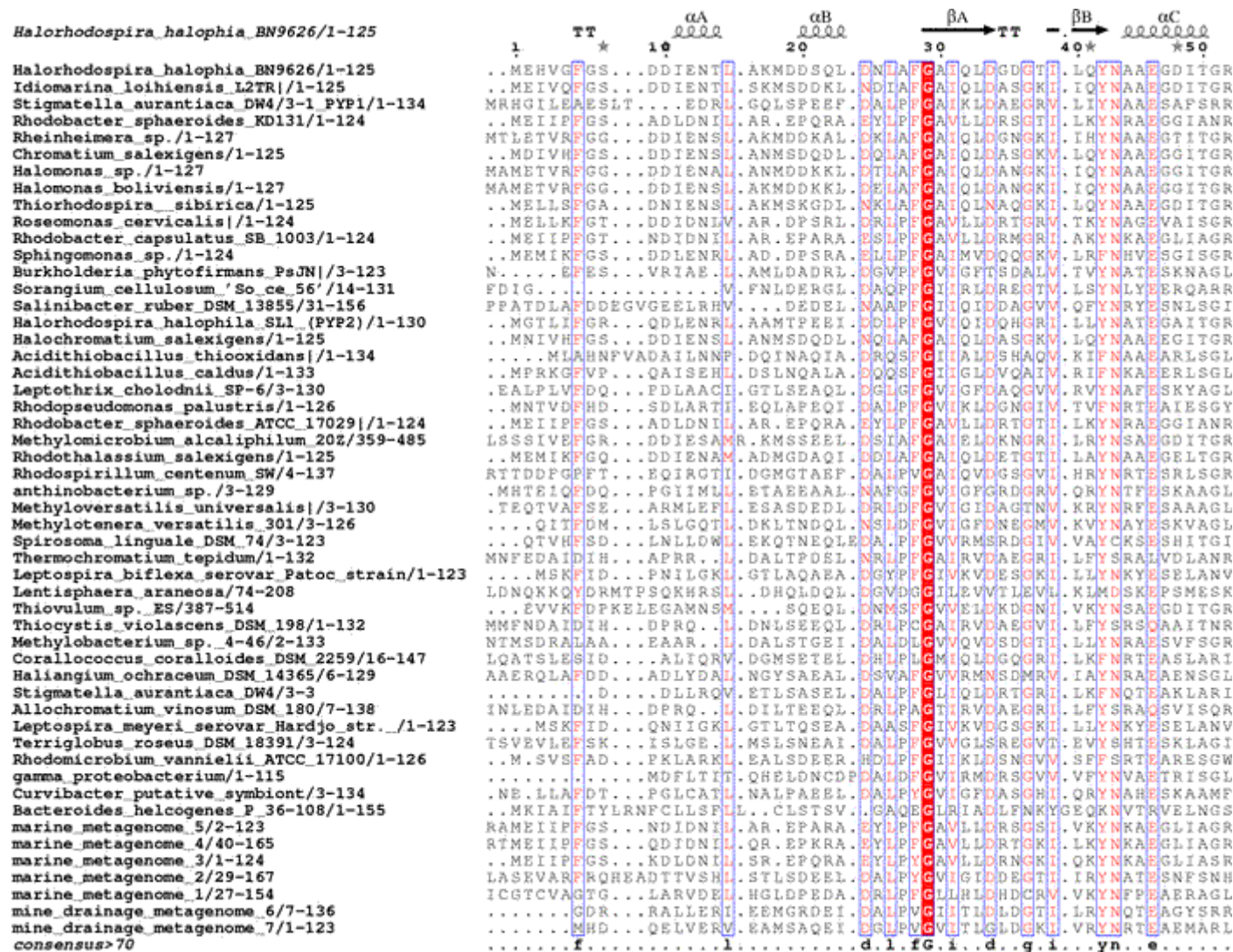


Figure 5.2: Sequence alignment of homologous PYP: The accession numbers from NCBI database and corresponding sequence. The sequence was compared with PYP from Hhal with COBALT alignment. The secondary structure elements of PYP from Hhal are indicated above the sequence.

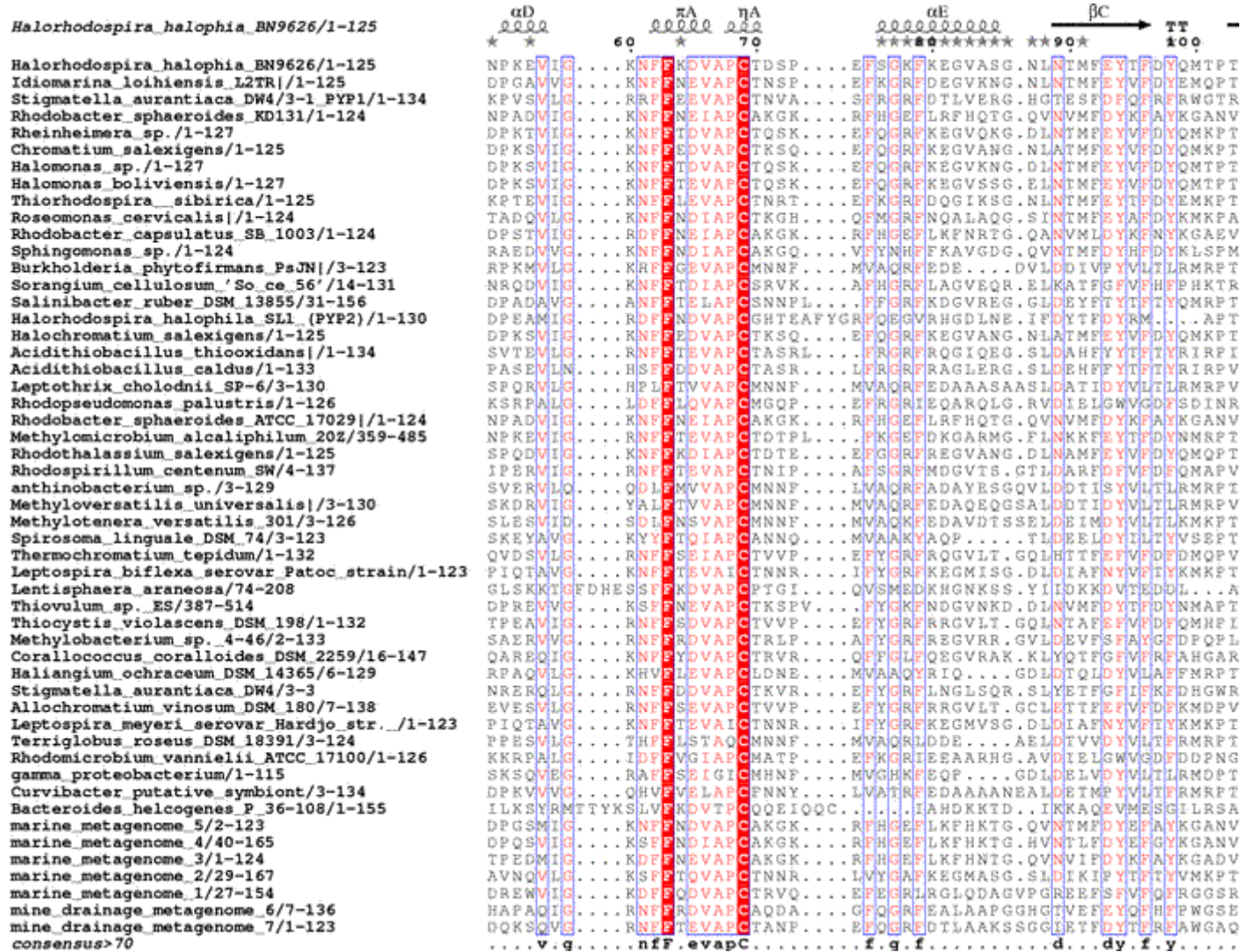


Figure 5.2—continued from previous page

	βD	βE
	110	*120
<i>Halorhodospira halophia</i> _BN9626/1-125	KVKKVHMK...KALS...GD..SYWV.....FVKKRV.....	
<i>Idiomarina loihiensis</i> _L2TR/1-125	KVKKVHMK...KALT...GD..TYWV.....FVKKRL.....	
<i>Stigmatella aurantiaca</i> _DW4/3-1_PYP1/1-134	NVRIHLMVLG...D...GSR...WV.....FVTAVLTALIPLGE	
<i>Rhodobacter sphaeroides</i> _KD131/1-124	GVKIHMKSQP...D...GQ..SCWL.....FVKKRV.....	
<i>Rheinheimera</i> _sp./1-127	KVKKVHMK...KAMT...GD..SPWI.....FVKKRL.....	
<i>Chromatium salexigens</i> /1-125	KVKKVHMK...KALV...DD..SYWI.....FVKKRL.....	
<i>Halomonas</i> _sp./1-127	KVKKVHMK...KALS...GD..TFWI.....FVKKRL.....	
<i>Halomonas boliviensis</i> /1-127	KVKKVHMK...KALS...GD..TYWI.....FVKKRL.....	
<i>Thiorhodospira sibirica</i> /1-125	KVKKVHMK...KALV...DD..TYWV.....FVKKRV.....	
<i>Roseomonas cervicalis</i> /1-124	KVKKVHMKSVS...I...DQ..GIWV.....FVKKRL.....	
<i>Rhodobacter capsulatus</i> _SB_1003/1-124	AVKIHLMKSN...D...GQ..FCWL.....FVKKRA.....	
<i>Sphingomonas</i> _sp./1-124	NVRIHLMKSN...A...SH..GIWI.....FVKKRV.....	
<i>Burkholderia phytofirmans</i> _PsJN/3-123	PVRIHLLKAT...D...CA..TRFV.....LVERRATN.....	
<i>Sorangium cellulosum</i> '_So_ce_56'/14-131	HVDVSLFYKAAARQ...DD..AVWV.....FVIRG.....	
<i>Salinibacter ruber</i> _DSM_13855/31-156	LVDVRLYRDE...AEN...N...WI.....LVQKR.....	
<i>Halorhodospira halophila</i> _SLL_(PYP2)/1-130	KVKKVHMK...RALS...GD..TYWI.....FVKRISAPAA...	
<i>Halochromatium salexigens</i> /1-125	KVKKVHMK...KALV...DD..SYWI.....FVKKRL.....	
<i>Acidithiobacillus thiooxidans</i> /1-134	SAHVHMFYDMRKSPL...FPIFIDRI...LVLYEDLG.....	
<i>Acidithiobacillus caldus</i> /1-133	SAHVHMLYRP...AQ...SP..LVFL.....FVDRV..IPLFED.	
<i>Leptothrix cholodnii</i> _SP-6/3-130	KVRIHLLAAP...A...TA..LRYV.....LVQRP.....	
<i>Rhodopseudomonas palustris</i> /1-126	SLQVRIQSAS...D...DG..SLWI.....FVNLRDHA.....	
<i>Rhodobacter sphaeroides</i> _ATCC_17029/1-124	GVKIHMKSQP...D...GQ..SCWL.....FVKKRV.....	
<i>Methylomicrobium alcaliphilum</i> _20Z/359-485	KVKKVHMK...KALS...GD..TYWI.....FVKKRV.....	
<i>Rhodothalassium salexigens</i> /1-125	KVKKVHMK...RAIT...GD..SYWI.....FVKKRV.....	
<i>Rhodospirillum centenum</i> _SW4-137	RVDIHRMQNAG...V...PD..RYWI.....FVKRLEDLRP..PG	
<i>anthinobacterium</i> _sp./3-129	KVRIHLLSDP...A...AD..LSYV.....LVHRL.....	
<i>Methylotetrasphaera universalis</i> /3-130	KVRIHLLAAP...D...RA..LRYV.....LVQRP.....	
<i>Methylotenera versatilis</i> _301/3-126	KVRIHLLSSP...Q...FS..YSYV.....LVILRS.....	
<i>Spirosoma linguale</i> _DSM_74/3-123	KVRIHLLKSP...E...SR..YQYP.....LVNRKA.....	
<i>Thermochromatium tepidum</i> /1-132	QVRIHMHSTSE...R...PG..EPWI.....LVQPLALLPA..RN	
<i>Leptospira biflexa</i> _serovar_Patoc_strain/1-123	NVVIIH.LYHD...KG...TN..SNWI.....FVKKLR.....	
<i>Lentisphaera araneosa</i> /74-208	LLKLYYCKSKNNKALK...IILDSP...LVK...YQN	
<i>Thiovulum</i> _sp._ES/387-514	KVRIHMLKNAEEBDAK...DK..TYWI.....FVKKRL.....	
<i>Thiocystis violascens</i> _DSM_198/1-132	QVRIHMRASH...R...PG..EPWI.....LVLEPLRQLFP..RN	
<i>Methylobacterium</i> _sp._4-46/2-133	RVRIHVALRGS...T...PG..RYWI.....LVIRPVGQVTV..SE	
<i>Corallococcus coralloides</i> _DSM_2259/16-147	HVAITILFYS...DK...TD..SVWV.....LVSDKKM..PDAR.	
<i>Haliangium ochraceum</i> _DSM_14365/6-129	PVRIHLLKRA...A...HD..WSYL.....LVK...C	
<i>Stigmatella aurantiaca</i> _DW4/3-3	NVAITIMFYS...EK...TD..SVWV.....LVISQTSVTPPPAR.	
<i>Allochromatium vinosum</i> _DSM_180/7-138	RVRIHMRASD...R...PG..EPWI.....LVQPKNRLFP..RN	
<i>Leptospira meyeri</i> _serovar_Hardjo_str./1-123	NVVIIH.LYHD...NP...SN..TNWI.....FVKKLR.....	
<i>Terriglobus roseus</i> _DSM_18391/3-124	PVRIHLLKKA...E...YP..RSYL.....LVIR...L	
<i>Rhodomicrobium vannielii</i> _ATCC_17100/1-126	EMTVRIQSAA...D...DG..GIWI.....LVCDRPPDQG.....	
<i>gamma proteobacterium</i> /1-115	PVRIHLLRQG...D...EK..YQYL.....LVIQPI.....	
<i>Curvibacter putative symbiont</i> /3-134	RVQVRIHLLAQP...E...AS..LRFE.....LVLRTPAPAK..A	
<i>Bacteroides helcogenes</i> _P_36-108/1-155	YVQVKEIDRNGKRLNRYILFKTGKGLMATLIYIEGFLSEKEMMDMLYRP	
<i>marine metagenome</i> _5/2-123	PVRIHLLKQP...D...GQ..NCWL.....FV...L	
<i>marine metagenome</i> _4/40-165	KVRIHLLKSP...D...GQ..SCWM.....FVKKRV.....	
<i>marine metagenome</i> _3/1-124	GVKIHLLKSP...D...GQ..HCWM.....LVKKRV.....	
<i>marine metagenome</i> _2/29-167	NVVIIH.MVRC...QD...SR..SNWL.....LVHHTDSNGSLI.	
<i>marine metagenome</i> _1/27-154	LVHVLMSHSP...KA...GT.....LVILVEDQG.....	
<i>mine drainage metagenome</i> _6/7-136	RVLISFLRGS...DA...PR..IQL.....LVITWPAEQSKAPLD	
<i>mine drainage metagenome</i> _7/1-123	RVRIHTEVRKA...GR...DD..IDV.....LVITRMSA.....	
<i>consensus</i> >70	.v.i.m	v

Figure 5.2—continued from previous page

REFERENCES

1. Altschul, S. F., W. Gish, W. Miller, E. W. Myers and D. J. Lipman 1990. Basic Local Alignment Search Tool. *J. Mol. Biol.* **215**: 403-410.
2. Anderson, S., S. Crosson and K. Moffat 2004. Short hydrogen bonds in photoactive yellow protein. *Acta Crystallogr D.* **60**: 1008-1016.
3. Ansari, A., J. Berendzen, S. F. Bowne, H. Frauenfelder, I. E. T. Iben, T. B. Sauke, E. Shyamsunder and R. D. Young 1985. Protein states and protein quakes. *Proc. Natl. Acad. Sci. U.S.A.* **82**: 5000-5004.
4. Ashkenazy, H., E. Erez, E. Martz, T. Pupko and N. Ben-Tal 2010. ConSurf 2010: calculating evolutionary conservation in sequence and structure of proteins and nucleic acids. *Nucleic Acids Res.* **38**: W529-W533.
5. Aurora, R. and G. D. Rose 1998. Helix capping. *Protein Sci.* **7**: 21-38.
6. Austin, R. H., K. W. Beeson, L. Eisenstein, H. Frauenfelder and I. C. Gunsalus 1975. Dynamics Of Ligand-Binding To Myoglobin. *Biochemistry* **14**: 5355-5373.
7. Baca, M., G. E. O. Borgstahl, M. Boissinot, P. M. Burke, D. R. Williams, K. A. Slater and E. D. Getzoff 1994. Complete chemical-structure of photoactive yellow protein - novel thioester-linked 4-hydroxycinnamyl chromophore and photocycle chemist. *Biochemistry* **33**: 14369-14377.
8. Baedeker, M. and G. E. Schulz 2002. Autocatalytic peptide cyclization during chain folding of histidine ammonia-lyase. *Structure* **10**: 61-67.
9. Baltuska, A., I. H. M. vanStokkum, A. Kroon, R. Monshouwer, K. J. Hellingwerf and R. vanGrondelle 1997. The primary events in the photoactivation of yellow protein. *Chem. Phys. Letters* **270**: 263-266.
10. Baranowski, J. D. and C. W. Nagel 1983. Properties of alkyl hydroxycinnamates and effects on *Pseudomonas fluorescens*. *Appl. Environ. Microb.* **45**: 218-222.
11. Bateman, A., L. Coin, R. Durbin, R. D. Finn, V. Hollich, S. Griffiths-Jones, A. Khanna, M. Marshall, S. Moxon, E. L. L. Sonnhammer, D. J. Studholme, C. Yeats and S. R. Eddy 2004. The Pfam protein families database. *Nucleic Acids Res.* **32**: D138-D141.
12. Benjamin, L. and G. C. Benson 1963. A deuterium isotope effect on the excess enthalpy of methanol—water solutions. *J. Phys. Chem.* **67**: 858-861.
13. Bernard, C., K. Houben, N. M. Derix, D. Marks, M. A. van der Horst, K. J. Hellingwerf, R. Boelens, R. Kaptein and N. A. J. van Nuland 2005. The solution structure of a transient photoreceptor intermediate: Delta 25 photoactive yellow protein. *Structure* **13**: 953-962.
14. Boehm, A., S. Steiner, F. Zaehring, A. Casanova, F. Hamburger, D. Ritz, W. Keck, M. Ackermann, T. Schirmer and U. Jenal 2009. Second messenger signalling governs *Escherichia coli* biofilm induction upon ribosomal stress. *Mol. Microbiol.* **72**: 1500-1516.
15. Borgstahl, G. E. O., D. R. Williams and E. D. Getzoff 1995. 1.4 Angstrom structure of photoactive yellow protein, a cytosolic photoreceptor - unusual fold, active site, and chromophore. *Biochemistry* **34**: 6278-6287.
16. Born, B., S. J. Kim, S. Ebbinghaus, M. Gruebele and M. Havenith 2009. The terahertz dance of water with the proteins: the effect of protein flexibility on the dynamical hydration shell of ubiquitin. *Faraday Discuss.* **141**: 161-173.

17. Brejc, K., T. K. Sixma, P. A. Kitts, S. R. Kain, R. Y. Tsien, M. Ormo and S. J. Remington 1997. Structural basis for dual excitation and photoisomerization of the *Aequorea victoria* green fluorescent protein. *Proc. Natl. Acad. Sci. USA* **94**: 2306-2311.
18. Byrne, M. P., R. L. Manuel, L. G. Lowe and W. E. Stites 1995. Energetic contribution of side chain hydrogen bonding to the stability of staphylococcal nuclease. *Biochemistry* **34**: 13949-13960.
19. Cacace, M. G., E. M. Landau and J. J. Ramsden 1997. The Hofmeister series: salt and solvent effects on interfacial phenomena. *Q. Rev. Biophys.* **30**: 241-277.
20. Careri, G. G., A 1979. Lysozyme film hydration events: An IR and gravimetric study. *Biopolymers* **18**: 1187-1203.
21. Chen, J., A. R. Zou, I. Splawski, M. T. Keating and M. C. Sanguinetti 1999. Long QT syndrome-associated mutations in the Per-Arnt-Sim (PAS) domain of HERG potassium channels accelerate channel deactivation. *J. Biol. Chem.* **274**: 10113-10118.
22. Cleland, W. W. and M. M. Kreevoy 1994. Low-barrier hydrogen-bonds and enzymatic catalysis. *Science* **264**: 1887-1890.
23. Collins, K. D. 2004. Ions from the Hofmeister series and osmolytes: effects on proteins in solution and in the crystallization process. *Methods* **34**: 300-311.
24. Collins, K. D. and M. W. Washabaugh 1985. The Hofmeister effect and the behavior of water at interfaces. *Q. Rev. Biophys.* **18**: 323-422.
25. Cordfunke, R., R. Kort, A. Pierik, B. Gobets, G. J. Koomen, J. W. Verhoeven and K. J. Hellingwerf 1998. trans/cis (Z/E) photoisomerization of the chromophore of photoactive yellow protein is not a prerequisite for the initiation of the photocycle of this photoreceptor protein. *Proc. Natl. Acad. Sci. U.S.A.* **95**: 7396-7401.
26. Cotter, P. A. and S. Stibitz 2007. c-di-GMP-mediated regulation of virulence and biofilm formation. *Curr. Opin. Microbiol.* **10**: 17-23.
27. Craven, C. J., N. M. Derix, J. Hendriks, R. Boelens, K. J. Hellingwerf and R. Kaptein 2000. Probing the nature of the blue-shifted intermediate of photoactive yellow protein in solution by NMR: hydrogen-deuterium exchange data and pH studies. *Biochemistry* **39**: 14392-14399.
28. Crosson, S., S. Rajagopal and K. Moffat 2003. The LOV domain family: Photoresponsive signaling modules coupled to diverse output domains. *Biochemistry* **42**: 2-10.
29. Cusanovich, M. A. and T. E. Meyer 2003. Photoactive yellow protein: A prototypic PAS domain sensory protein and development of a common signaling mechanism. *Biochemistry* **42**: 4759-4770.
30. Das, A., S. Mahale, V. Prashar, S. Bihani, J. L. Ferrer and M. V. Hosur 2010. X-ray Snapshot of HIV-1 Protease in Action: Observation of Tetrahedral Intermediate and Short Ionic Hydrogen Bond SIHB with Catalytic Aspartate. *J. Am. Chem. Soc.* **132**: 6366-6373.
31. Deechongkit, S., H. Nguyen, E. T. Powers, P. E. Dawson, M. Gruebele and J. W. Kelly 2004. Context-dependent contributions of backbone hydrogen bonding to beta-sheet folding energetics. *Nature* **430**: 101-105.
32. Derix, N. M., R. W. Wechselberger, M. A. van der Horst, K. J. Hellingwerf, R. Boelens, R. Kaptein and N. A. J. van Nuland 2003. Lack of negative charge in the

- E46Q mutant of photoactive yellow protein prevents partial unfolding of the blue-shifted intermediate. *Biochemistry* **42**: 14501-14506.
33. Devanathan, S., R. Brudler, B. Hessling, T. T. Woo, K. Gerwert, E. D. Getzoff, M. A. Cusanovich and G. Tollin 1999. Dual photoactive species in Glu46Asp and Glu46Ala mutants of photoactive yellow protein: A pH-driven color transition. *Biochemistry* **38**: 13766-13772.
 34. Doig, A. J. and R. L. Baldwin 1995. N- and C-capping preferences for all 20 amino acids in alpha-helical peptides. *Protein Sci.* **4**: 1325-1336.
 35. Donachie, S. P., S. B. Hou, T. S. Gregory, A. Malahoff and M. Alam 2003. *Idiomarina loihiensis* sp nov., a halophilic gamma-Proteobacterium from the L(o)ver-bar-'ihi submarine volcano, Hawai'i. *Int. J. Syst. Evol. Micr.* **53**: 1873-1879.
 36. Dong, A., P. Huang and W. S. Caughey 1990. Protein secondary structures in water from second-derivative amide I infrared spectra. *Biochemistry* **29**: 3303-3308.
 37. Dong, A., P. Huang and W. S. Caughey 1992. Redox-dependent changes in beta-extended chain and turn structures of cytochrome c in water solution determined by second derivative amide I infrared spectra. *Biochemistry* **31**: 182-189.
 38. Doscher, M. S. and F. M. Richards 1963. Activity of an enzyme in crystalline state - Ribonuclease S. *J. Biol. Chem.* **238**: 2399.
 39. Dux, P., G. Rubinstenn, G. W. Vuister, R. Boelens, F. A. A. Mulder, K. Hard, W. D. Hoff, A. R. Kroon, W. Crielaard, K. J. Hellingwerf and R. Kaptein 1998. Solution structure and backbone dynamics of the photoactive yellow protein. *Biochemistry* **37**: 12689-12699.
 40. Ebbinghaus, S., S. J. Kim, M. Heyden, X. Yu, U. Heugen, M. Gruebele, D. M. Leitner and M. Havenith 2007. An extended dynamical hydration shell around proteins. *Proc. Natl. Acad. Sci. U. S. A.* **104**: 20749-20752.
 41. Fenimore, P. W., H. Frauenfelder, B. H. McMahon and R. D. Young 2004. Bulk-solvent and hydration-shell fluctuations, similar to alpha- and beta-fluctuations in glasses, control protein motions and functions. *Proc. Natl. Acad. Sci. U. S. A.* **101**: 14408-14413.
 42. Fersht, A. R., J. P. Shi, J. Knilljones, D. M. Lowe, A. J. Wilkinson, D. M. Blow, P. Brick, P. Carter, M. M. Y. Waye and G. Winter 1985. Hydrogen bonding and biological specificity analysed by protein engineering. *Nature* **314**: 235-238.
 43. Finn, R. D., J. Mistry, J. Tate, P. Coghill, A. Heger, J. E. Pollington, O. L. Gavin, P. Gunasekaran, G. Ceric, K. Forslund, L. Holm, E. L. L. Sonnhammer, S. R. Eddy and A. Bateman 2010. The Pfam protein families database. *Nucleic Acids Res.* **38**: D211-D222.
 44. Fisher, S. Z., S. Anderson, R. Henning, K. Moffat, P. Langan, P. Thiyagarajan and A. J. Schultz 2007. Neutron and X-ray structural studies of short hydrogen bonds in photoactive yellow protein (PYP). *Acta Crystallogr. D Biol. Crystallogr.* **63**: 1178-1184.
 45. Frauenfelder, H., G. Chen, J. Berendzen, P. W. Fenimore, H. Jansson, B. H. McMahon, I. R. Stroe, J. Swenson and R. D. Young 2009. A unified model of protein dynamics. *Proc. Natl. Acad. Sci. U. S. A.* **106**: 5129-5134.

46. Frauenfelder, H., S. G. Sligar and P. G. Wolynes 1991. The Energy Landscapes And Motions Of Proteins. *Science* **254**: 1598-1603.
47. Freindorf, M., E. Kraka and D. Cremer 2012. A comprehensive analysis of hydrogen bond interactions based on local vibrational modes. *Int. J. Quant. Chem.* **112**: 3174-3187.
48. Fuhrmann, C. N., M. D. Daugherty and D. A. Agard 2006. Subangstrom crystallography reveals that short ionic hydrogen bonds, and not a His-Asp low-barrier hydrogen bond, stabilize the transition state in serine protease catalysis. *J. Am. Chem. Soc.* **128**: 9086-9102.
49. Fukushima, Y., K. Okajima, Y. Shibata, M. Ikeuchi and S. Itoh 2005. Primary intermediate in the photocycle of a blue-light sensory BLUF FAD-protein, Tll0078, of *Thermosynechococcus elongatus* BP-1. *Biochemistry* **44**: 5149-5158.
50. Genick, U. K., G. E. O. Borgstahl, K. Ng, Z. Ren, C. Pradervand, P. M. Burke, V. Srajer, T. Y. Teng, W. Schildkamp, D. E. McRee, K. Moffat and E. D. Getzoff 1997. Structure of a protein photocycle intermediate by millisecond time-resolved crystallography. *Science* **275**: 1471-1475.
51. Genick, U. K., S. Devanathan, T. E. Meyer, I. L. Canestrelli, E. Williams, M. A. Cusanovich, G. Tollin and E. D. Getzoff 1997. Active site mutants implicate key residues for control of color and light cycle kinetics of photoactive yellow protein. *Biochemistry* **36**: 8-14.
52. Getzoff, E. D., K. N. Gutwin and U. K. Genick 2003. Anticipatory active-site motions and chromophore distortion prime photoreceptor PYP for light activation. *Nat. Struct. Biol.* **10**: 663-668.
53. Gomelsky, M. and G. Klug 2002. BLUF: a novel FAD-binding domain involved in sensory transduction in microorganisms. *Trends Biochem. Sci.* **27**: 497-500.
54. Goodey, N. M. and S. J. Benkovic 2008. Allosteric regulation and catalysis emerge via a common route. *Nat. Chem. Biol.* **4**: 474-482.
55. Grabowski, M., A. Joachimiak, Z. Otwinowski and W. Minor 2007. Structural genomics: keeping up with expanding knowledge of the protein universe. *Curr. Opin. Struc. Biol.* **17**: 347-353.
56. Gulick, A. M., X. F. Lu and D. Dunaway-Mariano 2004. Crystal structure of 4-chlorobenzoate : CoA ligase/synthetase in the unliganded and aryl substrate-bound states. *Biochemistry* **43**: 8670-8679.
57. Guthrie, J. P. 1996. Short strong hydrogen bonds: Can they explain enzymic catalysis? *Chem. Biol.* **3**: 163-170.
58. Gutteridge, A. and J. M. Thornton 2005. Understanding nature's catalytic toolkit. *Trends. Biochem. Sci.* **30**: 622-629.
59. Haker, A., J. Hendriks, I. H. M. van Stokkum, J. Heberle, K. J. Hellingwerf, W. Crielaard and T. Gensch 2003. The two photocycles of photoactive yellow protein from *Rhodobacter sphaeroides*. *J. Biol. Chem.* **278**: 8442-8451.
60. Haker, A., J. Hendriks, T. Gensch, K. Hellingwerf and W. Crielaard 2000. Isolation, reconstitution and functional characterisation of the *Rhodobacter sphaeroides* photoactive yellow protein. *FEBS Lett.* **486**: 52-56.

61. Harigai, M., M. Kataoka and Y. Imamoto 2006. A single CH/ π weak hydrogen bond governs stability and the photocycle of the photoactive yellow protein. *J. Am. Chem. Soc.* **128**: 10646-10647.
62. Harigai, M., M. Kataoka and Y. Imamoto 2008. Interaction between N-terminal loop and beta-scaffold of photoactive yellow protein. *Photochem. Photobiol.* **84**: 1031-1037.
63. Harigai, M., S. Yasuda, Y. Imamoto, F. Yoshihara, F. Tokunaga and M. Kataoka 2001. Amino acids in the N-terminal region regulate the photocycle of photoactive yellow protein. *J. Biochem.* **130**: 51-56.
64. Harigai, M., Y. Imamoto, H. Kamikubo, Y. Yamazaki and M. Kataoka 2003. Role of an N-terminal loop in the secondary structural change of photoactive yellow protein. *Biochemistry* **42**: 13893-13900.
65. Harris, T. K. and G. J. Turner 2002. Structural basis of perturbed pK(a) values of catalytic groups in enzyme active sites. *IUBMB Life* **53**: 85-98.
66. He, W. Z., W. R. Newell, P. I. Haris, D. Chapman and J. Barber 1991. Protein secondary structure of the isolated photosystem II reaction center and conformational changes studied by Fourier transform infrared spectroscopy. *Biochemistry* **30**: 4552-4559.
67. Hefti, M. H., K. J. Francoijs, S. C. de Vries, R. Dixon and J. Vervoort 2004. The PAS fold - A redefinition of the PAS domain based upon structural prediction. *European Journal of Biochemistry* **271**: 1198-1208.
68. Hellingwerf, K. J., J. Hendriks and T. Gensch 2003. Photoactive Yellow Protein, a new type of photoreceptor protein: Will this "yellow lab" bring us where we want to go? *J. Phys. Chem. A* **107**: 1082-1094.
69. Hendriks, J., I. H. M. van Stokkum and K. J. Hellingwerf 2003. Deuterium isotope effects in the photocycle transitions of the photoactive yellow protein. *Biophys. J.* **84**: 1180-1191.
70. Hendriks, J., T. Gensch, L. Hviid, M. A. van der Horst, K. J. Hellingwerf and J. J. van Thor 2002. Transient exposure of hydrophobic surface in the photoactive yellow protein monitored with Nile red. *Biophys. J.* **82**: 1632-1643.
71. Henzler-Wildman, K. and D. Kern 2007. Dynamic personalities of proteins. *Nature* **450**: 964-972.
72. Herzog, E., T. Frigato, V. Helms and C. R. Lancaster 2006. Energy barriers of proton transfer reactions between amino acid side chain analogs and water from ab initio calculations. *J. Comput Chem.* **27**: 1534-1547.
73. Hickman, J. W., D. F. Tifrea and C. S. Harwood 2005. A chemosensory system that regulates biofilm formation through modulation of cyclic diguanylate levels. *Proc. Natl. Acad. Sci. USA* **102**: 14422-14427.
74. Hoff, W. D. 1995. Photoactive yellow protein. A new family of Eubacterial blue-light photoreceptors. Doctorate Dissertation Doctorate.
75. Hoff, W. D., A. Xie, I. H. M. Van Stokkum, X. J. Tang, J. Gural, A. R. Kroon and K. J. Hellingwerf 1999. Global conformational changes upon receptor stimulation in photoactive yellow protein. *Biochemistry* **38**: 1009-1017.

76. Hoff, W. D., I. H. M. Van Stokkum, J. Gural and K. J. Hellingwerf 1997. Comparison of acid denaturation and light activation in the eubacterial blue-light receptor photoactive yellow protein. *BBA-Bioenergetics* **1322**: 151-162.
77. Hoff, W. D., P. Dux, K. Hard, B. Devreese, I. M. Nugterenroodzant, W. Crielaard, R. Boelens, R. Kaptein, J. Vanbeeumen and K. J. Hellingwerf 1994. Thiol ester-linked p-coumaric acid as a new photoactive prosthetic group in a protein with rhodopsin-like photochemistry. *Biochemistry* **33**: 13959-13962.
78. Hoff, W. D., P. Dux, K. Hard, B. Devreese, I. M. Nugterenroodzant, W. Crielaard, R. Boelens, R. Kaptein, J. Vanbeeumen and K. J. Hellingwerf 1994. Thiol ester-linked p-coumaric acid as a new photoactive prosthetic group in a protein with rhodopsin-like photochemistry. *Biochemistry* **33**: 13959-13962.
79. Holm, L., S. Kaariainen, P. Rosenstrom and A. Schenkel 2008. Searching protein structure databases with DaliLite v.3. *Bioinformatics* **24**: 2780-2781.
80. Hospes, M. 2012. Light responses of bacteria: site-directed mutagenesis study of PYP & photo-inactivation of *E. coli* and *B. subtilis*. Doctorate Dissertation, University of Amsterdam
81. Hou, S. B., J. H. Saw, K. S. Lee, T. A. Freitas, C. Belisle, Y. Kawarabayasi, S. P. Donachie, A. Pikina, M. Y. Galperin, E. V. Koonin, K. S. Makarova, M. V. Omelchenko, A. Sorokin, Y. I. Wolf, Q. X. Li, Y. S. Keum, S. Campbell, J. Denery, S. I. Aizawa, S. Shibata, A. Malahoff and M. Alam 2004. Genome sequence of the deep-sea gamma-proteobacterium *Idiomarina loihiensis* reveals amino acid fermentation as a source of carbon and energy. *Proc. Natl. Acad. Sci. USA* **101**: 18036-18041.
82. Howell, I. and G. W. Neilson 1996. Li⁺ hydration in concentrated aqueous solution. *J. Phys-Condens. Mat.* **8**: 4455-4463.
83. Ihee, H., S. Rajagopal, V. Srajer, R. Pahl, S. Anderson, M. Schmidt, F. Schotte, P. A. Anfinrud, M. Wulff and K. Moffat 2005. Visualizing reaction pathways in photoactive yellow protein from nanoseconds to seconds. *Proc Natl Acad Sci U S A* **102**: 7145-7150.
84. Imamoto, Y. and M. Kataoka 2007. Structure and photoreaction of photoactive yellow protein, a structural prototype of the PAS domain superfamily. *Photochem Photobiol* **83**: 40-49.
85. Imamoto, Y., H. Kamikubo, M. Harigai, N. Shimizu and M. Kataoka 2002. Light-induced global conformational change of photoactive yellow protein in solution. *Biochemistry* **41**: 13595-13601.
86. Imamoto, Y., H. Koshimizu, K. Mihara, O. Hisatomi, T. Mizukami, K. Tsujimoto, M. Kataoka and F. Tokunaga 2001. Roles of amino acid residues near the chromophore of photoactive yellow protein. *Biochemistry* **40**: 4679-4685.
87. Imamoto, Y., K. Mihara, O. Hisatomi, M. Kataoka, F. Tokunaga, N. Bojkova and K. Yoshihara 1997. Evidence for proton transfer from Glu-46 to the chromophore during the photocycle of photoactive yellow protein. *J. Biol. Chem.* **272**: 12905-12908.
88. Imamoto, Y., S. Tatsumi, M. Harigai, Y. Yamazaki, H. Kamikubo and M. Kataoka 2008. Diverse roles of glycine residues conserved in photoactive yellow proteins. *Biophys. J.* **94**: 3620-3628.

89. Imamoto, Y., T. Ito, M. Kataoka and F. Tokunaga 1995. Reconstitution photoactive yellow protein from apoprotein and p-coumaric acid derivatives. *FEBS Lett.* **374**: 157-160.
90. Imhoff, J. F. and J. Suling 1996. The phylogenetic relationship among Ectothiorhodospiraceae: a reevaluation of their taxonomy on the basis of 16S rDNA analyses. *Archives of microbiology* **165**: 106-113.
91. Janiak-Spens, F., J. M. Sparling, M. Gurfinkel and A. H. West 1999. Differential stabilities of phosphorylated response regulator domains reflect functional roles of the yeast osmoregulatory SLN1 and SSK1 proteins. *J. Bacteriol.* **181**: 411-417.
92. Jiang, Z. Y., L. R. Swem, B. G. Rushing, S. Devanathan, G. Tollin and C. E. Bauer 1999. Bacterial photoreceptor with similarity to photoactive yellow protein and plant phytochromes. *Science* **285**: 406-409.
93. Joshi, C. P., H. Otto, D. Hoersch, T. E. Meyer, M. A. Cusanovich and M. P. Heyn 2009. Strong Hydrogen Bond between Glutamic Acid 46 and Chromophore Leads to the Intermediate Spectral Form and Excited State Proton Transfer in the Y42F Mutant of the Photoreceptor Photoactive Yellow Protein. *Biochemistry* **48**: 9980-9993.
94. Jung, K. H., V. D. Trivedi and J. L. Spudich 2003. Demonstration of a sensory rhodopsin in eubacteria. *Mol. Microbiol.* **47**: 1513-1522.
95. Kabsch, W. and C. Sander 1983. Dictionary of protein secondary structure: pattern recognition of hydrogen-bonded and geometrical features. *Biopolymers* **22**: 2577-2637.
96. Kennis, J. T., S. Crosson, M. Gauden, I. H. van Stokkum, K. Moffat and R. van Grondelle 2003. Primary reactions of the LOV2 domain of phototropin, a plant blue-light photoreceptor. *Biochemistry* **42**: 3385-3392.
97. Kim, M., R. A. Mathies, W. D. Hoff and K. J. Hellingwerf 1995. Resonance raman evidence that the thioester-linked 4-hydroxycinnamyl chromophore of photoactive yellow protein is deprotonated. *Biochemistry* **34**: 12669-12672.
98. Kim, M., R. A. Mathies, W. D. Hoff and K. J. Hellingwerf 1995. Resonance raman evidence that the thioester-linked 4-hydroxycinnamyl chromophore of photoactive yellow protein is deprotonated. *Biochemistry* **34**: 12669-12672.
99. Kort, R., H. Vonk, X. Xu, W. D. Hoff, W. Crielaard and K. J. Hellingwerf 1996. Evidence for trans-cis isomerization of the p-coumaric acid chromophore as the photochemical basis of the photocycle of photoactive yellow protein. *FEBS Lett.* **382**: 73-78.
100. Kort, R., W. D. Hoff, M. VanWest, A. R. Kroon, S. M. Hoffer, K. H. Vlieg, W. Crielaard, J. J. VanBeeumen and K. J. Hellingwerf 1996. The xanthopsins: A new family of eubacterial blue-light photoreceptors. *EMBO J.* **15**: 3209-3218.
101. Kortemme, T., A. V. Morozov and D. Baker 2003. An orientation-dependent hydrogen bonding potential improves prediction of specificity and structure for proteins and protein-protein complexes. *J. Mol. Biol.* **326**: 1239-1259.
102. Kroon, A. R., W. D. Hoff, H. P. Fennema, J. Gijzen, G. J. Koomen, J. W. Verhoeven, W. Crielaard and K. J. Hellingwerf 1996. Spectral tuning, fluorescence, and photoactivity in hybrids of photoactive yellow protein,

- reconstituted with native or modified chromophores. *J. Biol. Chem.* **271**: 31949-31956.
103. Kumauchi, M., M. T. Hara, P. Stalcup, A. H. Xie and W. D. Hoff 2008. Identification of six new photoactive yellow proteins - Diversity and structure-function relationships in a bacterial blue light photoreceptor. *Photochem. Photobiol.* **84**: 956-969.
 104. Kumauchi, M., N. Hamada, J. Sasaki and F. Tokunaga 2002. A role of methionine100 in facilitating PYPM-decay process in the photocycle of photoactive yellow protein. *Journal of Biochemistry* **132**: 205-210.
 105. Kumauchi, M., S. Kaledhonkar, A. F. Philip, J. Wycoff, M. Hara, Y. X. Li, A. H. Xie and W. D. Hoff 2010. A conserved helical capping hydrogen bond in PAS domains controls signaling kinetics in the superfamily prototype photoactive yellow protein. *J. Am. Chem. Soc.* **132**: 15820-15830.
 106. Kunz, W., J. Henle and B. W. Ninham 2004. 'Zur Lehre von der Wirkung der Salze' (about the science of the effect of salts): Franz Hofmeister's historical papers. *Curr. Opin. Colloid. In* **9**: 19-37.
 107. Kurokawa, H., D. S. Lee, M. Watanabe, I. Sagami, B. Mikami, C. S. Raman and T. Shimizu 2004. A redox-controlled molecular switch revealed by the crystal structure of a bacterial heme PAS sensor. *J. Biol. Chem.* **279**: 20186-20193.
 108. Kurokawa, H., D. S. Lee, M. Watanabe, I. Sagami, B. Mikami, C. S. Raman and T. Shimizu 2004. A redox-controlled molecular switch revealed by the crystal structure of a bacterial heme PAS sensor. *Journal of Biological Chemistry* **279**: 20186-20193.
 109. Kyndt, J. A., F. Vanrobaeys, J. C. Fitch, B. V. Devreese, T. E. Meyer, M. A. Cusanovich and J. J. Van Beeumen 2003. Heterologous production of *Halorhodospira halophila* holo-photoactive yellow protein through tandem expression of the postulated biosynthetic genes. *Biochemistry* **42**: 965-970.
 110. Kyndt, J. A., J. K. Hurley, B. Devreese, T. E. Meyer, M. A. Cusanovich, G. Tollin and J. J. Van Beeumen 2004. *Rhodobacter capsulatus* photoactive yellow protein: Genetic context, spectral and kinetics characterization, and mutagenesis. *Biochemistry* **43**: 1809-1820.
 111. Kyndt, J. A., T. E. Meyer and M. A. Cusanovich 2004. Photoactive yellow protein, bacteriophytochrome, and sensory rhodopsin in purple phototrophic bacteria. *Photoch. Photobio. Sci.* **3**: 519-530.
 112. Lagarias, D. M., S. H. Wu and J. C. Lagarias 1995. Atypical phytochrome gene structure in the green alga *Mesotaenium caldariorum*. *Plant Mol. Biol.* **29**: 1127-1142.
 113. Larson, S. M., I. Ruczinski, A. R. Davidson, D. Baker and K. W. Plaxco 2002. Residues participating in the protein folding nucleus do not exhibit preferential evolutionary conservation. *J. Mol. Biol.* **316**: 225-233.
 114. Lawrence, R. M. and R. F. Kruh 1967. X-Ray Diffraction Studies Of Aqueous Alkali-Metal Halide Solutions. *J. Chem. Phys.* **47**: 4758-4765.
 115. Lee, B. C., A. Pandit, P. A. Croonquist and W. D. Hoff 2001. Folding and signaling share the same pathway in a photoreceptor. *Proc. Natl. Acad. Sci. USA* **98**: 9062-9067.

116. Lide, D. V. and H. P. R. Frederikse 1997-1998. CRC Handbook of Chemistry and Physics, CRC Press LLC.
117. Louie, G. V., M. E. Bowman, M. C. Moffitt, T. J. Baiga, B. S. Moore and J. P. Noel 2006. Structural determinants and modulation of substrate specificity in phenylalanine-tyrosine ammonia-lyases. *Chem. Biol.* **13**: 1327-1338.
118. Lu, H. M., D. C. Yin, Y. M. Liu, W. H. Guo and R. B. Zhou 2012. Correlation between Protein Sequence Similarity and Crystallization Reagents in the Biological Macromolecule Crystallization Database. *Int. J.Mol. Sci* **13**: 9514-9526.
119. Man, D. L., W. W. Wang, G. Sabehi, L. Aravind, A. F. Post, R. Massana, E. N. Spudich, J. L. Spudich and O. Beja 2003. Diversification and spectral tuning in marine proteorhodopsins. *EMBO J.* **22**: 1725-1731.
120. Manikandan, K. and S. Ramakumar 2004. The occurrence of C-H center dot center dot center dot O hydrogen bonds in alpha-helices and helix termini in globular proteins. *Proteins Struct. Funct. Bioinf.* **56**: 768-781.
121. Mason, P. E., S. Ansell and G. W. Neilson 2006. Neutron diffraction studies of electrolytes in null water: a direct determination of the first hydration zone of ions. *J. Phys-Condens. Mat.* **18**.
122. Masuda, S. and C. E. Bauer 2002. AppA is a blue light photoreceptor that antirepresses photosynthesis gene expression in *Rhodobacter sphaeroides*. *Cell* **110**: 613-623.
123. Masuda, S., K. Hasegawa, A. Ishii and T. A. Ono 2004. Light-induced structural changes in a putative blue-light receptor with a novel FAD binding fold sensor of blue-light using FAD (BLUF); Slr1694 of *synechocystis* sp. PCC6803. *Biochemistry* **43**: 5304-5313.
124. Maxwell, P. H., G. U. Dachs, J. M. Gleadle, L. G. Nicholls, A. L. Harris, I. J. Stratford, O. Hankinson, C. W. Pugh and P. J. Ratcliffe 1997. Hypoxia-inducible factor-1 modulates gene expression in solid tumors and influences both angiogenesis and tumor growth. *Proc. Natl. Acad Sci USA* **94**: 8104-8109.
125. McCammon, J. A. 1984. Protein Dynamics. *Rep. Prog. Phys.* **47**:1-47.
126. McRee, D. E., T. E. Meyer, M. A. Cusanovich, H. E. Parge and E. D. Getzoff 1986. Crystallographic Characterization Of A Photoactive Yellow Protein With Photochemistry Similar To Sensory Rhodopsin. *J. Biol. Chem.* **261**: 3850-3851.
127. Memmi, S., J. Kyndt, T. Meyer, B. Devreese, M. Cusanovich and J. Van Beeumen 2008. Photoactive yellow protein from the halophilic bacterium *Salinibacter ruber*. *Biochemistry* **47**: 2014-2024.
128. Meot-Ner, M. 2005. The ionic hydrogen bond. *Chem. Rev.* **105**: 213-284.
129. Meyer, T. E. 1985. Isolation And Characterization Of Soluble Cytochromes, Ferredoxins And Other Chromophoric Proteins From The Halophilic Phototrophic Bacterium *Ectothiorhodospira-Halophila*. *Biochim. Biophys. Acta* **806**: 175-183.
130. Meyer, T. E., E. Yakali, M. A. Cusanovich and G. Tollin 1987. Properties Of A Water-Soluble, Yellow Protein Isolated From A Halophilic Phototrophic Bacterium That Has Photochemical Activity Analogous To Sensory Rhodopsin. *Biochemistry* **26**: 418-423.
131. Meyer, T. E., G. Tollin, J. H. Hazzard and M. A. Cusanovich 1989. Photoactive yellow protein from the purple phototrophic bacterium, *Ectothiorhodospira*

- halophila. Quantum yield of photobleaching and effects of temperature, alcohols, glycerol, and sucrose on kinetics of photobleaching and recovery. *Biophys. J.* **56**: 559-564.
132. Meyer, T. E., J. A. Kyndt, S. Memmi, T. Moser, B. Colon-Acevedo, B. Devreese and J. J. Van Beeumen 2012. The growing family of photoactive yellow proteins and their presumed functional roles. *Photochem. Photobiol. Sci.* **11**: 1495-1514.
 133. Meyer, T. E., S. Devanathan, T. Woo, E. D. Getzoff, G. Tollin and M. A. Cusanovich 2003. Site-specific mutations provide new insights into the origin of pH effects and alternative spectral forms in the photoactive yellow protein from *Halorhodospira halophila*. *Biochemistry* **42**: 3319-3325.
 134. Mihara, K., O. Hisatomi, Y. Imamoto, M. Kataoka and F. Tokunaga 1997. Functional expression and site-directed mutagenesis of photoactive yellow protein. *J. Biochem.* **121**: 876-880.
 135. Mildvan, A. S., M. A. Massiah, T. K. Harris, G. T. Marks, D. H. T. Harrison, C. Viragh, P. M. Reddy and I. M. Kovach 2002. Short, strong hydrogen bonds on enzymes: NMR and mechanistic studies. *J. Mol. Struct.* **615**: 163-175.
 136. Mirny, L. and E. Shakhnovich 2001. Evolutionary conservation of the folding nucleus. *J. Mol. Biol.* **308**: 123-129.
 137. Morishita, T., M. Harigai, Y. Yamazaki, H. Kamikubo, M. Kataoka and Y. Imamoto 2007. Array of aromatic amino acid side chains located near the chromophore of photoactive yellow protein. *Photochem. Photobiol.* **83**: 280-285.
 138. Nambu, J. R., J. O. Lewis, K. A. Wharton, Jr. and S. T. Crews 1991. The *Drosophila* single-minded gene encodes a helix-loop-helix protein that acts as a master regulator of CNS midline development. *Cell* **67**: 1157-1167.
 139. Narten, A. H., F. Vaslow and H. A. Levy 1973. Diffraction Pattern And Structure Of Aqueous Lithium-Chloride Solutions. *J. Chem. Phys.* **58**.
 140. Nathans, J., D. Thomas and D. S. Hogness 1986. Molecular genetics of human color vision: the genes encoding blue, green, and red pigments. *Science* **232**: 193-202.
 141. Neilson, G. W. and N. Skipper 1985. K⁺ Coordination In Aqueous-Solution. *Chem. Phys. Lett.* **114**.
 142. Nie, B. N., J. Stutzman and A. H. Xie 2005. A vibrational spectral marker for probing the hydrogen-bonding status of protonated Asp and Glu residues. *Biophys. J.* **88**: 2833-2847.
 143. Nishio, M. 2011. The CH/[small pi] hydrogen bond in chemistry. Conformation, supramolecules, optical resolution and interactions involving carbohydrates. *Phys. Chem. Chem. Phys.* **13**: 13873-13900.
 144. Nishio, M. 2011. The CH/[small pi] hydrogen bond in chemistry. Conformation, supramolecules, optical resolution and interactions involving carbohydrates. *Phys. Chem. Chem. Phys.* **13**: 13873-13900.
 145. Ohtomo, N. and K. Arakawa 1980. Neutron Diffraction Study of Aqueous Ionic Solutions. II. Aqueous Solutions of Sodium Chloride and Potassium Chloride. *Bull. Chem. Soc. Jpn* **53**: 1789-1794.
 146. Okajima, K., S. Yoshihara, Y. Fukushima, X. X. Geng, M. Katayama, S. Higashi, M. Watanabe, S. Sato, S. Tabata, Y. Shibata, S. Itoh and M. Ikeuchi 2005.

- Biochemical and functional characterization of BLUF-type flavin-binding proteins of two species of cyanobacteria. *J. Biochem* **137**: 741-750.
147. Orengo, C. A. and J. M. Thornton 2005. Protein families and their evolution - A structural perspective. *Annu. Rev. Biochem.* **74**: 867-900.
 148. O'Toole, G. A. and R. Kolter 1998. Flagellar and twitching motility are necessary for *Pseudomonas aeruginosa* biofilm development. *Mol. Microbiol.* **30**: 295-304.
 149. Pace, C. N., F. Vajdos, L. Fee, G. Grimsley and T. Gray 1995. How To Measure And Predict The Molar Absorption-Coefficient Of A Protein. *Protein Sci.* **4**: 2411-2423.
 150. Pace, C. N., G. Horn, E. J. Hebert, J. Bechert, K. Shaw, L. Urbanikova, J. M. Scholtz and J. Sevcik 2001. Tyrosine hydrogen bonds make a large contribution to protein stability. *J. Mol. Biol.* **312**: 393-404.
 151. Papadopoulos, J. S. and R. Agarwala 2007. COBALT: constraint-based alignment tool for multiple protein sequences. *Bioinformatics* **23**: 1073-1079.
 152. Paul, R., S. Weiser, N. C. Amiot, C. Chan, T. Schirmer, B. Giese and U. Jenal 2004. Cell cycle-dependent dynamic localization of a bacterial response regulator with a novel di-guanylate cyclase output domain. *Gene. Dev.* **18**: 715-727.
 153. Pauling, L., R. B. Corey and H. R. Branson 1951. The structure of proteins. 2. Hydrogen-bonded helical configurations of the polypeptide chain. *Proc. Natl. Acad. Sci. USA* **37**: 205-211.
 154. Pellequer, J. L., K. A. Wager-Smith, S. A. Kay and E. D. Getzoff 1998. Photoactive yellow protein: a structural prototype for the three-dimensional fold of the PAS domain superfamily. *Proc. Natl. Acad. Sci. U S A* **95**: 5884-5890.
 155. Perrin, C. L. and J. B. Nielson 1997. "Strong" hydrogen bonds in chemistry and biology. *Ann. Rev. Phys. Chem.* **48**: 511-544.
 156. Philip, A. F., K. T. Eisenman, G. A. Papadantonakis and W. D. Hoff 2008. Functional Tuning of Photoactive Yellow Protein by Active Site Residue 46. *Biochemistry* **47**: 13800-13810.
 157. Philip, A. F., M. Kumauchi and W. D. Hoff 2010. Robustness and evolvability in the functional anatomy of a PER-ARNT-SIM (PAS) domain. *Proc. Natl. Acad. Sci. U S A* **107**: 17986-17991.
 158. Philip, A. F., R. A. Nome, G. A. Papadantonakis, N. F. Scherer and W. D. Hoff 2010. Spectral tuning in photoactive yellow protein by modulation of the shape of the excited state energy surface. *Proc. Natl. Acad. Sci. USA* **107**: 5821-5826.
 159. Ponting, C. P. and L. Aravind 1997. PAS: a multifunctional domain family comes to light. *Curr. Biol.* **7**: R674-R677.
 160. Protein Purification Handbook, 1999. GE life sciences.
 161. Purcell, E. B. and S. Crosson 2008. Photoregulation in prokaryotes. *Curr. Opin. Microbiol.* **11**: 168-178.
 162. Purcell, E. B., D. Siegal-Gaskins, D. C. Rawling, A. Fiebig and S. Crosson 2007. A photosensory two-component system regulates bacterial cell attachment. *Proc. Natl. Acad. Sci. U S A* **104**: 18241-18246.
 163. Quiocho, F. A. and F. M. Richards 1966. Ezymic behavior of carboxypeptidase A in solid state. *Biochemistry* **5**: 4062-&.

164. Radu, I., M. Schleegeer, C. Bolwien and J. Heberle 2009. Time-resolved methods in biophysics. 10. Time-resolved FT-IR difference spectroscopy and the application to membrane proteins. *Photochem. Photobiol. S.* **8**: 1517-1528.
165. Rajagopal, S., S. Anderson, V. Srajer, M. Schmidt, R. Pahl and K. Moffat 2005. A structural pathway for signaling in the E46Q mutant of photoactive yellow protein. *Structure* **13**: 55-63.
166. Rinaldi, J., M. Gallo, S. Klinke, G. Paris, H. R. Bonomi, R. A. Bogomolni, D. O. Cicero and F. A. Goldbaum 2012. The beta-scaffold of the LOV domain of the *Brucella* light-activated histidine kinase is a key element for signal transduction. *J. Mol. Biol.* **420**: 112-127.
167. Rubinstenn, G., G. W. Vuister, F. A. A. Mulder, P. E. Dux, R. Boelens, K. J. Hellingwerf and R. Kaptein 1998. Structural and dynamic changes of photoactive yellow protein during its photocycle in solution. *Nat. Struct. Biol.* **5**: 568-570.
168. Ryjenkov, D. A., M. Tarutina, O. V. Moskvina and M. Gomelsky 2005. Cyclic diguanylate is a ubiquitous signaling molecule in bacteria: Insights into biochemistry of the GGDEF protein domain. *J. Bacteriol.* **187**: 1792-1798.
169. Sadhukhan, S., D. Muñoz, C. Adamo and G. E. Scuseria 1999. Predicting proton transfer barriers with density functional methods. *Chem. Phys. Lett.* **306**: 83-87.
170. Saito, K. and H. Ishikita 2012. Energetics of short hydrogen bonds in photoactive yellow protein. *Proc. Natl. Acad. Sci. USA* **109**: 167-172.
171. Scheiner, S. 2000. Calculation of isotope effects from first principles. *Biochim. Biophys. Acta* **1458**: 28-42.
172. Scheiner, S. and M. Čuma 1996. Relative Stability of Hydrogen and Deuterium Bonds. *J. Am. Chem. Soc.* **118**: 1511-1521.
173. Schmidt, A. J., D. A. Ryjenkov and M. Gomelsky 2005. The ubiquitous protein domain EAL is a cyclic diguanylate-specific phosphodiesterase: Enzymatically active and inactive EAL domains. *J. Bacteriol.* **187**: 4774-4781.
174. Schneider, K., K. Hovel, K. Witzel, B. Hamberger, D. Schomburg, E. Kombrink and H. P. Stüble 2003. The substrate specificity-determining amino acid code of 4-coumarate : CoA ligase. *Proc. Natl. Acad. Sci. USA* **100**: 8601-8606.
175. Schobert, B., J. Cupp-Vickery, V. Hornak, S. O. Smith and J. K. Lanyi 2002. Crystallographic structure of the K intermediate of bacteriorhodopsin: Conservation of free energy after photoisomerization of the retinal. *J. Mol. Biol.* **321**: 715-726.
176. Schultz, J., F. Milpetz, P. Bork and C. P. Ponting 1998. SMART, a simple modular architecture research tool: Identification of signaling domains. *Proc. Natl. Acad. Sci. USA* **95**: 5857-5864.
177. Semenza, G. L. 2000. Surviving ischemia: adaptive responses mediated by hypoxia-inducible factor 1. *J. Clin. Invest.* **106**: 809-812.
178. Serrano, L., J. Sancho, M. Hirshberg and A. R. Fersht 1992. α -Helix stability in proteins: I. Empirical correlations concerning substitution of side-chains at the N and C-caps and the replacement of alanine by glycine or serine at solvent-exposed surfaces. *J. Mol. Biol.* **227**: 544-559.
179. Shan, S. O., S. Loh and D. Herschlag 1996. The energetics of hydrogen bonds in model systems: implications for enzymatic catalysis. *Science* **272**: 97-101.

180. Sharrock, R. A. 2008. The phytochrome red/far-red photoreceptor superfamily. *Genome Biol.* **9**.
181. Shi, X., P. Abbyad, X. Shu, K. Kallio, P. Kanchanawong, W. Childs, S. J. Remington and S. G. Boxer 2007. Ultrafast excited-state dynamics in the green fluorescent protein variant S65T/H148D. 2. Unusual photophysical properties. *Biochemistry* **46**: 12014-12025.
182. Shirley, B. A., P. Stanssens, U. Hahn and C. N. Pace 1992. Contribution of hydrogen bonding to the conformational stability of ribonuclease T1. *Biochemistry* **31**: 725-732.
183. Sigala, P. A., M. A. Tsuchida and D. Herschlag 2009. Hydrogen bond dynamics in the active site of photoactive yellow protein. *Proc. Natl. Acad. Sci. USA* **106**: 9232-9237.
184. Sigler, P. B. and H. C. W. Skinner 1963. Reaction of diisopropylfluorophosphate with crystals of gamma-chymotrypsin. *Biochem. Biophys. Res. Commun.* **13**: 236-&.
185. Sprenger, W. W., W. D. Hoff, J. P. Armitage and K. J. Hellingwerf 1993. The eubacterium *ectothiorhodospira-halophila* is negatively phototactic, with a wavelength dependence that fits the absorption-spectrum of the photoactive yellow protein. *J. Bacteriol.* **175**: 3096-3104.
186. Stanley, N. R. and B. A. Lazazzera 2004. Environmental signals and regulatory pathways that influence biofilm formation. *Mol. Microbiol.* **52**: 917-924.
187. Steiner, T. 2002. The hydrogen bond in the solid state. *Angew. Chem. Int Edit.* **41**: 49-76.
188. Stryer, L. 1995. *Biochemistry* New York - Basingstoke, W. H. Freeman and Company.
189. Sugishima, M., N. Tanimoto, K. Soda, N. Hamada, F. Tokunaga and K. Fukuyama 2004. Structure of photoactive yellow protein (PYP) E46Q mutant at 1.2 angstrom resolution suggests how Glu46 controls the spectroscopic and kinetic characteristics of PYP. *Acta Crystallogr. D Biol. Crystallogr.* **60**: 2305-2309.
190. Sundberg, S. A., M. Alam and J. L. Spudich 1986. Excitation signal processing times in *Halobacterium halobium* phototaxis. *Biophys. J.* **50**: 895-900.
191. Swartz, T. E., S. B. Corchnoy, J. M. Christie, J. W. Lewis, I. Szundi, W. R. Briggs and R. A. Bogomolni 2001. The photocycle of a flavin-binding domain of the blue light photoreceptor phototropin. *J. Biol. Chem.* **276**: 36493-36500.
192. Takano, K., Y. Yamagata, M. Kubota, J. Funahashi, S. Fujii and K. Yutani 1999. Contribution of hydrogen bonds to the conformational stability of human lysozyme: Calorimetry and X-ray analysis of six Ser -> Ala mutants. *Biochemistry* **38**: 6623-6629.
193. Tamm, L. K. and S. A. Tatulian 1997. Infrared spectroscopy of proteins and peptides in lipid bilayers. *Q. Rev. Biophys.* **30**: 365-429.
194. Taylor, B. L. and I. B. Zhulin 1999. PAS domains: Internal sensors of oxygen, redox potential, and light. *Microbiol. Mol. Biol. R.* **63**: 479-506.
195. Terekhova, D. S. and I. V. Radchenko 1969. X-ray diffraction study of aqueous ammonium and potassium chloride solutions. *J. structural chemistry* **10**: 980-982.

196. Thomas, S. A., J. A. Brewster and R. B. Bourret 2008. Two variable active site residues modulate response regulator phosphoryl group stability. *Mol. Microbiol.* **69**: 453-465.
197. Timasheff, S. N. and G. D. Fasman, Eds. 1969. The comparison of protein structure in the crystal and in solution. Biological macromolecules. New York, MARCEL DEKKER Inc.
198. Tsai, C.-J., A. Del Sol and R. Nussinov 2009. Protein allostery, signal transmission and dynamics: a classification scheme of allosteric mechanisms. *Mol. Biosyst.* **5**: 207-216.
199. Ujj, L., S. Devanathan, T. E. Meyer, M. A. Cusanovich, G. Tollin and G. H. Atkinson 1998. New photocycle intermediates in the photoactive yellow protein from *Ectothiorhodospira halophila*: Picosecond transient absorption spectroscopy. *Biophys. J.* **75**: 406-412.
200. van Aalten, D. M. F., A. Haker, J. Hendriks, K. J. Hellingwerf, L. Joshua-Tor and W. Crielaard 2002. Engineering photocycle dynamics - Crystal structures and kinetics of three photoactive yellow protein hinge-bending mutants. *J. Biol. Chem.* **277**: 6463-6468.
201. Van Beeumen, J. J., B. V. Devreese, S. M. Van Bun, W. D. Hoff, K. J. Hellingwerf, T. E. Meyer, D. E. McRee and M. A. Cusanovich 1993. Primary structure of a photoactive yellow protein from the phototrophic bacterium *Ectothiorhodospira halophila*, with evidence for the mass and the binding site of the chromophore. *Protein sci.* **2**: 1114-1125.
202. Van der Horst, M. A. 2004. Structure/function relations in Photoactive Yellow Protein. Ph.D. Dissertation, University of Amsterdam.
203. van der Horst, M. A. and K. J. Hellingwerf 2004. Photoreceptor proteins, "star actors of modern times": a review of the functional dynamics in the structure of representative members of six different photoreceptor families. *Acc. Chem. Res.* **37**: 13-20.
204. van der Horst, M. A., I. H. van Stokkum, W. Crielaard and K. J. Hellingwerf 2001. The role of the N-terminal domain of photoactive yellow protein in the transient partial unfolding during signalling state formation. *FEBS Lett.* **497**: 26-30.
205. van der Horst, M. A., J. C. Arents, R. Kort and K. J. Hellingwerf 2007. Binding, tuning and mechanical function of the 4-hydroxy-cinnamic acid chromophore in photoactive yellow protein. *Photochem. Photobiol. Sci.* **6**: 571-579.
206. van der Horst, M. A., J. Key and K. J. Hellingwerf 2007. Photosensing in chemotrophic, non-phototrophic bacteria: let there be light sensing too. *Trends Microbiol.* **15**: 554-562.
207. van der Horst, M. A., T. P. Stalcup, S. Kaledhonkar, M. Kumauchi, M. Hara, A. Xie, K. J. Hellingwerf and W. D. Hoff 2009. Locked chromophore analogs reveal that photoactive yellow protein regulates biofilm formation in the deep sea bacterium *Idiomarina loihiensis*. *J. Am. Chem. Soc.* **131**: 17443-17451.
208. van der Horst, M. A., W. Laan, S. Yeremenko, A. Wende, P. Palm, D. Oesterhelt and K. J. Hellingwerf 2005. From primary photochemistry to biological function in the blue-light photoreceptors PYP and AppA. *Photochem. Photobiol. S* **4**: 688-693.

209. VanBrederode, M. E., W. D. Hoff, I. H. M. VanStokkum, M. L. Groot and K. J. Hellingwerf 1996. Protein folding thermodynamics applied to the photocycle of the photoactive yellow protein. *Biophys. J.* **71**: 365-380.
210. Varo, G. and L. Eisenstein 1987. Infrared Studies Of Water Induced Conformational-Changes In Bacteriorhodopsin. *Eur. Biophys. J. Biophys.* **14**: 163-168.
211. Vonhippe, P. H. and K. Y. Wong 1965. On conformational stability of globular proteins -Effects of various electrolytes and nonelectrolytes on thermal ribonuclease transition. *J. Biol. Chem.* **240**: 3909-&.
212. Xie, A. H., L. Kelemen, J. Hendriks, B. J. White, K. J. Hellingwerf and W. D. Hoff 2001. Formation of a new buried charge drives a large-amplitude protein quake in photoreceptor activation. *Biochemistry* **40**: 1510-1517.
213. Xie, A. H., W. D. Hoff, A. R. Kroon and K. J. Hellingwerf 1996. Glu46 donates a proton to the 4-hydroxycinnamate anion chromophore during the photocycle of photoactive yellow protein. *Biochemistry* **35**: 14671-14678.
214. Yamaguchi, S., H. Kamikubo, K. Kurihara, R. Kuroki, N. Niimura, N. Shimizu, Y. Yamazaki and M. Kataoka 2009. Low-barrier hydrogen bond in photoactive yellow protein. *Proc. Natl. Acad. Sci. USA* **106**: 440-444.
215. Yamato, T., T. Ishikura, T. Kakitani, K. Kawaguchi and H. Watanabe 2007. Spectral tuning of photoactive yellow protein. *Photochem. Photobiol.* **83**: 323-327.
216. Yan, B., T. Takahashi, R. Johnson and J. L. Spudich 1991. Identification of signaling states of a sensory receptor by modulation of lifetimes of stimulus-induced conformations: the case of sensory rhodopsin II. *Biochemistry* **30**: 10686-10692.
217. Yoda, M., H. Houjou, Y. Inoue and M. Sakurai 2001. Spectral tuning of photoactive yellow protein. Theoretical and experimental analysis of medium effects on the absorption spectrum of the chromophore. *J. Phys. Chem. B* **105**: 9887-9895.
218. Zhang, J. and Y. B. Yan 2005. Probing conformational changes of proteins by quantitative second-derivative infrared spectroscopy. *Anal. Biochem.* **340**: 89-98.

APPENDIX A

PYP Sample Preparation Protocol for FTIR measurements



A1: Basic information:

PYP: Photoactive yellow protein (over-expression from *E. coli* pET16b (DE3))

MW: 14021 Dalton (g/mol)

Extinction coefficient: $45.5 \text{ mM}^{-1}\text{cm}^{-1}$ (Meyer et al. 1991)

Weight of PYP per sample: $\sim 0.3 \text{ mg}$ ($3.0 \text{ }\mu\text{l}$) (Hhal PYP)

Final volume of PYP sample: $\sim 10 \text{ }\mu\text{l}$

Final protein concentration: 8-11 mM

Buffer concentration: 50 mM (5 buffer molecules per PYP)

UV/vis peak absorbance: 0.43-0.60 OD @ 446 nm with $12 \text{ }\mu\text{l}$ spacer

Amide I peak ($\sim 1640 \text{ cm}^{-1}$) absorbance: 0.60-0.80 OD (for D_2O samples)

Spacers: $12 \text{ }\mu\text{m}$. For samples in H_2O $6 \text{ }\mu\text{m}$, in that case UV/VIS and amide-I OD will reduce to half.

A2: Prepare PYP Samples for FTIR Experiments

The main goals for preparing FTIR PYP samples:

- (1) Right protein concentration (8-11 mM)
 - (2) Right pH (pH 7.50 at room temperature)
 - (3) For PYP in D₂O samples, low H₂O contamination (<1% of H₂O)
- *Weight of PYP: 1.1-1.2 mg* (Some protein may lost during concentration and washing process)
 - *The final volume: ~ 10 μ L* (volume per FTIR sample: 2.5-3.0 μ L)

Equipment:

5415 C microcentrifuge (eppendorf)
F-45-18-11 rotor (rotor comes with the centrifuge.)
Amicon 0.5 filters and centrifuge tube (Cutoff MW: 10,000D)
Adaptor (between filter and 0.5 mL tube, OSU physics machine shop made)
0.5 mL tube with O-ring cap (for storage)

Start from a liquid PYP sample

Use **Amicon 0.5** filter firstly concentrate PYP.
Set centrifugation speed to: 9000 rpm (RCF g =6,610)
Centrifugation time: 10 minutes



Two washes are sufficient for FTIR measurement.

First wash is meant for maintaining pH, while 2nd wash is meant for reducing water contamination.

Purge Microcentrifuge before closing the cap of the rotor and the cover of the centrifuge.
Centrifuge machine is operated at room temperature.

Starting Volume of sample before washing ~30 μ L

Note: Before centrifugation, calculate protein quantity by measuring UV/Vis absorption

The first wash:

Step 1: add 370 μ L of 50 mM potassium phosphate buffer in D₂O (pH=7.50) and ~30 μ L concentrated PYP sample in **Amicon 0.5** filter.

Wrap parafilm on top of washing tube to minimize H₂O exchange during washing.

(a) Set centrifugation speed to: 9000 rpm (RCF=6,610)

(b) Centrifugation time: 10 minutes

Make sure that >200 μ L of buffer solution is collected in the tube below the filter.

Step 2: Increase the centrifugation speed: 13,000 rpm (RCF g =11750)

Centrifugation time: 30 minutes

Make sure ~370 μ L of buffer is collected in the tube.

Comments:

(1) After adding 370 μL of buffer to 30 μL of 3.3 mM PYP, the resulting protein concentration is ~ 0.2 mM. Therefore, the buffer to protein ratio is 500:2 or 250:1. One wash is sufficient for pH adjustment. For H_2O samples 1 wash is enough to adjust the pH, however in case of D_2O samples second wash needed for reducing H_2O contamination.

(2) The H_2O contamination is $25 \mu\text{L} / 400 \mu\text{L} = 6.25\%$. A second wash is needed to further reduce the water contamination.

The second wash:

Step 1: add 370 μL of buffer (pH=7.50) to the concentrated PYP from the first wash set
Wrap parafilm on top of washing tube to minimize H_2O exchange during washing.

(a) Set centrifugation speed to: 9000 rpm (RCF=6,610)

(b) Centrifugation time: 10 minutes

Make sure $> 200 \mu\text{L}$ of buffer is collected in the tube.

Step 2: Increase the centrifugation speed: 13,000 rpm (RCF=11750)

Centrifugation time: *30 minutes

Make sure $\sim 370 \mu\text{L}$ of buffer is collected in the tube.

The H_2O contamination after second wash is $6.25\% * (25 \mu\text{L} / 400 \mu\text{L}) = 0.39\%$.

NOTE: Check by eye sight if $\sim 20 \mu\text{L}$ is left in the Amicon 0.5 filter, before proceeding to second wash measure volume collected in the tube by 250 μL syringe. The volume collected in the tube should be $\sim 370 \mu\text{L}$. Error = $|30 \pm 5 / 30| * 100\% = 16.7\%$

Step 3: Dilute PYP solution to 2.5 folds by adding 32.5 μL D_2O (total volume is 90 μL)

(a) Set centrifugation speed to: 13000 rpm (RCF=6,610)

(b) Centrifugation time: 10 minutes

Collect 25 μL of PYP in to 0.5 ml test tube

When $\sim 30 \mu\text{L}$ of the PYP solution is remained in filter, dismantle the filter and connect it to the adapter and fix this adapter to a small 500 μL tube. Balance with an identical setup in the opposite end. Run centrifuge for several seconds in order to get sample off the filter without introducing much water contamination.

After second wash: The H_2O contamination is $6.25\% * (25 \mu\text{L} / 400 \mu\text{L}) * (25 \mu\text{L} / 72.5 \mu\text{L}) = 0.13\%$. A second wash is sufficient to reduce the water contamination to $< 1.0\%$.

The other H_2O contamination comes from air during sample handling and the centrifugation.

Concentrating PYP using vacuum freeze dry

1: Place the 500 μL in Styrofoam cup containing LN2 to freeze

2: Replace the cap with 4 hole and place the 500 μL test tube inside home made vacuum chamber.

- 3: Close the vacuum lid and close the vent knob.
- 4: Start vacuum and open vacuum chamber fully. Wait for 17 minutes to remove the D₂O/H₂O.
- Step 5:** Vent off the vacuum chamber and replace cap with closed one. Perform this step under N₂ purging.

A3: Preparation of Stock Buffer, 1M 500 μ L potassium phosphate buffer in D₂O, pH=7.50 (pH* =7.10)

Check if the stock buffer has been prepared and stored in the freezer. Note: the three pK_a values of potassium phosphate buffers are: 2.15, 7.20 and 12.37.

Chemicals:

- (1) Potassium phosphate dibasic trihydrate (Sigma Aldrich P5504-100G) K₂HPO₄·3H₂O, MW 228.33 g/mol
- (2) Potassium phosphate monobasic (Sigma Aldrich P0662-25G) KH₂PO₄, MW 136.09 g/mol
- (3) D₂O (Cambridge Isotope 100 ml bottle 99.9 %)
- (4) Purified deionized water (18 M Ω) water purification system

Equipments:

- Pipettes :1 mL,200 μ l
- 1 mL tips (for pipette)
- 0.5 mL MicroTest Tubes (BioRad (with O-Ring Screw caps))
- pH meter (Accument AR 15)
- Calibration buffers for pH meter (pH 4.0, 7.0 and 10.0)
- Analytical balance
- Weighing papers (or trays)

Step 1: Preparing 500 μ L 1.0 M potassium phosphate dibasic (stock buffer)

- (a) Weigh 114.10 mg of potassium phosphate dibasic in a weighing paper using the analytical balance.
- (b) Transfer the chemical to 0.50 ml tube
- (c) Add 500.0 μ L of H₂O in another 0.50 mL tube as reference
- (e) Add 470.0 μ L of D₂O (or H₂O) to the buffer tube until it reaches 500 μ L by comparing it with the 500 μ L H₂O tube. Close the tube with an o-ring cap and gently shake it until fully dissolved.

Step 2: Prepare 500 μ L 1.0 M of potassium phosphate monobasic (stock buffer)

- (a) Weigh 68.0 mg of potassium phosphate monobasic in a weighing paper using the analytical balance

Repeat the process of (b-e) of the step 1

Step 3: Prepare 1.0 mL 50 mM potassium phosphate buffers at pH* 7.10 (in D₂O) + Prepare 1.0 mL 50mM potassium phosphate buffers at pH 7.50 (in H₂O)

(a) Mix 40 μ L of 1M potassium phosphate dibasic with 10 μ L of 1M potassium phosphate monobasic

(b) Add 900 μ L of D₂O Measure and adjust the pH of the mixed buffer:

For potassium phosphate buffer in D₂O

If pH* value < pH*7.10 add 0.50 M NaOD.

If pH* value > pH*7.10, add 0.50 M DCl.

For potassium phosphate buffer in H₂O:

If pH value < pH 7.50, add 0.50 M NaOD.

If pH value > pH 7.50, add 0.50 M DCl

(c) Add additional D₂O to make 1000.0 μ L of total volume.

Reference:

1. Meyer, T. E., G. Tollin, T. P. Causgrove, P. Cheng and R. E. Blankenship 1991. Picosecond decay kinetics and quantum yield of fluorescence of the photoactive yellow protein from the halophilic purple phototrophic bacterium, *Ectothiorhodospira halophila*. *Biophys J* **59**: 988-991.

APPENDIX B

Operation protocol of Brilliant laser

B1: Laser Information

Safety Officer: Sandip Kaledhonkar

- Model:- Quantel Bigsky Laser (Brilliant) with OPOTEK OPO (Serial No:-Z31BR)

Table 1: Laser energy

Principal radiation	1064 nm	532 nm	355 nm	OPO energy
Laser energy /pulse	400 mJ	200 mJ	100 mJ	10-22 mJ

- Tunable OPO wavelength window: 410-680 nm
- Laser pulse duration: 5 ns
- Nd:YAG (Neodymium-doped Yttrium Aluminum Garnet; Nd:Y₃Al₅O₁₂)
- Class IV: Diffuse reflections of the laser beam can be hazardous to skin or eye



Figure 1: Nd:YAG laser components (A) Brilliant Laser (B)OPOTEK OPO (C) remote control box (D) Delay generator (SRS DG 535) (E) Laser power supply unit (F) OPOTEK OPO stepper motor driver

B2: Laser safety

- 1) Wear laser goggles when use fundamental, second and third harmonic oscillator. Laser goggles are located at 220D HBRC bench areas D1-D5.
- 2) Never look directly into laser beam, even when laser is having problems or laser flashes are not visible.
- 3) Be aware of scattered and reflected beams. Block the scattered and reflected beam with black metal sheets.
- 4) While working with laser remove wrist watches, jewelry with reflective surface to avoid accidental reflections.
- 5) Do not expose any part of body to the laser beam.
- 6) Turn on warning sign “LASER IN USE” and slide the black curtains in the laser working area.
- 7) Before operating laser always read Brilliant instruction manual.
- 8) Contact laser safety officer to test laser safety knowledge.

B3: Tuning OPO wavelength

Follow this procedure if you want to change the wavelength from previous experiment, if not follow procedure C5.

The laser wavelength is set at 475 nm using OPOTEK motor driver for OPO. This wavelength is meant to excite the wild type (wt) photoactive yellow protein (PYP) from *H. Halorodhospira* (*Hhal*). Below is the reference for OPO motor position at 475 and 500 nm.

Table 2: Reference for OPO stepper motor position

Wavelength (nm)	OPO motor position
475	36207
500	39279

Note: After desired wavelength has been set, switch off the OPO motor driver. After switching off the motor driver, motor position locked and stays at the same wavelength. This way motor position needs not to be changed every day.

- To change the wavelength to other wavelength, follow procedure below.
- 1) Turn the control key on the front panel of the laser box to the “I” position if it is in “O”. (“I”=ON, “O”=OFF) (When key is turned to “I” position, both Power and Interlock LED should Lit on Remote Box panel.)
 - 2) Wait about 15 minutes until the water temperature equilibrates for flashlamp operation. Water temperature should reach 39 °C.
 - 3) Turn on the OPOTEK computer. Wait until Windows has started.
 - 4) Turn on the OPOTEK OPO motor driver.
 - 5) Double click file C:\opotek\Vibrant_OPOLETTEver5.3.3poly6.
 - 6) Home the OPO stepper motor by selecting “Yes”. And wait until motor homes (Figure 2A). Wait for 1 minute to home the stepping motor.
 - 7) Select “Edit system parameter” and change the settings to internal laser control. Press “save and exit” to go to main menu. (Figure 2B)
 - 8) Press “Start Flashlamp” button on main menu to start flashlamp. Wait for 30 minutes to warm up the laser.
 - 9) Enter the desired wavelength number in box, click “Tune” button to adjust the stepper motor. (Figure 3). Wait for ~ 1 minute until stepper motor is moved.

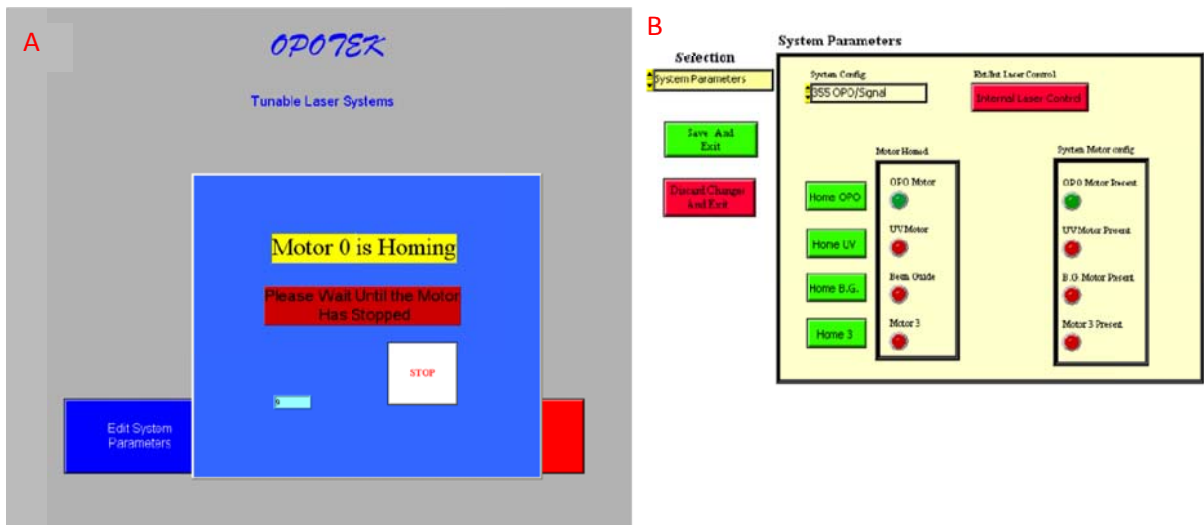


Figure 2: Display of OPO stepper motor homing (A) OPOTEK software system parameter set up display (B)

10) Switch off the OPOTEK OPO stepper motor.

11) Close the OPOTEK software by pressing “Return” button.

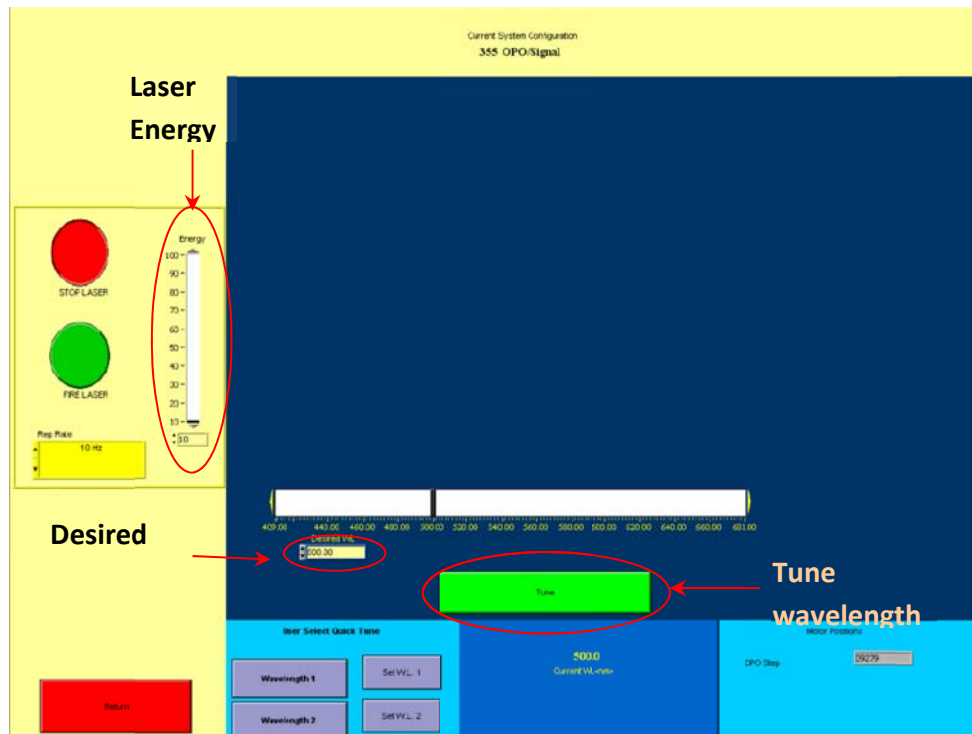


Figure 3: Tuning the OPO wavelength and selecting laser energy

B4: Internal/external triggering mode

Usually flashlamp and Q-switch will be in internal triggering mode settings.

- 1) To change triggering mode from internal to external or vice versa, select main menu on remote control box.
- 2) Select Flashlamp, move cursor to second line of display and press “+” to set in external mode (“-” to set internal mode) .
- 3) Select Q-switch, move cursor to second line of display and press “+” to set in external mode (“-” to set internal mode).

Comment: For flash photolysis, time-resolved rapid-scan and step-scan FTIR measurement laser repetition rate is set at 9.85 Hz to avoid noise from line frequency with mains 60 Hz using delay generators.

Please follow protocols for time-resolved rapid-scan and step-scan FTIR to learn how to trigger flashlamp and Q-switch using delay generators (Standford Research System DG535)

Synchronization of Laser using delay generators

Delay generator on internal triggering mode: laser master clock

Delay generator on external triggering mode: FTIR master clock, laser slave

B5: Daily startup procedure

- 1) Turn the control key on the front panel of the laser box to the “I” position if it is in “O”. (“I”=ON, “O”=OFF) (When key is turned to “I” position, both Power and Interlock LED should lit on remote control box.)
- 2) Wait about 15 minutes until the water temperature equilibrates for flashlamp operation. Water temperature should reach 39 °C.
- 3) Set the flashlamp and Q-switch in internal mode using remote control box.
- 4) Start the flashlamp and wait for 30 minutes for warming up. (Flashlamp voltage 1410 V)
- 5) Select the laser output energy to 10% by changing Q-switch delay time to 272 μ s. Laser repetition rate is 10 Hz.
- 6) To change the Q-switch delay time on remote select FL_QS Dly.
Below is the chart for selecting Q-switch time delay to control laser output delay.

- 7) Align power probe (Molelectron POWERMAX 500D), and press single shot button on remote to check whether laser beam is at the center of probe.
- 8) Set the laser output energy to 100% by changing Q-switch delay time to 192 μ s.
- 9) Check the 100% laser energy at 10Hz. 100% laser energy at 475 nm with 10 Hz repetition rate should be \sim 22 mJ/pulse.

Laser energy %	Q-switch delay time (μ s)
20	298
30	285
40	272
50	258
60	245
70	232
80	219
90	205
100	192

Table 3: Q-switch delay time and corresponding laser energy in percentage

B6: Laser Shutdown procedure

- 1) Stop the laser emission by pressing the “stop” buttons of the Q-Switch on the remote control box
- 2) Press “ stop” button for flashlamp on the remote control box.
- 2) In remote box change the triggering mode to internal.
- 2) Turn the control key on front panel of the laser box to “O” position.

Note: To disconnect the laser head from power supply discharge the capacitor by pushing the capacitor discharge knob inside as shown on back side of laser power supply unit.

B7: Trouble Shootings:

Laser is not flashing.

-Check flashlamp and Q-switch triggering mode is in either internal or external mode.

B8: Maintenance:

Change the cartridge and deionized water once in every 4 months.

Cartridge may need not to change every 4 months however it is mandatory to change deionized water every 4 months.

Procedure for changing cartridge and deionized water:

- 1) Switch off power supply unit, unplug the AC power cord and push capacitor discharge switch.
- 2) Unscrew the screws on left side to open the cooling group unit (CGU).
- 3) Refer to diagram of CGU in the manual and put the water tank below valve of CGU.
- 4) Open the cap of water tank and drain the water.
- 5) Place the draining hose back to its initial position.
- 6) Replace cartridge
- 7) Fill up water tank with deionized water.
- 8) Close the cap of water tank.
- 9) Take the air-cock connector in hand and pull it above the CG level. Press for about a minute this connectore with finger on the half of its area to remove air bubble.
- 10) Pull the capacitor switch and connect the power supply unit to mains.
- 11) Turn the key on the front panel of power supply unit to “I” position and wait for three minutes before turning it back to “O” position.
- 12) Unplug the main cord from mains and push the capacitor discharge switch.
- 13) Put back in place cabinet side and pull the capacitor discharge switch.

APPENDIX C

Protocol for time-resolved rapid-scan FTIR measurement of PYP sample

C1: Checklist:

- Temperature controller is on (takes 20-30 minutes for temperature equilibration)
- Cool down MCT Detector with liquid nitrogen
- Vacuum on (EVAC. IF/ VENT SM on the FTIR)
- IR beam is not blocked (Check signal in OPUS-NT)
- IR signal (no sample) at the centerburst should be in the range of ± 0.50 and ADC count is around ± 20000 with sample signal gain 1.
- Purge the N₂ in the sample chamber with flow rate 80 (2.21 L/min, glass ball).
- Measurement parameters in OPUS are OK.

C2: Checklist at the end of day:

- Vent optics and turn off the vacuum pump
- Turn off purging nitrogen gas.
- **Slow down the scanner velocity to 10 kHz step by step**
- Turn off the temperature controller
- Remove the samples from sample chamber and clean the windows (**for BaF₂ windows, need to clean the windows immediately after each day's measurement**)
- Back up the experimental data on CD (two copies) at the end of experiments

C3: Experimental procedure:

Part I: Prepare for experiments

1. Turn on the NESLAB RTE-111 temperature controller. Set temperature to 25°C.
2. Turn on the Cary 300 spectrometer
3. Cool down the MCT detector.
4. Evacuate FTIR optics compartment.

Check the checklist for the starting of the experiments

Part II: Load the sample

1. Take the sample from the freezer and thaw for 5 min at room temperature, then centrifuge at 3000 rpm for 2 min in order to remove the micro air bubbles.
2. Clean two CaF₂/BaF₂ windows (15 mm diameter x 2 mm thickness) using ethanol. Cut optical cleaning tissue. Fold it with the help of plastic fork. Wipe the window with ethanol soaked paper in one direction.
3. Clean the spacer (6 or 12 micrometer thick, home made from the big sheet) using distilled water and dry it.
4. Place 3 micro-drops of 0.5 µl D₂O on indium foil of sample holder with help of syringe. This will help sample to rehydrate during experiment.
5. Place one window in the sample holder.
6. Place the spacer flat on the window.
7. For deuterated sample, keep gentle purging with dry N₂ while loading the sample.
8. Take 3.0 µl of sample (optimal is 2.5 µl to save sample) using 10 µl pipette (small, 10 µl tips), load the sample in the center of the window.
!!!In order to prevent air bubbles in the sample, cautions must be exercised for the next two steps!!!
9. !!! Place the second window in order to prevent air bubbles. First keep one edge of the 2nd window on the first, use a needle or inoculating loop to support the 2nd window, slowly lower it until it touches the drop of the sample and continue to lower down the window.
10. !!! Place the sample hold cover on the top of window. Use two fingers of left hand (weaker hand) to evenly, gently and steadily press the window, tighten screws gradually in 3-4 rotations using hexagonal screw driver (size=2 mm).
11. Repeat the process 2-9 to load the buffer in the identical sample holder.



Part III: Measure the UV/vis absorption spectrum of the sample

Measure the UV/vis spectrum of each sample before and after the FTIR measurements. Make sure to get a spectrum with publication quality.

1. Load the sample to a lens holder in the sample beam position
!!! If the sample is placed off the focal position, so that the monitoring beam is slightly smaller than the sample cross-section and concentric, it can reduce the light activation caused by the probe beam.
2. No sample is mounted in the reference beam position (Air as reference)
3. Set the Cary spectrometer to the following parameters.
4. Set the directory: eg. D:\name\
5. Measure the UV/vis absorption spectrum, repeat the measurement if necessary to achieve high quality spectrum (high S/N, minimal discontinuity around 350 nm).
6. Print two copies of the spectrum, one for data collection notebook, one for result binder.
7. If the buffer is KHPO₄ or NaHPO₄, no measurement of buffer is needed.
8. UV absorption at λ_{max} should be 0.40-0.60 OD. (No further experiment should be done if UV absorption is not in this region in order to get publication quality of data)

Experimental Parameters for Cary 300 UV/Vis spectrometer

Range: 250 – 550 nm
Double Beam Mode
SBW: 2.0 nm
Baseline Correction: ON
Scan Rate: 150 nm/min, 0.4 seconds per data point
Data Interval: 1.0 nm
Mode: Absorption

Part IV: Measure the FTIR absorption spectrum of the sample and the buffer

!!!Measure the infrared spectrum of each sample before and after the FTIR measurements. Make sure that pre-rapid-scan spectrum has the publication quality.

1. Insert PYP sample FTIR sample chamber (Bruker IFS66v). (Position 1: sample, Position 2: buffer, Position 3: CaF₂ windows).
2. Set the temperature controller to 25°C. 10 minutes are required for equilibration after the coolant reached the desired temperature or after loading the sample holder with sample.
3. Start purging N₂ in the sample chamber (with flow rate 80 (2.21 L/min, glass ball)).
4. Make sure that step motor's power cable is unplugged from power unit.

5. Move 3 sample exchanger's position 3 (reference) to IR beam; check the interferogram using MCT detector. Magnitude of center burst should be less than 0.50. If magnitude is greater than 0.50, reduce signal gain or vice versa.
6. Move the 3 sample exchanger's position 1 (sample) to IR beam. Plug in power cable of step motor to power unit. (Correct SI program should have been loaded to step motor driver)
7. Measure the IR absorption spectrum using 3 sample exchanger and rapid scan (copy experimental files to the data folder).
8. Amide-I absorption should be 0.60-0.80 OD. Saturated D₂O absorption in region of 2000-2500 cm⁻¹ should be more than 2.0 OD.

Acquisition mode: Double sided forward backward

For FTIR Absorption measurement use following settings.

D:\OPUS\MEAS\0_Experimental files\Rapidscan_3sample_exchanger

Xpm File:- abs_2cm_3sampleExchanger.XPM

TRS File:- RPD_3sampleexchanger_2cm_1scan_40kHz.TRS

Optic settings

Detector: 2; MCT; -800; 0.9
 Aperture: 5 mm
 Scanner Velocity: 40.0 kHz
 Sample Signal Gain: 4 (with no sample ADC count is 20000)

Advanced settings

Spectral resolution: 2 cm⁻¹
 Save data from 4000 cm⁻¹ to 850 cm⁻¹
 Data blocks to be saved: Single Channel and Sample Interferogram.

Acquisition settings

High Folding Limit: 6000 cm⁻¹
 Low Folding Limit: 0.00 cm⁻¹
 Wanted High Frequency: 4200 cm⁻¹
 Wanted Low Frequency: 800 cm⁻¹
 Acquisition mode: Double-sided forward backward

FT settings

Phase resolution: 16 cm⁻¹
 Phase Correction Mode: Mertz
 Apodization Function: Blackman-Harris 3-Term
 Zero filling factor: 4
 Perform interferogram nonlinearity correction before FT.

Connections of BNC cable

Connect the BIT 0 BNC cable to 3 sample exchanger

Part V : Rapid-scan AND Quadruple splitting rapid scan measurement

Experimental setup

XPM :- wtPYP_rpsc_norm_4.5cm_200kHz.XPM

TRS:- RPD_4S_norm_4.5cm_200kHz.TRS

Optic settings

Detector: 2; MCT; -800; 0.9

Aperture: 5 mm

Scanner Velocity: 100.0 kHz

Note: actual scanner velocity during time-resolved rapid-scan measurement is 200 kHz. In TRS file the scanning velocity is slowly increased to 200 kHz from 100 kHz. This is to prevent interlocking of laser during experiment and step by step increase in scanner velocity.

Advanced settings

Spectral resolution: 4.5 cm^{-1}

Save data from 4000 cm^{-1} to 850 cm^{-1}

Data blocks to be saved: Single Channel and Sample Interferogram.

Acquisition settings

High Folding Limit: 6000 cm^{-1}

Low Folding Limit: 0.00 cm^{-1}

Wanted High Frequency: 4200 cm^{-1}

Wanted Low Frequency: 800 cm^{-1}

Acquisition mode: Double-sided forward backward

FT settings

Phase resolution: 16 cm^{-1}

Phase Correction Mode: Mertz

Apodization Function: Blackman-Harris 3-Term

Zero filling factor: 4

Perform interferogram nonlinearity correction before FT.

Connections of BNC cable

Connect the BIT 0 BNC cable to rapid scan BNC cable.

Procedure

1. (Before Absorption Measurement) Check optics setup in sample chamber. Make sure measurement pathway is not blocked and excited light is focused on the sample
2. Load files for rapid scan measurement to OPUS measurement window.
3. Click on start measurement, a pop up window will appear.

4. Press the start button for Flashlamp on Laser remote control box, then wait until 80 flash and press start button for Q-switch
5. Click on pop up window to start rapid scan measurement.
6. Measure one rapid scan for testing; 10 loops, test band positions, decay time.
7. Measure rapid scan on the protein sample.
8. Repeat for several data set.
9. Measure IR absorption spectrum again. The absorption of 5% protein bleaching is acceptable.
10. Measure VIS absorption spectrum of the protein sample.

Delay Generators

All the output signals are TTL (inverted normal) signals. FTIR FWD signal triggers the delay generator slave 1.

DG1 Delay generator 1 triggered by FTIR FWD				DG2 Delay generator 2 triggered by DG1			
A	B	C	D	A	B	C	D
T+10ms	A+30 μ s	A+220 μ s	C+30 μ s	T+8.94ms	T+985ms	T+20ms	C+70ms
AB: flashlamp		CD: Q-switch		AB: not connected T+ 985 ms laser repetition rate		CD: not connected	
				T: Electronic shutter triggered by DG2 Exposure time 90 ms			

XPM:- wtPYP_rpsc_QS_4.5cm_200kHz.XPM

TRS:- RPD_4S_QS_4.5cm_200kHz.TRS

For quadruple splitting measurement, change the delay time for the 1st, 2nd, 3rd and 4th measurements to 10 ms, 23 ms, 59 ms, and 72 ms respectively of A of slave 1 delay generators. This delay time has been set considering that 1 full scan at 200 kHz scanner velocity takes 98.7 ms.

C4: Data analysis for rapid scan using macro programs:

1. Load all the rapid-scan measurement files in OPUS window.
2. Delete all the data files in C:\Program Files\OPUS\WORK\ directory.
3. Select “Run Macro” in the OPUS-NT “Macro” pull down menu.
4. Open the main macro program for rapid-scan data analysis “E:\OPUS_macro\macro_NT\RPDSCAN\RPD_NORM\updates\RPD_NORM.MTX”.
5. Select all the single beam spectra and drag them to the blank space labeled “Rapidscan(s)” in the popup window.

6. Specify the “First block to extract” to be 1 and “Last block to extract” (Find the last block number by showing parameters in “Trace/Multiple” of the rapid-scan OPUS files.
7. Select “Calculate mOD”.
8. Click “OK”.
9. The difference absorption spectra will be loaded to the screen. They are saved in C:\Program Files\OPUS\WORK\ folder.

Copy and Paste them to your local directory and delete them from the WORK folder to prevent loading wrong set of data for next data analysis

C5: Data analysis for quadruple-split rapid scan using macro programs:

10. Load all the rapid-scan measurement files in OPUS window.
 11. Delete all the data files in C:\Program Files\OPUS\WORK\ directory.
 12. Select “Run Macro” in the OPUS-NT “Macro” pull down menu.
 13. Open the main macro program for rapid-scan data analysis “E:\OPUS_macro\macro_NT\RPDSCAN\RPD_SHFT\updates\RPD_SHFTMTX”.
 14. Select all the single beam spectra for first time delay and drag them to the blank space labeled “Rapidscan(s)” in the popup window.
 15. Specify the “First block to extract” to be 4 and “Last block to extract” (Find the last block number by showing parameters in “Trace/Multiple” of the rapid-scan OPUS files.
 16. Specify the “No of data sets”.
 17. Select “Calculate mOD” and “Average”.
 18. Click “Continue”.
 19. For next pop up window, select single beam of 2nd delay time measurement. Click continue and repeat for single beam of 3rd and 4th delay time measurement.
 20. Click “Continue” at the fourth pop up window.
 21. OPUS will start extracting data blocks.
 22. The difference absorption spectra will be loaded to the screen. They are saved in C:\Program Files\OPUS\WORK\ folder.
 23. Copy and Paste them to your local directory and delete them from the WORK folder to prevent loading wrong set of data for next data analysis.
- Measure IR absorption once done with quadruple rapid scan.

APPENDIX D

Experimental Protocol for Step-scan FTIR of wt-PYP

D1: Checklist:

- Warm up the laser according to laser startup procedure
- Photovoltaic MCT Detector is cooled down
- Vacuum on (EVAC. IF/ VENT SM on the FTIR)
- Table is floating (pressure 23.6 psi, 6 mm higher)
- Turn the switch to step-scan scan mode
- Temperature controller is on
- IR filter is placed in the sample compartment. Cutoff: 1900 cm^{-1} (5% transmission).
- IR beam is not blocked (Check signal in OPUS-NT)
- IR signal (no sample) at the centerburst should be in the range of ± 0.75 and ADC count is around 22000 with Sample signal gain of 8 (DC mode). If the interferogram is off zero, use the screwdriver to offset.
- Laser is aligned for step-scan
- Laser energy before sample (0.066 mJ/mm^2 , 7.46 mJ on 6 mm area)
- Test the control of sample exchanger
- Purge the LN_2 in the sample chamber (with higher flow rate 140 (3.62 L/min, glass ball) for ~5 minute and then reduce it to ~80 (2.21 L/min, glass ball)).

D2: Checklist at the end of day:

- Vent optics and turn off the vacuum pump
- Turn off purging nitrogen gas
- Turn off the high pressure nitrogen to stop floating table
- Turn down the laser according to laser shutdown procedure
- Turn off the temperature controller
- Turn off the delay generators and power meter
- Remove the samples from sample chamber and clean the windows (for BaF₂ windows, need to clean the windows immediately after each day's measurement)
- Back up the experimental data on CD (two copies) at the end of experiments

D3: Measurements settings:

UV-Vis absorption

Experimental Parameters for Cary UV/Vis spectrum

Range: 250 – 550 nm

Double Beam Mode

SBW: 2.0 nm

Baseline Correction: ON

Scan Rate: 600 nm/min

Data Interval: 1.0 nm

Mode: Absorption

Experimental Parameters for standard measurement (saved at D:\OPUS\MEAS\XPM\norm_FTIR_2cm-1.xpm).

FTIR absorption

Optic settings

Detector: Detector 3

Aperture: 6 mm

Scanner Velocity: 20.0 kHz

Sample Signal Gain: 4 (with no sample ADC count is 22000, DC mode)

Advanced settings

Spectral resolution: 2 cm⁻¹

Save data from 4000 cm⁻¹ to 850 cm⁻¹

Acquisition settings

High Folding Limit: 7899.94 cm⁻¹

Low Folding Limit: 0.00 cm⁻¹

Wanted High Frequency: 6000 cm⁻¹

Wanted Low Frequency: 800 cm⁻¹

Acquisition mode: Double-sided forward backward

FT settings

Phase resolution: 4 cm^{-1}
Phase Correction Mode: Mertz
Apodization Function: Blackman-Harris 3-Term
Zero filling factor: 4

Experimental Parameters for step-scan FTIR (saved at
D:\OPUS\MEAS\XPM\wtPYP_stsc_010506.xpm).

Recorder settings

Device: Internal ADC (± 10 V)
Time resolution: 5 μs (200 KHz)
No. of time slices 2000 (10 ms)
Timebase: Linear Timescale
Input range: ± 10 V
Repetition/Coadd. Count: 6 mirror position (2 for each sample)
Trigger mode: External Positive Edge
Experiment recovery time: 0 ms
Stabilization delay after mirror movements: 20 ms

Optic settings

Detector: MCT Photovoltaic (Detector 3)
Aperture: 2.5-3 mm (depending upon saturation of signal)
Scanner Velocity: 20.0 kHz
Sample Signal Gain: 1 (with 11 mM wt-PYP sample ADC count is 20800, DC mode)

Advanced settings

Spectral resolution: 4.5 cm^{-1}
Save data from 1850 cm^{-1} to 990 cm^{-1}

Acquisition settings

High Folding Limit: 1974.75 cm^{-1}
Low Folding Limit: 987.38 cm^{-1}
Wanted High Frequency: 1850 cm^{-1}
Wanted Low Frequency: 990 cm^{-1}

Acquisition mode: Single sided

FT settings

Phase resolution: 32 cm⁻¹

Phase Correction Mode: Mertz

Apodization Function: Blackman-Harris 3-Term

Zero filling factor: 4

DC output of MCT detector is connected to Detector X Input Analog Input.

The number of mirror positions is determined by spectral resolution and phase resolution (See the table below)

Phase resolution	4.5 cm ⁻¹	6 cm ⁻¹
32	423	330
16	475	382
8	580	487

Number of mirror positions at different phase and spectral resolutions with folding of 929 – 1858 cm⁻¹

No. of spectra averaged until the noise is ≤10⁻⁵ OD (≤10⁻⁴ OD?)

Calculation of measurement time

6 co-addition				9 co-addition			
Sample recovery time	DG Slave D	Mirror position	Meas. time	Sample recovery time	DG Slave D	Mirror position	Meas. time
2 s	0.667 s	475	31.7 m	2 s	0.667 s	475	47.6 m
4 s	1.333 s		1.06 h	4 s	1.333 s		1.59 h
6 s	2 s		1.58 h	6 s	2 s		2.37 h
8 s	2.667 s		2.11 h	8 s	2.667 s		3.17 h

Explanation (wt-PYP for example)

6 coadd/mirror positions means 3 flashes/sample.

6 coadd. \times 449 mirror position \times 4 s \times 1/3 = 2694 s, \sim 95 min for one spectra series of 6 averages (plus \sim 5 min for FT). This is 1425 flashes/sample. One sample can be used for 3 step-scan measurements: \sim 4000 flashes (the absorption of 5% protein bleaching is acceptable). 120 averages: \sim 21 hrs. In the literature 4 – 8 cm^{-1} resolution is used.

D4: Delay Generators and synchronization

During the measurement (i) the Start of the measurement, (ii) the laser flash, (iii) the 3 sample exchanger and (iv) the shutter are synchronized. DG1 is internally triggered with 9.85Hz, and it triggers DG2.

Start of measurement is triggered from DG2 such that there're 256 background spectra before the laser flash. For 5 μ s resolution it is 1.28 ms.

Laser flash is triggered from DG1: normal AB triggers flashlamp, normal CD triggers Q-switch

3 sample exchanger is triggered by DG2's normal CD output. Its own program is downloaded to its driver unit.

Shutter is triggered by DG2's T output. It is set up on its driver unit such that it remains open for 90 ms, so one and only one flash can be transmitted

DG1				DG2			
A	B	C	D	A	B	C	D
T+10ms	A+30 μ s	A+220 μ s	C+30 μ s	T+8.94ms	T+985ms	T+20ms	C+70ms
AB: flashlamp		CD: Q-switch		AB: start of stepscan		CD: 3 sample exch.	
				T: shutter			

- The start of the measurement signal has to come before the laser flash. The delay is determined by the Q-switch delay (DG1, C point). Set the DG1's A delay to 10 ms and DG2's A output to 10ms - 1.28ms + 220 μ s = 8.94ms. Use DG2's normal AB output's positive edge to trigger the measurement which with this setup comes 1.28 ms before the laser flash. DG2's B delay is set to determine how frequently the sample is illuminated. It should be set to around 1s if 3 samples are used.
- With this setting the laser runs with 10Hz, and the shutter selects the flash to excite the sample.

Experimental procedure:

Measure single beam spectra of the sample holder with (1) no sample and (2) the buffer only. This will be used as background and it needs to be collected only once before starting the few-days step-scan measurements.

D5: Daily procedure**Part I: Setting up experiment and loading sample**

1. Change trigger mode in Opetek control software from internal to external
2. Turn on Flashlamp and Q-switch with internal triggering using remote control box and block the laser beam
3. Use Syringe to load 3 x 2.5 μ l samples in the small sample holders (Sample has been degassed by vacuum to remove the air bubbles).
4. Measure the three samples' VIS absorption spectrum using Cary 300 UV/Vis spectrometer. The variation in the absorption of 3 samples should be within 0.05 OD (less than 10%) from each other.
5. Insert samples into FTIR sample chamber (Bruker IFS66v).
6. Switch triggering mode of flashlamp from internal to external.
7. Turn on the flashlamp and Q-switch using remote control box and block the laser beam.
8. Start purging with higher flow rate 140 (3.62 L/min, glass ball) for ~5 minute and then reduce it to ~80 (2.21 L/min, glass ball).
9. Offset the DC output signal so that the baseline of interferogram is close to 0, make sure the interferogram is properly amplified (within ± 0.75 , ADC counts around 14000 with protein sample and sample signal gain of 32, DC mode).
10. Set the desired temperature. Wait an extra 10 min for equilibration after the sample reached the desired temperature.

Part 2: Experimental measurements

1. Measure IR absorption spectrum. Check IR absorption, Amide I OD. Take special care for the water vapor bands.
2. Make sure the switch is on Rapid-scan
3. Measure rapid scan on each sample for testing following the RapidsScan protocol; 50 averages, test band positions, decay time.
4. Make sure the switch is on Step-scan and change delay generator settings for step-scan
5. Start step motor control for sample exchanger
6. Remove the block of the laser
7. Measure step scan spectra on the three samples.
8. As soon as the scanner finish the last mirror position and Fourier transforming starts (may change the macro program to convert interferograms to single beam later so that we will save

time on data collection), block the laser immediately and disconnect the cable for step motor driver from Delay Generator “B” output.

9. Before repeating step-scan experiments, make sure the sample exchanger is position 1, connect the power cord for step motor driver if it is not connected, remove the block of the laser, connect the cable for step motor driver to the Delay Generator, press the button for “Start Step-scan Measurement” in OPUS window.
10. Repeat two more step-scan measurements
11. Take time-resolved rapid-scan measurement again, check the Amide I amplitude.
12. Measure VIS absorption spectrum of the three samples (5% photo damage is acceptable).

D6: Data analysis using macro programs:

1. Load all the step-scan measurement files in OPUS window.
2. Delete files in C:\Program Files\OPUS\WORK folder
3. Select “Run Macro” in the OPUS-NT “Macro” pull down menu.
4. Open the main macro program for step-scan data analysis “E:\OPUS_macro\macro_NT\STEPSCAN\STP_MAIN.MTX”.
5. Select all the single beam spectra to be averaged and drag them to the blank space labeled “Stepscan(s)” in the popup window.
6. Specify the block number 48 for “Last preflash block”, “First block to extract” to be 49 and “Last block to extract” to be 1498.
7. Select “Calc mOD” and “Average”.
8. Click “Continue”.
9. Specify the data blocks for averaging in the following window according to “step-scan data logarithmic averaging” scheme only in “First block” and “Last block” boxes.
10. Click “Continue”.

Time points after laser flash	Actual time points	First block to extract	Last block to extract	No. of Coaddition	No. of spectra
1 – 8	0 – 8	99	107	1	9
10 – 16	9 – 16	108	115	2	4
20 – 32	18 – 33	117	132	4	4
40 – 70	35 – 74	134	173	10	4
80 – 160	70 – 169	169	268	20	5
200 – 320	180 – 339	279	438	40	4
400 – 700	400 – 899	499	998	100	5

APPENDIX E

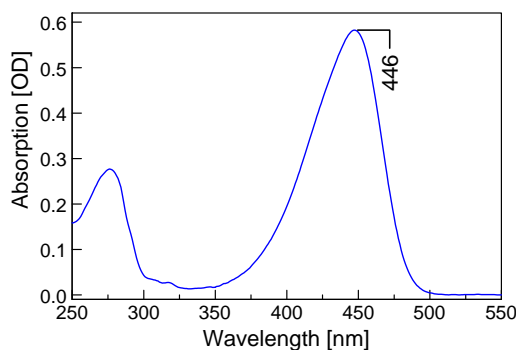
Over-expression and Purification of Photoactive Yellow Protein (PYP)

Major Steps of PYP Over-expression and Purification

- E1. Media preparation
- E2. Over-expression of E. coli
- E3. Reconstitution of apo-PYP to holo PYP
- E4. Protein purification

The purity index (PI) of PYP:

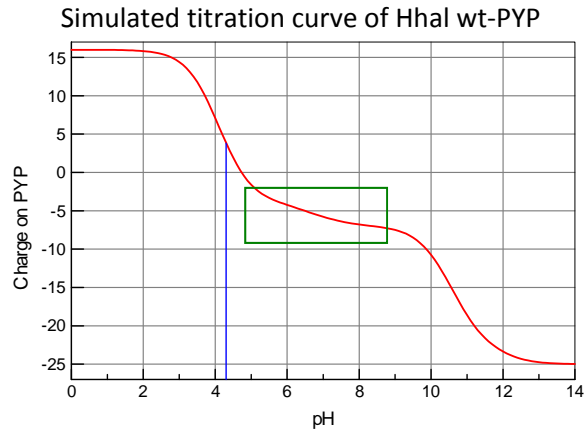
- (1) Definition: $PI = Abs(278nm) / Abs(446nm)$. The 446 nm absorption arises from the PYP chromophore, whereas the 278 nm absorption originates from Trp, Tyr, and Phe.
- (2) The optimal PI of hHal wtPYP is 0.42: we use PYP with $PI \leq 0.43$ for publication and PI of 0.44-48 for testing experiments.



Three basic principles for PYP purification:

- (1) **Solubility & stability:** PYP is highly water soluble and stable. The net charge of PYP is zero at pH 4.3.
- (2) **Ion exchange:** Proteins with different net charges and charge distributions can be separated using ion exchange column. (PYP contains 19 carboxylic groups (12 Asp, 7 Glu), 5 Tyr, 2 Arg, 2 His, 11 Lys residues.) Anion exchange column is used for PYP purification. The preferable pH range for ion exchange of PYP should be 6.5-8.5.

- (3) **Size exclusion:** Proteins can also be separated by size exclusion. For size exclusion, it is critical to start with very concentrated proteins, 1-2 ml only and use a long column (1 meter long). Concentration of protein should be 0.5/2 % of column volume (CV)



To ensure high yield of PYP purification ($\geq 80\%$), make sure that PYP is stable and soluble during each purification step.

E1. Media preparation

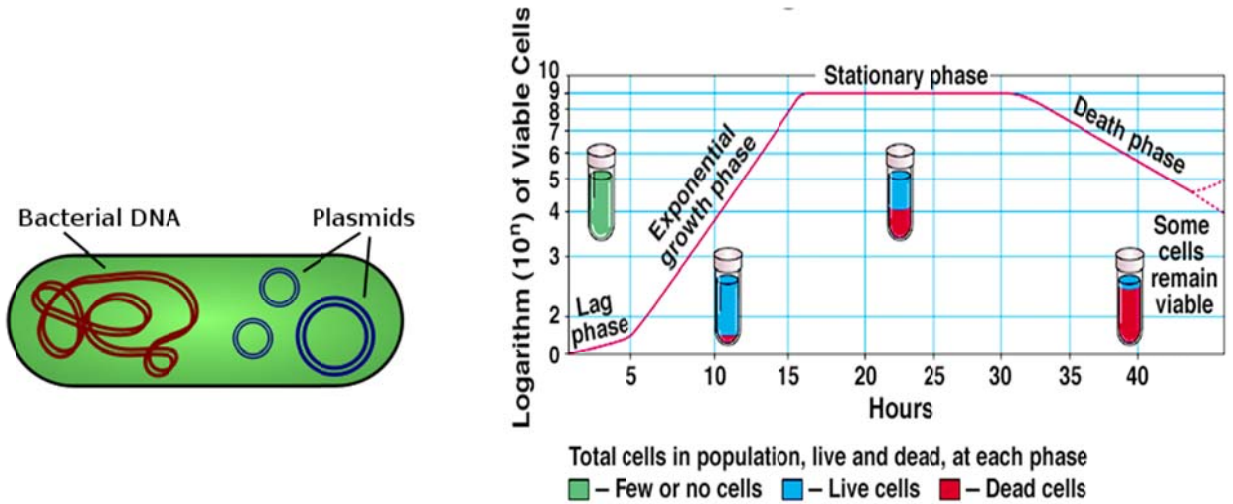
To facilitate oxygen intake to growth medium, large surface/volume ratio is preferred. Thus, we grow 1 L of bacterial culture in 2.8 L flask with wide base.

- 1) Add 25 g LB broth and 1 L of distil deionized water to 2.8 L flask.
- 2) Add 50 μ l antifoam and dissolve the LB broth in water.
- 3) Transfer 50 ml of culture to 250 ml flask.
- 4) Cover each flask with aluminum foil and stick autoclave tape.
- 5) Autoclave culture at 121 $^{\circ}$ C on liquid P13 cycle for 30 minutes.
- 6) Cool down culture to room temperature after autoclaving and add 1 ml (50 mg/ml) ampicillin.



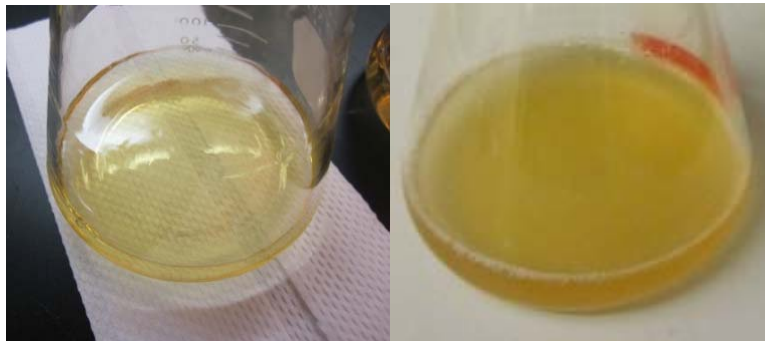
E2. Over-expression of PYP

PYP which is over expressed is originally from *Halorhodospira halophilla* (*Hhal*) bacterium. However the *Hhal* bacteria growth is slower. *E.Coli* bacterium PYP gene is introduced in *E.Coli*'s circular DNA (PETBL2) which over-expresses PYP. It takes about 20 minutes to reproduce one generation *E.Coli* bacteria in LB broth medium.



E2.1 Over-expression

- 1) Inoculate 50 μ l of bacterial stock (stored at -80°C) to the 50 ml culture. Work near flame.
- 2) Place the culture in incubator (Innova, 4230).
- 3) Incubate culture \sim 9 hrs (overnight) at 210 rpm, 37°C .
- 4) Monitor OD at 600 nm. When OD is reached at 1, transfer the bacterial culture to 1 L culture.
- 5) Grow 1 L culture for 4 hours until OD at 600 nm reaches to 1
- 6) Add 1 ml 1M IPTG for induction of PYP.
- 7) Incubate it further for 6 hours at 210 rpm and 37°C .



E2.2 Harvest cell

Equipments

- 1) SLC-6000 Rotor
- 2) 1L plastic bottles
- 3) Centrifuge: Sorval Evolution RC



Procedure

- 1) Pre cool the SLC-6000 rotor to 4 °C.
- 2) Transfer the 0.5 L culture to two 1 L bottles and balance them
- 3) Centrifuge bottles at 4000 rpm (3510 g) at 4 °C for 10 minutes.
- 4) Dispose the supernatant and collect the cell pallet.
- 5) Transfer the cell pallets to 250 ml bottle and resuspend the cells in 500 µl 50 mM Tris buffer pH 7.50

E2.3 Cell lysis

- 1) Add 75 ml of 8 M urea to cell pallets.
- 2) Stir the solution with magnetic stirrer for 30 minutes at room temperature
- 3) Add 75 ml of 50 mM Tris buffer (pH=7.50) to dilute to 4 M urea.



Preparation of pCA anhydride

Add 300 mg pCA, 500 mg DCC to 10 ml DMF in tube, vortex, Put the tubes in boiling water for 15 min until the solution turned to yellow. Put the tube in -80 degree in 30 min. Take out the tube, spin down the precipitant and keep the supernatant for use.

E3. Reconstitution of apo-PYP to holo-PYP

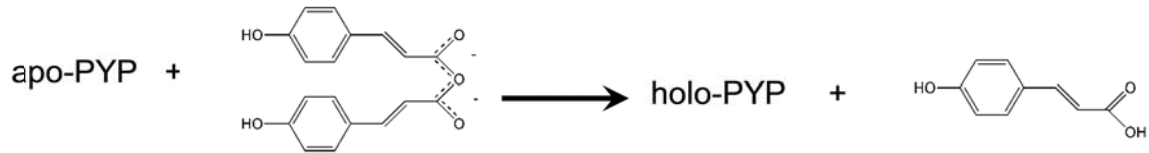
E3.1 Addition of pCA anhydride

- 1) Add 400 µl of pCA anhydride to 4 M urea solution
- 2) Keep the bottle on ice and in dark.

- 3) Stir the solution in dark for 30 minutes

apo-PYP: PYP without pCA. Partially unfolded

holo-PYP: pCA linked to Cys69 in PYP, folded and active



E3.2 Precipitation of extra pCA anhydride and cell membranes

- 1) Distribute the solution in 4 pairs of centrifuge tubes.
- 2) Balance each pair with 0.01 g accuracy.
- 3) Place the balanced centrifuge tubes in 70 Ti, T 395 rotor.
- 4) Run ultrahigh centrifuge (Blackman Coulter Optima L-90) at 25,000 rpm (46,000 g)
- 5) Collect the supernatant and discard precipitant.

E4. Protein Purification

E4.1 Dialysis

- 1) Cut two 30 cm dialysis tubing (Spectrapore 5.1 ml/cm, MWCO 6-8000)
- 2) Put tubing into 100 ml beaker and add DDW until brim
- 3) Microwave for 2 minutes
- 4) Remove the tubing from hot water and rinse it with cold DDW.
- 5) Tie one end of the tubing and transfer the 75 ml PYP solution to each tubing using long neck funnel.
- 6) Suspend the PYP tubing in 3 L bucket filled with 3 L 15 mM Tris pH 8.50 buffer
- 7) Put the bucket on magnetic stirrer and stir it overnight at 4 °C.
- 8) Next morning change the dialysis buffer and stir it for another 6 hours.
- 9) Collect the PYP solution in bottle and keep it on ice.

D4.2 First course purification

Goal : To remove the chemicals (urea, pCA anhydride) and unwanted proteins.

Equipments/ chemicals

- 1) Column C25/40
- 2) Resin DEAE sepharose Fast Flow
- 3) 20 mM Tris buffer
- 4) 150 mM NaCl buffer

Procedure for running first Anion exchange column

- 1) Equilibrate column using 20 mM Tris buffer pH 8.50 (2CV)
- 2) Load PYP with 20 cm/hr flow rate.
- 3) After loading PYP solution wash column with 1 CV of 20 mM Tris pH 8.50 buffer
- 4) Elute column with 150 mM NaCl in 20 mM Tris buffer pH 8.50.
- 5) Collect the PYP in ~ 15 fractions. In the beginning and ending collect 1.0 ml fraction, while in middle 2.0 ml fraction.
- 6) Measure Purity Index (PI) using Cary 300
- 7) Combine the fractions with PI less than 1.00 and perform dialysis against 20 mM Tris pH 8.50 buffer overnight to reduce the concentration of NaCl less than 5 mM.

E4.3 Regeneration of Column

- 1) Wash column with 2 M NaCl, 2 CV with flow rate
- 2) Wash column with 1 M NaOH, 4 CV with flow rate
- 3) Wash column with 2 M NaCl, 2 CV with flow rate
- 4) Wash column with DDW, 2 CV with flow rate
- 5) Wash column with 20 mM Tris pH 8.50 buffer 4 CV with flow rate



E5. Second Fine purification

Goal : 90 % PYP can be purified with PI~0.450-0.500

Equipments/Chemicals

- 1) C16/20 Column 12 ml , 6 cm bed height
- 2) Q-sepharose Fast Flow
- 3) Gradient maker
- 4) Peristaltic pump
- 5) 20 mM Tris buffer pH 8.50

Procedure

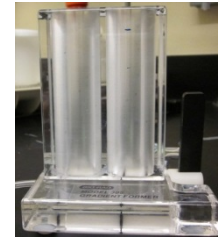
- 1) Load PYP with 20 cm/hr flow rate. After loading, there is a uniform yellow band for the good column.
- 2) Wash with 1 CV buffer to make all the protein bind to the gel.
- 3) Apply gradient maker, 50 mM NaCl (55 ml) to 400 mM NaCl (55 ml), protein eluted at 130 mM NaCl.
- 4) Collect PYP with 1ml fractions in the beginning and ending 2 tubes, 2ml in the middle.
- 5) Measure Purity index of proteins.



- 6) Combine the fractions with $PI < 0.500$, dialysis against 20 mM tris buffer $pH=6.9$ to make sure the salt concentration smaller than 5.0 mM.
- 7) Regenerate with 1M NaCl (2CV), 1M NaOH(4CV), 1M NaCl (2CV), DDW (4CV), $pH8.5$ 20mM Tris buffer (4CV)



Comment: This step is fine purification; the PI of protein can be improved a lot. In the collecting process, the small fractions in the beginning and the end can avoid bad proteins to mix with good protein to improve the recovery of the good protein. The air bubbles will damage the column, remove the air bubbles in the pumps and tubes.



E6. Third Fine Purification

Goal: 60 % wt PYP can be purified with $PI \leq 0.430$, Mutants PYP with $PI \leq 0.400$

Equipment/ Chemicals

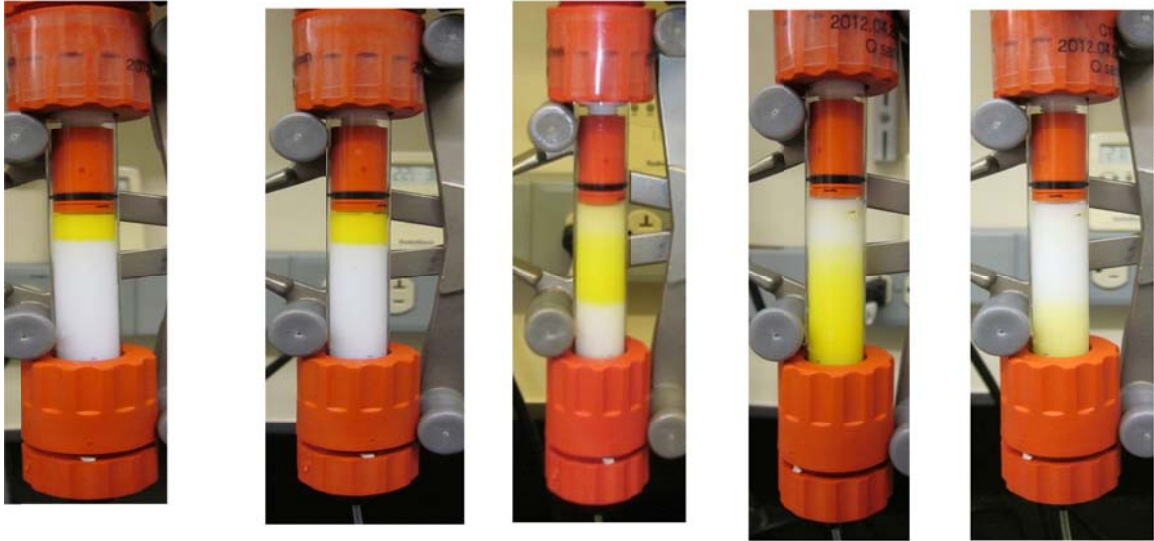
- 1) C10/10, 5 ml, 6 cm bed height
- 2) Q-sepharose high performance
- 3) Gradient maker
- 4) Peristaltic pump
- 5) 20 mM Bis-Tris $pH 6.90$ buffer
- 6) 300 mM NaCl in 20 mM Bis-Tris $pH 6.90$

Elution: Gradient maker, 80 mM NaCl buffer (55 ml) in mixing chamber, 300 mM NaCl buffer (55 ml) in reservoir chamber. The volume can be changed depending on the amount of protein.

Procedure

- 1) Load PYP with 15cm/hr flow rate. After loading, there is a uniform yellow band for the good column.
- 2) Wash with 1 CV buffer to make all the protein bind to the gel.
- 3) Apply gradient maker, 80 mM NaCl (55 ml) to 300 mM NaCl (55 ml) for 30 mg proteins, protein eluted at about 100 mM NaCl.
- 4) Collect PYP with 0.20 ml fractions in the beginning and ending 2 tubes, 0.50ml in the middle.
- 5) Measure Purity index of proteins.
- 6) Distribute 2mg protein per tube, store in -80 degree and update the protein bank document.
- 7) Regenerate 1M NaCl (4CV), DDW (4CV), $pH 6.9$ 20 mM Tris buffer (4CV)

Comment: The uniform band is important to get proteins with good PI. Also collecting small fractions to separate PYP with bad PI is important to get good recovery of the proteins. The air bubbles will damage the column, remove the air bubbles in the pumps and tubes.



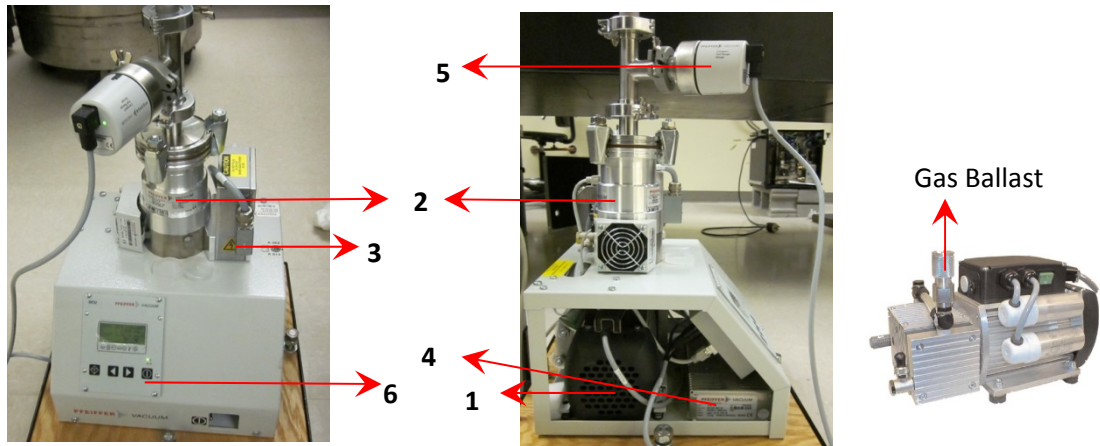
Elution of PYP: Above picture shows the elution of PYP during final purification steps. In first picture PYP bind to media and forms a uniform layer. As The NaCl concentration increases the PYP band spreads and starts elution process.

APPENDIX F

Operation Procedure for Pfeiffer Turbo Pump

F1: Components

- 1) Rough Pump (Diaphragm Vacuum Pump Model # MVP 015-2)
- 2) Turbomolecular Drag Pump (Model # TMH 071P)
- 3) TC 600 electronic Drive unit
- 4) Power supply: TPS 100
- 5) Vacuum Gauge:
- 6) Digital Controlled Unit (DCU)



F2: Procedure to changing parameter value

Select parameter from DCU unit.

- a) Press forward (▶) and backward (◀) buttons on DCU simultaneously
- b) Arrow should appear, change the settings to desired value by pressing forward or backward button.
- c) Press forward and backward buttons on DCU simultaneously until arrow disappears to set the desired value

F3: Procedure to turn on the turbomolecular pump:

- 1) Turn on the power supply of rough pump.
- 2) Locate the gas ballast of rough pump and open the gas ballast by pulling down the sleeve.
- 3) Turn on DCU by turning on TPS 100 unit.
- 4) Wait 1-2 minutes until self-testing is finished. If no error message shows then the system is ready to operate.

Make sure parameters P010 and P023 are off at this time.
Check parameter list at the end of the protocol.

Caution: If Turbomolecular pump is connected to vacuum chamber make sure that valve to vacuum chamber is open and venting valve is closed.

- 5) Turn on the rough pump. Select parameter [P:010] on DCU unit.

Turning on procedure for rough pump

- a) Press forward (▶) and backward (◀) buttons on DCU simultaneously
 - b) Arrow should appear, change the settings to “ON” by pressing forward button.
 - c) Press forward and backward buttons on DCU simultaneously until arrow disappears to turn on rough pump.
- 6) Monitor the vacuum pressure reading on DCU.

Note: Wait for 10-15 minutes until pressure reaches below 10 mbar. This is crucial step before turning on turbomolecular pump.

- 7) Turn on Turbomolecular pump. Select parameter [P:023] on DCU unit.

Turning on procedure for Turbomolecular pump

- a) Press forward (▶) and backward (◀) buttons on DCU simultaneously
- b) Arrow should appear, change the settings to “ON” by pressing forward button.
- c) Press forward and backward buttons on DCU simultaneously until arrow disappears to turn on turbomolecular pump

- 8) Go to Parameter [P:309], monitor the rotation speed of turbo pump, wait (~ 5 minutes) until the frequency reaches setting value as Parameter [P: 308]
Current settings for P:308, 1500 Hz.

- 9) Monitor vacuum pressure reading on DCU for first 15 minutes, pressure should fall down fast. As pressure reading reaches at 10^{-2} mbar, monitor pressure every 5 minutes.

F4: Procedure to turn off the turbomolecular pump:

- 1) Close valve between vacuum pump and the chamber so that vacuum is restored in vacuum chamber.
- 2) Turn off turbo pump. Select Parameter [P:023] on DCU unit

Turning off procedure for Turbomolecular pump

- a) Press forward (▶) and backward (◀) buttons on DCU simultaneously
- b) Arrow should appear, change the settings to “OFF” by pressing backward button.
- c) Press forward and backward buttons on DCU simultaneously until arrow disappears to turn off turbomolecular pump

3) Select Parameter [P:309], monitor the rotation speed of turbo pump, wait (~5 minutes) until the frequency reaches 0.

4) Select Parameter [P:012], make sure value is “on” (this enables venting function when pump is off)

5) Select Parameter [P:030], select venting mode: “0” for automatic venting (venting takes place when turbo pump frequency drop to certain level after being turned off, set at Parameter [P:720] and will continue for a period of time set at Parameter [P:721]).

Current settings for parameter [P:012] “ON”

Current settings for parameter [P:030] “0” (numerical zero)

Current settings for parameter [P:720] “50” (50% of final rotation speed of turbomolecular pump).

Current settings for parameter [P:721] “3600 s” maximum venting time in seconds.

6) Turn off the rough pump. Select Parameter [P:010] on DCU unit

F5: Turning off procedure for rough pump

- a) Press forward (▶) and backward (◀) buttons on DCU simultaneously
- b) Arrow should appear, change the settings to “OFF” by pressing backward button.
- c) Press forward and backward buttons on DCU simultaneously until arrow disappears to turn off rough pump.

7) After the rough pump is turned off, the pump system will start to vent according to the settings at step 5. Wait until the pressure gauge reading reaches >2 mbar. (~ 15-20 minutes)

8) Vent the rough pump by opening the valve between vacuum pump and vented chamber.

9) Close the gas ballast of rough pump.

F6: Setting Commands (readable and writable)

#	Display	Description	min	max	factory settings	TC 600
001	Heating	Pre-selection heating ON/OFF	OFF	ON	OFF	•
002	Standby	Standby ON/OFF	OFF	ON	OFF	•
004	RUTime ctr	Run-up time monitoring ON/OFF	OFF	ON	ON	•
009	Error ackn	Error acknowledgement			-	•
010	Pump stat	Pumping station ON/OFF	OFF	ON	ON(*)	•
012	Vent enab	Venting enable ON/OFF	OFF	ON	ON(*)	•
013	Brake enab	Pre selection brake ON/OFF	OFF	ON	OFF	•
023	Motor	Motor Turbopump ON/OFF	OFF	ON	ON(*)	•
024	Conf. Out1	Configuration output KI: 0=switchpoint attained; 1=TMS	0	2	0	•
025	OpMode	Operations mode backing pump, 0=non-stop; 1=intermittent;	0	2	0	•
026	OpMode	Operations mode TMP 0=final rot. speed op.; 1=rot. speed	0	1	0(*)	•
027	Gas mode	Gas mode 0=heavy inert gases; 1=other gases	0	1	0	•
028	Opmode	Remote operations mode 0=standard, 1=Remote priority, 2	0	2	0	•
029	OpMode	Drive unit operations mode OFF=max., ON=reduced power	OFF	ON	OFF	•
030	Vent mode	Venting mode, 0=controlled venting; 1=no venting;	0	2	0	•
032	Conf Out4	Configuration heating output; 0=Heat/TMS operations;	0	1	0	•
035	Conf I/O1	Configuration accessories ON/Output 1 (see chapter 3.19)	0	3	0	-

036	Conf I/O2	Configuration accessories ON/Output 2 (see chapter 3.19)	0	3	1	-
055	Conf AO1	Configuration Analog Output 1 0=Rot Speed; 1=Power;	0	2	0	•

#	Display	Description	min	max	factory settings	TC 60
300		Unit remote controlled, not choosable by			-	•
301	Oil defec	Oil deficiency turbopump	-	-	-	•
302		Rotation switch point attained			-	•
303	Error code	Actual error code „no Err“, „Errxxx“ or „Wrnxxx“			-	•
304		Over temperature Electronic drive unit			-	•
305		Over temperature turbopump			-	•
306		Set rotation speed attained			-	•
307		Turbopump accelerates			-	•
308	Set rotspd	Set rotation speed TMP in Hz	0	2000	-	•
309	Act rotspd	Actual rotation speed TMP in Hz	0	2000	-	•
310	TMP I-Mot	Motor current TMP in A	0	15.0	-	•
311	TMP Op hrs	Operating hours TMP in h	0	99999	-	•
312	Drv Softw	Software version electronic drive unit			-	•
313	TMP	Motor voltage TMP in V	0	200.0	-	•
314	Drv Op hrs	Operating hours electronic drive unit	0	99999	-	•
315	TMP	Final rotation speed TMP in Hz	0	2000	-	•
316	TMP	Motor power TMP in W	0	1000	-	•
319	Cycl count	Cycle counter	0	99999	-	•
331	TMS	Heating TMS, actual value in °C	5	200	-	•
333	TMS	TMS regulator engaged ON/OFF	OFF	ON	-	•
334	TMS	Maximum TMS temperature occurred in °C	5	200	-	•
335	Heat type	Heating type 0=conventional heating, 1=TMS	0	1	-	•
340	Pressure	Actual pressure value in mbar ³⁾	1E-10	1E3	-	-
349	Drv Name	Unit type electronic drive unit			-	•
350	Ctrl Name	Unit type operating and display unit ³⁾			-	-
351	Ctrl Softw	Software version Display and Control Unit DCU ³⁾			-	-
360	Past Err1	Error storage, Position 1 (last error occuring)			-	•
361	Past Err2	Error storage, Position 2			-	•
362	Past Err3	Error storage, Position 3			-	•
363	Past Err4	Error storage, Position 4			-	•
364	Past Err5	Error storage, Position 5			-	•
365	Past Err6	Error storage, Position 6			-	•
366	Past Err7	Error storage, Position 7			-	•
367	Past Err8	Error storage, Position 8			-	•
368	Past Err9	Error storage, Position 9			-	•
369	Past Err10	Error storage, Position 10			-	•

Set values (readable and writable)

#	Display	Description	min	max	factory settings	TC 600
700	TMP	maximum run-up time in mins	1	120	154) / 85)	•
701	Switch pnt	Rotation speed switchpoint in %	50	97	80	•
704	TMSheats	TMS heating temperature set value in °C	30	90	40	•
707	TMProt set	Rotation speed set value in rotation speed setting operations	20.0	100.0	50.0(*)	•
708	DrvPwr set	Drive power set in %	10	100	80	•
710	BKP Poff	Pmin for backing-pump interval operations W	0	1000	0	•
711	BKP Pon	Pmax for backing-pump interval operations W	0	1000	0	•
717	Stbyrotset	Rotation speed set value at standby operations (%)	20	100	66	•
719	Switch pnt2	Rotation speed switchpoint2 in %	5	97	20	•
720	Vent frequ	Venting frequency as a % of the final rotation speed of the	40	98	50	•
721	Vent time	Venting time in s	6	3600	3600	•
738	Gaugetype	Vacuum pressure gauge type ³⁾			-	-
794	Param. set	Parameter set 0= basic parameter set; 1= extended parameter	0	1	0	-
795	ServiceLin	insert service line			795	-
797	Address	Unit address	1	255	1	•

F7. Parameter Overview, numerical, DCU5

Run-up time and rotation speed switchpoint

#	Display	Name, Description	min	max	factory setting
004	RUtime ctr	Run-up time monitoring, 0=OFF; 1=ON	OFF	ON	ON
700	TMP	maximum run-up time in mins	1	120	15/8
701	Switch pnt	Rotation speed switchpoint in %	50	97	80
719	Switch pnt2	Rotation speed switchpoint 2 in %	5	97	20

General operating information

#	Display	Name, Description	min	max	factory setting
315	TMP rnspsd	Final rotation speed TMP in Hz	0	2000	-
310	TMP I-Mot	Motor current TMP in A	0	15.0	-
313	TMP	Motor voltage TMP in V	0	200.0	-
316	TMP power	Motor power TMP in W	0	1000	-
311	TMP Op hrs	Operating hours TMP in h	0	99999	-

Operating adjustment turbopump

#	Display	Name, Description	min	max	factory setting
002	Standby	Standby ON/OFF	OFF	ON	OFF(*)
010	Pump stat	Pumping station ON/OFF	OFF	ON	-
023*	Motor TMP	Motor Turbopump ON/OFF	OFF	ON	-
026	OpMode	Operations mode TMP 0=final rot. speed oper., 1=rot. speed	0	1	0
027	gas mode	Gas mode 0=heavy inert gases; 1=other gases	0	1	0
029	OpMode	Operating mode drive unit OFF=max., ON=reduced power	OFF	ON	OFF
308	Set rotspd	Set rotation speed TMP in Hz	0	2000	-
309	Act rotspd	Actual rotation speed TMP in Hz	0	2000	-
717	Stbyrotset	Rotation speed set value at standby operations (%)	20	100	66
707	TMProt set	Rotation speed set value in rotation speed setting operations	20.0	100.0	50.0(*)

Vent valve controlling turbopump

#	Display	Name, Description	min	max	factory settings
012	Vent enab	Venting enable ON/OFF	OFF	ON	ON
030	Vent mode	Venting mode 0=automatic venting; 1=do not vent;	0	2	0(*)
720	Vent frequ	Venting frequency as a % of the final rotation speed of the	40	98	50
721	Vent time	Venting time in s	6	3600	3600

Pumping station controlling

#	Display	Name, Description	min	max	factory setting
025	Opmode	Operations mode backing pump, 0=non-stop; 1=intermittent;	0	2	0
035**	Conf I/O1	Configuration Accessories ON/Output 1	0	3	0
036**	Conf I/O2	Configuration Accessories ON/Output 2	0	3	1
340	Pressure	Actual pressure value in mbar	1E-10	1E3	-
738	Gaugetype	Vacuum pressure gauge type			-
710	BKP Poff	Pmin for backing-pump interval operations W	0	1000	0
711	BKP Pon	Pmax for backing-pump interval operations W	0	1000	0

Others

#	Display	Name, Description	min	max	factory setting
013*	Brake enab	Preselection Brake ON/OFF	OFF	ON	OFF
024*	Conf. Out1	Configuration output K1 0=switchpoint attained; 1=IMS	0	1	0
028	OpMode	Remote operations mode 0=standard, 1=Remote priority, 2	0	2	0
055	Conf AO1	Configuration Analogue Output 1	0	2	0
303	Error code	Actual error code „no Err“, „Errxxx“ oder „Wrnxxx“			-
312	Drv Softw	Software version electronic drive unit			-
351	Ctrl Softw	Software version Display and Control Unit			-
794	Param. set	Parameter set 0=basic parameter set; 1=extended parameter	0	1	0
795	Servicelin	insert serviceline			795
797	Address	Unit address	1	255	1

Table of failures

#	Display	Name, Description	min	max	factory setting
360	Past Err1	Error storage, Position 1 (last error occurring)			-
361	Past Err2	Error storage, Position 2			-
362	Past Err3	Error storage, Position 3			-
363	Past Err4	Error storage, Position 4			-
364	Past Err5	Error storage, Position 5			-
365	Past Err6	Error storage, Position 6			-
366	Past Err7	Error storage, Position 7			-
367	Past Err8	Error storage, Position 8			-
368	Past Err9	Error storage, Position 9			-
369	Past Err10	Error storage, Position 10			-

* only for TC 600/750

** only for TC 100 / TCK 100

(*) Function can only be affected via remote plug (X16)

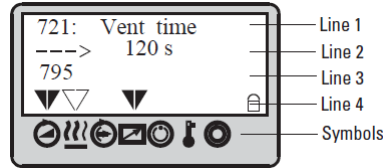
- Function can be called by RS 485

F8: Error codes

Code	Description	Occurs at	Error Elimination Action
E001	TMP excess rotation speed	Operating	- Inform PFEIFFER VACUUM Service. - If operations with mains voltage 90 - 132 VAC, check
E002	Power pack unit error	Self-test/	- Check power pack output voltage. - Check settings [P:013]
E006	Start-up time error When the start-up phase is completed, the rotation speed of the pump drops below the rotation speed of the pump.	Self-test/ Operating	- Set correct start-up time. - Open vacuum valve. - Reduce fore-vacuum pressure
E007	Operating fluid deficiency	Self-test/	- Check oil level. - Request status of the oil sensor via [P:301]
E008	Connection TC and pump	Self-test/	- Check connection TC and pump.
E014	The heating type identified in the self test has been changed by pulling the plug or by an error.	Operating	- Change configuration of heating or cooling unit.
E015	Error in the TC controller	Self-test/	- Reset the controller with mains ON/OFF with the pump at standstill (f=0 Hz)
E021	Incorrect pump identification resistance	Self-test/	- Inform PFEIFFER VACUUM Service.
E025	Error in the temperature monitoring TC	Self-test/	- Reset the controller with mains ON/OFF with the pump at standstill (f=0 Hz)
E026	Error of the temperature sensor inside the TC	Self-test/	- Reset the controller with mains ON/OFF with the pump at standstill (f=0 Hz)
E037	Error in the motor stages or control	Self-test/	- Possibly Inform PFEIFFER VACUUM Service.
E698	TC does not respond	Self-test/	- Check connection DCU - TC. - Change the DCU
E913	Error in the self test or when the pump	Self-test	- Error resets itself 5 times. Then switching off via «E006» - Possibly set the op. mode backing pump [P:025] up to "2"

F9: Symbols on DCU

Key	Explanation
	Reset (error acknowledgement). Acknowledges errors (red LED illuminates)
	Scroll back parameters Scrolls back a parameter
	Reduce a value (with arrow "←→")
	Scroll parameters forwards Scrolls forward a parameter
	Increases a value (with arrow "→←")
	Alters a value (⇒data editing mode) Access to a displayed value, if possible (arrow "→←" appears)
simultaneously	Confirm a value (⇒param. selection mode) Takes over an altered value (The arrow "→←" disappears)
	Pumping Station ON/OFF Switches the pumping station ON and OFF, equivalent to parameter 010: "Pump stat."



	Symbol	Arrow	Explanation
	Pump accelerates	–	No
		▼	yes
	Pre-selection heating	–	No pre-selection
		▽	Pre-selection heating, but switchpoint not attained
	Stand-by	–	Off
		▼	On
	Unit under remote control	–	No
		▼	Yes
	Switchpoint attained	–	No
		▼	Yes
	Excess-temperature	–	No excess temperatures
		▽	Excess temperature pump
		▼	Excess temperature pump elektronik
		▼	Excess temperature pump and pump elektronik
	Final rotation speed attained	–	No
		▼	Yes

Line 1: Number and name of the selected parameter

Line 2: Relating value. If an arrow (--->) is displayed, the displayed value can be altered

Line 3: Two functions

Function 1: Messages relating to operations and operating are displayed

Function 2: An optional second parameter in the form of >>Parameter number<< : >>value<<

is displayed. The function of this line enables setting via parameter [P:795] >>Servicelin<< at

line 1 . With >>Servicelin<< all parameters can be displayed. Error messages are displayed

independent of the selected function.

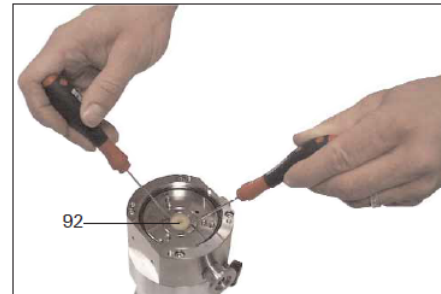
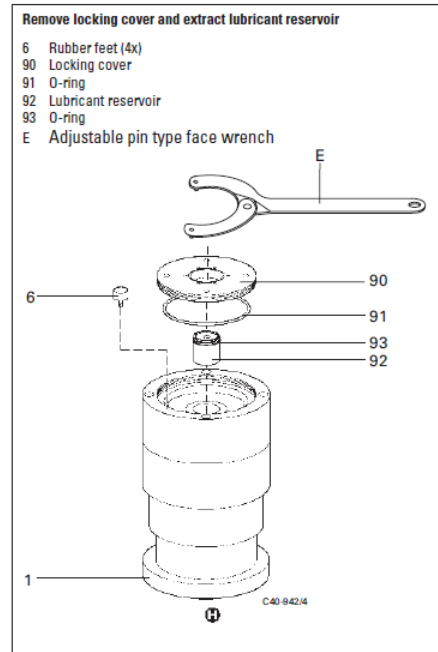
Line 4: Arrows which points to the underlying symbol. This restores the unit status.

F10: Maintenance

F10.1. Replacing the Lubricant Reservoir Recommended at least once a year

Following is the procedure for replacing Lubricant Reservoir

- 1) Turn off turbopump and vent to atmospheric pressure (~1 bar).
- 2) If necessary, remove turbopump from the system
- 3) Unscrew rubber feet (6) as illustrated in diagram, from the underside of the pump
- 4) Remove locking cover (90) from the underside of the pump with help of adjustable pin type face wrench (E)
- 5) Lever out lubricant reservoir (92) with help the help of two screwdrivers.
- 6) Clean off the dirt on pump and locking cover with soft tissue or fluff-free cloth
- 7) Insert new lubricant reservoir (92) up to the O-ring (93) in the pump.
- 8) Screw in locking cover (90) with O-ring (91).
Lubricant Reservoir is brought into the correct axial position with the locking cover.
- 9) Screw rubber feet (6) back in.



F10.2. Replacing the bearings Recommended once in 3 years

Turbopump has to send to company and company will replace the bearings. The cost of replacing bearings in 2012 was \$800

Company Contact information
Pfeiffer Vacuum, Inc.
24 Trafalgar Square
Nashua, NH 03063-1988, USA
Phone: (603) 578-6500

F11: Troubleshoot

Problem	Possible Causes	Remedy
Pump doesn't start; none of the integrated LEDs glow on the TC600	<ul style="list-style-type: none"> • Power supply interrupted • Incorrect operations voltage supplied • pins 1-3 & -14 on the remote plug not connected • No supply of operations voltage • Defect TC600 • Reduction in the voltage in the cable 	<ul style="list-style-type: none"> • Check fuse in the power pack unit • check plug contacts on the mains power unit • Check power unit feeder line • Check voltage on power unit (24V DC) at connection X2 • Supply correct operations voltage • Connect pins 1-3 & 1-4 on the remote plug • Check plug contacts on power supply • Inform Pfeiffer vacuum Service of need for repair • Use suitable cable
Pump doesn't attain nominal rotational speed within the start run-up time pump cuts out during operation	<ul style="list-style-type: none"> • Fore vacuum pressure too high • Leak or too much gas • Rotor sluggish caused by defective bearing • TC run-up time too short 	<ul style="list-style-type: none"> • Check backing pump function • check seals • Seek leak and repair • Reduce supply of process gas • Check bearing (noises), Inform Pfeiffer Vacuum service • Set longer start-up time with DCU or PC
pump doesn't attain final pressure	<ul style="list-style-type: none"> • Pump dirty • Leak in vacuum chamber, lines or pump 	<ul style="list-style-type: none"> • Break out pump • If seriously contaminated: Request Pfeiffer Vacuum service to clean • Seek leak starting with vacuum chamber • Repair leak
Unusual operating noises	<ul style="list-style-type: none"> • Bearing damaged • Rotor damages • Splinter shield (if fitted) not seals firmly 	<ul style="list-style-type: none"> • Inform Pfeiffer vacuum Service of need for repair • Inform Pfeiffer vacuum Service of need for repair • Check seat of splinter shield (for detail information see manual of TMH 071 P Section 3.2)

Red LED on TC 600 glows	<ul style="list-style-type: none"> • Collective malfunction 	<ul style="list-style-type: none"> • Rest via mains OFF/ON or remote pin 5 • Different malfunction display with the DCU possible
Red LED on TC 600 flashes	<ul style="list-style-type: none"> • Warning through -Mains power failure -Supply voltage short circuit to earth 	<ul style="list-style-type: none"> • Different warning message with DCU possible • Check power unit voltage • Check power unit mains connection • Check power unit voltage for short circuit to earth

F12: Technical information for Turbomolecular TMH- 071-P pump

Feature	TMH-071-P
Connection nominal diameter	63 ISO-K (2.5' O.D.)
Nominal rotation speed (1/min)	90,000
Final pressure backing pump (mbar)	<10
Maximum fore vacuum pressure for (mbar)	
N ₂	18
He	17
H ₂	8
Final pressure with diaphragm pumps (mbar)	<1·10 ⁻⁷
Lubricant	TL 011

*For more technical data refer manual for turbomolecular TMH-071-P pump section 9.

APPENDIX G

List of PYPs with accession number and amino acid sequence

Bacteria	Accession Number	Amino Acid Sequence
<i>Halorhodospira halophila</i> BN9626 PYP1	YP_001003384 125aa	MEHVAFGSEDIENLAKMDDGQLDGLAFGAIQLDGDGNILQYNAAE ¹ GDITGRDPKQVIGKNFFKDVAPC TDSPEFYGKFKEGVASGNLNTMFEYTFDYQMTPTKVKVHMKKALSGDSYWVFKRV
<i>Idiomarina loihiensis</i> L2TR	YP_156766 125 aa	MEIVQFGSDDIENTLSKMSDDKLNDFAGAIQLDASGKIIQYNAAE ¹ GDITGRDPGAVVGKNFFNEVAPC TNSPEFKGRFDEGVKNGNLNTMFEYVFDYEMQPTKVKVHMKKALTDGTYWVFKRL
<i>Stigmatella aurantiaca</i> DW4/3-1 PYP1	ZP_01461006 135 aa (34.1%)	MRHGILEAESLTEDRLGQLSPEEFDALPFGAIKLDAGEGRVLIYNAAE ¹ SAFSRRKPVSVLGRRFFEEVAPC TNVASFRGRFDLTVRERGHGTESDFQFRFRWGTRNVRIRLMVLGDGSRWVFTAVLTALIPLEG
<i>Rhodobacter sphaeroides</i> KD131	YP_002520069 124 aa	MEIIPFGSADLNILAREPQRAEYLPFGAVLLDRSGTILKYNRAE ¹ GGIANRNPADVIGKNFFNEIAPC AKGKRFHGEFLRFHQGTQVNVMFYKFAKGANVGVKIHMKSPDGGQSCWLVFKRV
<i>Rheinheimera</i> sp. A13L	ZP_08571126 127 aa	MTLETVRFGGDDIENSLAKMDDKALDKLAFGAIQLDNGKIIHYNAAE ¹ GTITGRDPKTVIGKNFFTDVAPC TQSKFQGRFKEGVQKGLNLTMFEYVFDYQMKPTKVKVHMKKAMTGDSTFWVFKRL
<i>Chromatium salexigen</i>	AAB3638 125 aa	MDIVHFGSDDIENSLANMSDQDLQLAFGAIQLDASGKVLQYNAAE ¹ GGITGRDPKSVIGKNFFEDVAPC TKSQEFQGRFKEGVANGNLATMFEYVFDYQMKPTKVKVHMKKALVDDSYWVFKRL
<i>Halomonas</i> sp. GFAJ-1	ZP_09290099 127 aa	MAMETVRFGGDDIENALANMDDKKLDTLAFGAIQLDANGKIIQYNAAE ¹ GGITGRDPKSVIGKNFFTDVAPC TQSKFQGRFKEGVANGNLATMFEYVFDYQMTPTKVKVHMKKALSGDTFWVFKRL
<i>Halomonas boliviensis</i> LC1	ZP_09187052 127 aa	MAMETVRFGGDDIENSLAKMDDKKLDELAFGAIQLDANGKIIQYNAAE ¹ GGITGRDPKSVIGKNFFTEVAPC TQSKFQGRFKEGVSSGELNLTMFEYVFDYQMTPTKVKVHMKKALSGDTFWVFKRL
<i>Thiorhodospira sibirica</i> ATCC 700588	ZP_08923137 125 aa	MELLSFGADNIENSLAKMSKGLNKLAFGAIQLNAQGGKILQYNAAE ¹ GDITGRKPTEVIGKNFFLEVAPC TNRTEFKGRFDQGIKSGNLNTMFEYTFDYEMKPTKVKVHMKKALVDDTYWVFKRV
<i>Roseomonas cervicalis</i> ATCC 49957	ZP_06896627 124 aa	MELLKFGTDD IDNLVARDP S RLDRLPFGAV LLDRTGRVTK YNAGE ¹ VAISG RTADQVLGKN FFNDIAPC TK GHQFMGRFNQ ALAQGSINTM FEYAFDYKMK PAKVRVHMKS VSIDQGIWVFIKRL
<i>Rhodobacter capsulatus</i> SB 1003	YP_003577233 124 aa	MEIIPFGTND IDNILAREPA RAESLPFGAV LLDRMGRIAK YNKA ¹ EGLIAG RDPSTVIGRD FFNEIAPC AK GKRFGHEFLK FNRTGQANVM LDYKFNYKGA EVAVKIHLKS QPDGQFCWLVFKRA
<i>Sphingomonas</i> sp. PAMC 26617	ZP_10425641 124 aa	MEMIKFGSDD LENRLADDP S RAELLPFGAI MVDQGGKVL R FNH ¹ VESGISG RRAEDVVGKN FNDIAPC AK GQVFYNHFFK AVGDGQVNTM FDYHFDYKLS PMNVRIHMKS ANASHGIWIFIKRV
<i>Burkholderia phytofirmans</i> PsJN	YP_001895217 123 aa	MDNEFESVRI AELAMLADR LDGVPFVGIV FTSDALVTY ¹ NATESKNAGL RPKMVLGKHFFGEVAPC MNN FMVAQRFEDE DVLDDIVPVV LTLRMRPTPV RLRLKATDC ATRFVLIERRATN
<i>Sorangium cellulosum</i> 'So ce 56'	YP_001611644 131 aa (39.7%)	MGSEERSTAG EFEFDIGVFN LDERGLDAQP FGIIRLDREG TVLSYNLYEER ¹ QARRNRQDV IGKNFFTDIAPC ¹ SRVKAHFG RFLAGVEQRE LKATFGVFH FPHKTRHVDV SLFYKAAARQ QDDAVWVFIRG
<i>Salinibacter ruber</i> DSM 13855	YP_446329 156 aa (30.3%)	MADSNQPY S Y LREDDPDSAP GDSGDADEPE PPATDLAFDD EGVGEELRHV DEDELNAAPFGIIQIDDAGVVQFY ¹ NRYESNLSGIDPADAVGANFFTELAPC SNNPLFFGR FKDGVREGGL DEYFTYFTY QMRPTLV DVR LYRDEAENNWLIQKR
<i>Halorhodospira halophila</i> SL1 (PYP2)	YP_001002902 130 aa	MGTLIFGRQD LENRLAAMP E EIDDLPGV I QIDQHGRIL LYNATE ¹ GAIT GRDPEAMIGR DFFNDVAPC G HTEAFYGRFQ EGVRHGLDNE IFDYTFDYRM APTKVRVHMK RALSGDTYWVFKRISAPAA
<i>Halochromatium salexigen</i>	P81046 125 aa	MNIVHFGSDD IENSLANMSD QDLNQLAFGA IQLDASGKVL QYNAAE ¹ EGIT GRDPKSVIGK FFEDVAPC ¹ T K SQEFQGRFK EGVANGNLAT MFEYVFDYQM KPTKVKVHMK KALVDDSYWVFKRL

Acidithiobacillus thiooxidans ATCC 19377	ZP_09998043 134 aa (34.6%)	MLAHNFVADA ILNNDPQINA QIADRQSFGI IALDSHAQVK IFNAE EARLS GLSVEVLGR NFFTEVAPC T ASRLFRGRFR QGIQEGSLDA HFFYTFTYRI RPISAHVHMF YDMRKSPLFF IFDRIIQLY EDLG
Acidithiobacillus caldus ATCC 51756	ZP_05291964 134 aa	MPRKGFVPQA ISEHLDSLNO ALADQQSFGI IGLDVQAIVR IFNKAE EERLS GLPASEVLNH SFFDDVAPC T ASRLFRGRFR AGLERGLSDE HFFYTFTYRI RPSVAHIHML YRPAQSPLVF LFVDRVIPLF EDLG
Leptothrix cholodnii SP-6	YP_001792566 130aa (69.3)	MNEALPLVFD QPDLAACIGT LSEAQLDGLG FGVIGFDAQG VVRV YNAFES KYAGLSPQRV LGHP LFTVVAPC MNFMVAQ RFEDAAASAA SLDATIDYVL TLRMRPVKVK LRLLAAPATA LRYVLVQRPA
Rhodopseudomonas palustris BisB5	YP_570463.1	MNTVDFHDSDLARTIEQLAPEQIDALPFGVIKLDGNGIVTV FNRT EAIESGYKSRPALGLD FFLQVAPC MGQPEFRGRIEQARQLGRVDIELGWVGFSDINRSLQVRIQSASDGLSWIFNLRDHA
Rhodobacter sphaeroides ATCC 17029	YP_001045536 124 aa	MEIIPFGSAD LDNILAREPQ RAEYLPFGAV LLDRTGTILK YNRAE GGIAN RNPADVIGKN FFNEIAPC AK GKRFGHEFLR FHQTGQVNM FDYKFAYKGA NVGVKIHMS QPDGQSC WLFVKRV
Methylomicrobium alcaliphilum 20Z	YP_004916954 485 aa	311 DISQSMRLIN ELAEANAQAM NQNQEVSQAL SQAQKLEKL VSNFKTNTLS SSIVEFRDD IESAMRKMS EELDSIAFGA IELDKNGRIL R YNSAE GDIT GRNPKEVIGRN FFTEVAPC T DTPLFKGEFD KGARMGFLNK KFEYTFDYNM RPTKVKVHMK KLSGSDTY WIFVKRV
Rhodothalassium salexigens	Q53120 125aa	MEMIKFGQDD IENAMADMGD AQIDDLAFGA IQLDETGTIL AYNAAE GELT GRSPQDVIGK NFFKDIAPC T DTEEFGRFR EGVANGDLNA MFEYVFDYQM QPTKVKVHMK RAITGDSY WIFVKRV
Rhodospirillum centenum SW	YP_002299398 883 aa	MPDRTTDDFG PFTEQIRGTI DGMGTAEFDA LPVGAIQVDG SGVIHR YNRT ESRLSGRIFE RVIGRN FFTEVAPC TNIPAF SGRFMDGVTS GTLDARFDFV FDFQMAPVRV QIRMQNAGVP DRY WIFVRKL
Janthinobacterium sp. PAMC 25724	ZP_10443803 129 aa	MNMHTEIQFD QPGIIMLET AEEAALNAFG FGVIGFGRDG RVQR YNTFES KAAGLSVERV LQQD LFMVVAPC MNFLVAQ RFADAYESGQ VLDDTISYVL TLRMRPTRVK LRLSDPAAD LSYVLVHRL
Methyloversatilis universalis FAM5	ZP_08505937 130 aa (62.4)	MNTEQTVAFS EARMLEFLES ASDELDRLD FGVIGIDAGT NVKR YNRFES AAAGLSKDRV IGYAL LFTVVAPC MNFMVAQ RFEDAQEQGS ALDDTIDYVL TLRMRPVKVK LRLLAAPDRA LRYVLVQRQT
Methylotenera versatilis 301	YP_003675031 126 aa (70.9)	MNQITFDMLS LGQTLDKLTN DQLNSLDFGV IGFNDEGMVK VYNAYE SKVA GLSLESVIDS DLFNSVAPC M NFMVAQKFE DAVDTSSELD EIMDYVLT LK MKPTRVKLRL LSSPQFSYSY VVILRS
Spirosoma linguale DSM 74	YP_003384973 123 aa (62.8)	MNQTVHFSDL NLLDWLEKQT NEQLEDAPFG VVRMSRDGIV VAY CKSE SHITGISKEYAVG KY YFTQIAPC ANNQMVAKY AQPTLDEELD YILTYVSEPT KVRLRLKSP ESRYQYFLVN RKA
Thermochromatium tepidum	ADV90265 1108 aa	MNFEDAIDH APRRLDALTP DELNRLPFGA IRVDAEGRIL FYSRAL VDLA NRQVDSVLGR NFFSEIAPC T VVPEFYGRFR QGVL TGQLHT TFEVDFDFM QPVQVRIAMH TSERPGEF WILVQPLALLPA
Leptospira biflexa serovar Patoc strain	YP_001964889	MSKFIDPNILGKGLTGAQAEADGYPFGIVKVDSESKILL YNKYE SELANVPIQTAVGKN FFTEVAIC TNNRIF YGRFKEGMISGDLIAFNFTYKMKPTNVVHLYHDKGTNSNWFVKLR
Thiovulum sp. ES	ZP_10404127 514 aa	331 VNKVDKSMHE IYEITETLD VAGDTDIAT EVAELSKTFA DAIDGKYDKN KTAKKLEVVK FDPKELEGAM NSMSQEQLDN MSFGVVELDK DGNIVK YNSAE GDITGRDRP EVVGKS FFNEVAPC TKSPVF YGKFNQGVNK DDLNVMFDYT FDYNMPTKV KIQMKNAE E E ADKDKTY WIFVKRL
Thiocystis violascens DSM 198	YP_006416171 1122 aa	1 MMFNDAIDH DPRQLDNLSE EQLDRLPCGA IRVDAEGLVIL FYSRSQA AIT NRTPEAVIGR NFFSDVAPC T VVPEFYGRFR RGVLTGQLNT AFEVDFDFM HPIQVRISMR ASHRPGEF WILIEPLRQLPP
Methylobacterium sp. 4-46	YP_001770032 864 aa	MNTMSD R ALA AEAARLDALS TGEIDALDLGVVQVDSGDI LLYN RAESV FSGR S AERVVG RNFFRDVAPC TRLPAYGRF REGV RR GVLD EVFSFAYGFD PQPLRV VAL RG SATPGRY WIVTR PVGQVT
Coralococcus coraloides DSM 2259	YP_005370094 147 aa (35.8%)	1 MNPTPYTPPT GEPFPLQATS LESIDALIQR VDGMSSETLD HLPLGMIQLD GQGRILK FNRT EASLARIQA REQIGKN FFYDVAPC TRVRQ FFGLFQEGVR AKKLYQTFGF VFRFAHGARH VAITLFYSDK TDSV WV LVSD KKMPDAR
Haliangium ochraceum DSM 14365	YP_003269899 129 aa (32.0%)	MSIEQAAERQ LAFDDADLYD ALNGYSAEAL DSVAFGVVRM NSDMRVIA YNRAE AENSGLR PAQVLGKHV FLEVAPC LDNE MVAAYRIQG DLDTQLDYVL AFFMRPTPVR LRLKRAAHD WSY LCVKKR
Stigmatella aurantiaca DW4/3-1	ZP_01464165 146 aa (31.6%)	MAPPSTSLASNA PPK TT P TDDLRLQVETLSASELDALPFGLIQLDRTGRILK FNQTE AKLARINRERQ LGRN FFDDVAPC TKVREFYGRFLNGLSQRSLYETFGFIFKFDHGWRNVAITMFYSEKTD SVWV LISQTSVT PPPAR
Allochromatium vinosum DSM 180	YP_003444998 1114 aa (31.6%)	1 MNRIEPINLE DAIDIHPRQ LDILTEEQLD RLPAGTIRVD AGRILF YSRAQ SVISQREV ESVLGRN FFSEVAPC TVVPE FYGRFRRGVL TGCLTTFEF VFDFKMDPVR VRITMRASDR PGEF WIV QP KNRLPPRNEG
Leptospira meyeri serovar Hardjo str. Went 5	EKJ85739 123 aa	MSKFIDQNI KGLGLTLQSE ADAASFGIVK VDGSGKILL YNKYE SELANV PIQTAVGKN FFTEVAIC TNN RIFYGRFKEG MVSGDLIAF NYVFTYKMKP TNVVIHLYHD NPSNTN WIFVKLR
Terriglobus roseus DSM 18391	YP_006423411 124 aa	MATSEVLEF SKISLGELMS LSNEAIDALP GVVGLSREGVTEV YSHT ESKLAGIPPESVLGTH FFLSTAQC MNFMVAQ RLDDAEALDT VVDYVLTFRM RPTPIRLRL KKAEPYRSYLLIQR
Rhodomicrobium	YP_004011389	MSVSFADPKL ARKLEALSDE ERHDLPGFII KLDNSGVVSF FSRTE ARESG WKKRPALGID FFVGIAPC

vanniellii ATCC 17100	126 aa (59.7)	MA TPEFKGRIEE AARHGAVDIE LGWVGDFDDP NGEMTVRIQS AADGGI W ICLDRPDQG
gamma proteobacterium NOR5-3	ZP_05127488 115 aa	MDFLTITQHE LDNCDPDALD FGVIRMDRSG VVVF YNVAET RISGLSKSQV EGRA FFSEIGIC MHNFMVGH KFEQPGDLDE LVDVYLTLRM DPTPVTLRLL RQGDEKYQYL LIQPI
Curvibacter putative symbiont of Hydra magnipapillata	CBA33201 134 aa	MNNELAFDTPGLCATLNALPAEELDALPYGVIGFDASGH IQR YNAHESK AAMFDPKVVVGGQHV FVELAPC FNNYLVA TR FEDAAAANEALDETMPYVLT FRMRPTRVQV RLLAQPEASL RFILVLRTPA PAKA
Gemmatimonas aurantiaca T-27	YP_002762618 162 aa	1 MPLDITRMLAPFLNRLSDE ELDSIPYGV I QLDPEGFVVS YNRAE AEENAG YCPRPIGRH FFREVAPS ANA PEFHGRFLRG VAEGRLDETF NFTYHCDLMP RRVQLRLYLS PQTQSVWLFV AKPDGTPLDW PSVDLTPVLT SKYVPRFTGF AALNATVDAL LA
Bacteroides helcogenes_P_36-108	YP_004162403	MKIAIFTYLRNFCLLSFLLCLSTSVGAQEGLRIADLFNKYGEQKN VTRVEL NGSILKSYRMTTYKSL VFKDVT PC QQEIQQCIADKDKTDIKAQEVMEGILRSAYYQLKEIDRNGKRLNRYILFKTGKGLMATLIYIEGFLSEK EMMDMLYRPQ
Lentisphaera araneosa HTCC2155	ZP_01876266 209 aa	1 MKVFLVSIVL HIIVLGLIYL NGGFEPVSS ENRRVNPQEV APEVKAREKS VPIKDSKKRV 61 LDEKEKEELI VKTLDNQQKQ YDRMTPSQKH RSLDHQLDQL DGVDGGILEV VTLEVLK LMSKE PSMESKG LSKKTGF DHE SS FFKDVAPC PTGIQVSMED KHGNKSSYII DKKDVTEDDL ALLKLYQKSK NNKALKIILD SFIKHYQNK
marine metagenome	EDJ53704 123 aa	IRA MEIIPFG SNDIDNILAR EPARAEYLPF GAVLLDRSGS IV KYNKA EGL IAGRDPGSMI GKN FFNDVAPC AKGKRFHGE FLKFHKTGQV NTMFDYEFAY KGANVKVRIH LKAQPDGQNC WLF
marine metagenome	EDJ36333 165 aa	MARSAASTTP PGRATTASSP IRRTPAERR PDQRLPREDR T MEIIPFGSQ DIDNILQREP KRAEYLPFGA VLLDRTGKIL KYNKA EGLIA GRDPQSVIGK FFNDIAPC A KGKRFHGEFL KFHKTHGHVNT LFDYEFYKYG ANVKVRIHLK SQPDGQSC WV MFVKRV
marine metagenome	ECM80370.1 124 aa	MEIIPFGSKD LDNLSREPQ RAEYLPYGAV LLDRNGKIQK YNKA EGLIAS RTPEDMIGKD FFNEVAPC AK GKRFHGEFLK FHNTGQVNV I FDYKFAYKGA DVGVKIHLKS QPDGQHC WMLV KRV
marine metagenome	ECJ6517 167 aa	GVTASTVKRW ADDGSLACER TAGGHRRFLA SEVARFRQHE ADTTVSHLST LSDEELDALPYGVIGIDDEG TIIR YNATES NFSNHAVNQV LGKS FFTQVAPC TNNRLVYG AFKEGMASGS LDIKIPYTFY YVMKPTNVVI HMVRCQDSRS NWLLI HHNTD SNGSLIV
marine metagenome	EBF15616 154 aa	MNHRVDCAWC GKMHGDLDS AVLSHGICGT CVAGTGLARV DELHGLDPED ADRLPFGLLH LDHDCRVV YNFPE AERAGL DREWVIGKD FFQDVAPC TRV QEFEGRLRGL QDAGVPGREE FSFVQFRGG SRLVHVLMSH SPKAGTVILV EDQG
mine drainage metagenome	CBH74763 150 aa	MLTSSEGDRR ALLERIEEMG RDEIDALPVG IITLDLDGTI LR YNQTE AGYSRRHAPAQIG RN FFRDVAPC AQDAGFQGRF EALAAPGGHG TVEFEYQHFH PWGSERV LIS FLRGSAPRI QLLIT WP AEQ GKAPLDASAN AHRRARSRRY
mine drainage metagenome	CBH75091 123 aa	MHDQELVERV EAMSAQEIDG LPVGVITLGL DGKIVR YNRTE AEMARLDQK SQVGRN FFTEVAPC TANPEF QGRFDTLAAK SSGGIETFDY TFRFAWGAQR VHITFVRKAG RDDIDVLITRMSA

VITA

Sandip Laxman Kaledhonkar

Candidate for the Degree of

Doctor of Philosophy/Education

Dissertation: STRUCTURAL DYNAMICS OF PHOTOACTIVE YELLOW PROTEIN

Major Field: Physics

Biographical:

Education:

Completed the requirements for the Doctor of Philosophy in Physics at Oklahoma State University, Stillwater, Oklahoma, USA in July, 2013.

Completed the requirements for the Master of Sciences in Physics at University of Pune, Pune, Maharashtra, India in 2004.

Completed the requirements for the Bachelor of Science in Physics at University of Pune, Pune, Maharashtra, India in 2002.

Experience:

Worked as project student at National Chemical Laboratory, Pune, India from Fall 2004-Fall 2005; employed as Junior Research Fellow at Defense Institute of Advanced Technology, Pune, India from Oct 2005-April 2006; employed as a teaching assistant in Department of Physics, Oklahoma State University in Fall 2006- , Fall 2012; employed as research assistant in Department of Physics, Oklahoma State University SU 07, SP 08, FA10, SP 11, SU 12, SP 13, SU 13.

Awards:

Received Outstanding Teaching assistant from Department of Physics, Oklahoma State University, in 2010; received Outstanding Research Assistant from Department of Physics, Oklahoma State University in 2012.

Professional Memberships:

American Physical Society since 2007.